The Design, Synthesis and Evaluation of a New Class of Antibiotic

Submitted in fulfilment of the degree

Doctor of Philosophy (Chemistry)

THE UNIVERSITY of ADELAIDE

Damian Leszek Stachura

B. Sc. (Hons.)

December 2022

Department of Chemistry

Supervisors: Prof. Andrew Abell and Dr. Thomas Avery

Table of Contents

Abstract

Biotin protein ligase (BPL) is a ubiquitous enzyme that catalyzes the conjugation of biotin and ATP to give biotinyl-5'-AMP **1.02**, a key intermediate in the activation of biotin dependent enzymes that are crucial to the survival of all cells. Inhibition of this enzyme critically damages bacteria and thus presents an important strategy to develop a new class of antibiotic. Described in this thesis is the design, synthesis, and biological assay of potent inhibitors of *Staphylococcus aureus* biotin protein ligase (*Sa*BPL) with a 1,2,3-triazole or sulfonamide based isostere.

Chapter One highlights the structure and catalytic mechanism of the target enzyme *Sa*BPL. A summary of the chemistry and *in vitro* biology of known 1,2,3-triazole-based and sulfonamide-based inhibitors, designed to mimic the natural intermediate biotinyl-5'-AMP **1.02**, is also discussed.

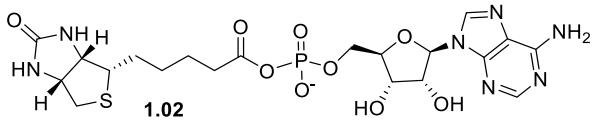

Chapter Two presents work on the development of a new *N1*-diphenylmethyl-triazole scaffold to replace the adenosine of biotinyl-5'-AMP **1.02**. A series of *N1*-diphenylmethyl-triazole analogues were designed and prepared, with the guidance of *in silico* docking, to maximise interactions with the active site of *Sa*BPL. This manifested in significant *in vitro* potency improvements over previous lead triazole-based inhibitors, where **12** and **13**, with imidazole and aminopyridine groups respectively, being the most potent inhibitors reported to date for this chemotype (K_i = 6.01 ± 1.01 and 8.43 ± 0.73 nM). Triazole **12** also demonstrated the best antimicrobial activity reported to date for the triazole-based *Sa*BPL inhibitors against *S. aureus* ATCC 49775, exhibiting a minimum inhibitory concentration (MIC) of 1 μg/mL.

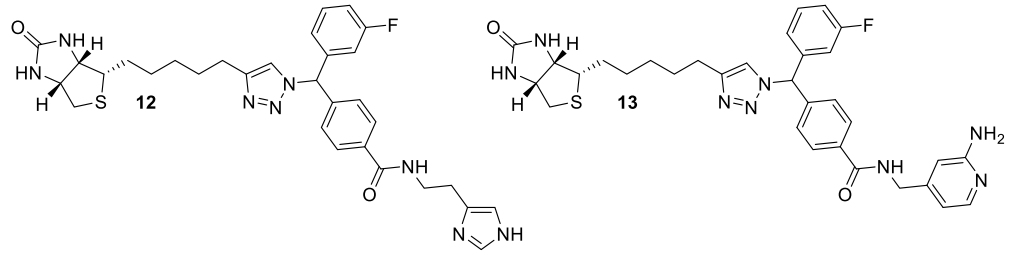

Chapter Three presents a series of potent *N1*-diphenylmethyl-triazole-based analogues targeted to exploit crucial hydrogen bond interactions within the adenine binding site of *Sa*BPL. The inhibitory activity against *Sa*BPL strongly correlated with the *in silico* docking, particularly analogues that were proposed to hydrogen bond to Asn212 and Ser128 within the adenine binding site. For example, the butanamide substituent of **14** was predicted by docking to hydrogen bond these key amino acids, which manifested in a K_i value of 10.2 ± 2.4 nM.

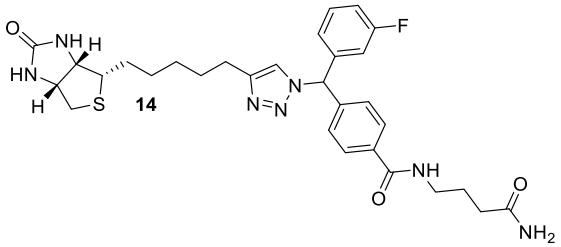

Chapter Four describes the design, detailed characterisation by NMR, and biological assay of a new 1,2,3-triazole-based inhibitor design. Inclusion of a carbonyl at the C10 position of a benzyl-triazole-based *Sa*BPL inhibitor (**1.07**) gave analogue **4.02**, which was shown by docking to hydrogen bond Lys187 within the phosphate binding region. This presumed hydrogen bonding interaction reflected the enhanced K_i value exhibited by **4.02** against *Sa*BPL, relative to triazole **1.07** (K_i = 0.12 ± 0.01 vs 0.25 ± 0.03 µM, respectively).

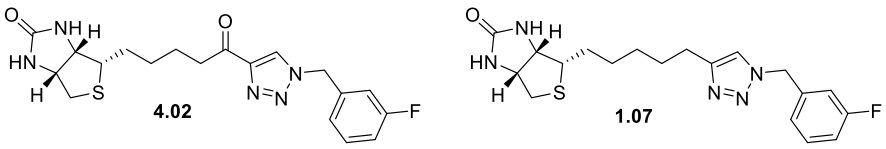

Chapter Five is concerned with the optimisation of the acidity of central NH comprising the sulfonyl linker of the highly effective sulfonamide based *Sa*BPL inhibitors. Acidity of the central NH has been proposed to influence *Sa*BPL inhibitory activity, and based on this, a series of sulfonylurea and sulfonylcarbamate linked analogues were prepared. The relative central sulfonyl NH acidity of these compounds was assessed by ^{1}H NMR, with inhibitor activity against *Sa*BPL shown to correlate with the relative acidity of the central NH. In particular, the acidic sulfonylcarbamate analogue (**5.76**) exhibited an excellent K_i value of 10.3 ± 3.8 nM, whilst also demonstrating potent whole cell activity against *S. aureus* ATCC 49775 (MIC = 4 µg/mL)

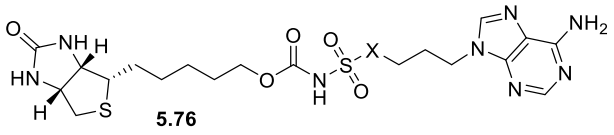

Chapter Six reports details of the biological protocols, docking method, and experimental synthetic procedures for compounds described throughout Chapters, Four, and Five.

Publications

The following publications comprise full chapters in this thesis:

Publication 1

Stachura, D. L.; Nguyen, S.; Polyak, S. W.; Jovcevski, B.; Bruning, J. B.; Abell, A. D., A New 1,2,3-Triazole Scaffold with Improved Potency Against *Staphlyococcus aureus* Biotin Protein Ligase., *ACS Infectious Diseases* **2022**, *8* (12), 2579 – 2585. https//doi.org/10.1021/acsinfecdis.2c00452

Publication 2

Stachura, D. L.; Nguyen, S.; Polyak, S. W.; Jovcevski, B.; Bruning, J. B.; Abell, A. D., A Structural Study of Potent Triazole-based Inhibitors of *Staphylococcus aureus* Biotin Protein Ligase. *Submitted for Peer Review to ACS Medicinal Chemistry Letters* **2022**.

Declaration

I certify that this work contains no material which has been accepted for the award of any other degree or diploma in my name, in any university or other tertiary institution and, to the best of my knowledge and belief, contains no material previously published or written by another person, except where due reference has been made in the text. In addition, I certify that no part of this work will, in the future, be used in a submission in my name, for any other degree or diploma in any university or other tertiary institution without the prior approval of the University of Adelaide and where applicable, any partner institution responsible for the joint-award of this degree.

I acknowledge that copyright of published works contained within this thesis resides with the copyright holder(s) of those works.

I also give permission for the digital version of my thesis to be made available on the web, via the University's digital research repository, the Library Search and also through web search engines, unless permission has been granted by the University to restrict access for a period of time.

I acknowledge the support I have received for my research through the provision of an Australian Government Research Training Program Scholarship.

Damián Leszek Stachura

12/12/2022

……..

Date

Acknowledgments

First and foremost, I would like to sincerely thank my supervisor, Prof. Andrew Abell, for his guidance over the course of my candidature. His remarkable breadth of knowledge, support, and enthusiasm towards all aspects of research has helped me grow as a researcher. I would also like to thank Andrew for his tireless effort in drafting and revising this thesis.

Secondly, I want to thank Dr. Thomas Avery and Dr. John Horsley, for all their constant support over the course of my candidature and assisting the development of my scientific writing skills.

I would like to thank all the past and present members of the Abell group for the welcoming and stimulating working environment. I would like to especially thank. Dr. Kwang Jun Lee who willingly helped me any time I had questions related to my work.

I thank all collaborators associated with the BPL project for all their hard work and time dedicated to help bring the project to where it is now. Particularly, Dr. Blagojce Jovcevski, for allowing me to use his lab space for enzymatic and bacterial work; Dr. Steven Polyak for all useful discussions associated with the project; and Stephanie Nguyen for preparing enzyme stocks required for all assay work.

I wish also to thank all my incredible friends for their support, encouragement, and overall memorable times over the course of this amazing and lengthy journey.

I would be remiss to leave out thanking my parents, Dorota and Leszek, for their encouragement and constant support during the course of all my studies throughout my life. Without them I would not be where I am today as a person, and I feel very fortunate to be their son.

Abbreviations

*Aa*BPL	*A. aeolicus* biotin protein ligase
ABL	ATP binding loop
ACC	Acetyl-CoA carboxylase
$AlCl_3$	Aluminium chloride
AMP	Adenosine monophosphate
AMR	Antimicrobial resistance
ATP	Adenosine triphosphate
BBL	Biotin binding loop
BBL	Biotin binding loop
BCCP	Biotin carboxyl carrier protein
Boc	*tert*-Butyloxycarbonyl
BPL	Biotin protein ligase
Br_2	Bromine
BSA	Bovine serum albumin
BTMSA	Bis(trimethylsilyl)acetylene
Bz	Benzoyl
BzCl	Benzoyl chloride
CAM	Cerium ammonium molybdate
CD_3OD	Deuterated methanol
$CDCl_3$	Deuterated chloroform
CH_3NO_2	Nitromethane
$CHCl_3$	Chloroform
COSY	^1H-^1H Correlation Spectroscopy
Cs_2CO_3	Caesium carbonate
CSI	Chlorosulfonyl isocyanate
$Cu(ClO_4)_2$	Copper perchlorate
CuAAC	Copper alkyne azide cycloaddition
CuI	Copper iodide
DBU	1,8 – Diazabicyclo[5.4.0]undec – 7 – ene
DCM	Dichloromethane
DIPEA	*N*,*N*-Diisopropylethylamine
DMF	*N*,*N*-Dimethylformamide
DMSO	Dimethyl sulfoxide

DMSO-d_6	Deuterated dimethyl sulfoxide
DNA	Deoxyribonucleic acid
DPPA	Diphenylphosphoryl azide
DTT	Dithiothreitol
*Ec*BPL	*E. coli* biotin protein ligase
EDCI	1-Ethyl-3-(3-dimethylaminopropyl)carbodiimide
Eq	Equivalents
ESI	Electro-spray ionisation
EtOAc	Ethyl acetate
EtOH	Ethanol
$FeCl_3$	Ferric chloride
GST	Glutathione *S*-transferase
H_2O_2	Hydrogen peroxide
HATU	*O*-(azabenzotriazol-1-yl)-*N,N,N′,N′*-tetramethyluronium hexafluorophosphate
HBTU	*O*-(benzotriazol-1-yl)-*N,N,N′,N′*-tetramethyluronium hexafluorophosphate
HCl	Hydrochloric acid
HMBC	Heteronuclear Multiple Bond Correlation
HMPA	Hexamethylphosphoramide
HOSA	Hydroxylamine-*O*-sulfonic acid
HRMS	High resolution mass spectrometry
HSQC	Heteronuclear single quantum coherence
K_2CO_3	Potassium carbonate
KF	Potassium fluoride
K_i	Absolute inhibitory constant
KI	Potassium iodide
K_M	Michaelis constant
$KMnO_4$	Potassium permanganate
LC-MS	Liquid chromatography – mass spectrometry
LDA	Lithium diisopropylamide
$LiAlH_4$	Lithium aluminium hydride
LiBr	Lithium bromide
LiHMDS	Lithium *N,N*-bis(trimethylsilyl)amide
LiI	Lithium iodide
LiOH	Lithium hydroxide
m/z	Mass to charge ratio

m-CPBA	*meta*-Chloroperoxybenzoic acid
MeCN	Acetonitrile
MeLi	Methyllithium
MeOH	Methanol
$MgCl_2$	Magnesium chloride
MIC	Minimum inhibitory concentration
MRSA	Methicillin resistant *S. aureus*
*Mt*BPL	*M. tuberculosis* biotin protein ligase
Na_2SO_3	Sodium sulfite
Na_2SO_4	Sodium sulfate
$NaNO_2$	Sodium nitrite
NaOAc	Sodium acetate
NaOH	Sodium hydroxide
NaOMe	Sodium methoxide
n-BuLi	*n*-Butyllithium
NFSi	*N*-Fluorobenzenesulfonimide
NH_4OH	Ammonium hydroxide
NMR	Nuclear magnetic resonance
NOE	Nuclear Overhauser Effect
NOESY	Nuclear Overhauser Effect Spectroscopy
$(COCl)_2$	Oxalyl chloride
PC	Pyruvate carboxylase
PDB	Protein Data Bank
*Ph*BPL	*P. horikoshii* biotin protein ligase
PhMe	Toluene
PMB	*para*-methoxybenzyl
PMBCl	*para*-methoxybenzyl chloride
PPh_3	Triphenyl phosphine
PPi	Pyrophosphate
p-TsOH	*para*-Toluene sulfonic acid
Pyr	Pyridine
RMSD	Root mean square deviation
rt	Room temperature
S. aureus	*Staphylococcus aureus*
*Sa*BPL	*Staphylococcus aureus* biotin protein ligase

*Sa*PC90-GST	GST tagged 90 amino acid biotin-acceptor domain from PC
$SOCl_2$	Thionyl Chloride
TBAF	Tetra-*n*-butylammonium fluoride
TBS	Tris-buffered saline
TBTA	Tris(benzyltriazolylmethyl)amine
t-BuOH	*tert*-Butanol
TEA	Triethylamine
TFA	Trifluoroacetic acid
THF	Tetrahydrofuran
TLC	Thin layer chromatography
TMS	Trimethylsilyl
TMSCl	Trimethylsilyl chloride

Chapter One

The increasing incidence of antibiotic resistant bacteria is a leading global health issue,[1] with recent findings indicating that deaths attributed to bacterial infections has now overtaken that of malaria and HIV combined.[2] Alarmingly, 1.27 million global fatalities directly attributed to bacterial infections were reported in 2019,[2] with a treatment burden of $1,400 dollars per hospitalised patient in the United States (US) alone. This equates to a nation expenditure of $2.2 billion nationally per annum to combat bacterial infections.[3] This threat to human health is only expected to worsen, with global health cost expenditure and deaths projected to exceed $1 trillion and 10 million respectively, by the year 2050.[4–6] Alarmingly, the exit of most pharmaceutical companies from the antibiotic research space, has led to only five new classes of antibiotics being approved since the year 2000.[7,8] Thus, it is imperative that new antibiotic classes are developed to effectively combat this threat of antimicrobial resistance (AMR). A clinically important bacteria, *Staphylococcus aureus* (*S. aureus*), has attained resistance to a multitude of commonly prescribed antibiotics.[9] In particular, methicillin resistant *S. aureus* (MRSA) is responsible for the majority of blood based infections, which frequently leads to fatal sepsis.[10,11] Although countries such as Australia and the US have experienced a reduction in hospital acquired MRSA,[12,13] the threat of community acquired MRSA is on the rise,[14] accounting for 18 % of all reported MRSA infections.[15] An important strategy to combat antimicrobial resistance is to develop new antibiotic classes that affect novel drug targets, particularly those that have no pre-existing mechanisms for resistance. This thesis presents work on one such target *S. aureus* biotin protein ligase (*Sa*BPL), a protein that is critical in bacterial biotin biology, as a novel drug target for antibiotic research.

1.1: Biotin Protein Ligase

Biotin protein ligase (BPL) is a ubiquitous and essential enzyme found in all organisms. The primary role of BPL is to catalyse the post-translational modification of biotin (vitamin B7) onto a specific lysine residue of biotin dependent enzymes. This process is critical for the synthesis of membrane lipid synthesis, amino acid synthesis and gluconeogenesis.[16–19] Two essential enzymes dependent on this post-translational modification are pyruvate carboxylase (PC) and acetyl-CoA carboxylase (ACC).[20,21] The biotin activated PC is involved in the process of converting pyruvate to oxaloacetate, critical to the citric acid cycle. This cycle is central to a multitude of metabolic pathways, importantly the biosynthesis of amino acids.[22] The role of ACC upon biotinylation is the carboxylation of acetyl-CoA to malonyl-CoA, the first step in fatty acid biosynthesis.[23] Importantly, this metabolic pathway ultimately leads into cell membrane biogenesis and maintenance. Thus, inhibiting BPL targets multiple critical metabolic

pathways that are essential for the cell viability of *S. aureus*. Furthermore, knocking out the *birA* gene (the BPL encoding gene) from *S. aureus* prevented cell growth, thus indicating that there is no alternate pathway for the biotinylation of biotin-dependent proteins in bacteria.[24,25]

Additionally, *S. aureus* BPL (*Sa*BPL) has a secondary role, where it regulates uptake and biotin biosynthesis.[26–28] Low cellular concentrations of biotinylated biotin-dependent enzymes induce *Sa*BPL to form a homodimer. This homodimer acts as a transcriptional repressor that regulates biotin biosynthesis and transport, by binding specific promoter sequences on *S. aureus* DNA encoding these proteins.[29] This bifunctionality of *Sa*BPL makes it a promising drug target, as it is unlikely that *S. aureus* can develop target-based resistance due to the intimate involvement of *Sa*BPL in essential metabolic pathways.[28]

The process of biotinylation occurs through a concerted two-step mechanism as illustrated in Scheme 1.1.[30,31] Firstly, BPL catalyses the reaction between biotin **1.01** and ATP to give biotinyl-5'-AMP **1.02**, and pyrophosphate (PPi). The binding of biotin **1.01** to the active site of BPL stimulates an associated conformational change giving rise to the biotin binding loop (BBL) (Figure 1.1). This then permits subsequent binding of ATP, followed by nucleophilic attack on the α-phosphate of ATP by biotin to give biotinyl-5'-AMP **1.02**. The second step involves the post-translational modification of a biotin-dependent enzyme (e.g., ACC or PC). The BPL-**1.02** complex binds to a biotin carboxyl carrier protein (BCCP) domain located on the inactive biotin dependent enzyme. Once bound, the positively charged ε-amino group of the target lysine residue in the BCCP reacts with the biotin carbonyl of **1.02**. This results in the transfer and hence covalent attachment of biotin onto the biotin-dependent enzyme, with adenosine monophosphate (AMP) generated as a side product.

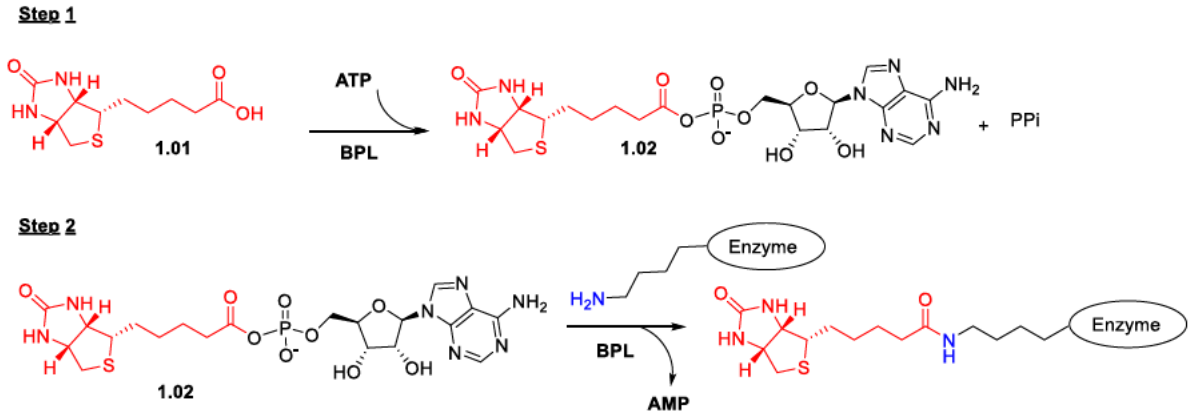

Scheme 1.1: The catalytic concerted two-step reaction of biotinylation.

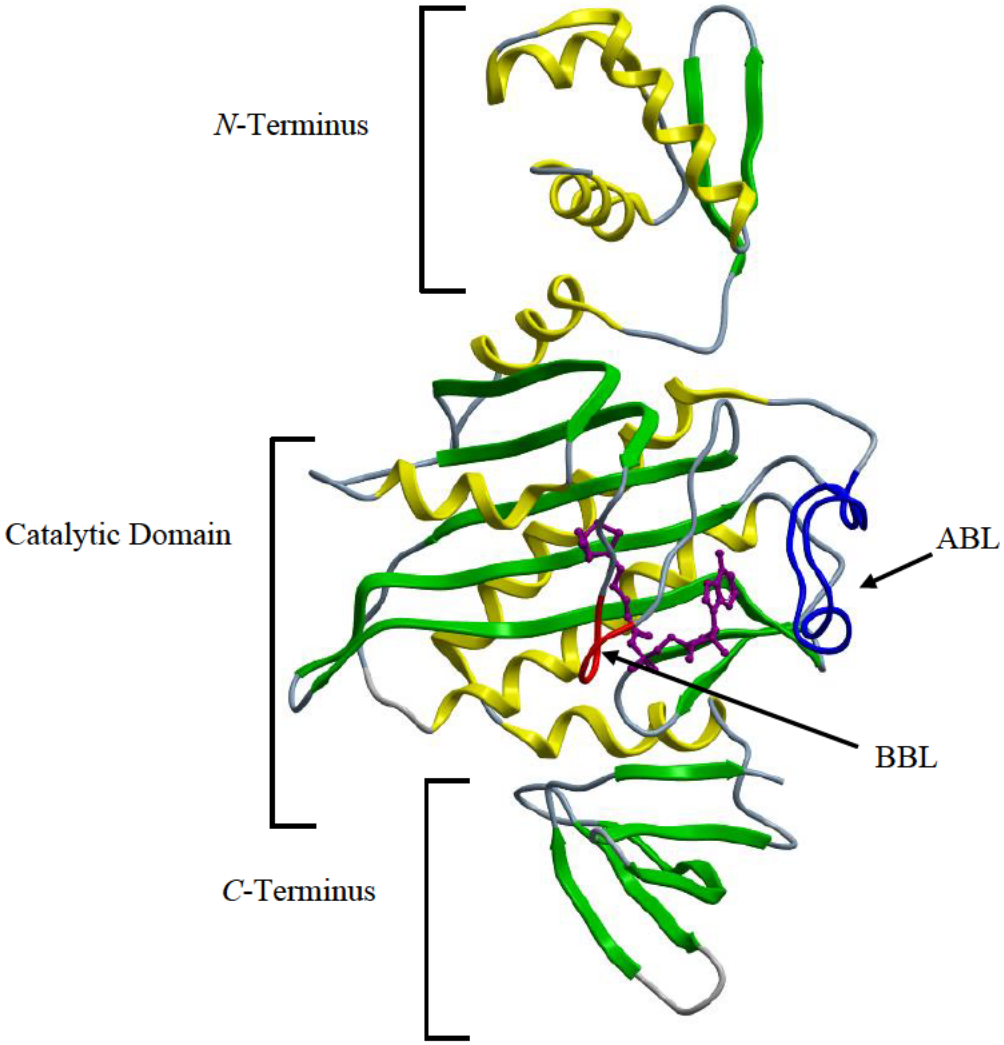

Figure 1.1: 3D depiction of *Sa*BPL in complex with biotinyl-5′-AMP **1.02** (PDB: 3V8L[32]). The β sheets are shown in yellow, α helices in green, biotin binding loop (BBL) in red, ATP binding loop (ABL) in blue, and biotinyl-5′-AMP **1.02** in purple.

1.1.1: Structural Classes of Biotin Protein Ligase

There are three divergent structural classes of BPL (Figure 1.2). Prokaryotic cells have BPLs that fall into either class I or II, whilst eukaryotic cells BPL (e.g., *Homo sapiens*) belong to class III. Class I BPLs are composed entirely of the conserved catalytic domain, which is essential for the biotinylation process. X-ray crystal structures of class I BPLs have been reported for *Aquifex aeolicus* (*A. aeolicus*),[33] *Pyrococcus horikoshii* (*P. horikoshii*)[34] and *Mycobacterium tuberculosis* (*M. tuberculosis*)[35]. Class II BPLs retain the conserved catalytic domain, but also

contain a *N*-terminal DNA binding domain. As a result, this class of BPL is suspected to have the bifunctionality of a ligase and a transcriptional repressor. X-ray crystal structures of class II BPLs have been reported for *S. aureus*[36] (the focus of this thesis) and *Escherichia coli* (*E. coli*)[20]. Class III BPLs also retain the conserved catalytic domain of the other two classes; however, this class possesses an extended *N*-terminus, that is distinct to the *N*-terminus of class II BPLs. Mutagenic and genetic studies have shown that this *N*-terminus extension has "proof-reading" activity, that assists in selecting correct enzymes for biotinylation.[37] The lack of atomic resolution structures of any class III BPL has hindered attempts to better analyse the structural and functional properties of these BPLs.[38] Comparing the conserved catalytic domain of *P. horikoshii* (class I BPL) and *S. aureus* (class II), it is evident that there is a disordered biotin binding loop (BBL) (depicted as a red loop in Figure 1.3) and ATP binding loops (ABL), (depicted as a purple loop in Figure 1.3). Further detail on the BBL and ABL are discussed below in section 1.1.2.

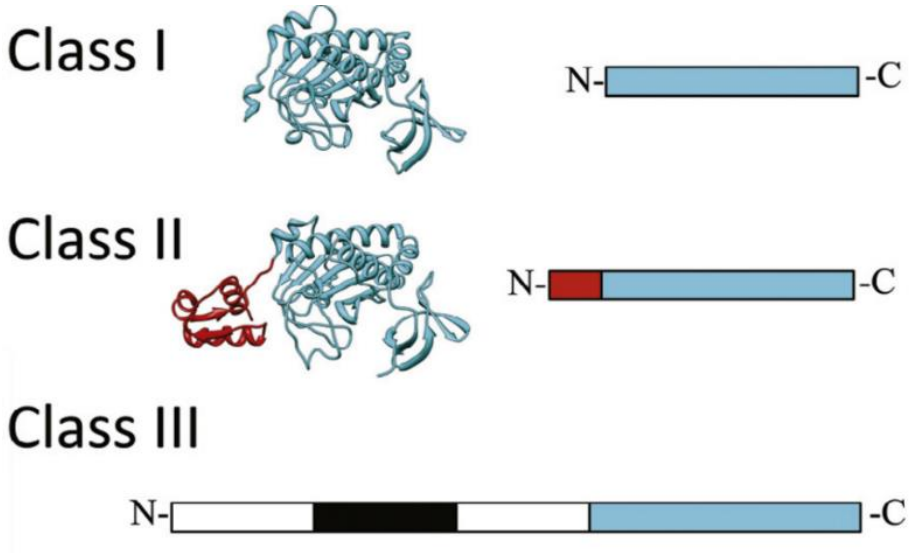

Figure 1.2: Schematic diagram of the three BPL classes. The conserved catalytic region is depicted in teal, the class II *N*-terminus DNA binding domain is shown in red and the proof-reading domain in eukaryotic BPL is boxed black. This figure is adapted from Satiaputra *et al*.[29]

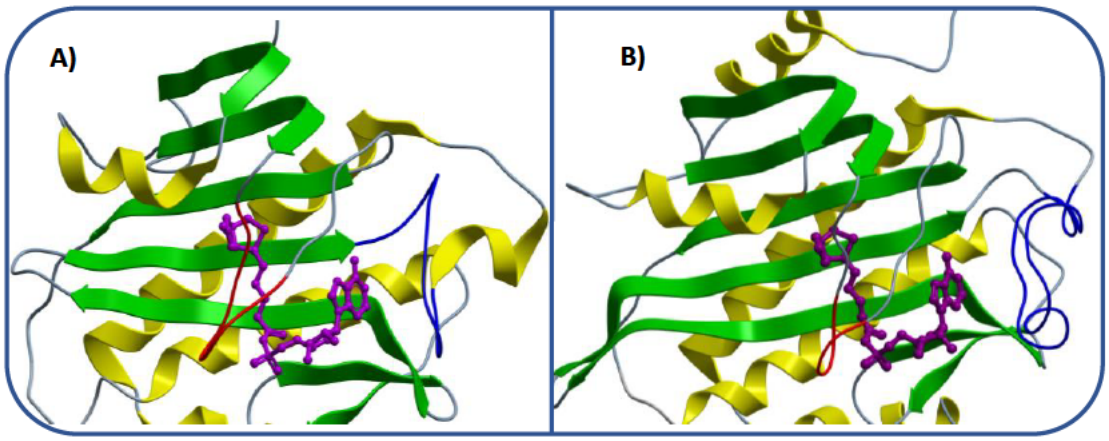

Figure 1.3: X-ray co-crystal structures of biotinyl-5'-AMP **1.02** bound to the active site of (**A**) class I BPL (*P. horikoshii* BPL, PDB: 1WQW[34]) and (**B**) class II BPL (*S. aureus* BPL, PDB: 3V8L[32]), biotin binding loop (BBL) in red, ATP binding loop (ABL) in blue and biotinyl-5′-AMP **1.02** in purple.

1.1.2: Biotin Protein Ligase Structural Characterisation

Biotin binding pocket

There are two distinct regions that biotin **1.01** binds within *Sa*BPL, a hydrophilic pit, and hydrophobic tunnel. The binding of both these regions by biotin **1.01** stimulates the ordering of the BBL, which stabilises the biotin ligand.[36] Binding into the hydrophilic pit is suggested to occur first, where the oxygen of the ureido group of biotin **1.01**, forms hydrogen bonds with residues Ser93, and Arg120, as shown in Figure 1.4. The ureido NH's also form hydrogen bonds with the side chain of Gln116 and the amide back-bone oxygen of Arg120. These residues are highly conserved in BPLs across most species.[39] Three hydrophobic β-sheets encase the valeric tail of biotin **1.01** upon binding of the ureido ring, giving rise to the hydrophobic tunnel. This tunnel is composed of amino acid residues Gly119, Gly210, Gly189, Leu192 and Ile209. Comparison of cocrystals of biotin **1.01** and biotinyl-5'-AMP **1.02** complexed to BPL show a high degree of conservation in the binding pocket of *Sa*BPL[36], *Ec*BPL (*E. Coli*)[30], *Ph*BPL (*P. horikoshii*)[40], *Mt*BPL (*M. tuberculosis*)[41], and *Aa*BPL (*A. aeolicus*)[33].

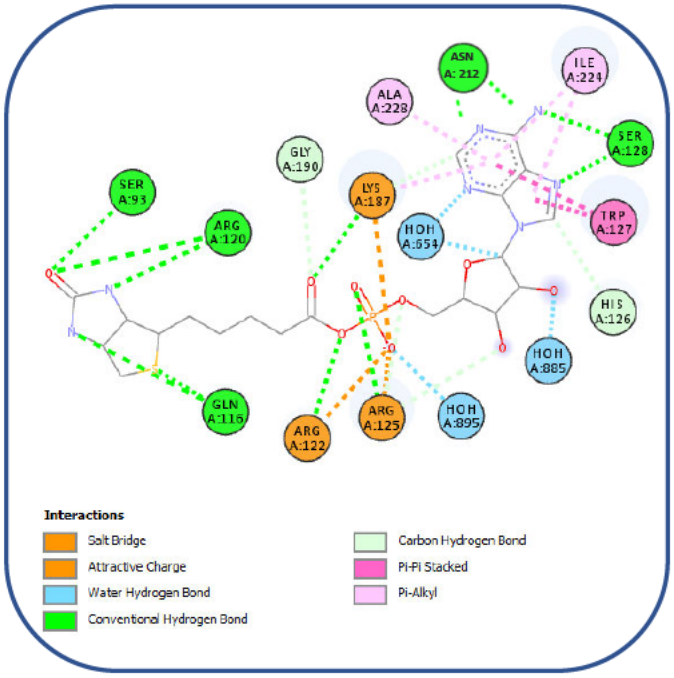

Figure 1.4: 2D interaction diagram of reaction intermediate biotinyl-5′-AMP **1.02** bound to *Sa*BPL. Key binding interactions between **1.02** and the active site of *Sa*BPL are shown. Structure was generated by Chimera, where hydrogen bonding is indicated in green with details omitted as dictated by the program.

Adenosine Triphosphate binding pocket

Structural ordering of the BBL results in the formation of the ATP binding site, a large crevasse that is solvent exposed. The amino acid residue Trp127 presents a nucleotide binding surface, whereby, the indole of Trp127 adopts π-π stacking interactions with the adenine of ATP.[39,42] Without prior ordering of the BBL, Trp127 is oriented such that it cannot establish this π-π stacking interaction.[34] This Trp127 is also highly conserved in BPLs across all species. The aryl amidine functionality of the adenine moiety of ATP also forms hydrogen bonds with Ser128 and Arg212 within the adenine binding site of BPL. Once ATP is bound to the active site, the first step (reaction of biotin with ATP) illustrated in Scheme 1.1 takes place, giving biotinyl-5'-AMP **1.02**.

The formation of the biotinyl-5'-AMP intermediate **1.02** results in the ordering of the ATP binding loop (ABL). The ABL will then proceed to encapsulate intermediate **1.02**, and stabilize it through amino acid residues Ile224, and Ala228. A mutagenesis study on *Ec*BPL confirmed that modifying these hydrophobic residues decreases the binding affinity of the ATP substrate,[42] thus confirming the proposed importance of these residues in the ABL.

Phosphate binding domain

A phosphate binding domain is situated between the biotin and ATP binding pockets. Multiple hydrogen bonding interactions occur between the phosphoanhydride linker of **1.02** and amino acids residues Arg122 Arg125 and Lys187 of *Sa*BPL.[21] Critically, a conserved 'Gly-Arg-Gly-Arg[122] -X' motif contained in all BPLs, shields biotinyl-5'-AMP from solvent.[30] Particularly important is residue Arg122 that plays the critical role of stabilising the binding domain by inducing the formation of a complex network of water-mediated hydrogen bonds with the side chain of Asp180.[21,39] Support for this observation was shown by a point mutation in *Ec*BPL (*E. coli*) of the equivalent residue (Arg118), which resulted in a 400-fold and 100-fold increase in the dissociation rate constant of biotinyl-5'-AMP **1.02** and biotin **1.01** respectively, from the mutant enzyme relative to wild type-BPL.[39]

1.2: *Sa*BPL Inhibitors – Preliminary Data

*Sa*BPL is an attractive novel target for antibiotic development, for multiple reasons. Firstly, the metabolic enzymes PC and ACC can only be biotinylated by *Sa*BPL.[43] Thus, targeting *Sa*BPL consequently disrupts crucial metabolic pathways critical for bacterial cell viability. Secondly, *Sa*BPL also regulates the biotin biosynthesis (*BioO*) and biotin transport (*BioY*) genes. Therefore, targeting *Sa*BPL will not only impact biotinylation of key metabolic enzymes, but also disrupt the supply of cellular biotin.[26,27] Thirdly, the allelic replacement mutagenesis of individual genes demonstrated that without BPL, limited cell growth will occur for *S. aureus*.[24] Lastly, *Sa*BPL is not a known target for any FDA approved antibiotics currently on market. Novel antibiotic classes are critical in combatting the growing threat of AMR, as resistance to one class often leads to resistance to antibiotic belonging to the same class.

1.2.1: Triazole-based SaBPL Inhibitors

One approach to inhibit BPL function is by preparing compounds that bind both the biotin and ATP binding sites, and that are linked by a stabilised isostere of the labile phosphoanhydride of biotinyl-5'-AMP **1.02**. This methodology has procured potent BPL inhibitors for other pathogenic bacterium such as *M. tuberculosis* and *E. coli*.[35,44,45] The first example of a low micromolar *Sa*BPL inhibitor was achieved by the replacing the electrophilic carbonyl of biotinyl-5'-AMP **1.02** for a methylene group, giving biotinol-5'-AMP **1.03** (K_i = 0.03 μM).[32] Unfortunately, **1.03** also inhibits *Homo sapiens* BPL (*Hs*BPL), however, replacing the phosphoanhydride linker of **1.03** with a 1,2,3-triazole, as in **1.04** (Figure 1.5), resulted in >1000-fold selectivity for *Sa*BPL over *Hs*BPL.[46] Furthermore, **1.04** lacks toxicity against mammalian HepG2 cell cultures, an essential trait for a potential antimicrobial therapeutic. The 1,2,3-

triazole core possesses significant advantages over the phosphate of **1.02** or **1.03**. The 1,2,3-triazole has three nitrogens that can act as hydrogen bond acceptors, while the triazole ring can adopt potential π-π stacking interactions, see Figure 1.5. The intrinsic stability of the 1,2,3-triazole is also of importance, as it is stable to oxidative and reductive conditions, acid/base hydrolysis, and metabolic degradation.[47] Moreover, 1,2,3-triazoles are readily prepared by a simple copper-catalysed azide alkyne cycloaddition (CuAAC)

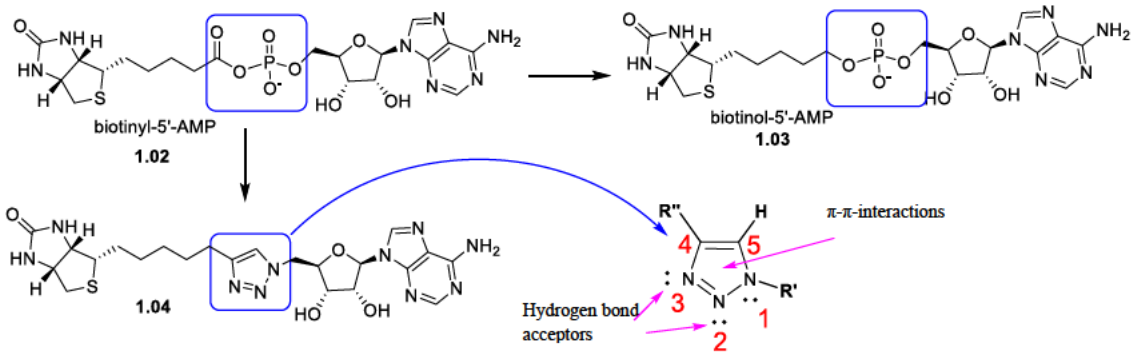

Figure 1.5: Chemical structures of biotinyl-5'-AMP **1.02**, and *Sa*BPL inhibitors **1.03** and **1.04**. Potential interactions with the 1,2,3-triazole scaffold is also shown.

An X-ray crystal structure of **1.04** bound to *Sa*BPL revealed that the 1,2,3-triazole nitrogen atoms form hydrogen bonds with Arg122, and, Arg125; however, not with Lys187.[32] Thus, as triazole **1.04** mimicked the same hydrogen bonds formed between the phosphoanhydride of **1.02** and *Sa*BPL, a series of 1,4-disubstituted-1,2,3-triazole based analogues (**1.05 – 1.09**, see Figure 1.6) were prepared and tested for inhibitory activity against *Sa*BPL.[32,46,48–50]

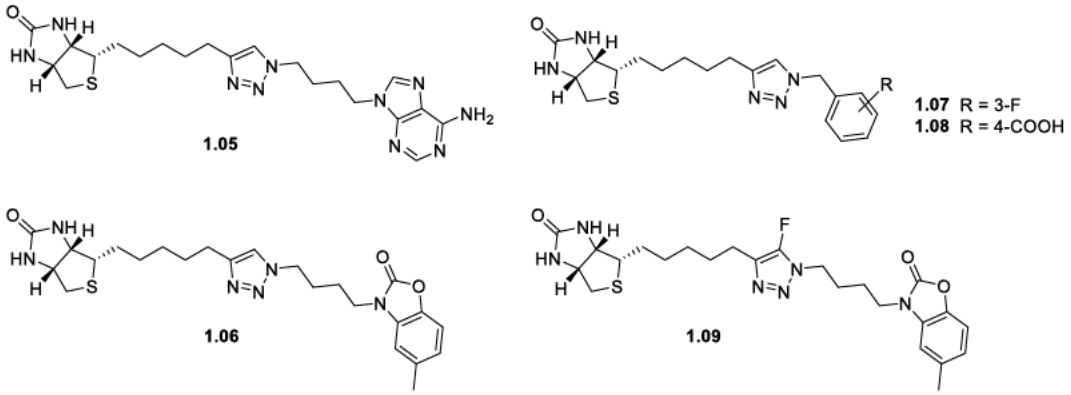

Figure 1.6: Chemical structures of previously reported 1,4-disubstituted-1,2,3-triazole based *Sa*BPL inhibitors.

The adenosine ribose of **1.04** (K_i = 1.17 μM[32]) was replaced with an aliphatic chain to give the more potent inhibitor **1.05** (K_i = 0.67 μM[32,49]), see Figure 1.5. The ribose of biotinyl-5'-AMP **1.02** is reported as superfluous to binding *Sa*BPL, which warranted this replacement. X-ray

crystallography revealed that the adenine ring of **1.05** π-π stacks with Trp123 of *Sa*BPL and hydrogen bonds with Ser129 and Asn212, in a similar manner to **1.02**.[32] Replacing the adenine of **1.05** with a 2-benzoxazolone moiety, as in **1.06**, further improved *Sa*BPL inhibition (K_i = 0.23 μM). Importantly, triazole **1.06** retains selectivity for *Sa*BPL over *Hs*BPL.[50] An X-ray cocrystal structure of **1.06**, bound to *Sa*BPL, showed a displaced π-π stacking interaction between Trp127 of *Sa*BPL, and the aromatic ring of **1.06**.[32] Surprisingly, truncating the alkyl-adenine moiety of **1.05** to a benzylic substituent, as in **1.07** and **1.08**, gave rise to highly potent *Sa*BPL inhibitors (K_i = 0.28 and 0.67 μM, respectively).[46,50] Although **1.05** – **1.08** showed promising *in vitro* potency, these analogues all exhibited poor whole cell activity against a clinical isolate of *S. aureus* (ATCC 49775), with only 60% growth reduction observed at 8 μg/mL for **1.06**.[32] This level of whole cell activity is substantially below what is required for a preclinical candidate.[51] Growth inhibition by 90% was demonstrated by fluorinating the triazole C5 carbon of **1.06** to give **1.09**,[50] where the addition of fluorine to drug-like compounds has been reported to increase the passive diffusion across a lipid membrane, thus, improving compound efficacy.[52–58] However, 5-proto triazoles **1.06** – **1.08** still exhibited superior *Sa*BPL inhibitory activity relative to the 5-fluoro triazole **1.09**. Hence, as **1.07** and **1.08** were potent and offered enhanced atom efficiency relative to **1.06**, these two analogues remained as drug leads for the triazole-based series.

An X-ray co-crystal structure of triazole **1.08** bound within *Sa*BPL revealed that its *p*-carboxy aryl ring is positioned geometrically similar to the ribose group of biotinyl-5'-AMP **1.02** when complexed with *Sa*BPL, see Figure 1.7. The *p*-carboxyl group of **1.08** is directed into the hydrophilic adenine binding site of *Sa*BPL, where no clear interaction is established between this substituent and *Sa*BPL. In contrast, X-ray crystallography of *Sa*BPL in complex with **1.07** revealed a complete lack of electron density for its *m*-F benzyl ring, see Figure 1.8. This lack of electron density reflects rotation of the benzyl ring about its N^1-methylene carbon within the active site. An unoccupied hydrophobic crevasse situated directly adjacent to the adenosine binding site was identified, which may bind the aryl ring of **1.07**. These promiscuous interactions within *Sa*BPL demonstrated by the aryl rings of **1.07** and **1.08**, signify that these inhibitors are not optimal binders of the enzyme. Thus, further chemical optimisation of triazoles **1.07** and **1.08** is warranted to establish all possible interactions within the adenosine binding region of *Sa*BPL, as discussed in this thesis.

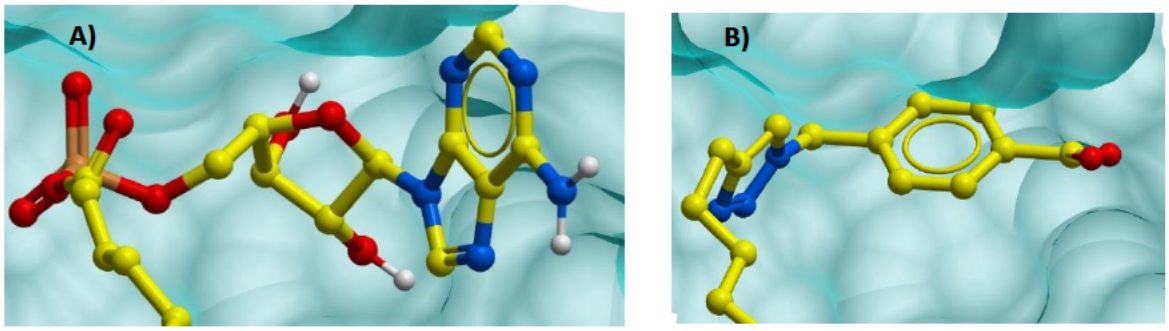

Figure 1.7: The X-ray cocrystal structure of biotinyl-5'-AMP **1.02** (PDB 3RIR[32]) (**A**) and triazole **1.08** (6APW[50]) (**B**) in the adenosine binding pocket region of *Sa*BPL.

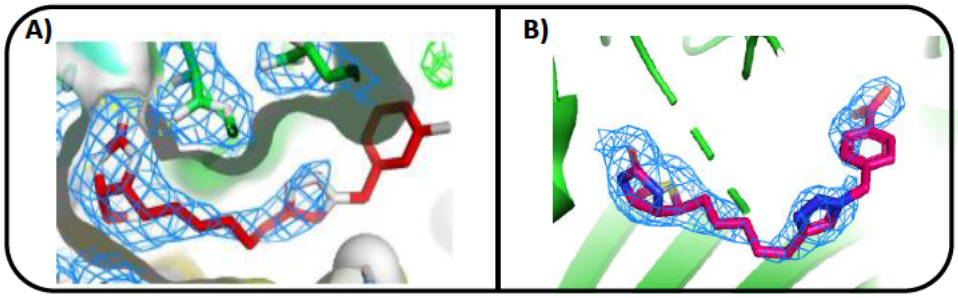

Figure 1.8: X-ray cocrystal structures of **1.07** (**A**) and **1.08** (**B**) in bound to *Sa*BPL (PDB: 6AQQ[50] and PDB: 6APW[50] respectively), with ligand electron density highlighted in a blue grid (*m*-F benzyl moiety shown in predicted conformation)

1.2.2: Sulfonamide-based SaBPL Inhibitors

Replacement of the phosphoanhydride linker of biointyl-5'-AMP **1.02** for a *N*-acyl sulfamate linker **1.10** (Figure 1.9) has also been reported to effectively inhibit BPL.[44,59] Previous studies have established sulfonamide groups as suitable and highly effective isosteres of the phosphoryl group.[58,60,61] However, sulfamate **1.10**, exhibits low inhibitory activity against *Ec*BPL, and rapidly degrades to **1.12** and **1.13** by a proposed intramolecular cyclization.[35,44] Duckworth *et al* reported a potent *Mt*BPL, inhibitor denoted Bio-AMS **1.11**, which binds 1700-fold more tightly to BPL than biotin **1.01**.[62] This BPL inhibitor was selective against *M. tuberculosis*, with minimum inhibitory concentrations (MICs) ranging from 0.16 – 0.63 μM against a number of multi-drug resistant strains (including the virulent H37Rv strain).[62] However, the analogue was shown to be inactive against gram-negative bacteria (e.g., *E. coli*, *P. aeruginosa*, *K. pneumoniae*) and gram-positive bacteria (e.g., *S. aureus*). Inspection of the X-ray cocrystal structure of the *Mt*BPL-Bio-AMS **1.11** complex revealed that amino acids Arg69, Arg72 and Asn130 (the equivalent of Arg122, Arg 125 and Asn179 in *Sa*BPL, respectively), form hydrogen bonds with the sulfonyl oxygens of **1.11**.[62] The carbonyl of the sulfamide is also shown to establish an electrostatic interaction with Lys138 (the equivalent of Lys187 in

*Sa*BPL). The conjugate base of the sulfamide linker of **1.11** is proposed to guide this electrostatic interaction.[62] Lee *et al*. hypothesised that this particular interaction is crucial to inhibitor activity, given the critical role of this lysine residue in biotinylation.[63,64]

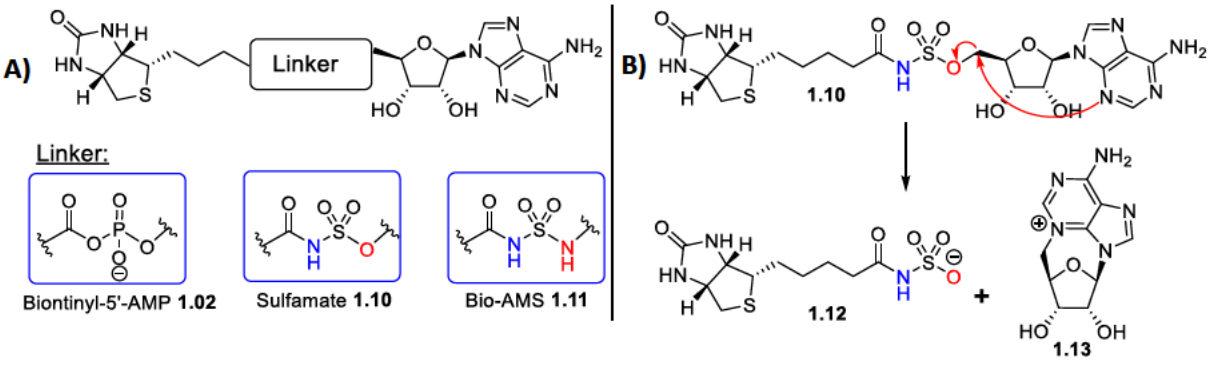

Figure 1.9: Reported sulfonamide-based BPL inhibitors **1.10** and **1.11** (**A**), and the proposed degradation pathway of **1.10** (**B**). The central NH of these sulfonamide-based inhibitors is highlighted in blue.

However, sulfamide of Bio-AMS **1.11** was similarly unstable as sulfamate **1.10**, degrading rapidly to sulfamonylamino adenosine and biotin **1.01** *in vivo*.[65,66] Problematically, *M. tuberculosis* has been shown to develop spontaneous resistance to Bio-AMS **1.11**, by overexpressing a type II alkyl sulfatase, Rv3406.[66] Interestingly, *S. aureus* lacks any equivalent sulfatase, suggesting this bacterium would be susceptible to a sulfonamide-based BPL inhibitor. Indeed, Lee *et al* demonstrated this susceptibility in *S. aureus* with sulfamide **1.14**, which inhibited *Sa*BPL with a K_i value of 7.00 ± 0.30 nM,[63] see Figure 1.10. Additionally, this analogue was shown to effectively inhibit growth of MRSA and other clinically relevant strains of *S. aureus* with MIC values ranging from 0.125 – 0.500 μg/mL.[63,67] Examining the X-ray cocrystal structure of **1.14** in complex with *Sa*BPL revealed an electrostatic interaction between Lys187 of *Sa*BPL and *N3* (central NH, highlighted blue in Figure 1.9) of the acyl sulfamide linker. Similar to **1.11**, analogue **1.14** degrades rapidly *in vivo* under physiological conditions.[63] This intrinsic instability of sulfonamide-based BPL inhibitors was addressed by the sulfonylurea linker of **1.15**. The sulfonylurea of **1.15** show improved *in vivo* stability, however was revealed to be less potent than sulfamide **1.14** against *Sa*BPL (K_i = 65 ± 3.0 vs 7.00 ± 0.30 nM, respectively).[63]

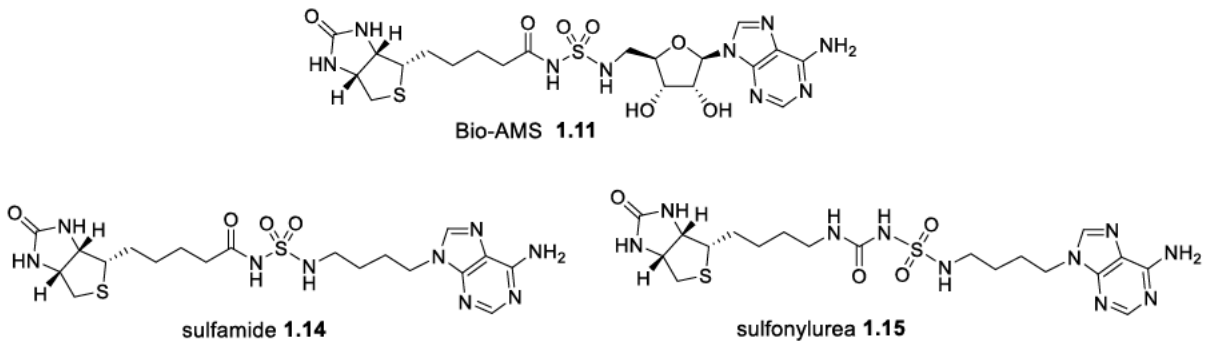

Figure 1.10: Reported sulfonamide-based inhibitors of BPL **1.11**, **1.14** and **1.15**

Interestingly, two distinct binding conformations are reported for **1.15** in complex with *Sa*BPL. The minor conformer binds Lys187 of *Sa*BPL via electrostatic interaction via the deprotonated central NH, whilst the protonated major conformer lacks this interaction, see Figure 1.11.[63] The tendency for the central NH of the linker being deprotonated was also observed for the *Sa*BPL-**1.14** complex, suggesting this is critical for sulfonamide-based inhibitors function. The relative acidity of the sulfonyl linker has been suggested to influence inhibitory activity against *Sa*BPL,[63] however, further investigation is required to elucidate this proposal.

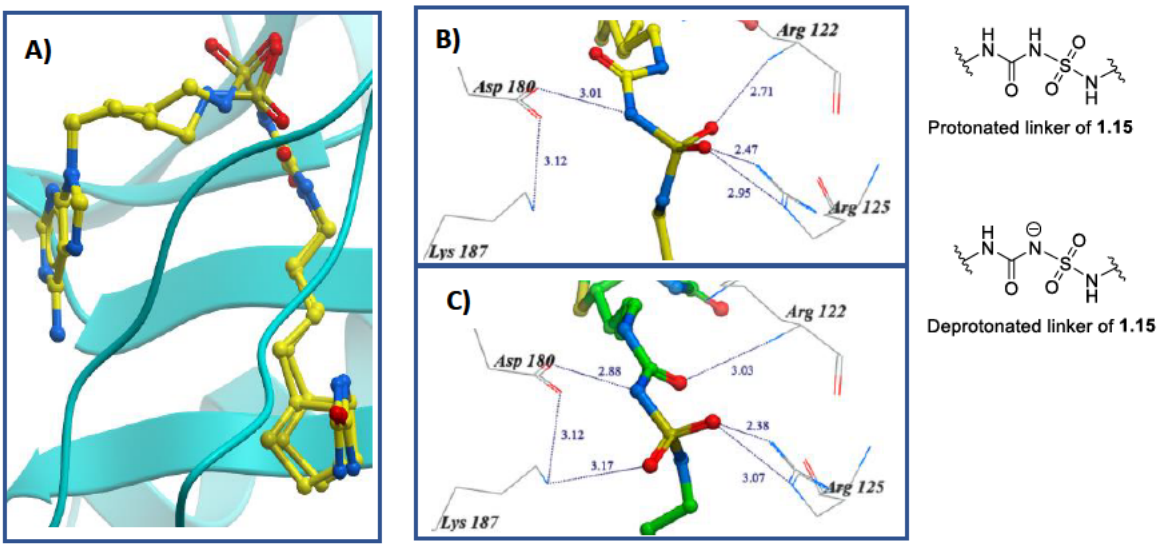

Figure 1.11: X-ray co-crystal structure of sulfonylurea **1.15** bound to *Sa*BPL. (**A**) The two major conformers of **1.15** superimposed within the *Sa*BPL active site. Enzyme-inhibitor interaction diagram of the protonated (**B**) and deprotonated (**C**) linker of **1.15**. Figure adaptations made from Lee *et al.*[63]

1.3: Work Described in this Thesis

As discussed above, *Sa*BPL has been established as an important, and novel drug target for the development of a new class of antibiotic to combat the serious global threat of AMR. The work described in this thesis outlines the design, synthesis, and biological assay of new classes of *Sa*BPL inhibitors with significantly improved potency against the enzyme, and importantly, excellent whole cell activity against *S. aureus*.

The contents of the thesis are as outlined:

Chapter Two presents work that combined the aryl rings of **1.07** and **1.08**, to give a N^1-diphenylmethyl-1,2,3-triazole scaffold. The most potent triazole-based *Sa*BPL inhibitors reported to date are presented in this Chapter.

Chapter Three presents findings that indicated hydrogen bonding amino acid residues Ser128 and Asn212 within the adenine binding region of *Sa*BPL is crucial for the preparation of highly potent N^1-diphenylmethyl-1,2,3-triazole-based inhibitors of *Sa*BPL. The work described in this Chapter was guided by the lead compounds presented in Chapter Two.

Chapter Four presents the design, detailed NMR characterisation, and assay of a new 1,2,3-triazole linker, which contains a carbonyl at the C10 position in order to better mimic the phosphoanhydride linker of biotinyl-5'-AMP **1.02**.

Chapter Five describes work on elucidating the correlation between sulfonyl linker acidity and inhibitory activity against *Sa*BPL for the sulfonamide-based *Sa*BPL inhibitor chemotype.

1.4: References for Chapter One

(1) Temkin, E.; Fallach, N.; Almagor, J.; Gladstone, B. P.; Tacconelli, E.; Carmeli, Y. Estimating the Number of Infections Caused by Antibiotic-Resistant Escherichia Coli and Klebsiella Pneumoniae in 2014: A Modelling Study. *Lancet Glob. Heal.* **2018**, *6* (9), e969–e979. https://doi.org/10.1016/S2214-109X(18)30278-X.

(2) Murray, C. J.; Ikuta, K. S.; Sharara, F.; Swetschinski, L.; Robles Aguilar, G.; Gray, A.; Han, C.; Bisignano, C.; Rao, P.; Wool, E.; Johnson, S. C.; Browne, A. J.; Chipeta, M. G.; Fell, F.; Hackett, S.; Haines-Woodhouse, G.; Kashef Hamadani, B. H.; Kumaran, E. A. P.; McManigal, B.; Agarwal, R.; Akech, S.; Albertson, S.; Amuasi, J.; Andrews, J.; Aravkin, A.; Ashley, E.; Bailey, F.; Baker, S.; Basnyat, B.; Bekker, A.; Bender, R.; Bethou, A.; Bielicki, J.; Boonkasidecha, S.; Bukosia, J.; Carvalheiro, C.; Castañeda-Orjuela, C.; Chansamouth, V.; Chaurasia, S.; Chiurchiù, S.; Chowdhury, F.; Cook, A. J.; Cooper, B.; Cressey, T. R.; Criollo-Mora, E.; Cunningham, M.; Darboe, S.; Day, N. P. J.; De Luca, M.; Dokova, K.; Dramowski, A.; Dunachie, S. J.; Eckmanns, T.; Eibach, D.; Emami, A.; Feasey, N.; Fisher-Pearson, N.; Forrest, K.; Garrett, D.; Gastmeier, P.; Giref, A. Z.; Greer, R. C.; Gupta, V.; Haller, S.; Haselbeck, A.; Hay, S. I.; Holm, M.; Hopkins, S.; Iregbu, K. C.; Jacobs, J.; Jarovsky, D.; Javanmardi, F.; Khorana, M.; Kissoon, N.; Kobeissi, E.; Kostyanev, T.; Krapp, F.; Krumkamp, R.; Kumar, A.; Kyu, H. H.; Lim, C.; Limmathurotsakul, D.; Loftus, M. J.; Lunn, M.; Ma, J.; Mturi, N.; Munera-Huertas, T.; Musicha, P.; Mussi-Pinhata, M. M.; Nakamura, T.; Nanavati, R.; Nangia, S.; Newton, P.; Ngoun, C.; Novotney, A.; Nwakanma, D.; Obiero, C. W.; Olivas-Martinez, A.; Olliaro, P.; Ooko, E.; Ortiz-Brizuela, E.; Peleg, A. Y.; Perrone, C.; Plakkal, N.; Ponce-de-Leon, A.; Raad, M.; Ramdin, T.; Riddell, A.; Roberts, T.; Robotham, J. V.; Roca, A.; Rudd, K. E.; Russell, N.; Schnall, J.; Scott, J. A. G.; Shivamallappa, M.; Sifuentes-Osornio, J.; Steenkeste, N.; Stewardson, A. J.; Stoeva, T.; Tasak, N.; Thaiprakong, A.; Thwaites, G.; Turner, C.; Turner, P.; van Doorn, H. R.; Velaphi, S.; Vongpradith, A.; Vu, H.; Walsh, T.; Waner, S.; Wangrangsimakul, T.; Wozniak, T.; Zheng, P.; Sartorius, B.; Lopez, A. D.; Stergachis, A.; Moore, C.; Dolecek, C.; Naghavi, M. Global Burden of Bacterial Antimicrobial Resistance in 2019: A Systematic Analysis. *Lancet* **2022**, *399* (10325), 629–655. https://doi.org/10.1016/S0140-6736(21)02724-0.

(3) Thorpe, K. E.; Joski, P.; Johnston, K. J. Antibiotic-Resistant Infection Treatment Costs Have Doubled since 2002, Now Exceeding $2 Billion Annually. *Health Aff.* **2018**, *37* (4), 662–669. https://doi.org/10.1377/hlthaff.2017.1153.

(4) Chokshi, A.; Sifri, Z.; Cennimo, D.; Horng, H. Global Contributors to Antibiotic Resistance. *J. Glob. Infect. Dis.* **2019**, *11* (1), 36–42. https://doi.org/10.4103/jgid.jgid_110_18.

(5) Dadgostar, P. Antimicrobial Resistance: Implications and Costs. *Infect. Drug Resist.* **2019**, *12*, 3903–3910. https://doi.org/10.2147/IDR.S234610.

(6) de Kraker, M. E. A.; Stewardson, A. J.; Harbarth, S. Will 10 Million People Die a Year Due to Antimicrobial Resistance by 2050? *PLoS Med.* **2016**, *13* (11), e1002184. https://doi.org/10.1371/journal.pmed.1002184.

(7) Penchovsky, R.; Traykovska, M. Designing Drugs That Overcome Antibacterial Resistance: Where Do We Stand and What Should We Do? *Expert Opin. Drug Discov.* **2015**, *10* (6), 631–650.

https://doi.org/10.1517/17460441.2015.1048219.

(8) Dantes, R.; Mu, Y.; Belflower, R.; Aragon, D.; Dumyati, G.; Harrison, L. H.; Lessa, F. C.; Lynfield, R.; Nadle, J.; Petit, S.; Ray, S. M.; Schaffner, W.; Townes, J.; Fridkin, S. National Burden of Invasive Methicillin-Resistant Staphylococcus Aureus Infections, United States, 2011. *JAMA Intern. Med.* **2013**, *173* (21), 1970–1979. https://doi.org/10.1001/jamainternmed.2013.10423.

(9) Rasmussen, R. V; Fowler Jr, V. G.; Skov, R.; Bruun, N. E. Future Challenges and Treatment of Staphylococcus Aureus Bacteremia with Emphasis on MRSA. *Future Microbiol.* **2010**, *6* (1), 43–56. https://doi.org/10.2217/fmb.10.155.

(10) Yang, Y.; Hu, Z.; Shang, W.; Hu, Q.; Zhu, J.; Yang, J.; Peng, H.; Zhang, X.; Liu, H.; Cong, Y.; Li, S.; Hu, X.; Zhou, R.; Rao, X. Molecular and Phenotypic Characterization Revealed High Prevalence of Multidrug-Resistant Methicillin-Susceptible Staphylococcus Aureus in Chongqing, Southwestern China. *Microb. Drug Resist.* **2017**, *23* (2), 241–246. https://doi.org/10.1089/mdr.2016.0078.

(11) Turnidge, J. D.; Nimmo, G. R.; Pearson, J.; Gottlieb, T.; Collignon, P. J. Epidemiology and Outcomes for Staphylococcus Aureus Bacteraemia in Australian Hospitals, 2005-06: Report from the Australian Group on Antimicrobial Resistance. *Commun. Dis. Intell. Q. Rep.* **2007**, *31* (4), 398–403.

(12) Infections, M.; Bulens, S.; Reingold, A.; Petit, S.; Gershman, K.; Ray, S. M.; Harrison, L. H.; Lynfield, R.; Schaffner, W. Health Care – Associated Invasive MRSA. **2012**, *304* (6), 2005–2008.

(13) Ferguson, J. Healthcare-Associated Methicillin-Resistant Staph Aureus (MRSA) Control in Australia and New Zealand - 2007 Australasian Society for Infectious Diseases (ASID) Conference Forum Convened by Healthcare Infection Control Special Interest Group (HICSIG). *Healthc. Infect.* **2007**, *12* (2), 60–66.

(14) Klein, E.; Smith, D. L.; Laxminarayan, R. Hospitalizations and Deaths Caused by Methicillin-Resistant Staphylococcus Aureus, United States, 1999-2005. *Emerg. Infect. Dis.* **2007**, *13* (12), 1840–1846. https://doi.org/10.3201/eid1312.070629.

(15) Cameron, J. K.; Hall, L.; Tong, S. Y. C.; Paterson, D. L.; Halton, K. Incidence of Community Onset MRSA in Australia: Least Reported Where It Is Most Prevalent. *Antimicrob. Resist. Infect. Control* **2019**, *8* (1), 1–9. https://doi.org/10.1186/s13756-019-0485-7.

(16) Eisenreich, W.; Dandekar, T.; Heesemann, J.; Goebel, W. Carbon Metabolism of Intracellular Bacterial Pathogens and Possible Links to Virulence. *Nat. Rev. Microbiol.* **2010**, *8* (6), 401–412. https://doi.org/10.1038/nrmicro2351.

(17) Gago, G.; Diacovich, L.; Arabolaza, A.; Tsai, S.-C.; Gramajo, H. Fatty Acid Biosynthesis in Actinomycetes. *FEMS Microbiol. Rev.* **2011**, *35* (3), 475–497. https://doi.org/10.1111/j.1574-6976.2010.00259.x.

(18) Park, S.; Klotzsche, M.; Wilson, D. J.; Boshoff, H. I.; Eoh, H.; Manjunatha, U.; Blumenthal, A.; Rhee, K.; Barry, C. E.; Aldrich, C. C.; Ehrt, S.; Schnappinger, D. Evaluating the Sensitivity of Mycobacterium Tuberculosis to Biotin Deprivation Using Regulated Gene Expression. *PLoS Pathog.* **2011**, *7* (9), 3–12. https://doi.org/10.1371/journal.ppat.1002264.

(19) Salaemae, W.; Azhar, A.; Booker, G. W.; Polyak, S. W. Biotin Biosynthesis in Mycobacterium Tuberculosis: Physiology, Biochemistry and Molecular Intervention. *Protein Cell* **2011**, *2* (9), 691–695. https://doi.org/10.1007/s13238-011-1100-8.

(20) Feng, J.; Paparella, A. S.; Booker, G. W.; Polyak, S. W.; Abell, A. D. Biotin Protein Ligase Is a Target for New Antibacterials. *Antibiotics* **2016**, *5* (3). https://doi.org/10.3390/antibiotics5030026.

(21) Soares Da Costa, T. P.; Tieu, W.; Yap, M. Y.; Zvarec, O.; Bell, J. M.; Turnidge, J. D.; Wallace, J. C.; Booker, G. W.; Wilce, M. C. J.; Abell, A. D.; Polyak, S. W. Biotin Analogues with Antibacterial Activity Are Potent Inhibitors of Biotin Protein Ligase. *ACS Med. Chem. Lett.* **2012**, *3* (6), 509–514. https://doi.org/10.1021/ml300106p.

(22) Wallace, J. C.; Jitrapakdee, S.; Chapman-Smith, A. Pyruvate Carboxylase. *Int. J. Biochem. Cell Biol.* **1998**, *30* (1), 1–5. https://doi.org/10.1016/S1357-2725(97)00147-7.

(23) Bloch, K.; Vance, D. Control Mechanisms in the Synthesis of Saturated Fatty Acids. *Annu. Rev. Biochem.* **1977**, *46* (1), 263–298. https://doi.org/10.1146/annurev.bi.46.070177.001403.

(24) Payne, D. J.; Gwynn, M. N.; Holmes, D. J.; Pompliano, D. L. Drugs for Bad Bugs: Confronting the Challenges of Antibacterial Discovery. *Nat. Rev. Drug Discov.* **2007**, *6* (1), 29–40. https://doi.org/10.1038/nrd2201.

(25) Forsyth, R. A.; Haselbeck, R. J.; Ohlsen, K. L.; Yamamoto, R. T.; Xu, H.; Trawick, J. D.; Wall, D.; Wang, L.; Brown-Driver, V.; Froelich, J. M.; Kedar, G. C.; King, P.; McCarthy, M.; Malone, C.; Misiner, B.; Robbins, D.; Tan, Z.; Zhu, Z. Y.; Carr, G.; Mosca, D. A.; Zamudio, C.; Foulkes, J. G.; Zyskind, J. W. A Genome-Wide Strategy for the Identification of Essential Genes in Staphylococcus Aureus. *Mol. Microbiol.* **2002**, *43* (6), 1387–1400. https://doi.org/10.1046/j.1365-2958.2002.02832.x.

(26) Rodionov, D. A.; Mironov, A. A.; Gelfand, M. S. Conservation of the Biotin Regulon and the BirA Regulatory Signal in Eubacteria and Archaea. *Genome Res.* **2002**, *12* (10), 1507–1516. https://doi.org/10.1101/gr.314502.

(27) Abbott, J.; Beckett, D. Cooperative Binding of the Escherichia Coli Repressor of Biotin Biosynthesis to the Biotin Operator Sequence. *Biochemistry* **1993**, *32* (37), 9649–9656. https://doi.org/10.1021/bi00088a017.

(28) Beckett, D. Biotin Sensing at the Molecular Level. *J. Nutr.* **2009**, *139* (1), 167–170. https://doi.org/10.3945/jn.108.095760.

(29) Satiaputra, J.; Shearwin, K. E.; Booker, G. W.; Polyak, S. W. Mechanisms of Biotin-Regulated Gene Expression in Microbes. *Synth. Syst. Biotechnol.* **2016**, *1* (1), 17–24. https://doi.org/10.1016/j.synbio.2016.01.005.

(30) Wood, Z. A.; Weaver, L. H.; Brown, P. H.; Beckett, D.; Matthews, B. W. Co-Repressor Induced Order and Biotin Repressor Dimerization: A Case for Divergent Followed by Convergent Evolution. *J. Mol. Biol.* **2006**, *357* (2), 509–523. https://doi.org/10.1016/j.jmb.2005.12.066.

(31) Bagautdinov, B.; Kuroishi, C.; Sugahara, M.; Kunishima, N. Crystal Structures of Biotin Protein Ligase

from Pyrococcus Horikoshii OT3 and Its Complexes: Structural Basis of Biotin Activation. *J. Mol. Biol.* **2005**, *353* (2), 322–333. https://doi.org/https://doi.org/10.1016/j.jmb.2005.08.032.

(32) Soares Da Costa, T. P.; Tieu, W.; Yap, M. Y.; Pendini, N. R.; Polyak, S. W.; Pedersen, D. S.; Morona, R.; Turnidge, J. D.; Wallace, J. C.; Wilce, M. C. J.; Booker, G. W.; Abell, A. D. Selective Inhibition of Biotin Protein Ligase from Staphylococcus Aureus. *J. Biol. Chem.* **2012**, *287* (21), 17823–17832. https://doi.org/10.1074/jbc.M112.356576.

(33) Tron, C. M.; McNae, I. W.; Nutley, M.; Clarke, D. J.; Cooper, A.; Walkinshaw, M. D.; Baxter, R. L.; Campopiano, D. J. Structural and Functional Studies of the Biotin Protein Ligase from Aquifex Aeolicus Reveal a Critical Role for a Conserved Residue in Target Specificity. *J. Mol. Biol.* **2009**, *387* (1), 129–146. https://doi.org/10.1016/j.jmb.2008.12.086.

(34) Samols, D.; Thornton, C. G.; Murtif, V. L.; Kumar, G. K.; Haase, F. C.; Wood, H. G. Evolutionary Conservation among Biotin Enzymes. *J. Biol. Chem.* **1988**, *263* (14), 6461–6464. https://doi.org/10.1016/s0021-9258(18)68661-2.

(35) Duckworth, B. P.; Geders, T. W.; Tiwari, D.; Boshoff, H. I.; Sibbald, P. A.; Barry, C. E.; Schnappinger, D.; Finzel, B. C.; Aldrich, C. C. Bisubstrate Adenylation Inhibitors of Biotin Protein Ligase from Mycobacterium Tuberculosis. *Chem. Biol.* **2011**, *18* (11), 1432–1441. https://doi.org/10.1016/j.chembiol.2011.08.013.

(36) Pendini, N. R.; Yap, M. Y.; Polyak, S. W.; Cowieson, N. P.; Abell, A.; Booker, G. W.; Wallace, J. C.; Wilce, J. A.; Wilce, M. C. J. Structural Characterization of Staphylococcus Aureus Biotin Protein Ligase and Interaction Partners: An Antibiotic Target. *Protein Sci.* **2013**, *22* (6), 762–773. https://doi.org/10.1002/pro.2262.

(37) Mayende, L.; Swift, R. D.; Bailey, L. M.; Da Costa, T. P. S.; Wallace, J. C.; Booker, G. W.; Polyak, S. W. A Novel Molecular Mechanism to Explain Biotin-Unresponsive Holocarboxylase Synthetase Deficiency. *J. Mol. Med.* **2012**, *90* (1), 81–88. https://doi.org/10.1007/s00109-011-0811-x.

(38) Sternicki, L. M.; Nguyen, S.; Pacholarz, K. J.; Barran, P.; Pendini, N. R.; Booker, G. W.; Huet, Y.; Baltz, R.; Wegener, K. L.; Pukala, T. L.; Polyak, S. W. Biochemical Characterisation of Class III Biotin Protein Ligases from Botrytis Cinerea and Zymoseptoria Tritici. *Arch. Biochem. Biophys.* **2020**, *691* (June), 108509. https://doi.org/10.1016/j.abb.2020.108509.

(39) Kwon, K.; Beckett, D. Function of a Conserved Sequence Motif in Biotin Holoenzyme Synthetases. *Protein Sci.* **2000**, *9* (8), 1530–1539. https://doi.org/10.1110/ps.9.8.1530.

(40) Bagautdinov, B.; Matsuura, Y.; Bagautdinova, S.; Kunishima, N. Protein Biotinylation Visualized by a Complex Structure of Biotin Protein Ligase with a Substrate. *J. Biol. Chem.* **2008**, *283* (21), 14739–14750. https://doi.org/10.1074/jbc.M709116200.

(41) Purushothaman, S.; Gupta, G.; Srivastava, R.; Ramu, V. G.; Surolia, A. Ligand Specificity of Group I Biotin Protein Ligase of Mycobacterium Tuberculosis. *PLoS One* **2008**, *3* (5), 1–12. https://doi.org/10.1371/journal.pone.0002320.

(42) Naganathan, S.; Beckett, D. Nucleation of an Allosteric Response via Ligand-Induced Loop Folding. *J.*

Mol. Biol. **2007**, *373* (1), 96–111. https://doi.org/10.1016/j.jmb.2007.07.020.

(43) Rozwarski, D. A.; Vilchèze, C.; Sugantino, M.; Bittman, R.; Sacchettini, J. C. Crystal Structure of the Mycobacterium Tuberculosis Enoyl-ACP Reductase, InhA, in Complex with NAD+ and a C16 Fatty Acyl Substrate. *J. Biol. Chem.* **1999**, *274* (22), 15582–15589. https://doi.org/10.1074/jbc.274.22.15582.

(44) Brown, P. H.; Cronan, J. E.; Grøtli, M.; Beckett, D. The Biotin Repressor: Modulation of Allostery by Corepressor Analogs. *J. Mol. Biol.* **2004**, *337* (4), 857–869. https://doi.org/10.1016/j.jmb.2004.01.041.

(45) Bockman, M. R.; Kalinda, A. S.; Petrelli, R.; De La Mora-Rey, T.; Tiwari, D.; Liu, F.; Dawadi, S.; Nandakumar, M.; Rhee, K. Y.; Schnappinger, D.; Finzel, B. C.; Aldrich, C. C. Targeting Mycobacterium Tuberculosis Biotin Protein Ligase (MtBPL) with Nucleoside-Based Bisubstrate Adenylation Inhibitors. *J. Med. Chem.* **2015**, *58* (18), 7349–7369. https://doi.org/10.1021/acs.jmedchem.5b00719.

(46) Feng, J.; Paparella, A. S.; Tieu, W.; Heim, D.; Clark, S.; Hayes, A.; Booker, G. W.; Polyak, S. W.; Abell, A. D. New Series of BPL Inhibitors To Probe the Ribose-Binding Pocket of Staphylococcus Aureus Biotin Protein Ligase. *ACS Med. Chem. Lett.* **2016**, *7* (12), 1068–1072. https://doi.org/10.1021/acsmedchemlett.6b00248.

(47) Rostovtsev, V. V.; Green, L. G.; Fokin, V. V.; Sharpless, K. B. A Stepwise Huisgen Cycloaddition Process: Copper(I)-Catalyzed Regioselective "Ligation" of Azides and Terminal Alkynes. *Angew. Chemie - Int. Ed.* **2002**, *41* (14), 2596–2599. https://doi.org/10.1002/1521-3773(20020715)41:14<2596::AID-ANIE2596>3.0.CO;2-4.

(48) Tieu, W.; Polyak, S. W.; Paparella, A. S.; Yap, M. Y.; Soares Da Costa, T. P.; Ng, B.; Wang, G.; Lumb, R.; Bell, J. M.; Turnidge, J. D.; Wilce, M. C. J.; Booker, G. W.; Abell, A. D. Improved Synthesis of Biotinol-5′-AMP: Implications for Antibacterial Discovery. *ACS Med. Chem. Lett.* **2015**, *6* (2), 216–220. https://doi.org/10.1021/ml500475n.

(49) Tieu, W.; Soares Da Costa, T. P.; Yap, M. Y.; Keeling, K. L.; Wilce, M. C. J.; Wallace, J. C.; Booker, G. W.; Polyak, S. W.; Abell, A. D. Optimising in Situ Click Chemistry: The Screening and Identification of Biotin Protein Ligase Inhibitors. *Chem. Sci.* **2013**, *4* (9), 3533–3537. https://doi.org/10.1039/c3sc51127h.

(50) Paparella, A. S.; Lee, K. J.; Hayes, A. J.; Feng, J.; Feng, Z.; Cini, D.; Deshmukh, S.; Booker, G. W.; Wilce, M. C. J.; Polyak, S. W.; Abell, A. D. Halogenation of Biotin Protein Ligase Inhibitors Improves Whole Cell Activity against Staphylococcus Aureus. *ACS Infect. Dis.* **2018**, *4* (2), 175–184. https://doi.org/10.1021/acsinfecdis.7b00134.

(51) Tieu, W.; Jarrad, A. M.; Paparella, A. S.; Keeling, K. A.; Soares Da Costa, T. P.; Wallace, J. C.; Booker, G. W.; Polyak, S. W.; Abell, A. D. Heterocyclic Acyl-Phosphate Bioisostere-Based Inhibitors of Staphylococcus Aureus Biotin Protein Ligase. *Bioorganic Med. Chem. Lett.* **2014**, *24* (19), 4689–4693. https://doi.org/10.1016/j.bmcl.2014.08.030.

(52) Gillis, E. P.; Eastman, K. J.; Hill, M. D.; Donnelly, D. J.; Meanwell, N. A. Applications of Fluorine in Medicinal Chemistry. *J. Med. Chem.* **2015**, *58* (21), 8315–8359. https://doi.org/10.1021/acs.jmedchem.5b00258.

(53) Gerebtzoff, G.; Li-Blatter, X.; Fischer, H.; Frentzel, A.; Seelig, A. Halogenation of Drugs Enhances

Membrane Binding and Permeation. *ChemBioChem* **2004**, *5* (5), 676–684. https://doi.org/10.1002/cbic.200400017.

(54) Kuhn, B.; Mohr, P.; Stahl, M. Intramolecular Hydrogen Bonding in Medicinal Chemistry. *J. Med. Chem.* **2010**, *53* (6), 2601–2611. https://doi.org/10.1021/jm100087s.

(55) Stump, B.; Eberle, C.; Schweizer, W. B.; Kaiser, M.; Brun, R.; Krauth-Siegel, R. L.; Lentz, D.; Diederich, F. Pentafluorosulfanyl as a Novel Building Block for Enzyme Inhibitors: Trypanothione Reductase Inhibition and Antiprotozoal Activities of Diarylamines. *ChemBioChem* **2009**, *10* (1), 79–83. https://doi.org/10.1002/cbic.200800565.

(56) Weiss, M. M.; Williamson, T.; Babu-Khan, S.; Bartberger, M. D.; Brown, J.; Chen, K.; Cheng, Y.; Citron, M.; Croghan, M. D.; Dineen, T. A.; Esmay, J.; Graceffa, R. F.; Harried, S. S.; Hickman, D.; Hitchcock, S. A.; Horne, D. B.; Huang, H.; Imbeah-Ampiah, R.; Judd, T.; Kaller, M. R.; Kreiman, C. R.; La, D. S.; Li, V.; Lopez, P.; Louie, S.; Monenschein, H.; Nguyen, T. T.; Pennington, L. D.; Rattan, C.; San Miguel, T.; Sickmier, E. A.; Wahl, R. C.; Wen, P. H.; Wood, S.; Xue, Q.; Yang, B. H.; Patel, V. F.; Zhong, W. Design and Preparation of a Potent Series of Hydroxyethylamine Containing β-Secretase Inhibitors That Demonstrate Robust Reduction of Central β-Amyloid. *J. Med. Chem.* **2012**, *55* (21), 9009–9024. https://doi.org/10.1021/jm300119p.

(57) Dalvit, C.; Vulpetti, A. Intermolecular and Intramolecular Hydrogen Bonds Involving Fluorine Atoms: Implications for Recognition, Selectivity, and Chemical Properties. *ChemMedChem* **2012**, *7* (2), 262–272. https://doi.org/10.1002/cmdc.201100483.

(58) Patrone, J. D.; Yao, J.; Scott, N. E.; Dotson, G. D. Selective Inhibitors of Bacterial Phosphopantothenoylcysteine Synthetase. *J. Am. Chem. Soc.* **2009**, *131* (45), 16340–16341. https://doi.org/10.1021/ja906537f.

(59) Brown, P. H.; Beckett, D. Use of Binding Enthalpy to Drive an Allosteric Transition. *Biochemistry* **2005**, *44* (8), 3112–3121. https://doi.org/10.1021/bi047792k.

(60) Forrest, A. K.; Jarvest, R. L.; Mensah, L. M.; O'Hanlon, P. J.; Pope, A. J.; Sheppard, R. J. Aminoalkyl Adenylate and Aminoacyl Sulfamate Intermediate Analogues Differing Greatly in Affinity for Their Cognate Staphylococcus Aureus Aminoacyl TRNA Synthetases. *Bioorganic Med. Chem. Lett.* **2000**, *10* (16), 1871–1874. https://doi.org/10.1016/S0960-894X(00)00360-7.

(61) Yu, X. Y.; Hill, J. M.; Yu, G.; Wang, W.; Kluge, A. F.; Wendler, P.; Gallant, P. Synthesis and Structure-Activity Relationships of a Series of Novel Thiazoles as Inhibitors of Aminoacyl-TRNA Synthetases. *Bioorganic Med. Chem. Lett.* **1999**, *9* (3), 375–380. https://doi.org/10.1016/S0960-894X(98)00738-0.

(62) Duckworth, B. P.; Geders, T. W.; Tiwari, D.; Boshoff, H. I.; Sibbald, P. A.; Barry, C. E. 3rd; Schnappinger, D.; Finzel, B. C.; Aldrich, C. C. Bisubstrate Adenylation Inhibitors of Biotin Protein Ligase from Mycobacterium Tuberculosis. *Chem. Biol.* **2011**, *18* (11), 1432–1441. https://doi.org/10.1016/j.chembiol.2011.08.013.

(63) Lee, K. J.; Tieu, W.; Blanco-Rodriguez, B.; Paparella, A. S.; Yu, J.; Hayes, A.; Feng, J.; Marshall, A. C.; Noll, B.; Milne, R.; Cini, D.; Wilce, M. C. J.; Booker, G. W.; Bruning, J. B.; Polyak, S. W.; Abell, A. D.

Sulfonamide-Based Inhibitors of Biotin Protein Ligase as New Antibiotic Leads. *ACS Chem. Biol.* **2019**, *14* (9), 1990–1997. https://doi.org/10.1021/acschembio.9b00463.

(64) Ma, Q.; Akhter, Y.; Wilmanns, M.; Ehebauer, M. T. Active Site Conformational Changes upon Reaction Intermediate Biotinyl-5'-AMP Binding in Biotin Protein Ligase from Mycobacterium Tuberculosis. *Protein Sci.* **2014**, *23* (7), 932–939. https://doi.org/10.1002/pro.2475.

(65) Bockman, M. R.; Engelhart, C. A.; Dawadi, S.; Larson, P.; Tiwari, D.; Ferguson, D. M.; Schnappinger, D.; Aldrich, C. C. Avoiding Antibiotic Inactivation in Mycobacterium Tuberculosis by Rv3406 through Strategic Nucleoside Modification. *ACS Infect. Dis.* **2018**, *4* (7), 1102–1113. https://doi.org/10.1021/acsinfecdis.8b00038.

(66) Tiwari, D.; Park, S. W.; Essawy, M. M.; Dawadi, S.; Mason, A.; Nandakumar, M.; Zimmerman, M.; Mina, M.; Ho, H. P.; Engelhart, C. A.; Ioerger, T.; Sacchettini, J. C.; Rhee, K.; Ehrt, S.; Aldrich, C. C.; Dartois, V.; Schnappinger, D. Targeting Protein Biotinylation Enhances Tuberculosis Chemotherapy. *Sci. Transl. Med.* **2018**, *10* (438). https://doi.org/10.1126/scitranslmed.aal1803.

(67) Hayes, A. J.; Satiaputra, J.; Sternicki, L. M.; Paparella, A. S.; Feng, Z.; Lee, K. J.; Blanco-Rodriguez, B.; Tieu, W.; Eijkelkamp, B. A.; Shearwin, K. E.; Pukala, T. L.; Abell, A. D.; Booker, G. W.; Polyak, S. W. Advanced Resistance Studies Identify Two Discrete Mechanisms in Staphylococcus Aureus to Overcome Antibacterial Compounds That Target Biotin Protein Ligase. *Antibiotics* **2020**, *9* (4). https://doi.org/10.3390/antibiotics9040165.

Chapter Two

This chapter consists of a publication submitted to ACS Infectious Diseases in September 2022 and accepted in November 2022. The publication is entitled “A New 1,2,3-Triazole Scaffold with Improved Potency Against *Staphylococcus aureus* Biotin Protein Ligase”. Copies of key ^{1}H and ^{13}C NMR spectra are included in this Chapter as required by the journal.

ACS Infectious Diseases, **2022**, *8* (12), 2579 – 2585

Damian L. Stachura, Stephanie Nguyen, Steven W. Polyak, Blagojce Jovcevski, John B. Bruning, Andrew D. Abell

Statement of Authorship

Title of Paper	A New 1,2,3-Triazole Scaffold with Improved Potency against *Staphylococcus aureus* Biotin Protein Ligase
Publication Status	☑ Published ☐ Accepted for Publication ☐ Submitted for Publication ☐ Unpublished and Unsubmitted work written in manuscript style
Publication Details	Stachura, D. L.; Nguyen, S.; Polyak, S. W.; Jovcevski, B.; Bruning, J. B.; Abell, A. D., New 1,2,3-Triazole Scaffold with Improved Potency Against *Staphylococcus aureus* Biotin Protein Ligase., *ACS Infectious Diseases* **2022,** ASAP. https://doi.org/10.1021/acsinfecdis.2c00452

Principal Author

Name of Principal Author (Candidate)	Damian Leszek Stachura
Contribution to the Paper	Performed the synthesis, characterization of analogues, analysis of data, *in vitro* biological assays, provided advanced draft of manuscript and subsequent revisions
Overall percentage (%)	70
Certification:	This paper reports on original research I conducted during the period of my Higher Degree by Research candidature and is not subject to any obligations or contractual agreements with a third party that would constrain its inclusion in this thesis. I am the primary author of this paper.
Signature	Date 6/12/22

Co-Author Contributions

By signing the Statement of Authorship, each author certifies that:

i. the candidate's stated contribution to the publication is accurate (as detailed above);
ii. permission is granted for the candidate in include the publication in the thesis; and
iii. the sum of all co-author contributions is equal to 100% less the candidate's stated contribution.

Name of Co-Author	Stephanie Nguyen
Contribution to the Paper	Prepared *Sa*BPL and *Sa*PC90-GST enzyme stocks essential for the *in vitro* biochemical assays
Signature	Date 30/11/2022

Name of Co-Author	Steven Polyak
Contribution to the Paper	Worked closely with the principal authors of the manuscript and supervised the biological testing.
Signature	Date 30/11/22

Name of Co-Author	Blagojce Jovcevski		
Contribution to the Paper	Performed antimicrobial assay of analogues **12** and **13** and supervised the biological testing.		
Signature		Date	30/11/22

Name of Co-Author	John B. Bruning		
Contribution to the Paper	Supervised the biological aspects of the manuscript		
Signature		Date	30/11/2022

Name of Co-Author	Andrew D. Abell		
Contribution to the Paper	Supervised the medicinal chemistry of the project and revised manuscript. A corresponding author.		
Signature		Date	6/12/2022

2.1: Abstract

Staphylococcus aureus (*S. aureus*), a key ESKAPE bacteria, is responsible for most blood-based infections, and as a result is a major economic healthcare burden requiring urgent attention. Here we report *in silico* docking, synthesis, and assay of N^1-diphenylmethyl triazole-based analogues (**7-13**) designed to interact with the entire binding site of *S. aureus* biotin protein ligase (*Sa*BPL), an enzyme critical for the regulation of gluconeogenesis and fatty-acid biosynthesis. The second aryl ring of these compounds enhances both *Sa*BPL potency and whole cell activity against *S.aureus*, relative to previously reported mono-benzyl triazoles. Analogues **12** and **13**, with added substituents to better interact with the adenine binding site, are particularly potent with K_i values of 6.01 ± 1.01 and 8.43 ± 0.73 nM, respectively. These analogues are the most active triazole-based inhibitors reported to date and importantly inhibit the growth of a clinical isolate strain of *S. aureus*, ATCC 49775, with minimum inhibitory concentrations of 1 and 8 µg/mL respectively.

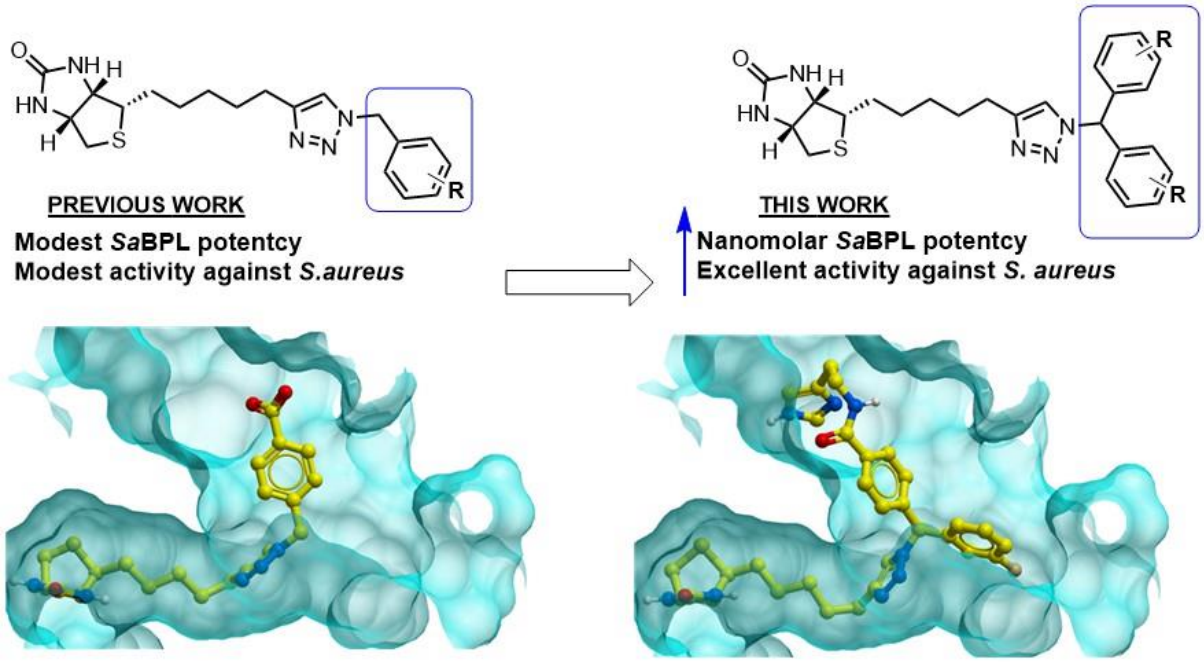

The N^1-diphenylmethyl-1,2,3-triazole maximises interactions within *Sa*BPL, which significantly enhances inhibitory activity relative to previously reported triazole-based inhibitors.

2.2: Introduction

The World Health Organisation (WHO) has warned that antibiotic resistance is a major threat to global health,[1] with mortality rates directly attributable to drug-resistant bacterial infections expected to rise to 10 million global annual deaths by 2050.[2,3] *Staphylococcus aureus* (*S. aureus*) is central to this dogma with methicillin resistant strains (MRSA) being responsible for the majority of bloodstream infections,[4–6] making it an extremely important burden on world health.[7–9] New classes of antibiotics are desperately required to counter this threat[10] and *S. aureus* biotin protein ligase (*Sa*BPL) is a promising drug target in this context.[11–13] BPL is responsible for the covalent attachment of biotin onto biotin-dependent enzymes, a process central to bacterial survival that is also found in humans.[14–16] Acetyl-CoA carboxylase and pyruvate carboxylase, enzymes critical to gluconeogenesis and fatty acid synthesis respectively, are biotinylated and hence activated in this way.[17,18]

Biotinylation occurs through a concerted two-step process with *Sa*BPL promoting ligation of biotin and ATP to form the reactive intermediate biotinyl-5′-AMP **1**.[14,16] The labile phosphoanhydride linker of **1** has been replaced with a non-hydrolysable bio-isostere to give *Sa*BPL inhibitors, for example see the 1,2,3-triazole **2** in Figure 1, which has a modest K_i of 1.17 μM. Importantly, triazole inhibitors of this type show selectivity for *Sa*BPL over the human BPL homologue.[11,12,19–21] Replacement of the adenosine substituent of **2** with a simpler benzyl group, as in **4** and **5** (see Figure 1), retains activity against *Sa*BPL with K_i values of 0.29 ± 0.05 μM and 0.67 ± 0.06 μM, respectively. Substitution of the phosphoanhydride of **1** for a sulfonamide linker gave **3**, which was potent against a *Mycobacterium tuberculosis* homologue, but inactive against MRSA.[22,23] Interestingly, removal of the ribose group of **3** gives rise to the potent *Sa*BPL inhibitor (Sulfonamide **6** K_i : 0.007 ± 0.03 μM) that also displays excellent whole cell activity against *S. aureus* and MRSA.[12,24]

While the triazole-based inhibitors (such as **4** and **5**) lack some *Sa*BPL potency and whole cell activity against clinical isolates of *S. aureus,* they are simpler to prepare than the sulfonamides and thus warrant further investigation. Here we present a new series of N^1-di-phenylmethyl 1,2,3-triazoles (**7-13**, see Figure 2), with an additional aryl group designed to interact with the entire *Sa*BPL active site as discussed below. Studies are also presented on introducing an aryl substituent to better mimic the adenine of **1**, see compounds **12** and **13**.

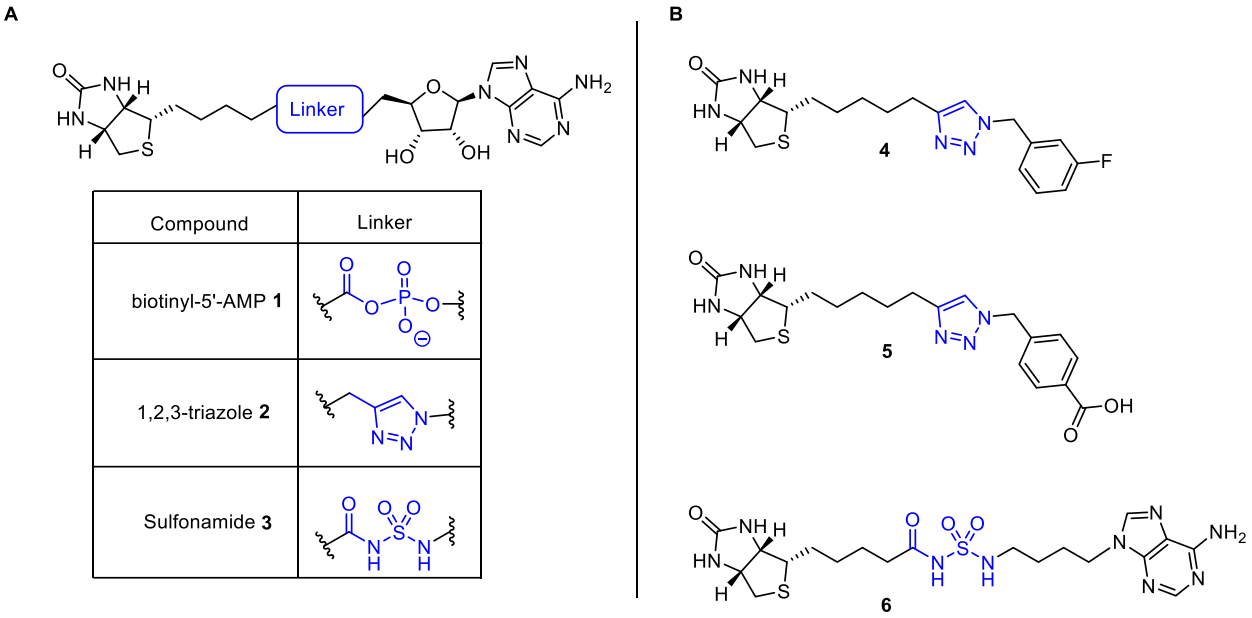

Figure 1: (A) Chemical structures of biotinyl-5'-AMP **1**, and sulfonamide and 1,2,3-triazole based bioisostere **2**, **3**. **(B)** Chemical structures of recently reported *Sa*BPL inhibitors **4-6**.

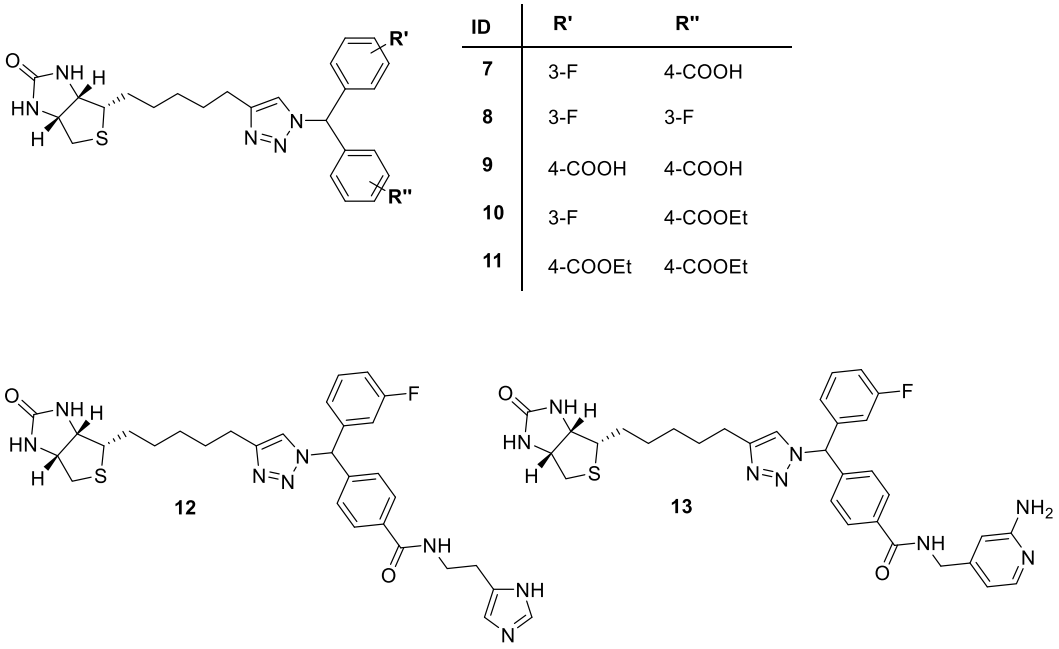

ID	R'	R"
7	3-F	4-COOH
8	3-F	3-F
9	4-COOH	4-COOH
10	3-F	4-COOEt
11	4-COOEt	4-COOEt

Figure 2: Proposed N^1-di-phenylmethyl 1,2,3-triazole *Sa*BPL inhibitors **7-13**.

2.3: Results and Discussion

Our previously reported X-ray co-crystal structure of mono-benzyl triazole inhibitor **4** bound to the active site of *Sa*BPL,[11] reveals a lack of electron density associated with its benzylic substituent. Unlike the aryl group of **5**, the position of the *m*-F-benzyl substituent of **4** is less defined in the structure, with rotation about the N^1-methylene bond resulting in two different interactions. Closer inspection of the active site of this structure reveals an alternate binding pocket adjacent to the adenosine binding pocket into which this group binds, as suggested by *in silico* docking. This suggests that the addition of a second aryl substituent as in **7-13** should allow occupation of both binding sites as developed in this paper. The alternate binding site region is highlighted in Figure 3.

2.3.1: Docking of Triazoles 7-13:

The proposed analogues **7-13** were docked with *Sa*BPL in order to validate the design using the above mentioned[11] X-ray co-crystal structure of *Sa*BPL. A rigid protein model was used in accordance with other docking studies of *Sa*BPL.[11] As anticipated, the triazole core of all analogues bound to *Sa*BPL in an analogous fashion to the phosphoanhydride linker of natural intermediate **1**, which positions one aryl ring in the adenosine binding pocket and the second in the adjacent binding pocket as mentioned above. Interestingly, the *in silico* docking suggests the *p*-carboxy aryl rings of **7** and of the mono-benzyl triazole **5** bind in the same way to the adenosine binding site. Both diastereomers of **7** docked with essentially the same binding conformations (see SI. Figure S1). Docking of the ester analogue **10**, positions its *p*-ethoxy carbonyl group deep within the adenine binding pocket of *Sa*BPL. However, no clear interactions were apparent between the ethyl chain and adenine binding region. The published X-ray cocrystal structure[19] of natural intermediate **1** bound to *Sa*BPL revealed hydrogen bonds between the adenine binding site amino acid residues Ser128 and Asn212 and the adenine ring of **1** (see Figure 3). Analogues **12** and **13**, with their respective imidazole and aminopyridine substituents were designed to better exploit these natural interactions. Docking of **12** and **13** then revealed the expected hydrogen bonds between the imidazole and aminopyridine with Asn212 and/or Ser128 respectively, thus mimicking interactions observed for the adenine of **1** and *Sa*BPL. Again, the diastereomeric pairs of **12** and **13** show similar binding conformations on docking to *Sa*BPL (see SI, Figures S6, S7).

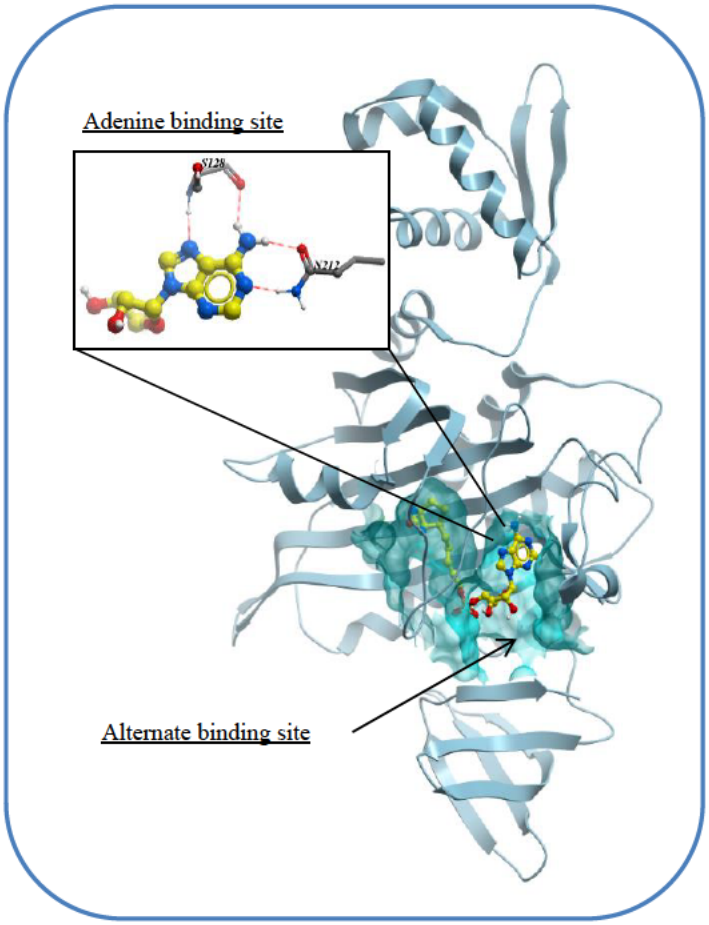

Figure 3: Previously reported X-ray co-crystal structure of biotinyl-5'-AMP **1** bound to *Sa*BPL (PDB: 3V8L).[19] Hydrogen bonds between the adenine ring of **1** and amino acid residues Ser128 and Asn212 of the *Sa*BPL adenine binding site are shown (red lines). The alternate binding site is also highlighted.

2.3.2: Synthesis of Triazoles 7-13:

Triazoles **7-13** were prepared by azide-alkyne Huisgen cycloaddition of biotin acetylene **14**[19] with the respective azides (**28-30**, Scheme 1). The azides were prepared from the corresponding benzophenones **18**, **20** and **21**. Benzophenone **18**, required for the synthesis of azide **29**, was prepared in three steps. Friedel Crafts reaction between acid chloride **15** and toluene, in the presence of $AlCl_3$, gave **16** in a 74 % yield. Subsequent benzylic oxidation of **16** with $KMnO_4$ then gave the carboxylic acid **17** (55 %), which was esterified to give the ethyl ester benzophenone **18** in 66 %. The di-ethyl ester benzophenone **20**, required for the preparation of azide **30**, was prepared by refluxing commercial di-acid **19** in EtOH in the presence of *p*-TsOH, as shown in Scheme 1. The benzophenones **18**, **20** and **21** were then separately reduced to the corresponding alcohols **22**, **23** and **24** with $NaBH_4$. Each of these alcohols was treated with $SOCl_2$ and the resulting acid chlorides (**25**, **26**, **27**) were reacted with NaN_3 to give the required azides **28**, **29** and **30** in 89, 91 and 91 % respectively.[11]

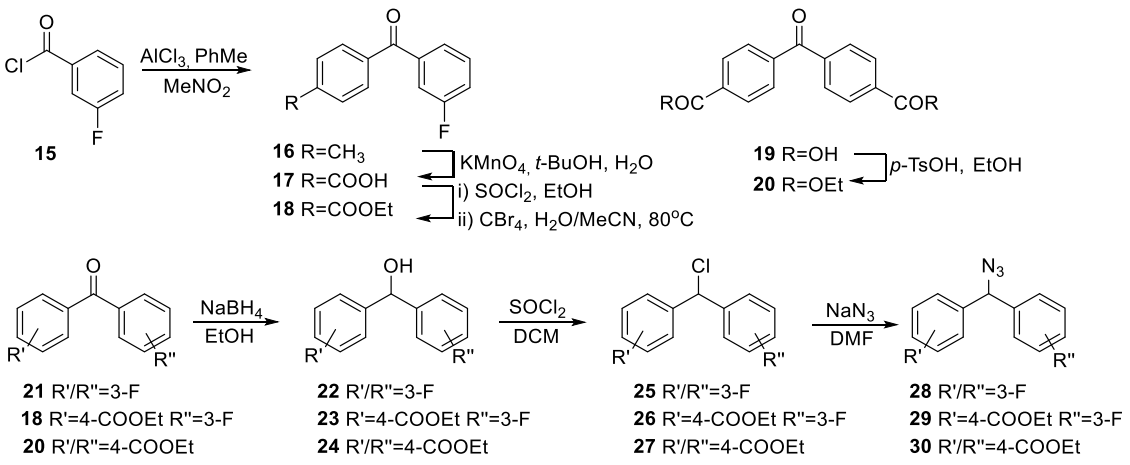

Scheme 1: Synthesis of azides **28**, **29**, **30**.

Biotin-acetylene **14**[19] was separately reacted with each azide (**28**, **29** and **30**), in the presence of copper nanopowder, to give 1,4-disubstituted-1,2,3-triazoles **8**, **10** and **11** in 54 , 69 and 82 % yields respectively (Scheme 2). The ethyl esters of **10** and **11** were hydrolysed with LiOH to give the corresponding carboxylic acids **7** and **9** in 96 and 93 %, respectively. Finally, samples of the carboxylic acid **7** were coupled with either histamine or 4-(aminomethyl)pyridin-2-amine, in the presence of HATU and DIPEA, to give analogues **12** and **13** in 61 and 41 %, respectively. Triazoles **7**, **10**, **12** and **13** were all tested against *Sa*BPL and *S. aureus* as mixtures of diastereomers as discussed below.

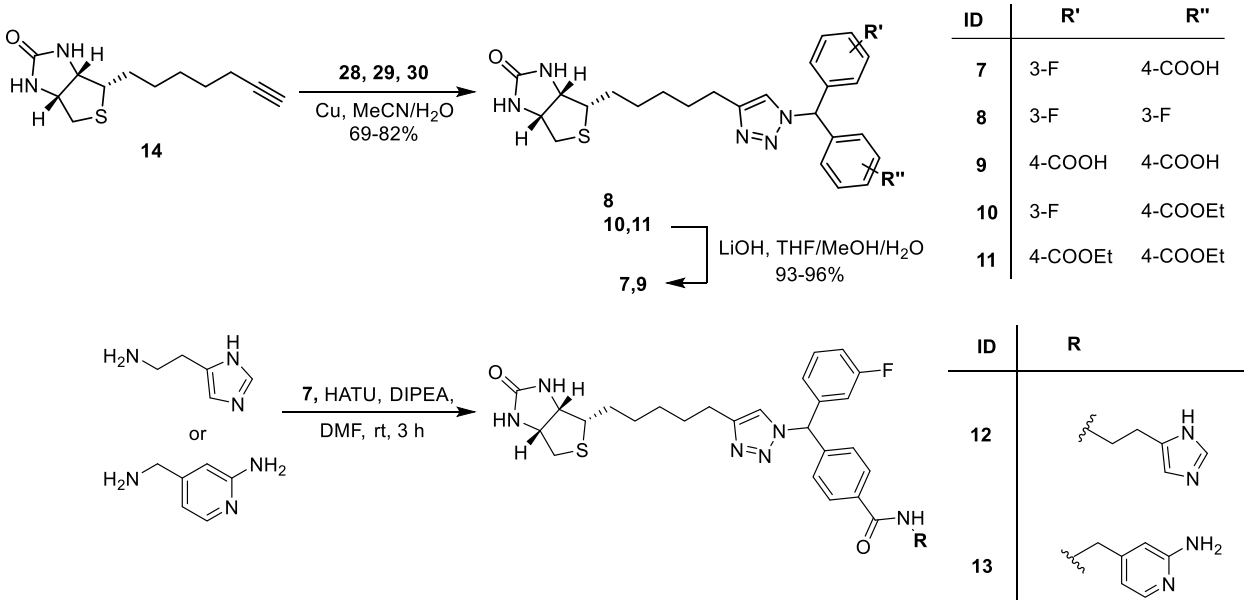

Scheme 2: Synthesis of analogues **7-13**

2.3.3: Biochemical and Antimicrobial Assay of Triazoles 7-13:

Triazoles **7**-**13** were assayed against *Sa*BPL using our published *in vitro* biotinylation assay,[11] with the results shown in Table 1. Importantly, compounds containing the additional aryl ring, as in N^1-diphenylmethyl-triazoles (**7**-**13**), were generally more potent than the previously reported mono-benzyl triazoles (c.f. **7**, **8**, **10**-**13** with **4** and **5**),[11] with the additional aryl ring presumably interacting with adjacent binding pocket as discussed above. For example, the di-phenylmethyl carboxylic acid **7** was approx. 2-fold more potent than the corresponding mono-benzyl derivative **5** (K_i: 0.40 ± 0.03 and 0.67 ± 0.06 μM[11] respectively). Interestingly, triazole **8,** with its two fluoro aryl groups, was equipotent to the mono-benzyl derivative **4** (K_i: 0.27 ± 0.04 and 0.28 ± 0.05 μM[11] respectively). However, there were differences in the whole cell data of these two compounds as discussed below.

The ethyl esters **10** and **11** were significantly more potent than the free acid analogues **7** and **9** respectively, see Table 1. Interestingly, triazoles **10** and **11** were similarly potent (K_i: 0.18 ± 0.03 and 0.20 ± 0.03 μM, respectively) despite both compounds presenting different aryl groups into the adjacent binding site based on *in silico* docking, see SI Figure S4 and S5. All this is consistent with the *in silico* docking, where the carboxylic acids of **7** and **9** only bind to the ribose binding site of *Sa*BPL, whereas the esters of **10** and **11** extend deeper into the adenine pocket. This effect is apparent in both the mono and N^1-diphenylmethyl series. The addition of imidazole and aminopyridine substituents, as in N^1-diphenylmethyl triazoles **12** and **13**, significantly improves potency (K_i: 6.01 ± 1.01 and 8.43 ± 0.73 nM respectively). Our docking suggests that these substituents interact with the adenine binding site of *Sa*BPL, resulting in an approx. 40-fold improvement relative to **7** with its carboxy substituent. Importantly, these analogues are the first triazole-based *Sa*BPL inhibitors with activity comparable to the best *Sa*BPL inhibitor reported to date, i.e. sulfonamide **6**, K_i: 7.00 ± 0.30 nM[12]. 1,2,3-Triazoles have the advantage of being resistant to biological degradation,[25,26] relative to the sulfonamide-based inhibitors that readily hydrolyse in whole blood.[12] Moreover, triazoles **12** and **13** are synthetically simpler to prepare relative to the sulfonamide-based *Sa*BPL inhibitors,[12] further highlighting the importance of this new series. This substantially improved potency of **12** and **13**, relative to existing triazole-based inhibitors, is likely due to the imidazole and aminopyridine substituents forming hydrogen bonds between amino acid residues Asn212 and/or Ser128 of *Sa*BPL, as discussed above.

The whole cell activity of *Sa*BPL inhibitors **7-13** against a clinical isolate strain of *S. aureus* (ATCC 49775) was also determined,[10] with results summarized in Table 1. All triazoles **7-13** significantly inhibited growth of the clinical isolate (see SI, Figure S8) with only one other 1,2,3-triazole reported to inhibit clinical isolate growth.[11] The triazoles **8**, and **10-13** were notably effective in inhibiting bacterial growth, with the MIC (i.e., >90 % inhibited growth) values shown in Table 1. However, the carboxylic acid examples **7** and **9** were less active, inhibiting growth by only 75 % at a concentration of 64 µg/mL, see SI. Figure S8. The corresponding and less polar esters **10** and **11**, showed improved whole cell activity, see Table 1. The di-phenylmethyl triazoles **7**, **8**, and **9**, possessing different combinations of the aryl groups of the mono-benzyl triazoles **4** and **5**, all display enhanced whole cell activity. This clearly indicates that the second aryl ring of **7**, **8**, and **9** crucially enhances whole cell activity relative to **4** and **5** (where **4** inhibits growth by 40 % and **5** lacks activity[20]).

The most active *Sa*BPL inhibitors, triazoles **12** and **13**, exhibited potent whole cell activity against the clinical isolate (MIC: 1 and 8 µg/mL, respectively) that is comparable to the most active sulfonamide-based *Sa*BPL inhibitor.[12] This study establishes triazoles **12** and **13** as the first 1,2,3-triazole-based nanomolar inhibitors of *Sa*BPL which have the added advantage of showing substantial whole cell activity against a clinical isolate of *S. aureus*.

Table 1: Biochemical and anti-staphylococcal properties of inhibitors **7-13**

Compound	K_i *Sa*BPL (µM) [a]	MIC *S. aureus* ATCC 49775 (µg/mL)
7	0.40 ± 0.03	>64
8	0.27 ± 0.04	32
9	1.39 ± 0.14	>64
10	0.18 ± 0.03	32
11	0.20 ± 0.03	8
12	0.006 ± 0.001	1
13	0.008 ± 0.001	8

[a]Inhibition constants (K_i) for the competitive inhibitors were derived from the IC_{50} for triazoles **7-11** and the Morrison equation for **12** and **13**. See "Methods" for further detail

2.4: Conclusion

Here we demonstrate for the first time, that the addition of a second aryl ring to mono-benzyl triazole-based *Sa*BPL inhibitors **4** and **5**,[11] to give N^1-diphenylmethyl-1,2,3-triazoles **7**-**13**, significantly enhances both *Sa*BPL and whole cell activity against a clinical isolate of *S. aureus*, ATCC 49775. *In silico* docking of these triazoles, against *Sa*BPL, suggests that that the second aryl ring of each analogue binds into an unexplored, and unoccupied binding pocket adjacent to the adenosine binding site. Critically, triazoles **12** and **13**, with their added imidazole and aminopyridine groups, are the most potent triazole-based inhibitors of *Sa*BPL reported to date, with K_i values of 6.01 ± 1.01 and 8.43 ± 0.73 nM respectively. Importantly, both analogues also display excellent whole cell activity against the clinical isolate (MIC: 1 and 8 µg/mL respectively). Docking suggests that the imidazole and aminopyridine groups of these inhibitors form hydrogen bonds with amino acid residues Ser128 and Asn212 of *Sa*BPL, as per the adenine group of the natural intermediate biotinyl-5'AMP **1**. Studies to further explore these interactions will be reported in due course.

2.5: Methods

Expression and Purification of Recombinant Protein

Recombinant *Sa*BPL fused to an *N*-terminal hexa-histidine tag, separated by a tobacco etch virus proteolytic cleavage site, was expressed in *Escherichia coli* BL21 (DE3-RIPL). Cells were cultured in Luria broth supplemented with Ampicillin (200 µg/mL) at 37 ºC until an optical density of 0.7 was reached. Protein expression was then induced with IPTG (0.25 mM) for 16 h at 16 ºC. Cells were collected via centrifugation and the pellets were stored at -80 ºC. Cells were lysed using a M110L microfluidizer processor and lysate was clarified by centrifugation. The cell lysate was loaded onto a 5 mL ZetaSep Nickel NTA column (EMP Biotech, Berlin, Germany) preequilibrated with Buffer A (20 mM Tris pH 8.0, 500 mM NaCl, 10 mM imidazole, 2 mM ß-mercaptoethanol). The column was then washed with 6 CV of 10% Buffer B (20 mM Tris pH 8.0, 500 mM NaCl, 250 mM imidazole, 2 mM ß-mercaptoethanol) and protein was eluted with an imidazole gradient from 10 mM to 250 mM. Fractions containing *Sa*BPL were then pooled and concentrated in an Amicon Ultra-15 Centrifugal Filter Unit (10 kDa MWCO) before loading onto a HiPrep 26/60 Sephacryl S-300 High Resolution size exclusion column preequilibrated in Storage Buffer (50 mM Tris pH 8.0, 0.5 mM EDTA, 5% glycerol, 1 mM DTT). Fractions containing *Sa*BPL were pooled, and protein purity was analysed via SDS-PAGE. *Sa*BPL was concentrated to 1.7 mg/mL, flash frozen in liquid nitrogen and stored at -80 ºC. Recombinant GST-*Sa*PC90 (a GST tagged 90 amino acid fragment of *S. aureus* pyruvate

carboxylase) was expressed and purified in *E. coli* BL21 (DE3) following methods described previously.[27]

SaBPL Assay:

The inhibitory activities of triazoles **7 – 11** was determined by measuring BPL activity in the presence of the inhibitor at various concentrations (25.0, 5.0, 1.0, 0.2, 0.04 and 0.008 μM). A reaction mixture was prepared containing 50 mM Tris HCl, pH 8.0, 3 mM ATP, 5 μM biotin, 5.5 mM $MgCl_2$, 100 mM KCl, 0.1 μM DTT, and 25 μM *Sa*PC90 fused to GST. Triazoles **7 – 11** were dissolved in DMSO and diluted into this reaction buffer to give a final concentration of 4% DMSO. The BPL reaction was initiated by the addition of *Sa*BPL at 37℃ (final [*Sa*BPL] = 6.25 nM). The reaction was terminated after 20 min by addition of 180 μL of stop buffer at 37℃, and three 50 μL aliquots were added to each well of a white Lumitrac-600 96-well plate (Greiner) that had been precoated with a polyclonal anti-GST antibody (Sigma-Aldrich, 50 μL per well, 1:40 000 dilution) at 4 °C overnight, followed by blocking for 2 h (200 μL per well) with 1% BSA in TBS at 37 °C and incubated at 37 °C for 1 h. The plate was then washed 5 times (200 μL per well) with TBS containing 0.1% Tween-20. Europium labelled streptavidin (PerkinElmer) was diluted to 0.1 μg/mL in TBS containing 0.1% Tween-20. The streptavidin probe (50 μL per well) was incubated for 30 min at 37 °C followed by washing 5 times with TBS containing 0.1% Tween-20 followed. Enhancement solution (PerkinElmer, 50 μL) was added to each well and incubated for 10 min before reading the plate using a PerkinElmer Victor X5 multilabel reader (time-resolved fluorescence settings, 340 nm excitation, and 612 nm emission).[28] The IC_{50} value of each compound was obtained from a dose–response curve, fitted in GraphPad prism version 9 using a nonlinear fit of "log(inhibitor) vs normalized response)", where the hillslope was constrained to -1 (see Figure S9 for normalized representative semi-log plots). The absolute inhibition constants (K_i) for triazoles **7 – 11** were determined using equation 1:[29]

$$K_i = \frac{IC_{50}}{1+\frac{[S]}{K_M}} \qquad \textbf{(Equation 1)}$$

where [*S*] is the concentration of biotin (5 μM) and K_M is the affinity of the enzyme for biotin (1 μM[20]).

The separate K_i values obtained for triazoles **7 – 11** were averaged, and the standard error means calculated. The K_i values for triazoles **12** and **13** were calculated using the Morrison equation,[30]

since equation 1 gave values approaching [*Sa*BPL] for these compounds. This data was fitted using equation 2 in GraphPad prism version 9:

$$Y = \frac{V_o(1-(((E_t+\mathrm{X}+(K_i(1+(\mathrm{S}/K_M))))-(((E_t+\mathrm{X}+(K_i(1+(\mathrm{S}/K_M))))^2)-4E_t\mathrm{X})^{0.5}))}{2E_t} \qquad \textbf{(Equation 2)}$$

where Y is the enzymatic activity, X is the concentration of inhibitor (in μM), [*S*] is the concentration of biotin (5 μM), E_t is the *Sa*BPL concentration (6.25 nM), K_M is the affinity of *Sa*BPL for biotin (1 μM[20]) and K_i is the absolute inhibition constant. Errors were calculated as per triazoles **7 – 11**.

Antibacterial Activity Evaluation:

Antibacterial activity was determined by a microdilution broth method as recommended by the CLSI (Clinical and Laboratory Standards Institute, Document M07-A8, 2009, Wayne, PA) using cation adjusted Mueller-Hinton broth (Trek Diagnostics Systems, U.K.). Compounds were dissolved in DMSO. Serial 2-fold dilutions of each compound were made using DMSO as the diluent. Trays were inoculated with 5 × 104 CFU of each strain in a volume of 100 μL (final concentration of DMSO was 3.2% (v/v)) and incubated at 35 °C for 16−20 h. Growth of the bacterium was quantified by measuring the absorbance at 620 nm.

Docking Studies:

Docking experiments were performed using ICM software version 3.8−7c (Molsoft L.L.C., San Diego, CA, USA). Proteins for docking were retrieved from RCSB protein data bank 6APW,[11] 3V8L.[19] Then, formal charges were assigned; protonation states of histidines were adjusted, and hydrogens, histidine, glutamine, and asparagine were optimized using the protein preparation procedure implemented in ICM.[31] The original bound ligand and all water molecules were removed from the binding site before docking. The binding site was defined as the cavity delimited by residues with at least one nonhydrogen atom within a 4.0 Å cutoff radius from the ligand **4** or **1.** The pocket was represented by 0.5 Å grid maps accounting for hydrogen bonding, hydrophobic, van der Waals, and electrostatic interactions. The molecules were flexibly docked into the rigid binding site and scored based on the ICM scoring function.

2.6: Acknowledgments

The authors thank Prof. Grant W. Booker (The University of Adelaide) for useful discussions.

2.7: References for Chapter Two

(1) Talebi Bezmin Abadi, A.; Rizvanov, A. A.; Haertlé, T.; Blatt, N. L. World Health Organization Report: Current Crisis of Antibiotic Resistance. *Bionanoscience* **2019**, *9* (4), 778–788. https://doi.org/10.1007/s12668-019-00658-4.

(2) de Kraker, M. E. A.; Stewardson, A. J.; Harbarth, S. Will 10 Million People Die a Year Due to Antimicrobial Resistance by 2050? *PLoS Med.* **2016**, *13* (11), e1002184. https://doi.org/10.1371/journal.pmed.1002184.

(3) Dadgostar, P. Antimicrobial Resistance: Implications and Costs. *Infect. Drug Resist.* **2019**, *12*, 3903–3910. https://doi.org/10.2147/IDR.S234610.

(4) Turner, N. A.; Sharma-Kuinkel, B. K.; Maskarinec, S. A.; Eichenberger, E. M.; Shah, P. P.; Carugati, M.; Holland, T. L.; Fowler, V. G. Methicillin-Resistant Staphylococcus Aureus: An Overview of Basic and Clinical Research. *Nat. Rev. Microbiol.* **2019**, *17* (4), 203–218. https://doi.org/10.1038/s41579-018-0147-4.

(5) Carretto, E.; Visiello, R.; Nardini, P. Methicillin Resistance in Staphylococcus Aureus. *Pet-to-Man Travel. Staphylococci A World Prog.* **2018**, *85* (Pt 1), 225–235. https://doi.org/10.1016/B978-0-12-813547-1.00017-0.

(6) Tak, V.; Mathur, P.; Lalwani, S.; Misra, M. C. Staphylococcal Blood Stream Infections: Epidemiology, Resistance Pattern and Outcome at a Level 1 Indian Trauma Care Center. *J. Lab. Physicians* **2013**, *5* (01), 46–50. https://doi.org/10.4103/0974-2727.115939.

(7) Lee, B. Y.; Singh, A.; David, M. Z.; Bartsch, S. M.; Slayton, R. B.; Huang, S. S.; Zimmer, S. M.; Potter, M. A.; Macal, C. M.; Lauderdale, D. S.; Miller, L. G.; Daum, R. S. The Economic Burden of Community-Associated Methicillin-Resistant Staphylococcus Aureus (CA-MRSA). *Clin. Microbiol. Infect.* **2013**, *19* (6), 528–536. https://doi.org/10.1111/j.1469-0691.2012.03914.x.

(8) Zhen, X.; Lundborg, C. S.; Zhang, M.; Sun, X.; Li, Y.; Hu, X.; Gu, S.; Gu, Y.; Wei, J.; Dong, H. Clinical and Economic Impact of Methicillin-Resistant Staphylococcus Aureus: A Multicentre Study in China. *Sci. Rep.* **2020**, *10* (1), 1–8. https://doi.org/10.1038/s41598-020-60825-6.

(9) Hübner, C.; Hübner, N. O.; Hopert, K.; Maletzki, S.; Flessa, S. Analysis of MRSA-Attributed Costs of Hospitalized Patients in Germany. *Eur. J. Clin. Microbiol. Infect. Dis.* **2014**, *33* (10), 1817–1822. https://doi.org/10.1007/s10096-014-2131-x.

(10) Soares Da Costa, T. P.; Tieu, W.; Yap, M. Y.; Zvarec, O.; Bell, J. M.; Turnidge, J. D.; Wallace, J. C.; Booker, G. W.; Wilce, M. C. J.; Abell, A. D.; Polyak, S. W. Biotin Analogues with Antibacterial Activity Are Potent Inhibitors of Biotin Protein Ligase. *ACS Med. Chem. Lett.* **2012**, *3* (6), 509–514. https://doi.org/10.1021/ml300106p.

(11) Paparella, A. S.; Lee, K. J.; Hayes, A. J.; Feng, J.; Feng, Z.; Cini, D.; Deshmukh, S.; Booker, G. W.; Wilce, M. C. J.; Polyak, S. W.; Abell, A. D. Halogenation of Biotin Protein Ligase Inhibitors Improves Whole Cell Activity against Staphylococcus Aureus. *ACS Infect. Dis.* **2018**, *4* (2), 175–184. https://doi.org/10.1021/acsinfecdis.7b00134.

(12) Lee, K. J.; Tieu, W.; Blanco-Rodriguez, B.; Paparella, A. S.; Yu, J.; Hayes, A.; Feng, J.; Marshall, A. C.; Noll, B.; Milne, R.; Cini, D.; Wilce, M. C. J.; Booker, G. W.; Bruning, J. B.; Polyak, S. W.; Abell, A. D. Sulfonamide-Based Inhibitors of Biotin Protein Ligase as New Antibiotic Leads. *ACS Chem. Biol.* **2019**, *14* (9), 1990–1997. https://doi.org/10.1021/acschembio.9b00463.

(13) Feng, J.; Paparella, A. S.; Booker, G. W.; Polyak, S. W.; Abell, A. D. Biotin Protein Ligase Is a Target for New Antibacterials. *Antibiotics* **2016**, *5* (3). https://doi.org/10.3390/antibiotics5030026.

(14) Satiaputra, J.; Shearwin, K. E.; Booker, G. W.; Polyak, S. W. Mechanisms of Biotin-Regulated Gene Expression in Microbes. *Synth. Syst. Biotechnol.* **2016**, *1* (1), 17–24. https://doi.org/10.1016/j.synbio.2016.01.005.

(15) Henke, S. K.; Cronan, J. E. Successful Conversion of the Bacillus Subtilis BirA Group II Biotin Protein Ligase into a Group I Ligase. *PLoS One* **2014**, *9* (5), e96757.

(16) McMahon, R. J. Biotin in Metabolism and Molecular Biology. *Annu. Rev. Nutr.* **2002**, *22*, 221–239. https://doi.org/10.1146/annurev.nutr.22.121101.112819.

(17) Polyak, S. W.; Abell, A. D.; Wilce, M. C. J.; Zhang, L.; Booker, G. W. Structure, Function and Selective Inhibition of Bacterial Acetyl-Coa Carboxylase. *Appl. Microbiol. Biotechnol.* **2012**, *93* (3), 983–992. https://doi.org/10.1007/s00253-011-3796-z.

(18) Pendini, N. R.; Yap, M. Y.; Polyak, S. W.; Cowieson, N. P.; Abell, A.; Booker, G. W.; Wallace, J. C.; Wilce, J. A.; Wilce, M. C. J. Structural Characterization of Staphylococcus Aureus Biotin Protein Ligase and Interaction Partners: An Antibiotic Target. *Protein Sci.* **2013**, *22* (6), 762–773. https://doi.org/10.1002/pro.2262.

(19) Soares Da Costa, T. P.; Tieu, W.; Yap, M. Y.; Pendini, N. R.; Polyak, S. W.; Pedersen, D. S.; Morona, R.; Turnidge, J. D.; Wallace, J. C.; Wilce, M. C. J.; Booker, G. W.; Abell, A. D. Selective Inhibition of Biotin Protein Ligase from Staphylococcus Aureus. *J. Biol. Chem.* **2012**, *287* (21), 17823–17832. https://doi.org/10.1074/jbc.M112.356576.

(20) Feng, J.; Paparella, A. S.; Tieu, W.; Heim, D.; Clark, S.; Hayes, A.; Booker, G. W.; Polyak, S. W.; Abell, A. D. New Series of BPL Inhibitors To Probe the Ribose-Binding Pocket of Staphylococcus Aureus Biotin Protein Ligase. *ACS Med. Chem. Lett.* **2016**, *7* (12), 1068–1072. https://doi.org/10.1021/acsmedchemlett.6b00248.

(21) Tieu, W.; Jarrad, A. M.; Paparella, A. S.; Keeling, K. A.; Soares Da Costa, T. P.; Wallace, J. C.; Booker, G. W.; Polyak, S. W.; Abell, A. D. Heterocyclic Acyl-Phosphate Bioisostere-Based Inhibitors of Staphylococcus Aureus Biotin Protein Ligase. *Bioorganic Med. Chem. Lett.* **2014**, *24* (19), 4689–4693. https://doi.org/10.1016/j.bmcl.2014.08.030.

(22) Duckworth, B. P.; Geders, T. W.; Tiwari, D.; Boshoff, H. I.; Sibbald, P. A.; Barry, C. E.; Schnappinger, D.; Finzel, B. C.; Aldrich, C. C. Bisubstrate Adenylation Inhibitors of Biotin Protein Ligase from Mycobacterium Tuberculosis. *Chem. Biol.* **2011**, *18* (11), 1432–1441. https://doi.org/10.1016/j.chembiol.2011.08.013.

(23) P. Duckworth, B.; M. Nelson, K.; C. Aldrich, C. Adenylating Enzymes in Mycobacterium Tuberculosis as Drug Targets. *Curr. Top. Med. Chem.* **2012**, *12* (7), 766–796. https://doi.org/10.2174/156802612799984571.

(24) Hayes, A. J.; Satiaputra, J.; Sternicki, L. M.; Paparella, A. S.; Feng, Z.; Lee, K. J.; Blanco-Rodriguez, B.; Tieu, W.; Eijkelkamp, B. A.; Shearwin, K. E.; Pukala, T. L.; Abell, A. D.; Booker, G. W.; Polyak, S. W. Advanced Resistance Studies Identify Two Discrete Mechanisms in Staphylococcus Aureus to Overcome Antibacterial Compounds That Target Biotin Protein Ligase. *Antibiotics* **2020**, *9* (4). https://doi.org/10.3390/antibiotics9040165.

(25) Staśkiewicz, A.; Ledwoń, P.; Rovero, P.; Papini, A. M.; Latajka, R. Triazole-Modified Peptidomimetics: An Opportunity for Drug Discovery and Development. *Front. Chem.* **2021**, *9* (May), 1–16. https://doi.org/10.3389/fchem.2021.674705.

(26) Pretzel, D.; Sandmann, B.; Hartlieb, M.; Vitz, J.; Hölzer, S.; Fritz, N.; Moszner, N.; Schubert, U. S. Biological Evaluation of 1,2,3-Triazole-Based Polymers for Potential Applications as Hard Tissue Material. *J. Polym. Sci. Part A Polym. Chem.* **2015**, *53* (16), 1843–1847. https://doi.org/10.1002/pola.27676.

(27) Sternicki, L. M.; Nguyen, S.; Pacholarz, K. J.; Barran, P.; Pendini, N. R.; Booker, G. W.; Huet, Y.; Baltz, R.; Wegener, K. L.; Pukala, T. L.; Polyak, S. W. Biochemical Characterisation of Class III Biotin Protein Ligases from Botrytis Cinerea and Zymoseptoria Tritici. *Arch. Biochem. Biophys.* **2020**, *691* (June), 108509. https://doi.org/10.1016/j.abb.2020.108509.

(28) Ng, B.; Polyak, S. W.; Bird, D.; Bailey, L.; Wallace, J. C.; Booker, G. W. Escherichia Coli Biotin Protein Ligase: Characterization and Development of a High-Throughput Assay. *Anal. Biochem.* **2008**, *376* (1), 131–136. https://doi.org/10.1016/j.ab.2008.01.026.

(29) Yung-Chi, C.; Prusoff, W. H. Relationship between the Inhibition Constant (KI) and the Concentration of Inhibitor Which Causes 50 per Cent Inhibition (I50) of an Enzymatic Reaction. *Biochem. Pharmacol.* **1973**, *22* (23), 3099–3108. https://doi.org/10.1016/0006-2952(73)90196-2.

(30) Tonge, P. J. Quantifying the Interactions between Biomolecules: Guidelines for Assay Design and Data Analysis. *ACS Infect. Dis.* **2019**, *5* (6), 796–808. https://doi.org/10.1021/acsinfecdis.9b00012.

(31) Neves, M. A. C.; Totrov, M.; Abagyan, R. Docking and Scoring with ICM: The Benchmarking Results and Strategies for Improvement. *J. Comput. Aided. Mol. Des.* **2012**, *26* (6), 675–686. https://doi.org/10.1007/s10822-012-9547-0.

SUPPORTING INFORMATION

S2.1: Figures S1 – S9

(A)

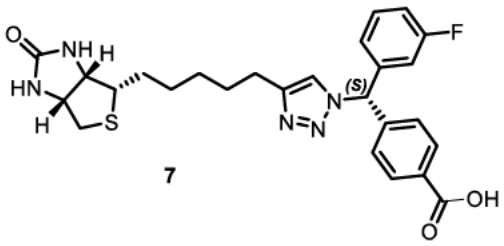

7

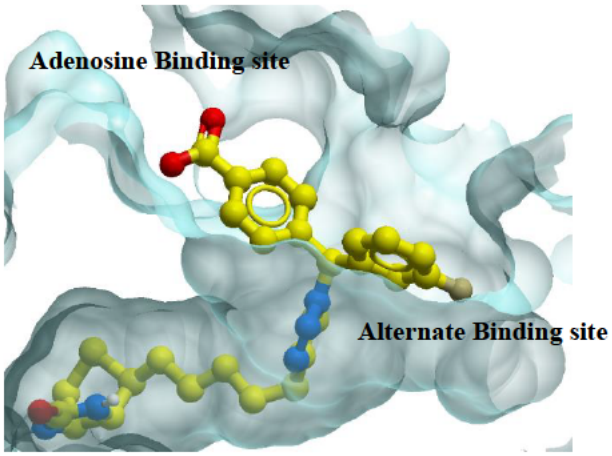

(B)

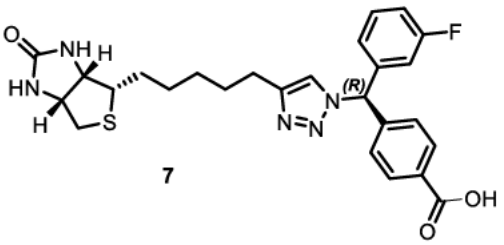

7

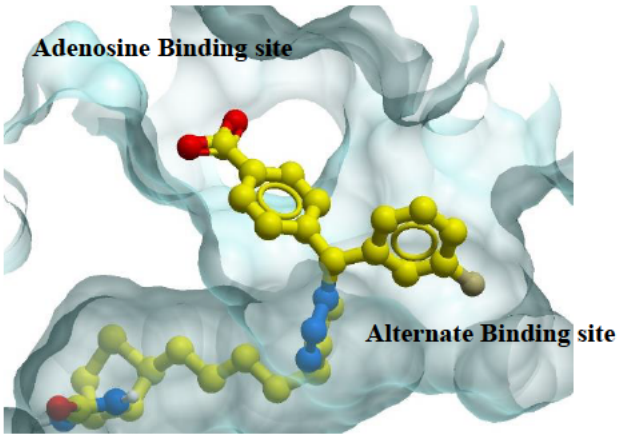

Figure S1: (**A**) Predicted binding conformation of the *S* diastereomer **7** in the active site of *Sa*BPL. (**B**) Predicted binding conformation of the *R* diastereomer **7** in the active site of *Sa*BPL.

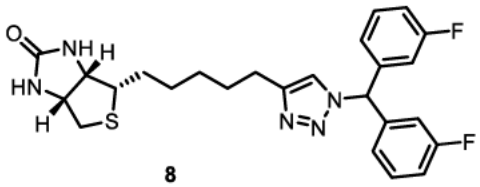

8

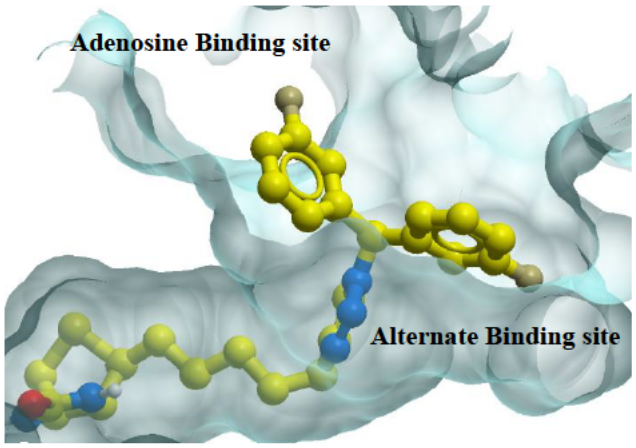

Figure S2: Predicted binding conformation of **8** in the active site of *Sa*BPL.

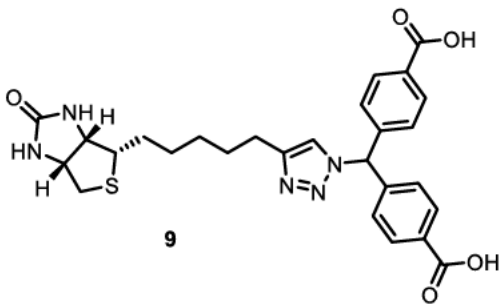

9

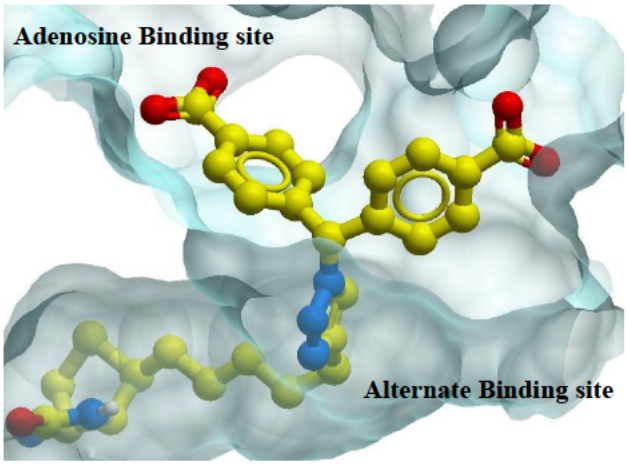

Figure S3: Predicted binding conformation of **9** in the active site of *Sa*BPL.

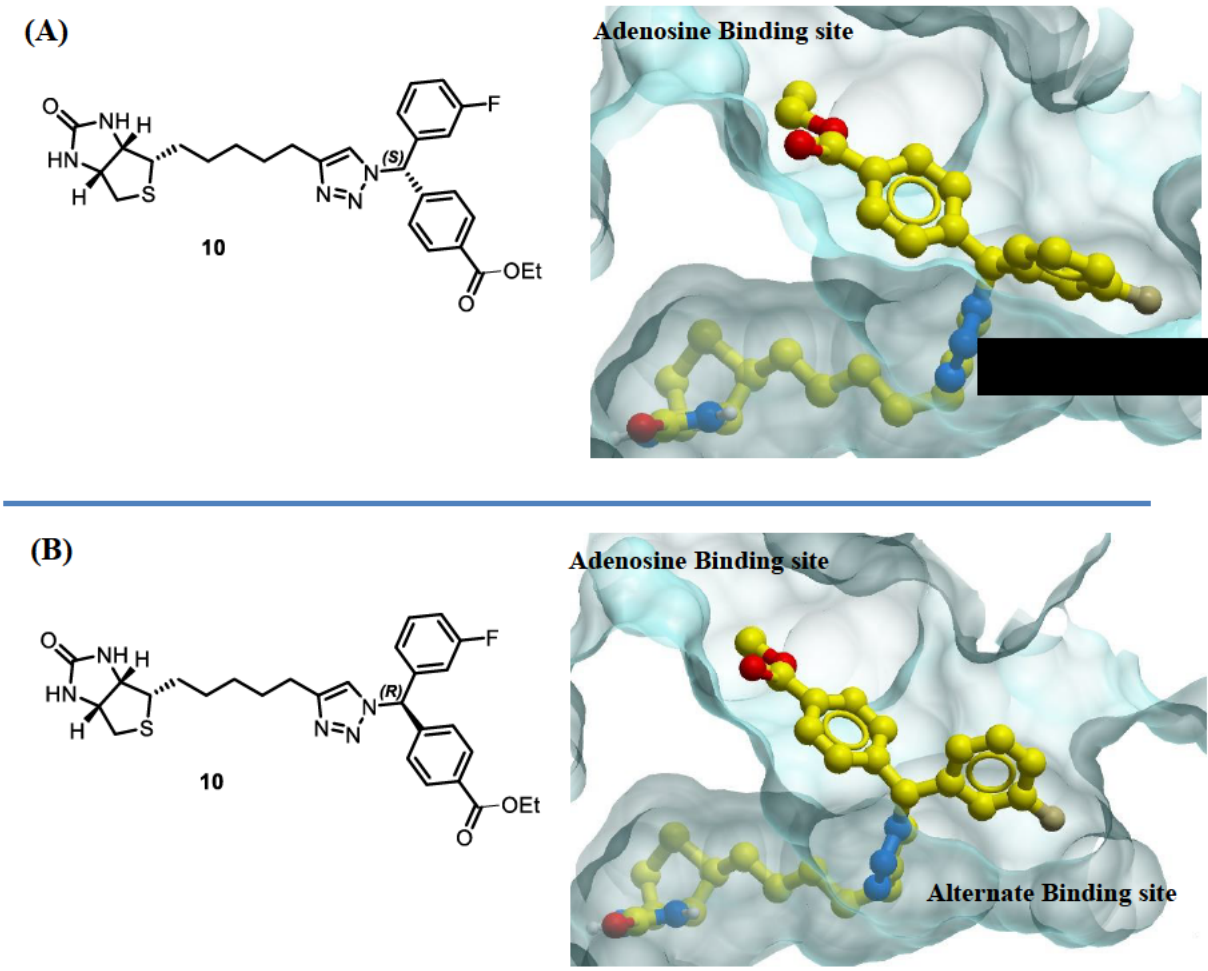

Figure S4: (**A**) Predicted binding conformation of the *S* diastereomer **10** in the active site of *Sa*BPL. (**B**) Predicted binding conformation of the *R* diastereomer **10** in the active site of *Sa*BPL.

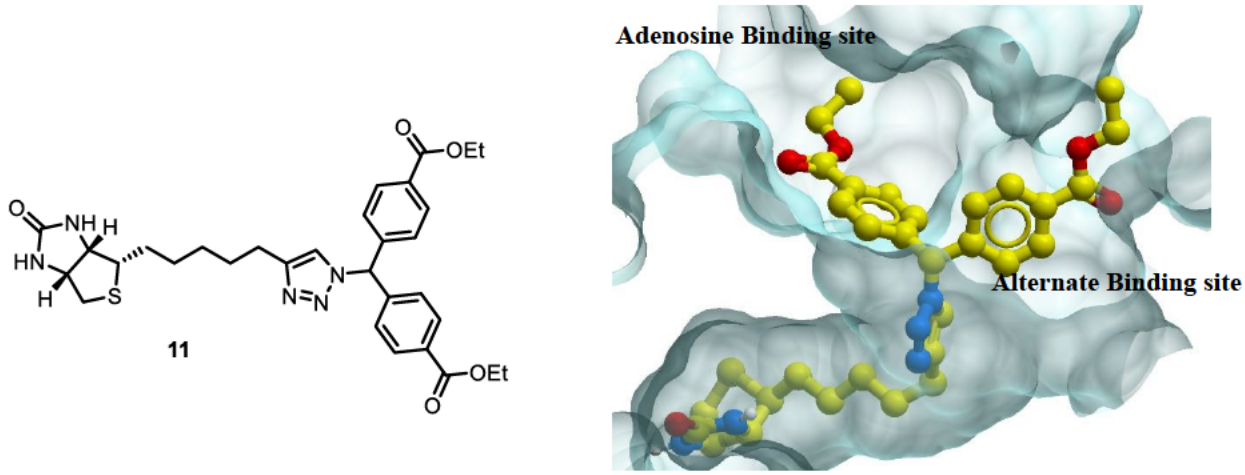

Figure S5: Predicted binding conformation of **11** in the active site of *Sa*BPL.

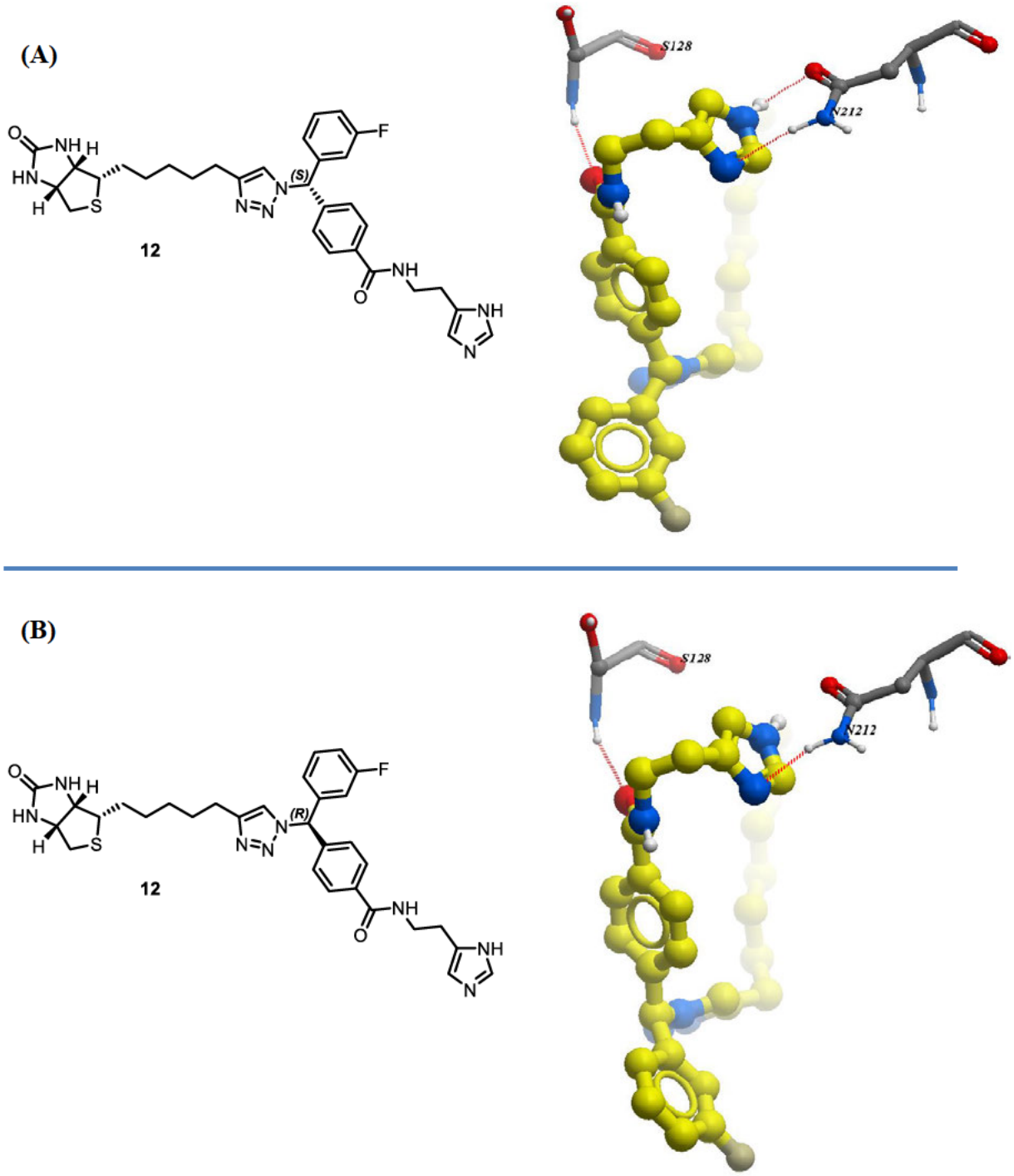

Figure S6: (**A**) Predicted binding conformation of the *S* diastereomer **12** within the active site of *Sa*BPL. Residues Ser128 and Asn212 are predicted to form hydrogen bonds to the imidazole functional handle, as indicated by the dotted redlines. (**B**) Predicted binding conformation of the *R* diastereomer **12** within the active site of *Sa*BPL. Residues Ser128 and Asn212 are predicted to form hydrogen bonds to the imidazole functional handle, as indicated by the dotted redlines.

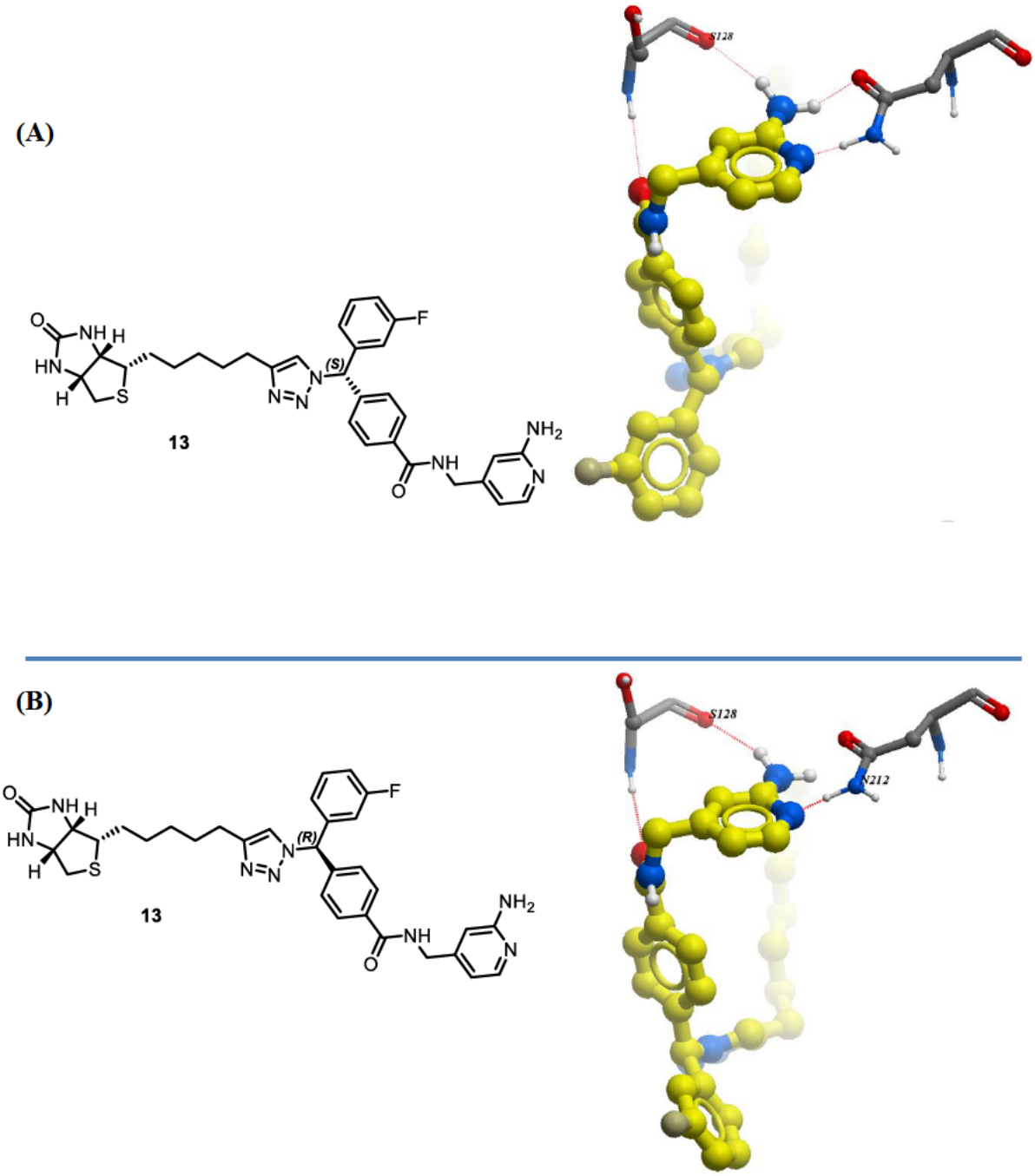

Figure S7: (**A**) Predicted binding conformation of the *S* diastereomer **13** within the active site of *Sa*BPL. Residues Ser128 and Asn212 are predicted to form hydrogen bonds to the aminopyridine functional handle, as indicated by the dotted redlines. (**B**) Predicted binding conformation of the *R* diastereomer **13** within the active site of *Sa*BPL. Residues Ser128 and Asn212 are predicted to form hydrogen bonds to the aminopyridine functional handle, as indicated by the dotted redlines.

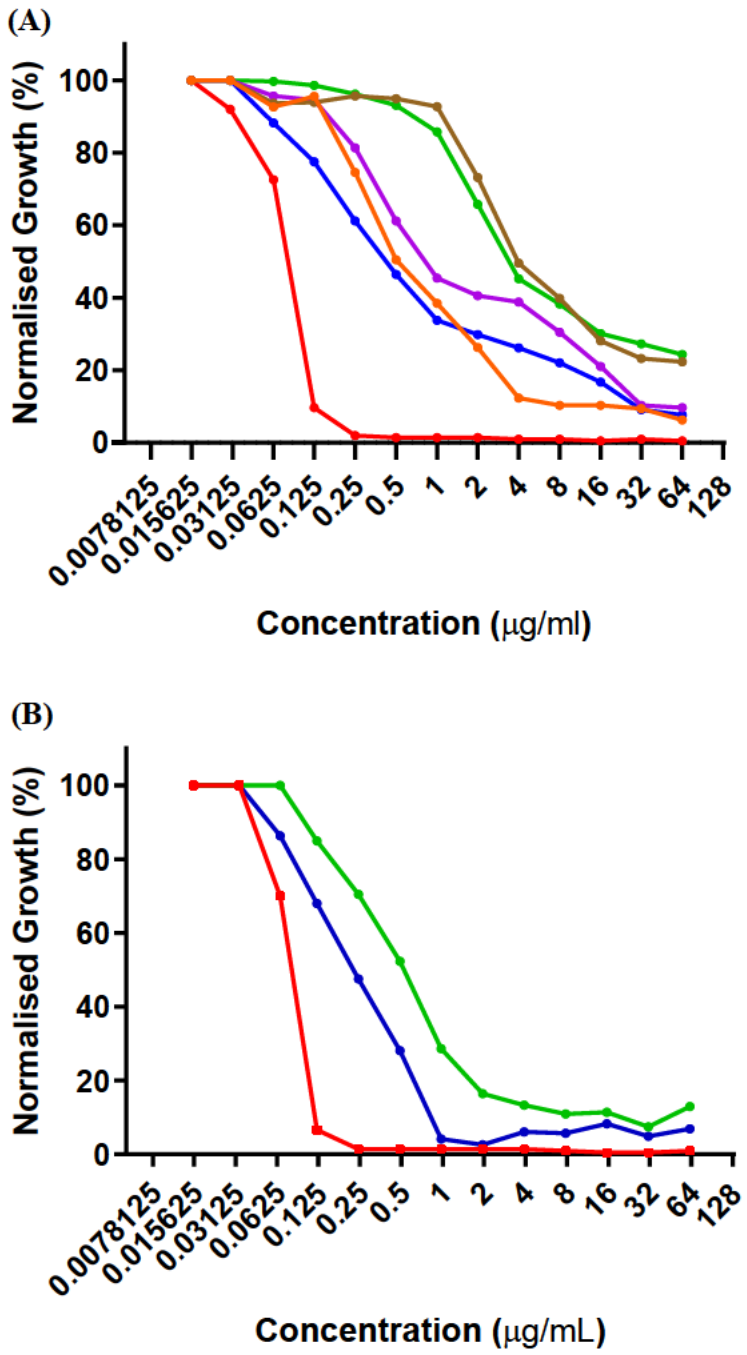

Figure S8: Inhibition growth of *S.aureus* growth *in vitro*. (**A**) Compounds **7** (green), **8** (blue), **9** (brown), **10** (purple), **11** (orange) and erythromycin (red) were tested against *S.aureus* ATCC 49775. (**B**) Compounds **12** (blue), **13** (green) and erythromycin (red) were tested against *S.aureus* ATCC 49775.

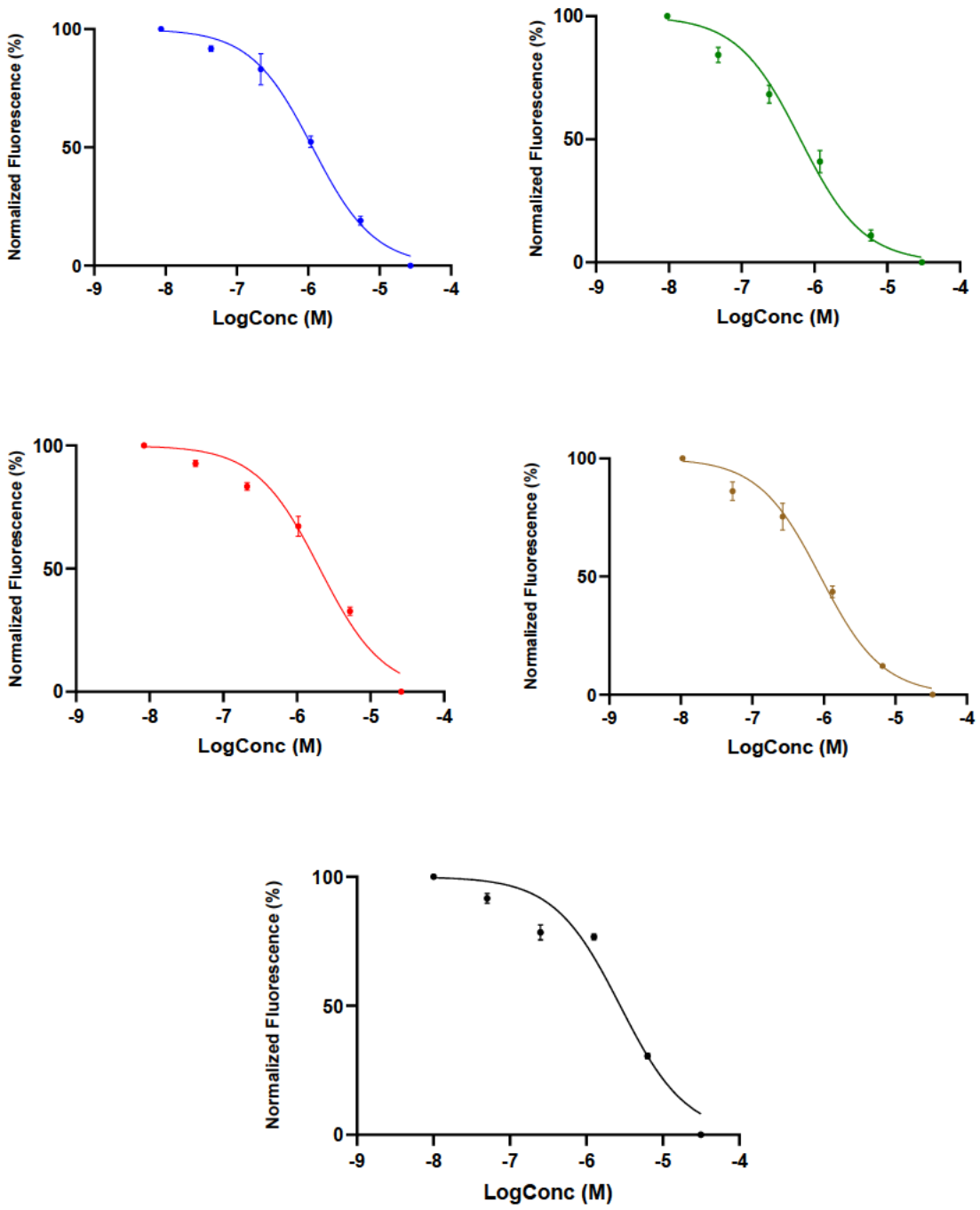

Figure S9: Normalized representative dose-response semi-log plots for triazoles **7** (black), **8** (brown), **9** (red), **10** (green), and **11** (blue) assayed against *Sa*BPL.

S2.2: Experimental Section

Chemistry: general Materials and Methods

All reagents were obtained from commercial sources and are of reagent grade or as specified. Solvents were also obtained from commercial sources, except for anhydrous THF and anhydrous DMF that were dried over solvent purifier (PS-Micro, Innovative Technology, USA). Reactions were monitored by TLC using precoated plates (silica gel 60 F254, 250 μm, Merck, Darmstadt, Germany), spots were visualised under ultraviolet light at 254 nm and with either sulfuric acid-vanillin spray, potassium permanganate dip or Hanessian's stain. Column chromatography was performed with silica gel (40-63 μm 60 Å, Davisil, Grace, Germany). ^{1}H and ^{13}C spectra were recorded on a Varian Inova 500 MHz or a Varian Inova 600 MHz. Chemical shifts are given in ppm (δ) relative to the residue signals, which in the case of DMSO-d_6 were 2.50 ppm for ^{1}H and 39.55 ppm for ^{13}C, and $CDCl_3$ were 7.26 ppm for ^{1}H and 77.23 ppm for ^{13}C. High-resolution mass spectra (HRMS) were recorded on an Agilent 6230 time of flight (TOF) liquid chromatography mass spectra (LC/MS) ($\Delta < 5$ ppm).

General procedure 2A: *Reduction of ketone to alcohol*: $NaBH_4$ (2 eq) was added portion-wise to a solution of the corresponding benzophenone (1 eq) in anhydrous ethanol (5 mL per 200 mg of benzophenone) with cooling in an ice bath. The resultant reaction mixture was then stirred with cooling in an ice bath for 2 h before being quenched with water. The reaction mixture was then concentrated *in vacuo*, with the resultant aqueous residue being extracted with EtOAc. The organic extract was dried over Na_2SO_4, filtered, and concentrated *in vacuo* to give a solid/oil that was used in subsequent steps without further purification. See individual experiments for details.

General procedure 2B: *Chlorination of alcohol*: $SOCl_2$ (1.2 eq) was added dropwise to a solution of the corresponding alcohol (1 eq) in DCM (6 mL per 1.00 g of alcohol) over 10 min. The reaction mixture was stirred at rt for 48 h, concentrated *in vacuo*. The resultant oil was purified by flash chromatography on silica gel eluting with a mixture of DCM and MeOH (v/v = 10:1). See individual experiments for details.

General procedure C: *Azidation of chlorides*: To a solution of the corresponding chloride (1 eq) in DMF (1 mL per 120 mg alkyl chloride) was added NaN_3 (1.3 eq). The resulting reaction mixture was stirred at rt for 48 h, poured onto water (15 mL per 1 mL of DMF) and extracted with diethyl ether. The organic extracts were combined and washed with water and brine. The

organic layer was dried over Na_2SO_4, filtered, and concentrated *in vacuo* to give a solid/oil that was used in subsequent steps without further purification. See individual experiments for details.

General procedure 2D: *CuACC*: To a solution of biotin acetylene **14**[1] (1 eq) and corresponding azide (1 eq) in MeCN and water (v/v = 2:1) (2 mL per 50mg of alkyne) was added copper nano-powder (0.2 eq). The reaction mixture was sonicated for 45 min, then stirred at room temperature for 24 h. The suspension was filtered through celite and, the resulting filtrate was concentrated *in vacuo*. The resultant residue was purified by flash chromatography on silica gel eluting with a mixture of DCM and MeOH (v/v = 20:1). See individual experiments for details.

General procedure 2E: *Ester hydrolysis*: LiOH (2.2 eq) was added to a solution of the ester **10** or **11** (1 eq) in a mixture of THF, MeOH, and water (v/v/v = 3:1:1) (1 mL per 20 mg of ester). The reaction mixture was stirred for 24 h at rt then, acidified to pH = 3 with 1 M aqueous HCl. The solution was diluted with EtOAc (10 mL per 1 mL of reaction mixture) and washed with 0.5 M aqueous HCl, water and brine. The organic layer was dried over Na_2SO_4, filtered, and concentrated *in vacuo* to give a solid that was used in subsequent steps without further purification. See individual experiments for details.

General procedure 2H: *Amide linkage formation*: Amine (1 eq) was added to a solution of carboxylic acid **7** (1 eq), HATU (1.1 eq), and DIPEA (4 eq) in DMF (1 mL per 20 mg of carboxylic acid), and the resultant reaction mixture was stirred for 16 h. The reaction mixture was diluted with conc. NH_4Cl (10 mL per 1 mL DMF), extracted with EtOAc, washed with water, brine, dried over Na_2SO_4, filtered, and concentrated *in vacuo*. See individual experiments for details

4-((*S*/*R*)-(3-Fluorophenyl)(4-(5-((3a*S*,4*S*,6a*R*)-2-oxohexahydro-1Hthieno[3,4*d*] imidazol-4yl)pentyl)- 1*H*-1,2,3-triazol-1-yl)methyl)benzoic acid (**7**)

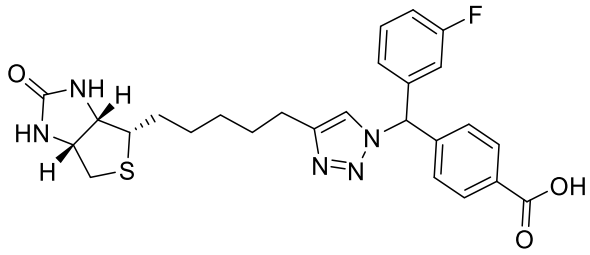

Compound **10** (0.100 g, 0.19 mmol) was hydrolysed according to **general procedure 2E**, to give **7** as a fine white solid (0.090 g, 96 %); **^{1}H NMR** (500 MHz, DMSO-d_6): δ 7.96 (d, *J* = 8.3 Hz, 2H), 7.92 (s, 1H), 7.49-7.43 (m, 1H), 7.36 (s, 1H), 7.30 (d, *J* = 8.3 Hz, 1H), 7.22 (td, *J* = 8.4, 2.0 Hz, 1H), 7.09 (d, *J* = 8.0 Hz, 1H), 7.05 (d, *J* = 9.9 Hz, 1H), 6.40 (s, 1H), 6.33 (s, 1H), 4.31 – 4.27 (m, 1H), 4.13 – 4.09 (m, 1H), 3.10 – 3.05 (m, 1H), 2.80 (dd, *J* = 12.4, 5.1 Hz, 1H), 2.62 (t, *J* = 7.7 Hz, 2H), 2.57 (d, *J* = 12.4 Hz, 1H), 1.65-1.55 (m, 2H), 1.50 – 1.29 (m, 6H); **^{13}C NMR** (126 MHz, DMSO-d_6): δ 166.79, 163.06, 162.66, 161.18, 147.15, 130.92, 130.85, 129.71, 128.05, 124.27, 122.17, 115.35, 115.18, 115.08, 114.90, 101.98, 79.20, 78.93, 78.67, 66.98, 65.40, 61.04, 59.16, 55.48, 39.78, 28.58, 28.26, 28.17, 25.09, 24.93; **HRMS** calcd. for (M + H$^+$) $C_{26}H_{29}FN_5O_3S^+$: requires 510.1970, found 510.1973.

(3a*S*,4*S*,6a*R*)4(5(1(Bis(3fluorophenyl)methyl)1H1,2,3triazol4yl)pentyl)tetrahydro 1H-thieno[3,4-*d*]imidazol-2(3H)-one (**8**)

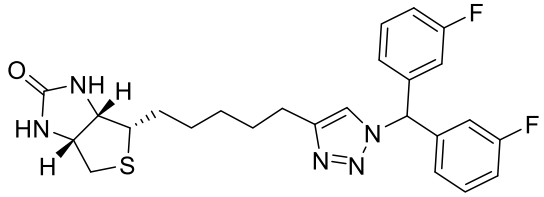

Di-phenylmethyl azide **28** (0.051 g, 0.25 mmol) was reacted according to **general procedure 2D**, to give **8** as a white solid (0.055 g, 54 %); **^{1}H NMR** (500 MHz, $CDCl_3$): δ 7.35 (td, *J* = 8.0, 6.1 Hz, 2H), 7.17 (s, 1H), 7.06 (td, *J* = 8.3, 2.3 Hz, 2H), 7.01 (s, 1H), 6.91 (d, *J* = 8.0 Hz, 2H), 6.81 (d, *J* = 9.2 Hz, 2H), 5.58 (s, 1H), 5.21 (s, 1H), 4.51 – 4.45 (m, 1H), 4.30 – 4.25 (m, 1H), 3.17 – 3.09 (m, 1H), 2.88 (dd, *J* = 12.8, 5.0 Hz, 1H), 2.74 – 2.66 (m, 3H), 1.73 – 1.59 (m, 4H), 1.48 – 1.34 (m, 4H); **^{13}C NMR** (126 MHz, $CDCl_3$): δ 164.10, 163.46, 162.13, 148.51, 140.33, 140.28, 130.86, 130.79, 123.94, 123.92, 123.90, 120.77, 116.06, 115.89, 115.47, 115.46, 115.29, 115.28, 66.95, 62.16, 60.23, 55.77, 40.68, 29.25, 29.11, 28.83, 28.68, 25.77; **HRMS** calcd. for (M + H$^+$) $C_{25}H_{28}F_2N_5OS^+$: requires 484.1977, found 484.1975.

4,4'-((4-(5-((3a*S*,4*S*,6a*R*)-2-Oxohexahydro-1H-thieno[3,4-*d*]imidazol-4-yl)pentyl)-1H-1,2,3-triazol-1-yl)methylene)dibenzoic acid (**9**)

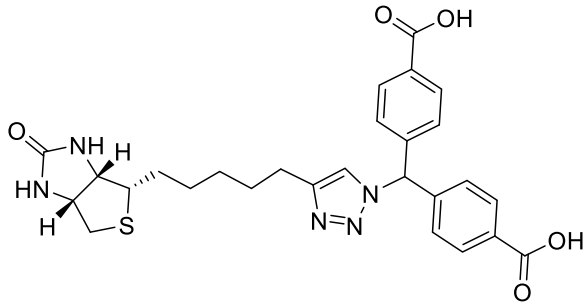

Compound **11** (0.030 g, 0.053 mmol) was hydrolysed according to **general procedure 2E**, to give **9** as a white solid (0.026 g, 93 %); **^{1}H NMR** (500 MHz, DMSO-d_6): δ 7.96 (d, *J* = 8.3 Hz, 4H), 7.92 (s, 1H), 7.43 (s, 1H), 7.32 (d, *J* = 8.3 Hz, 4H), 6.40 (s, 1H), 6.33 (s, 1H), 4.31 – 4.26 (m, 1H), 4.13 – 4.09 (m, 1H), 3.10 – 3.05 (m, 1H), 2.80 (dd, *J* = 12.4, 5.1 Hz, 1H), 2.62 (t, *J* = 7.6 Hz, 2H), 2.57 (d, *J* = 12.4 Hz, 1H), 1.62 – 1.29 (m, 8H); **^{13}C NMR** (126 MHz, DMSO-d_6): δ 166.77, 162.65, 147.14, 143.01, 130.66, 129.73, 128.24, 122.24, 65.64, 61.04, 59.16, 55.48, 39.78, 28.61, 28.58, 28.27, 28.16, 24.94; **HRMS** calcd. for (M + H$^+$) $C_{27}H_{30}N_5O_5S^+$: requires 536.1962, found 536.1961.

Ethyl-4-((S/R)-(3-fluorophenyl)(4-(5-((3aS,4S,6aR)-2-oxohexahydro-1H-thieno[3,4-d]imidazol-4-yl)pentyl)-1H-1,2,3-triazol-1-yl)methyl)benzoate (**10**)

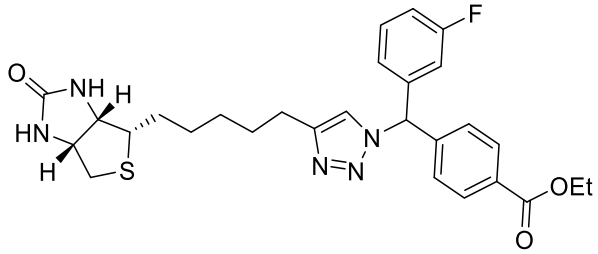

Di-phenylmethyl azide **29** (0.150 g, 0.50 mmol) was reacted according to **general procedure 2D**, to give **10** as a white solid (0.153 g, 69 %); **^{1}H NMR** (500 MHz, $CDCl_3$): δ 8.05 (d, *J* = 8.3 Hz, 2H), 7.39 – 7.33 (m, 1H), 7.19 (d, *J* = 8.3 Hz, 2H), 7.11 – 7.03 (m, 1H), 6.92 – 6.90(m, 1H), 6.80 – 6.78 (m, 1H), 5.23 (s, 1H), 4.93 (s, 1H), 4.51 – 4.48 (m, 1H), 4.38 (q, *J* = 7.1 Hz, 2H), 4.30 – 4.28 (m, 1H), 3.15 – 3.12 (m, 1H), 2.90 (dd, *J* = 12.8, 5.0 Hz, 1H), 2.72 – 2.69 (m, 3H), 1.71 – 1.65 (m, 4H), 1.47 – 1.40 (m, 4H), 1.39 (t, *J* = 7.1 Hz, 3H); **^{13}C NMR** (126 MHz, $CDCl_3$) δ 166.01, 163.93, 163.13, 162.28, 148.52, 142.48, 140.23, 140.19, 131.07, 130.90, 130.89, 130.84, 130.37, 128.14, 124.03, 124.01, 120.80, 116.11, 115.97, 115.53, 115.38, 67.17, 67.16, 62.10, 61.41, 60.18, 55.68, 40.68, 29.22, 29.13, 28.83, 28.66, 25.74, 14.45; **HRMS** calcd. for (M + H$^+$) $C_{28}H_{33}FN_5O_3S^+$: requires 538.2283, found 538.2282.

Diethyl 4,4'-((4-(5-((3a*S*,4*S*,6a*R*)-2-oxohexahydro-1H-thieno[3,4-*d*]imidazol-4-yl)pentyl)-1H-1,2,3-triazol-1-yl)methylene)dibenzoate (**11**)

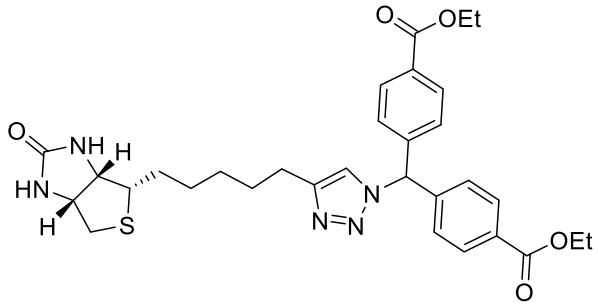

Di-phenylmethyl azide **30** (0.101 g, 0.25 mmol) was reacted according to **general procedure 2D**, to give **11** as a white solid (0.088 g, 82 %); **^{1}H NMR** (500 MHz, $CDCl_3$): δ 8.05 (d, *J* = 8.3 Hz, 4H), 7.18 (d, *J* = 8.2 Hz, 4H), 7.14 (s, 1H), 7.13 (s, 1H), 4.81 (s, 1H), 4.64 (s, 1H), 4.52 – 4.49 (m, 1H), 4.38 (q, *J* = 7.1 Hz, 4H), 4.32 – 4.28 (m, 1H), 3.17 – 3.12 (m, 1H), 2.91 (dd, *J* = 12.8, 5.1 Hz, 1H), 2.75 – 2.68 (m, 3H), 1.71 – 1.61 (m, 4H), 1.49 – 1.42 (m, 4H), 1.39 (t, *J* = 7.1 Hz, 6H); **^{13}C NMR** (126 MHz, $CDCl_3$) δ 166.00, 162.79, 148.52, 142.47, 131.18, 131.17, 130.40, 128.26, 128.25, 120.81, 67.48, 62.09, 61.41, 60.21, 55.56, 40.66, 29.20, 29.16, 28.82, 28.71, 25.74, 14.45; **HRMS** calcd. for (M + H^+) $C_{31}H_{38}N_5O_5S^+$: requires 592.2588, found 592.2590

N-(2-(1*H*-imidazol-5-yl)ethyl)-4-((3-fluorophenyl)(4-(5-((3a*S*,4*S*,6a*R*)-2-oxohexahydro-1*H*-thieno[3,4-*d*]imidazol-4-yl)pentyl)-1*H*-1,2,3-triazol-1-yl)methyl)benzamide (**12**)

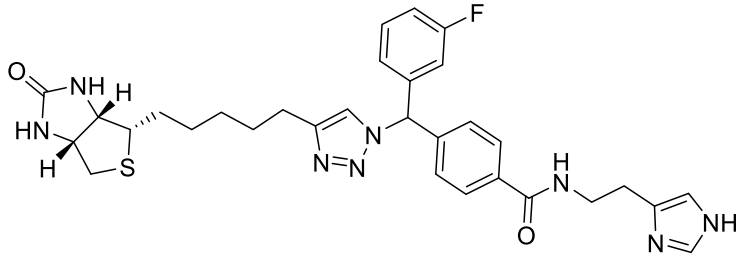

Histidine dihydrochloride (0.007 g, 0.038 mmol) was reacted according to **general procedure 2H**, and was purified by flash chromatography on silica gel eluting with DCM/MeOH (v/v = 6:1) to give **12** as white solid (0.014 g, 61 %); **^{1}H NMR** (600 MHz, DMSO-d_6) δ 11.81 (s, 1H), 8.56 (t, *J* = 5.5 Hz, 1H), 7.92 (s, 1H), 7.83 (d, *J* = 8.4 Hz, 2H), 7.52 (s, 1H), 7.48 – 7.44 (m, 1H), 7.33 (s, 1H), 7.25 (d, *J* = 8.4 Hz, 2H), 7.22 (td, *J* = 8.6, 2.5 Hz, 1H), 7.07 – 7.06 (m, 1H), 7.04 – 7.01 (m, 1H), 6.81 (s, 1H), 6.42 (s, 1H), 6.35 (s, 1H), 4.30 – 4.28 (m, 1H), 4.12 – 4.10 (m, 1H), 3.48 – 3.45 (m, 2H), 3.10 – 3.06 (m, 1H), 2.80 (dd, *J* = 12.5, 5.1 Hz, 1H), 2.74 (t, *J* = 6.5 Hz, 2H), 2.61 (t, *J* = 7.6 Hz, 2H), 2.56 (d, *J* = 12.5 Hz, 1H), 1.63 – 1.56 (m, 3H), 1.48 – 1.42 (m, 1H), 1.39 – 1.29 (m, 4H); **^{13}C NMR** (151 MHz, DMSO- d_6) δ 165.56, 162.94, 162.73,

161.31, 147.18, 141.30, 141.25, 141.22, 134.68, 134.59, 130.94, 130.88, 127.87, 127.60, 124.26, 124.24, 122.17, 115.31, 115.17, 115.02, 114.87, 65.45, 61.07, 59.19, 55.54, 39.94, 39.80, 39.66, 39.52, 39.38, 39.24, 39.10, 28.66, 28.61, 28.31, 28.20, 24.96; **HRMS** calcd. for ($M + H^+$) $C_{31}H_{35}FN_8O_2S^+$: requires 602.2588, found 602.2592.

N-((2-aminopyridin-4-yl)methyl)-4-((3-fluorophenyl)(4-(5-((3aS,4S,6aR)-2-oxohexahydro-1H-thieno[3,4-d]imidazol-4-yl)pentyl)-1H-1,2,3-triazol-1-yl)methyl)benzamide (**13**)

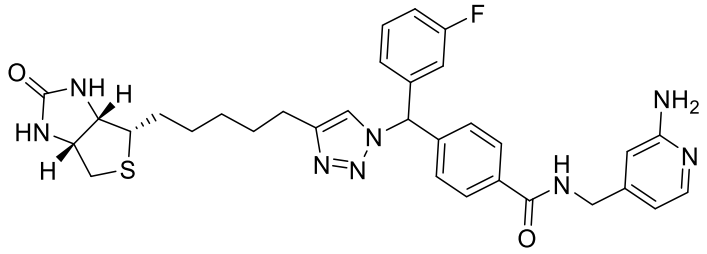

4-(aminomethyl)pyridine-2-amine hydrochloride (0.005 g, 0.041 mmol) was reacted according to **general procedure 2H** and was purified by flash chromatography on silica gel eluting with DCM/MeOH (v/v = 9:1) to give **13** as white solid (0.010 g, 41 %); **^{1}H NMR** (600 MHz, DMSO-d_6) δ 9.04 (t, *J* = 6.1 Hz, 1H), 7.96 – 7.90 (m, 3H), 7.80 (d, *J* = 5.2 Hz, 1H), 7.47 (td, *J* = 8.0, 6.1 Hz, 1H), 7.35 (s, 1H), 7.32 (d, *J* = 8.4 Hz, 2H), 7.22 (td, *J* = 8.4, 2.3 Hz, 1H), 7.10 – 7.07 (m, 1H), 7.05 – 7.02 (m, 1H), 6.43 – 6.41 (m, 1H), 6.40 (dd, *J* = 5.3, 1.5 Hz, 1H), 6.35 (d, *J* = 1.5 Hz, 1H), 6.32 (s, 1H), 5.83 (s, 2H), 4.32 (d, *J* = 6.0 Hz, 2H), 4.30 – 4.25 (m, 1H), 4.14 – 4.08 (m, 1H), 3.12 – 3.05 (m, 1H), 2.80 (dd, *J* = 12.5, 5.1 Hz, 1H), 2.62 (t, *J* = 7.6 Hz, 2H), 2.57 (d, *J* = 12.4 Hz, 1H), 1.63 – 1.57 (m, 3H), 1.47 – 1.42 (m, 1H), 1.36 – 1.27 (m, 4H); **^{13}C NMR** (151 MHz, dmso) δ 165.72, 162.95, 162.73, 161.32, 159.96, 149.10, 147.61, 147.20, 141.54, 141.27, 141.22, 134.07, 130.97, 130.91, 127.98, 127.78, 124.26, 124.24, 122.20, 115.34, 115.20, 115.02, 114.87, 110.64, 105.39, 65.45, 61.07, 59.19, 55.54, 41.76, 39.94, 39.80, 39.66, 39.52, 39.38, 39.24, 39.10, 28.68, 28.62, 28.32, 28.21, 24.96; **HRMS** calcd. for ($M + H^+$) $C_{32}H_{35}FN_8O_2S^+$: requires 614.2588, found 614.2595.

(3-Fluorophenyl)-(*p*-tolyl)-methanone (**16**)

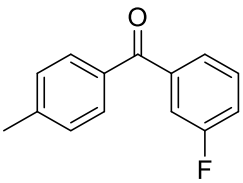

A solution of $AlCl_3$ (2.13 g, 16.0 mmol) in CH_3NO_2 (15 mL) was cooled to 20 ^{O}C. 3-Fluorobenzoyl chloride **15** (2.11 g, 13.3 mmol) was added drop-wise over 5 min to the solution, and the resultant solution was stirred for 30 min. Toluene (4.1 mL, 38.6 mmol) was added drop-wise to solution over 1 min, and the resultant reaction mixture was stirred for 2 h at rt. The reaction mixture was then poured over ice-cold 10% aqueous HCl (40 mL) and extracted with $CHCl_3$ (3 x 15 mL). The organic extracts were combined, washed with water (2 x 10 mL), and concentrated *in vacuo* to give a crude residue. The crude residue was dissolved in $CHCl_3$ (10 mL), washed with 15% aqueous NaOH (5 x 2.5 mL), water (2 x 5 mL), dried over Na_2SO_4, filtered, concentrated *in vacuo*, and recrystallised from hexane to give **16** as white/yellow crystals (2.10 g, 74 %); **^{1}H NMR** (500 MHz, $CDCl_3$): δ 7.72 (d, J = 8.1 Hz, 2H), 7.55 (d, J = 7.6 Hz, 1H), 7.50-7.43 (m, 2H), 7.31-7.25 (m, 3H), 2.45 (s, 3H); **^{13}C NMR** (126 MHz, $CDCl_3$): δ 195.14, 163.61, 161.63, 143.82, 140.25, 140.19, 134.52, 130.40, 130.06, 130.00, 129.26, 125.81, 125.78, 119.35, 119.19, 116.90, 116.72, 21.83.

4-(3-Fluorobenzoyl) benzoic acid (**17**)

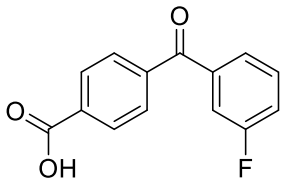

$KMnO_4$ (2.66 g, 16.8 mmol) was added to a rapidly stirring solution of **16** (2.10 g, 9.8 mmol) in *t*-BuOH / water (16 mL/5 mL) and refluxed for 2.5 h. Additional $KMnO_4$ (1.33 g, 8.4 mmol), and *t*-BuOH/ water (2.5 mL/ 2.5 mL) was added to the reaction mixture, and the reaction mixture was refluxed for a further 3 h, cooled to rt, filtered through celite, and concentrated *in vacuo*. The resultant residue was dissolved in a mixture of 15% aqueous NaOH (45 mL) and 1M aqueous NH_4OH (100 mL) and washed with diethyl ether (4 x 25 mL). The aqueous layer was acidified with 32% aqueous HCl with resultant precipitate collected by vacuum filtration to give **17** as a white/ yellow solid (1.29 g, 55 %); **^{1}H NMR** (500 MHz, $CDCl_3$): δ 8.23 (d, J = 8.4 Hz, 2H), 7.87 (d, J = 8.4 Hz, 2H), 7.58 (d, J = 7.7 Hz, 1H), 7.54 – 7.47 (m, 2H), 7.33 (td, J = 8.2, 1.8 Hz, 1H); **^{13}C NMR** (126 MHz, $CDCl_3$): δ 193.03, 163.75, 162.85, 141.54, 137.55, 137.50, 132.57, 130.40, 130.36, 130.34, 129.94, 126.24, 126.07, 126.05, 120.33, 120.16, 117.01, 116.83.

Ethyl 4-(3-fluorobenzoyl) benzoate (**18**)

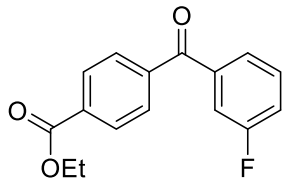

$SOCl_2$ (2.29 g, 19.3 mmol) was added dropwise to a solution of **17** (1.29 g, 5.3 mmol) in anhydrous ethanol (50 mL). The reaction mixture was stirred 24 h, concentrated *in vacuo* and purified by flash chromatography on silica gel using a mixture of hexane and EtOAc (v/v = 20:1). The resultant acetal (0.903 g, 2.60 mmol) was dissolved in a mixture of water and MeCN (v/v = 2:1) (9 mL), followed by addition of CBr_4 (0.172 g, 0.52 mmol). The resultant reaction mixture was heated at 80 ^oC for 6 h, cooled to rt, poured into saturated bicarbonate solution (30 mL), and extracted with diethyl ether (3 x 20 mL). The organic extracts were combined, washed with brine (30 mL), dried over Na_2SO_4, filtered and concentrated in vacuo to give **18** as a yellow solid (0.682 g, 66 %); **^{1}H NMR** (500 MHz, $CDCl_3$): δ 8.17 (d, J = 8.1 Hz, 2H), 7.84 (d, J = 8.1 Hz, 2H), 7.57 (d, J = 7.7 Hz, 1H), 7.53 – 7.46 (m, 2H), 7.32 (td, J = 8.1, 2.5 Hz, 1H), 4.43 (q, J = 7.1 Hz, 2H), 1.43 (t, J = 7.2 Hz, 3H); **^{13}C NMR** (126 MHz, $CDCl_3$): δ 194.82, 165.87, 163.51, 161.87, 140.70, 139.16, 139.12, 134.04, 130.33, 130.28, 129.86, 129.72, 126.06, 126.04, 120.20, 120.06, 116.99, 116.84, 61.67, 14.46.

Diethyl 4,4'-carbonyldibenzoate (**20**)

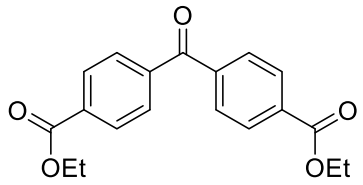

p-TsOH (1.40 g, 8.16 mmol) was added to a suspension di-carboxy acid **19** (0.480 g, 1.77 mmol) in EtOH (50 mL). The reaction mixture was refluxed for 16 h, cooled to rt, and concentrated *in vacuo*. The resultant residue was triturated with EtOAc, concentrated in vacuo, and purified by silica gel chromatography eluting with a mixture of hexane and EtOAc (v/v = 9:1) to give **20** as a white solid (0.402 g, 67 %); **^{1}H NMR** (500 MHz, $CDCl_3$): δ 8.17 (d, J = 8.1 Hz, 4H), 7.84 (d, J = 8.1 Hz, 4H), 4.43 (q, J = 7.1 Hz, 4H), 1.43 (t, J = 7.1 Hz, 6H); **^{13}C NMR** (126 MHz, $CDCl_3$): δ 195.55, 165.86, 140.67, 134.23, 129.96, 129.76, 61.67, 14.46.

Bis(3-fluorophenyl) methanol (**22**)

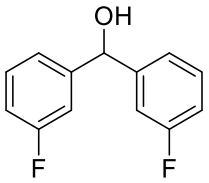

Benzophenone **21** (1.09 g, 5.01 mmol) was reacted according to **general procedure 2A**, to give **22** as a colourless oil (1.09 g, 99 %); **^{1}H NMR** (500 MHz, $CDCl_3$): δ 7.32 (td, J = 7.9, 5.9 Hz, 2H), 7.18-7.08 (m, 4H), 6.98 (td, J = 2.1 Hz, 2H), 5.83 (d, J = 3.4Hz, 1H), 2.30 (d, J = 3.4 Hz, 1H); **^{13}C NMR** (126 MHz, $CDCl_3$): δ 163.13, 161.85 145.93, 145.03, 130.30, 122.23, 114.89, 113.60, 75.26.

Ethyl 4-((3-fluorophenyl) (hydroxy)methyl) benzoate (**23**)

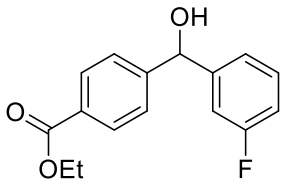

Benzophenone **18** (0.954 g, 3.5 mmol) was reacted according to **general procedure 2A**, to give **23** as a colourless oil (0.931 g, 99 %); **^{1}H NMR** (500 MHz, $CDCl_3$): δ 8.02 (d, J = 8.4 Hz, 1H), 7.45 (d, J = 8.2 Hz, 1H), 7.30 (td, J = 8.0, 5.9 Hz, 1H), 7.13 (d, J = 7.7 Hz, 1H), 7.11 – 7.08 (m, J = 9.7, 2.2 Hz, 1H), 6.99 – 6.94 (m, J = 8.4, 2.6, 1.3 Hz, 1H), 5.88 (d, J = 3.5 Hz, 1H), 4.37 (q, J = 7.1 Hz, 1H), 2.32 (d, J = 3.5 Hz, 1H), 1.38 (t, J = 7.1 Hz, 2H); **^{13}C NMR** (126 MHz, $CDCl_3$): δ 166.43, 164.12, 162.16, 148.08, 145.92, 145.87, 130.37, 130.30, 130.17, 130.06, 126.47, 122.30, 122.28, 115.01, 114.85, 113.74, 113.57, 75.51, 75.49, 61.15, 14.47.

Diethyl 4,4'-(hydroxymethylene)dibenzoate (**24**)

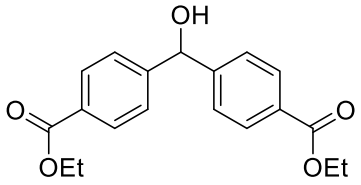

Benzophenone **20** (0.550 g, 1.71 mmol) was reacted according to **general procedure 2A**, to give **24** as a white solid (0.553 g, 99 %); **^{1}H NMR** (500 MHz, $CDCl_3$): δ 8.02 (d, J = 8.2 Hz, 4H), 7.45 (d, J = 8.2 Hz, 4H), 5.93 (d, J = 3.4 Hz, 1H), 4.37 (q, J = 7.1 Hz, 4H), 2.36 (d, J = 3.4 Hz, 1H), 1.38 (t, J = 7.1 Hz, 6H); **^{13}C NMR** (126 MHz, $CDCl_3$): δ 166.40, 148.04, 130.21, 130.09, 126.54, 75.75, 61.16, 14.47.

3,3'-(Chloromethylene)bis(fluorobenzene) (**25**)

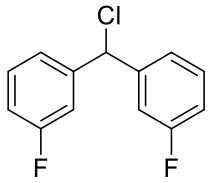

Compound **22** (1.09 g, 4.95 mmol) was reacted according to **general procedure 2B**, to give **25** as a colourless oil (0.736 g, 62 %); **^{1}H NMR** (500 MHz, $CDCl_3$): δ 7.32 (td, J = 8.0 Hz, 5.9 Hz, 2H), 7.20- 7.09 (m, 4H), 7.05-6.96 (m, 2H), 6.05 (s, 1H); **^{13}C NMR** (126 MHz, CDCl3): δ 163.96, 161.87, 143.12, 143.03, 130.36, 123.49, 115.48, 115.03, 62.52

Ethyl 4-(chloro(3-fluorophenyl)methyl)benzoate (**26**)

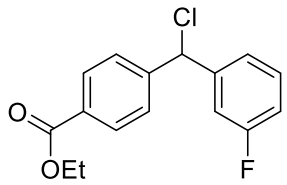

Compound **23** (0.931 g, 3.39 mmol) was reacted according to **general procedure 2B**, to give **26** as a colourless oil (0.885 g, 89 %); **^{1}H NMR** (500 MHz, $CDCl_3$): δ 8.04 (d, J = 8.3 Hz, 2H), 7.48 (d, J = 8.3 Hz, 2H), 7.34 – 7.29 (m, 1H), 7.15 (d, J = 7.8 Hz, 1H), 7.13 – 7.10 (m, 1H), 7.01 (td, J = 8.4, 2.5 Hz, 1H), 6.11 (s, 1H), 4.38 (q, J = 7.1 Hz, 2H), 1.39 (t, J = 7.1 Hz, 3H); **^{13}C NMR** (126 MHz, $CDCl_3$): δ 166.13, 163.92, 161.95, 145.18, 143.05, 142.99, 130.65, 130.41, 130.35, 130.09, 127.83, 123.54, 123.51, 115.58, 115.41, 115.16, 114.97, 62.73, 61.28, 14.47.

Diethyl 4,4'-(chloromethylene)dibenzoate (**27**)

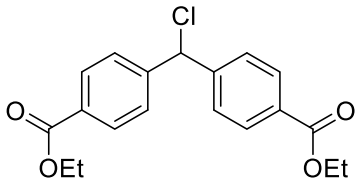

Compound **24** (0.553 g, 1.68 mmol) was reacted according to **general procedure 2B**, to give **27** as a white solid (0.504 g, 86 %); **^{1}H NMR** (500 MHz, $CDCl_3$): δ 8.03 (d, J = 8.4 Hz, 4H), 7.46 (d, J = 8.4 Hz, 4H), 6.16 (s, 1H), 4.38 (q, J = 7.1 Hz, 4H), 1.39 (t, J = 7.1 Hz, 6H); **^{13}C NMR** (126 MHz, $CDCl_3$): δ 166.12, 145.14, 130.66, 130.11, 127.86, 62.96, 61.29, 14.47.

3,3'-(Azidomethylene)bis(fluorobenzene) (**28**)

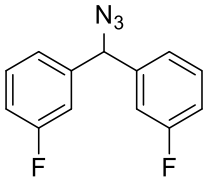

Compound **25** (0.736 g, 3.08 mmol) was reacted according to **general procedure 2C**, to give **28** as a clear yellow oil (0.673 g, 89 %); **^{1}H NMR** (500 MHz, $CDCl_3$): δ 7.37 – 7.32 (m, 2H), 7.09 (d, J = 7.8 Hz, 2H), 7.04 – 7.00 (m, 4H), 5.68 (s, 1H); **^{13}C NMR** (126 MHz, $CDCl_3$): δ 164.10, 162.13, 141.69, 141.64, 130.60, 130.53, 123.15, 123.13, 115.57, 115.40, 114.62, 114.44, 67.44.

Ethyl 4-(azido(3-fluorophenyl)methyl)benzoate (**29**)

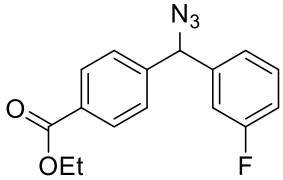

Compound **26** (0.885 g, 3.02 mmol) was reacted according to **general procedure 2C**, to give **29** as a clear yellow oil (0.820 g, 91 %); **^{1}H NMR** (500 MHz, $CDCl_3$): δ 8.05 (d, J = 8.1 Hz, 2H), 7.38 (d, J = 8.1 Hz, 1H), 7.36 – 7.31 (m, 1H), 7.09 – 7.06 (m, 1H), 7.04 – 6.99 (m, 1H), 5.74 (s, 1H), 4.38 (q, J = 7.1 Hz, 2H), 1.39 (t, J = 7.1 Hz, 3H); **^{13}C NMR** (126 MHz, $CDCl_3$): δ

166.19, 164.10, 162.13, 143.86, 141.58, 130.68, 130.63, 130.57, 130.26, 127.40, 123.21, 123.18, 115.60, 115.44, 114.67, 114.49, 67.69, 67.68, 61.27, 14.47.

Diethyl 4,4'-(azidomethylene)dibenzoate (**30**)

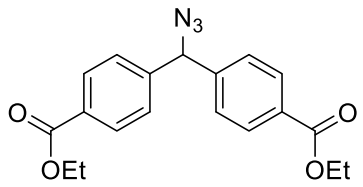

Compound **27** (0.504 g, 1.45 mmol) was reacted according to **general procedure 2C**, to give **30** as an orange solid (0.468 g, 91 %); **^{1}H NMR** (500 MHz, $CDCl_3$): δ 8.05 (d, J = 8.3 Hz, 4H), 7.39 (d, J = 8.3 Hz, 4H), 5.81 (s, 1H), 4.39 (q, J = 7.1 Hz, 4H), 1.40 (t, J = 7.1 Hz, 6H). **^{13}C NMR** (126 MHz, $CDCl_3$): δ 166.32, 145.24, 130.56, 130.01, 127.46, 69.96, 61.39, 14.47.

S2.3: ^{1}H and ^{13}C NMR of Triazoles 7 – 13

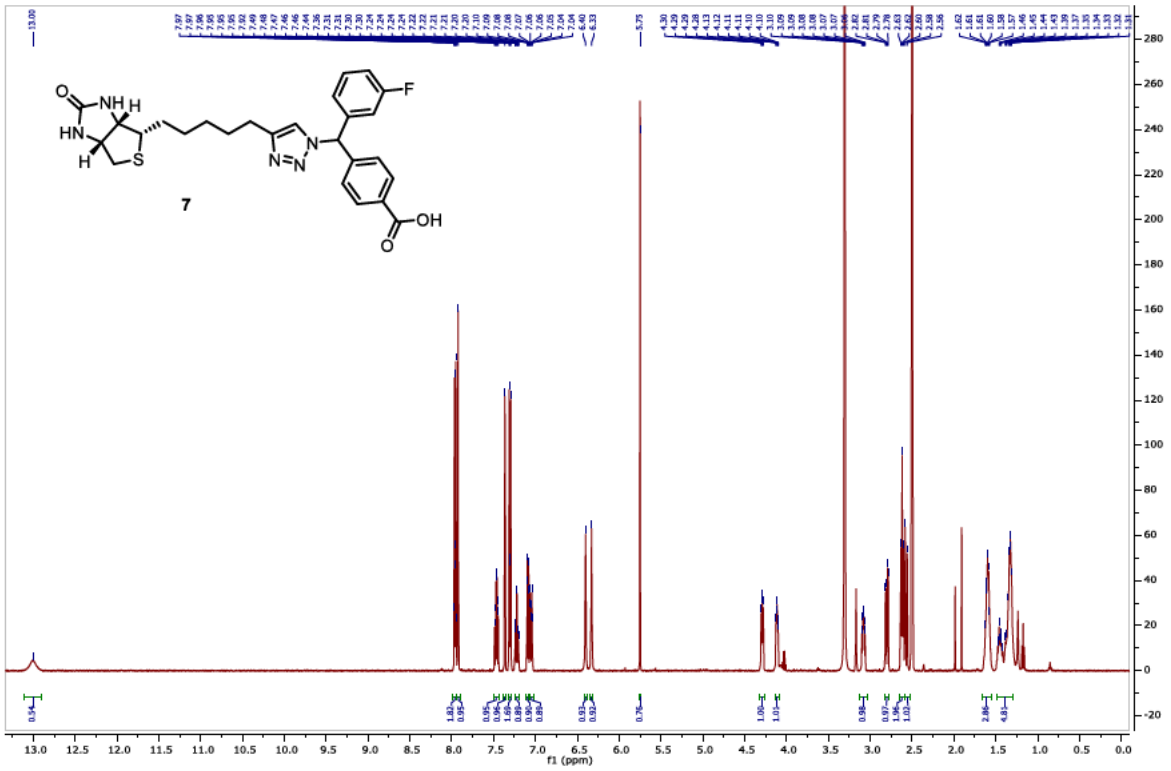

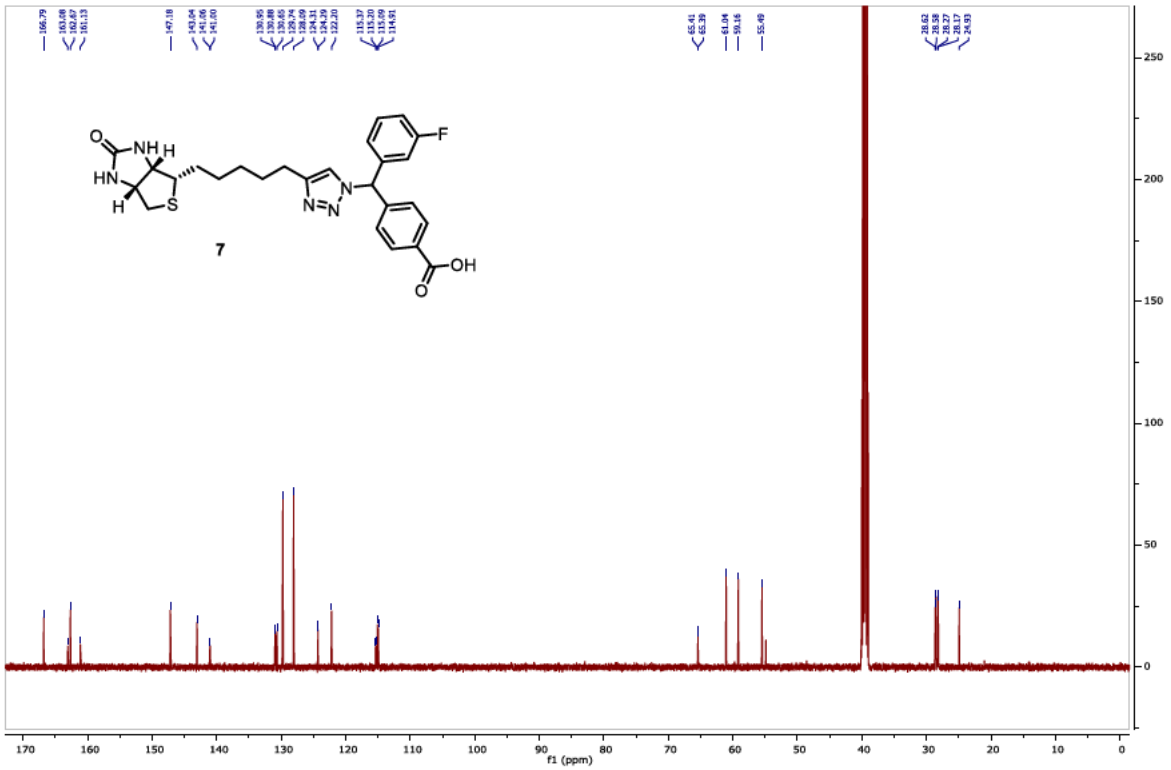

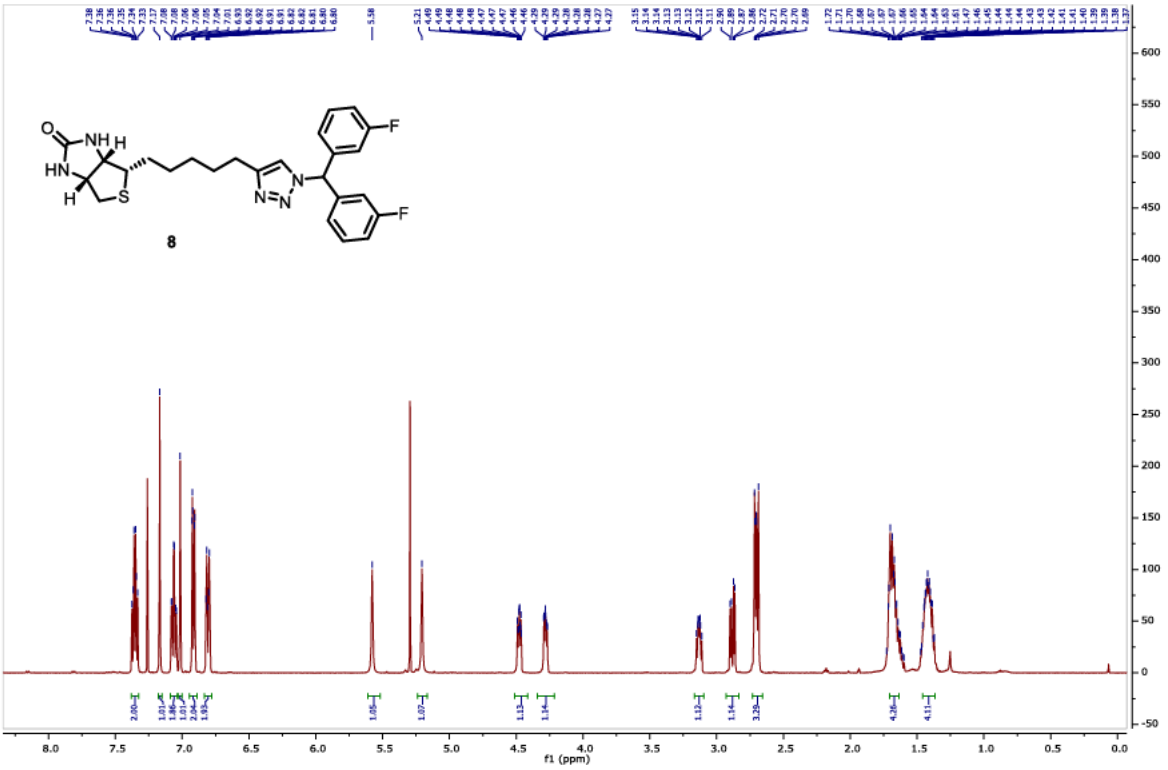
8
f1 (ppm)

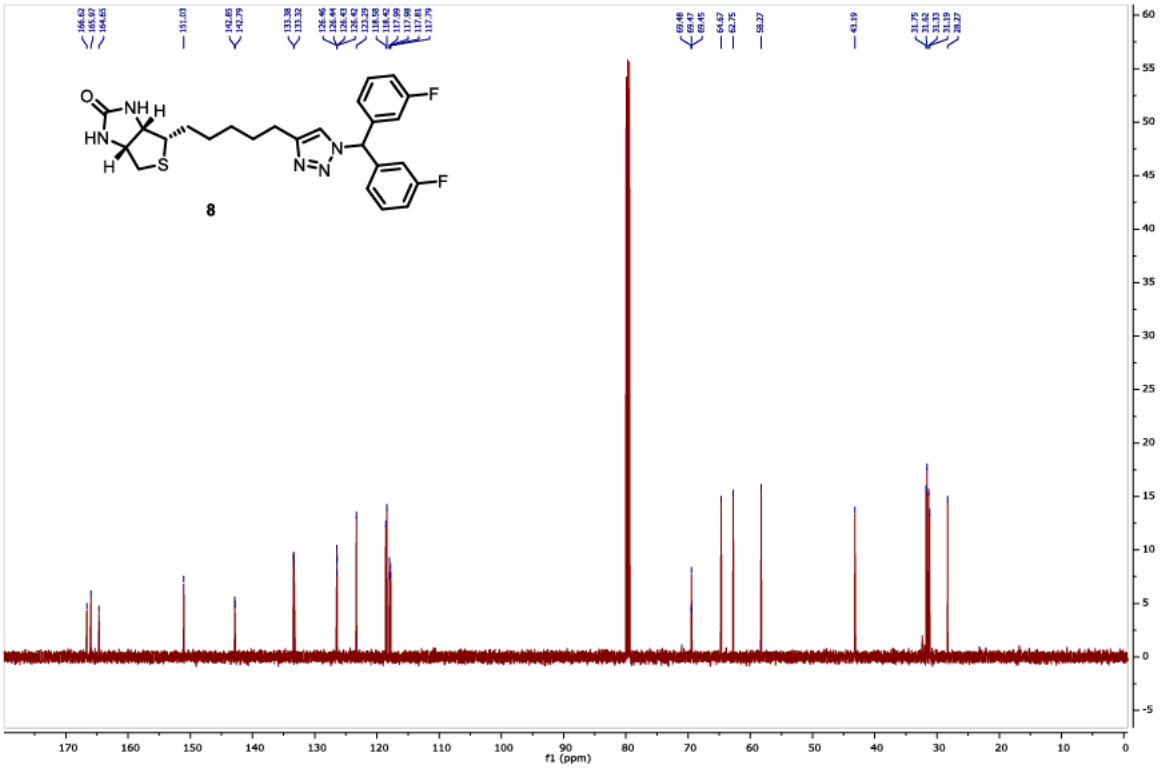
8
f1 (ppm)

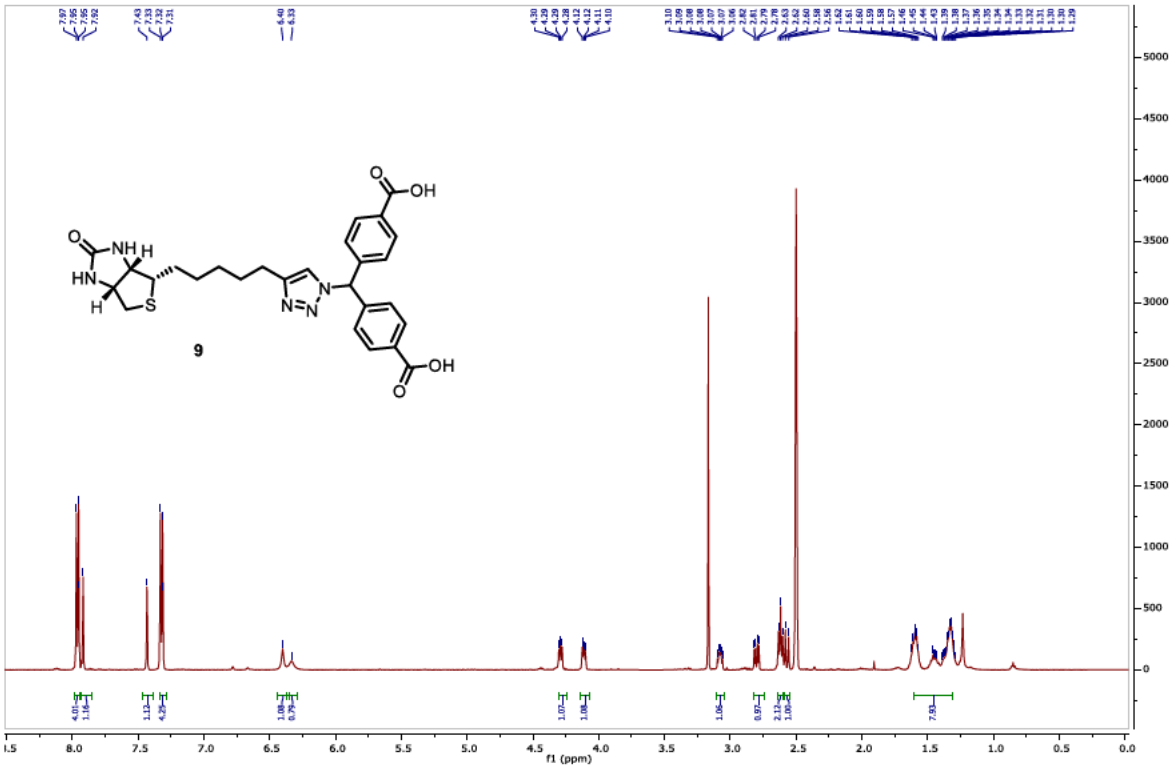
9
f1 (ppm)

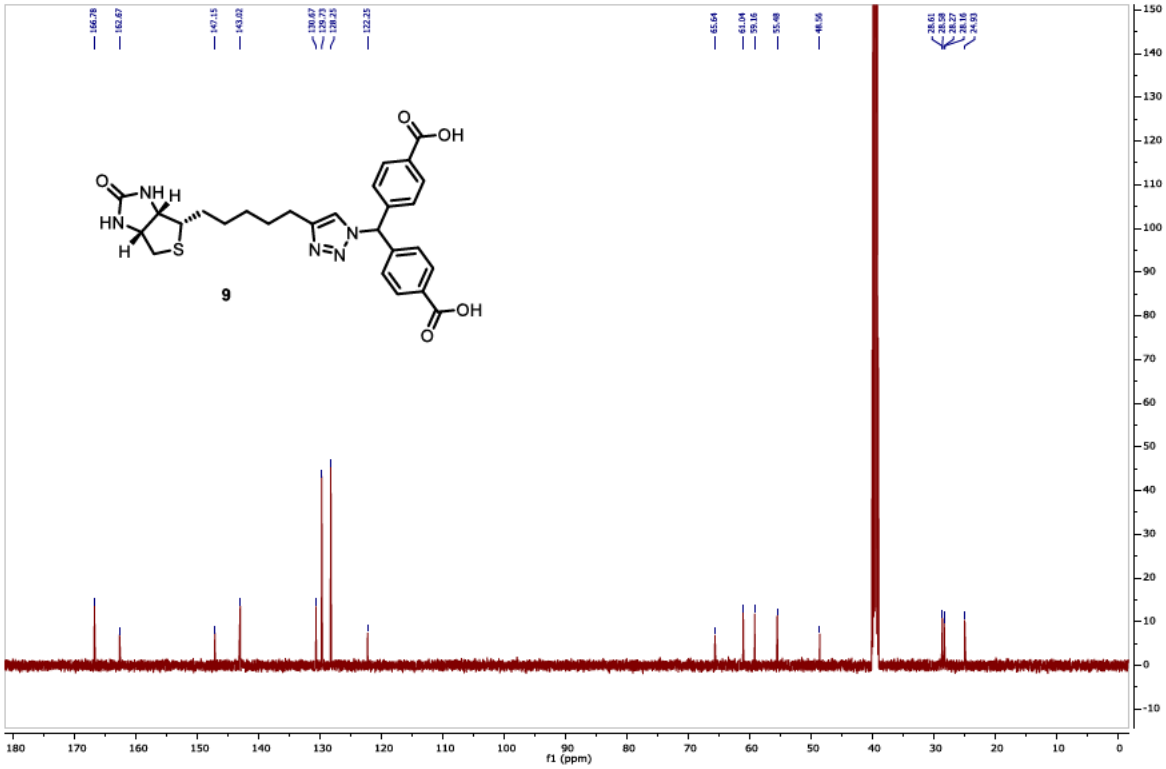
9
f1 (ppm)

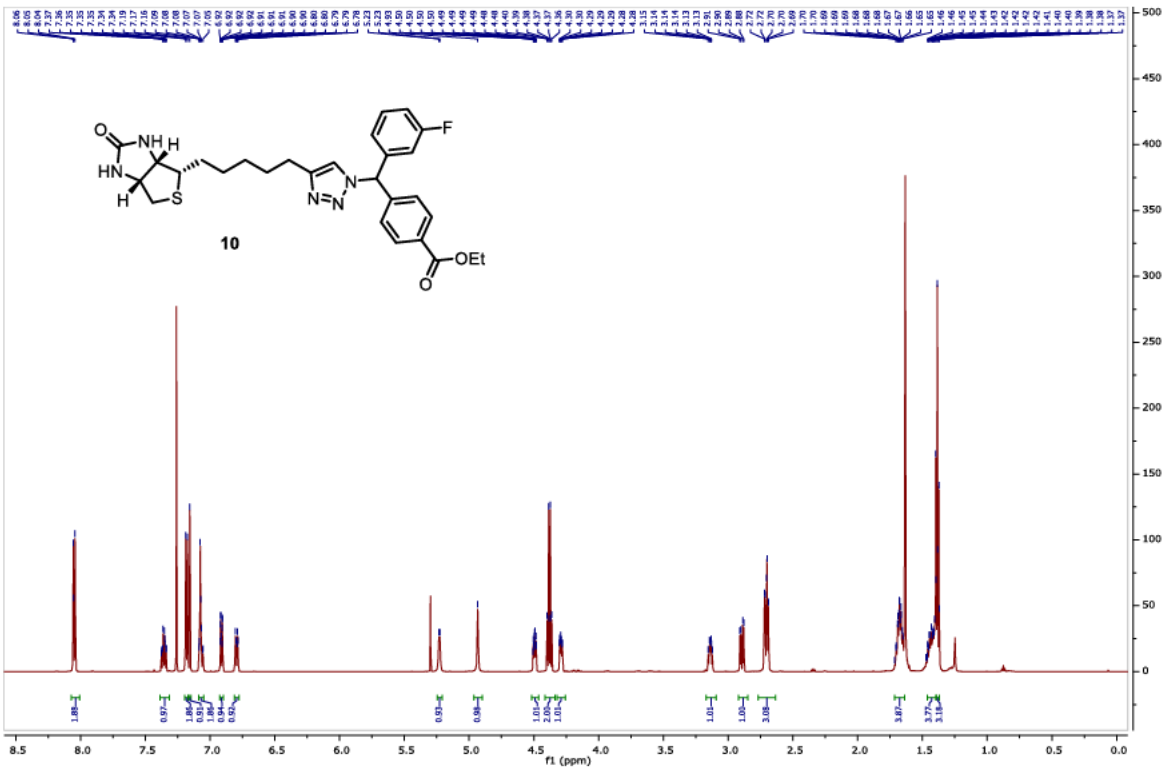
10
f1 (ppm)

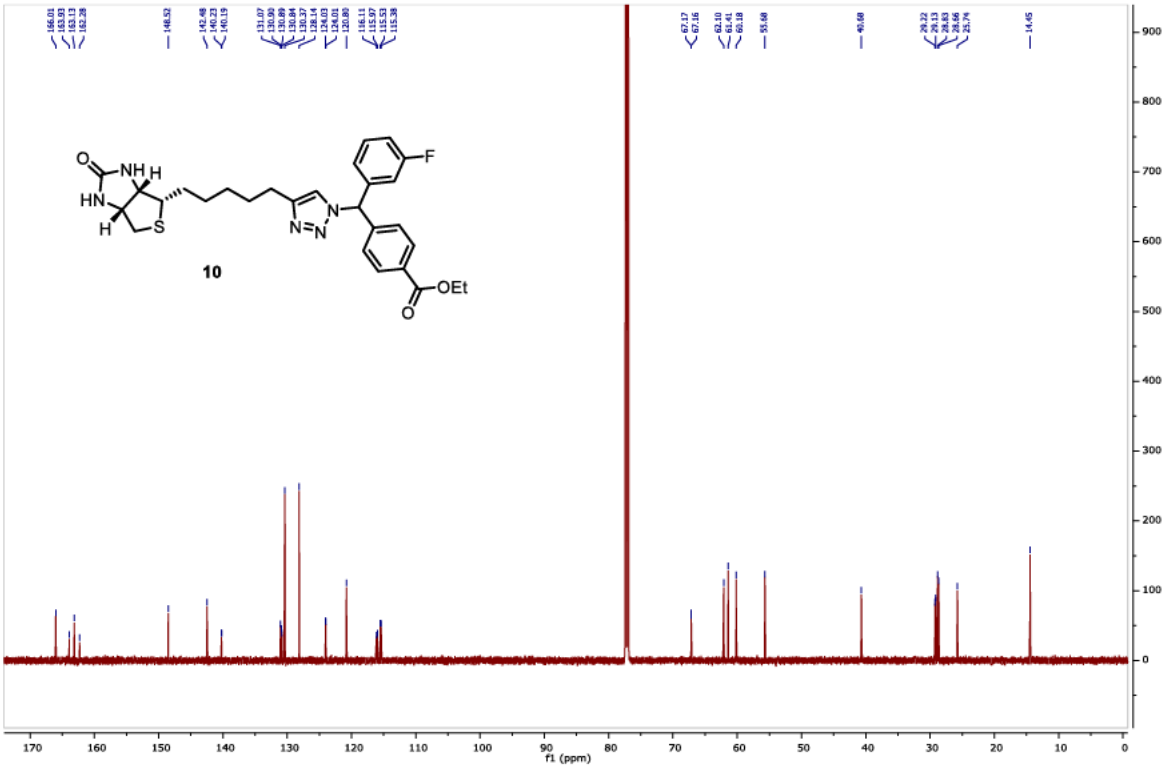
10
f1 (ppm)

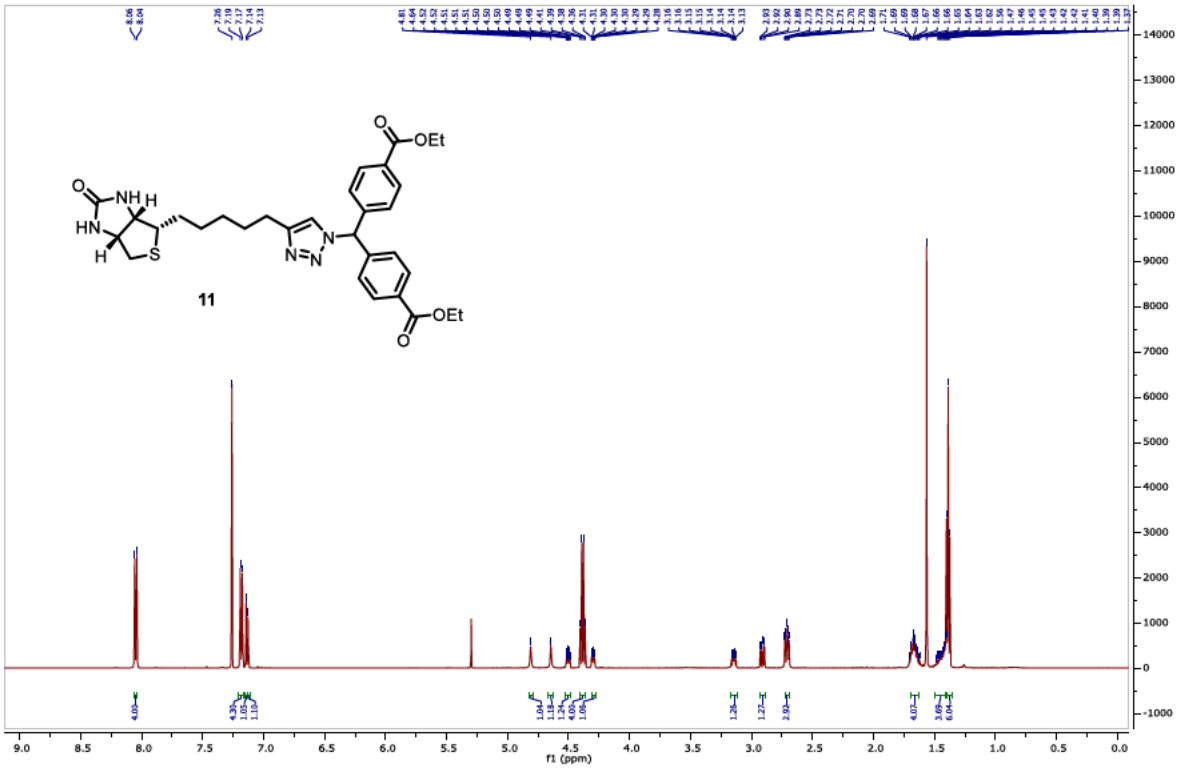
OEt
NH
H
HN
H
S
N
N=N
11
OEt
f1 (ppm)

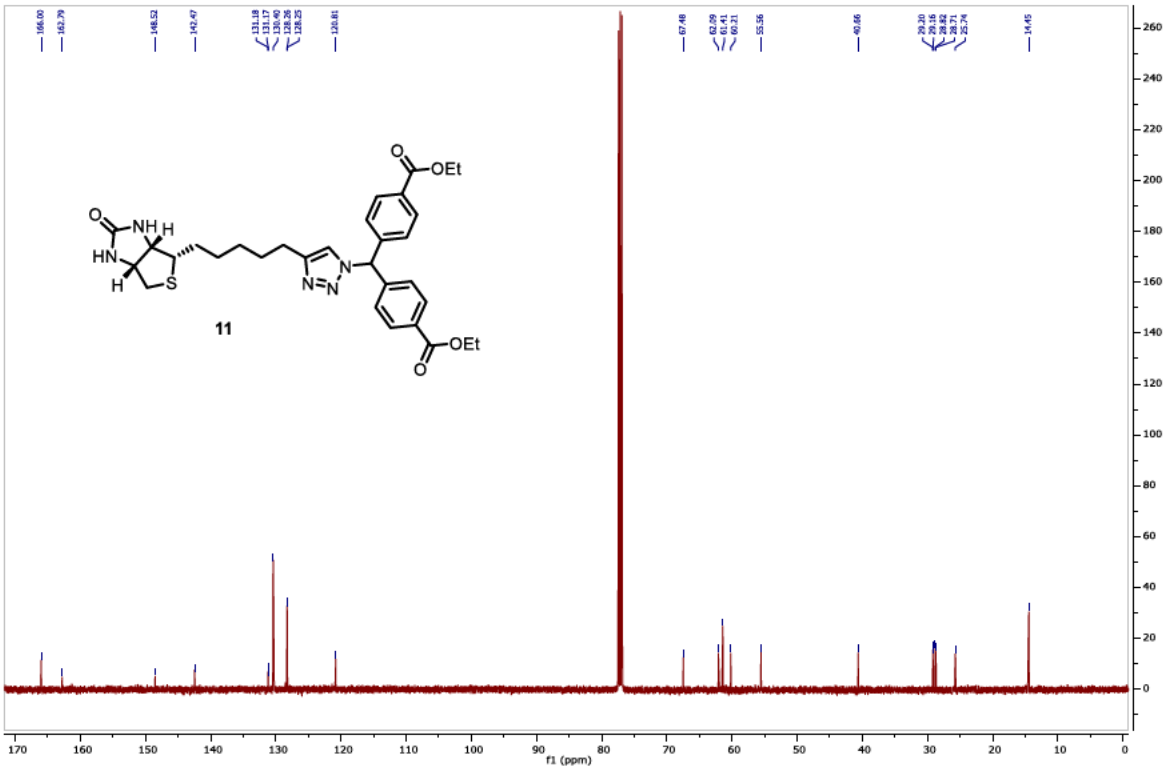
OEt
NH
H
HN
H
S
N
N=N
11
OEt
f1 (ppm)

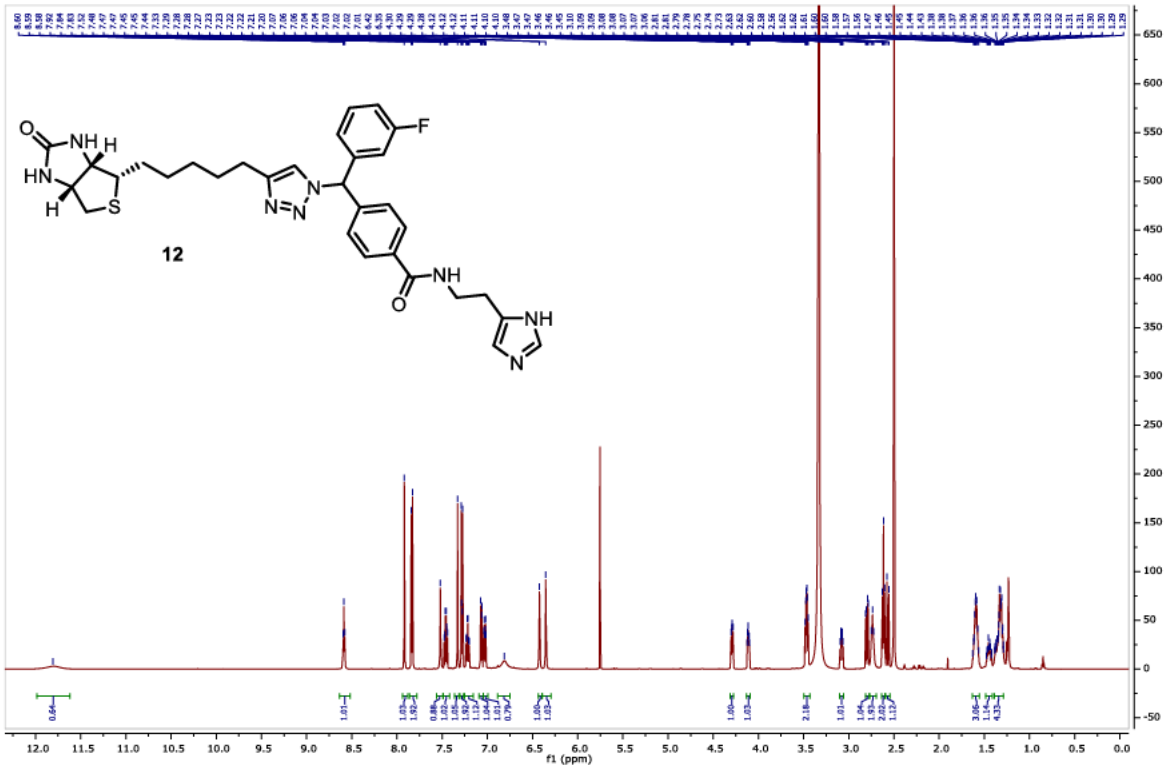
12
f1 (ppm)

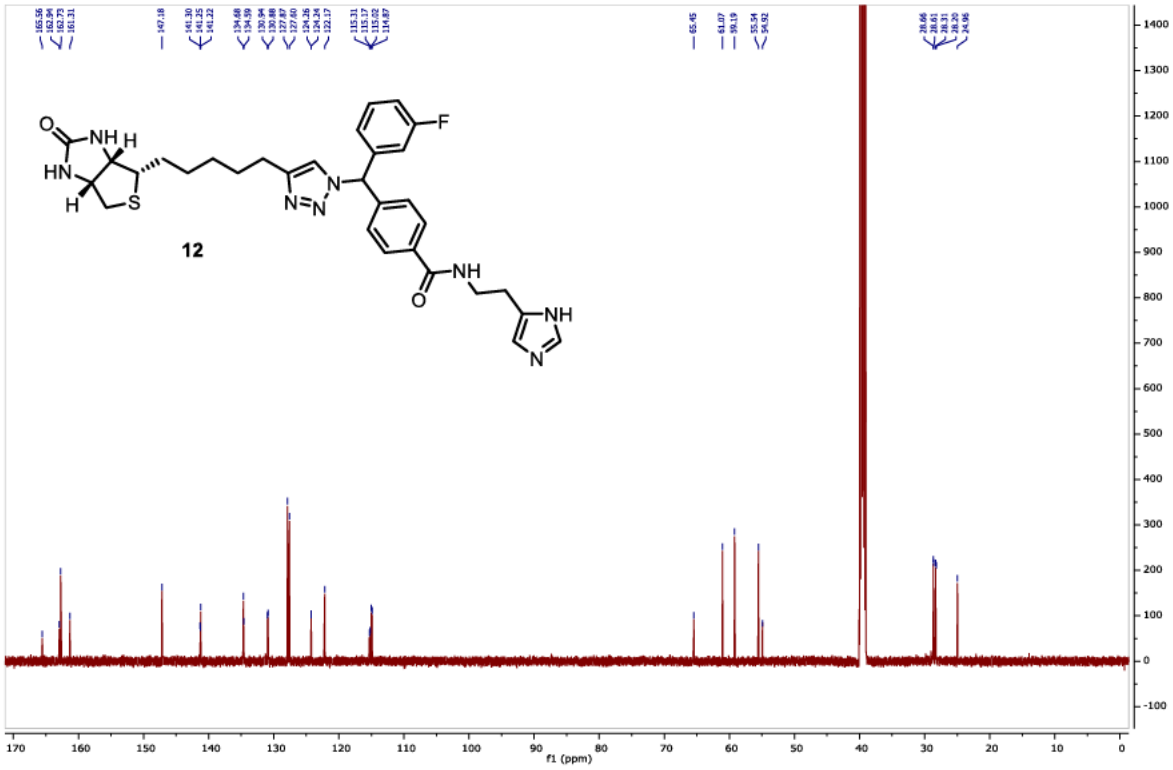
12
f1 (ppm)

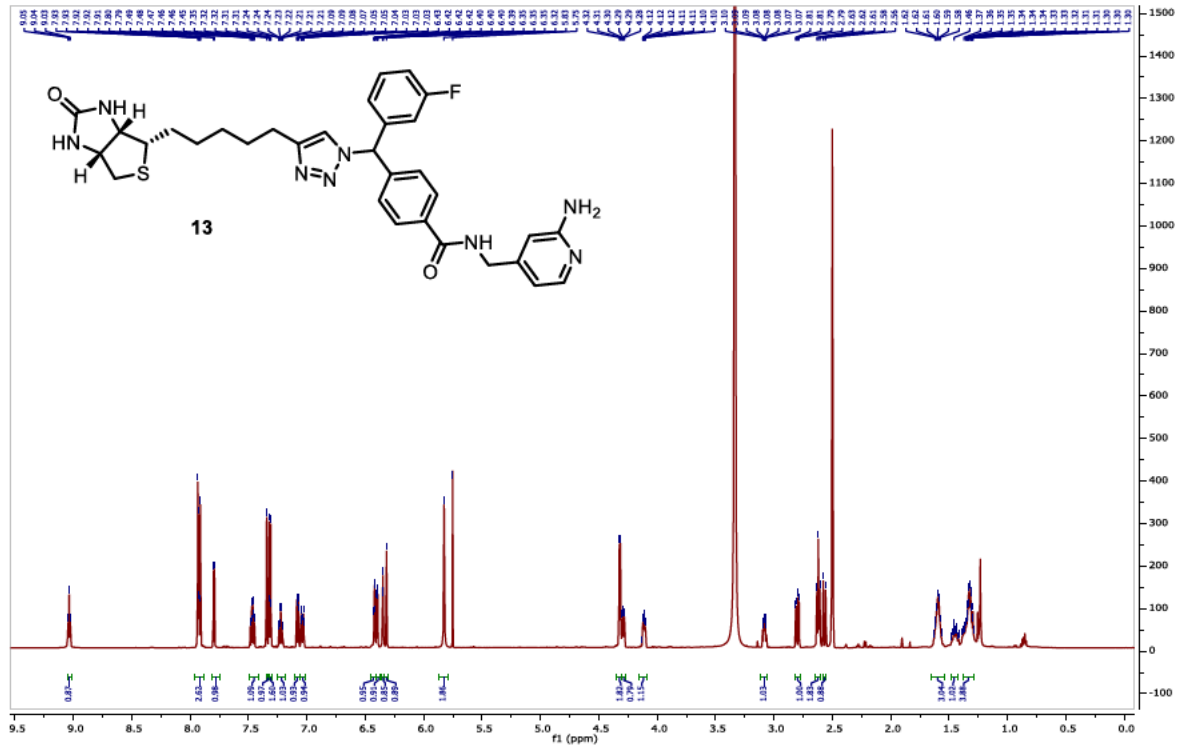
13
f1 (ppm)

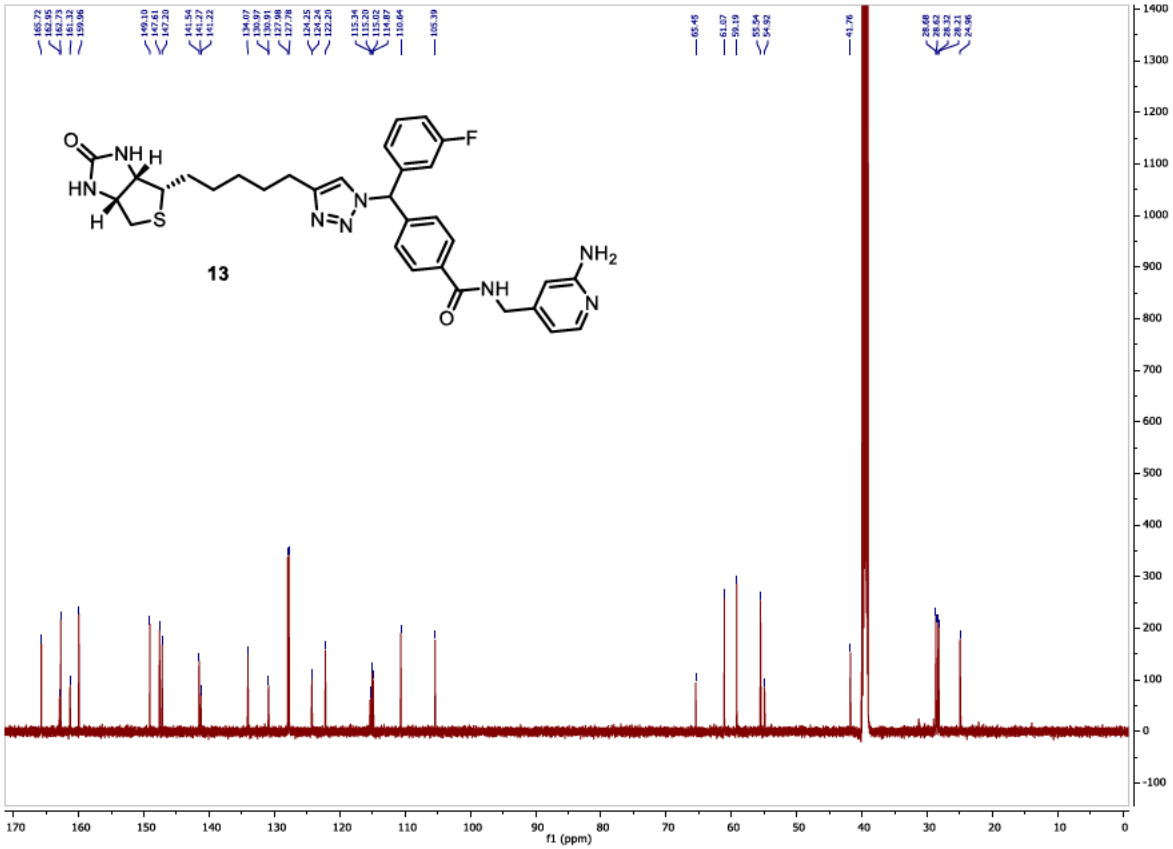
13
f1 (ppm)

S2.4: Supplementary References

(1) Soares Da Costa, T. P.; Tieu, W.; Yap, M. Y.; Pendini, N. R.; Polyak, S. W.; Pedersen, D. S.; Morona, R.; Turnidge, J. D.; Wallace, J. C.; Wilce, M. C. J.; Booker, G. W.; Abell, A. D. Selective Inhibition of Biotin Protein Ligase from Staphylococcus Aureus. *J. Biol. Chem.* **2012**, *287* (21), 17823–17832. https://doi.org/10.1074/jbc.M112.356576.

Chapter Three

This chapter consists of a publication submitted to ACS Medicinal Chemistry Letters in December 2022. The publication is entitled "A Structural Study of Potent Triazole-based Inhibitors of *Staphylococcus aureus* Biotin Protein Ligase". Copies of key ^{1}H and ^{13}C NMR spectra are included in this Chapter as required by the journal.

Damian L. Stachura, Stephanie Nguyen, Steven W. Polyak, Blagojce Jovcevski, John B. Bruning, Andrew D. Abell

Statement of Authorship

Title of Paper	A Structural Study of Potent Triazole-based inhibitors of *Staphylococcus aureus* Biotin Protein Ligase
Publication Status	☐ Published ☐ Accepted for Publication ☑ Submitted for Publication ☐ Unpublished and Unsubmitted w ork w ritten in manuscript style
Publication Details	Authors: Damian L. Stachura, Stephanie Nguyen, Steven Polyak, Blagojce Jovcevski, John Bruning, and Andrew D. Abell The manuscript was submitted to ACS Medicinal Chemistry Letters.

Principal Author

Name of Principal Author (Candidate)	Damian Leszek Stachura
Contribution to the Paper	Performed the synthesis, characterization of analogues, analysis of data, in vitro biological assays, provided advanced draft of manuscript and subsequent revisions.
Overall percentage (%)	70
Certification:	This paper reports on original research I conducted during the period of my Higher Degree by Research candidature and is not subject to any obligations or contractual agreements with a third party that would constrain its inclusion in this thesis. I am the primary author of this paper.
Signature	Date: 6/12/2022

Co-Author Contributions

By signing the Statement of Authorship, each author certifies that:

i. the candidate's stated contribution to the publication is accurate (as detailed above);
ii. permission is granted for the candidate in include the publication in the thesis; and
iii. the sum of all co-author contributions is equal to 100% less the candidate's stated contribution.

Name of Co-Author	Stephanie Nguyen
Contribution to the Paper	Prepared *Sa*BPL and *Sa*PC90-GST enzyme stocks essential for the in vitro biochemical assays
Signature	Date: 7/12/2022

Name of Co-Author	Steven Polyak
Contribution to the Paper	Worked closely with the principal authors and supervised the biological testing
Signature	Date: 8/12/2022

Name of Co-Author	Blagojce Jovcevski		
Contribution to the Paper	Provided supervision of the biological testing.		
Signature		Date	6/12/2022

Name of Co-Author	John B. Bruning		
Contribution to the Paper	Supervised the biological aspects of the manuscript		
Signature		Date	6/12/2022

Name of Co-Author	Andrew D. Abell		
Contribution to the Paper	Supervised the medicinal chemistry of the project and revised manuscript. A corresponding author.		
Signature		Date	6/12/2022

3.1: Abstract

The rise of multi drug-resistant bacteria, such as *Staphylococcus aureus* (*S. aureus*), has highlighted global urgency for new classes of antibiotics. Biotin protein ligase (BPL), a critical metabolic regulatory enzyme, is an important target that shows significant promise in this context. Here we report the *in silico* docking, synthesis, and biological assay of a new series of N^1-diphenylmethyl-1,2,3-triazole-based *S. aureus* BPL (*Sa*BPL) inhibitors (**8-19**) designed to probe the adenine binding site and define whole cell activity for this important class of inhibitor. Triazoles **13** and **14** with N^1-propylamine and -butanamide substituents respectively, were particularly potent with K_i values of 10 ± 2 and 30 ± 6 nM, respectively against *Sa*BPL. A strong correlation was apparent between the K_i values for **8-19** and the *in silico* docking, with hydrogen bonding to amino acid residues Ser128 and Asn212 of *Sa*BPL likely contributing to potent inhibition.

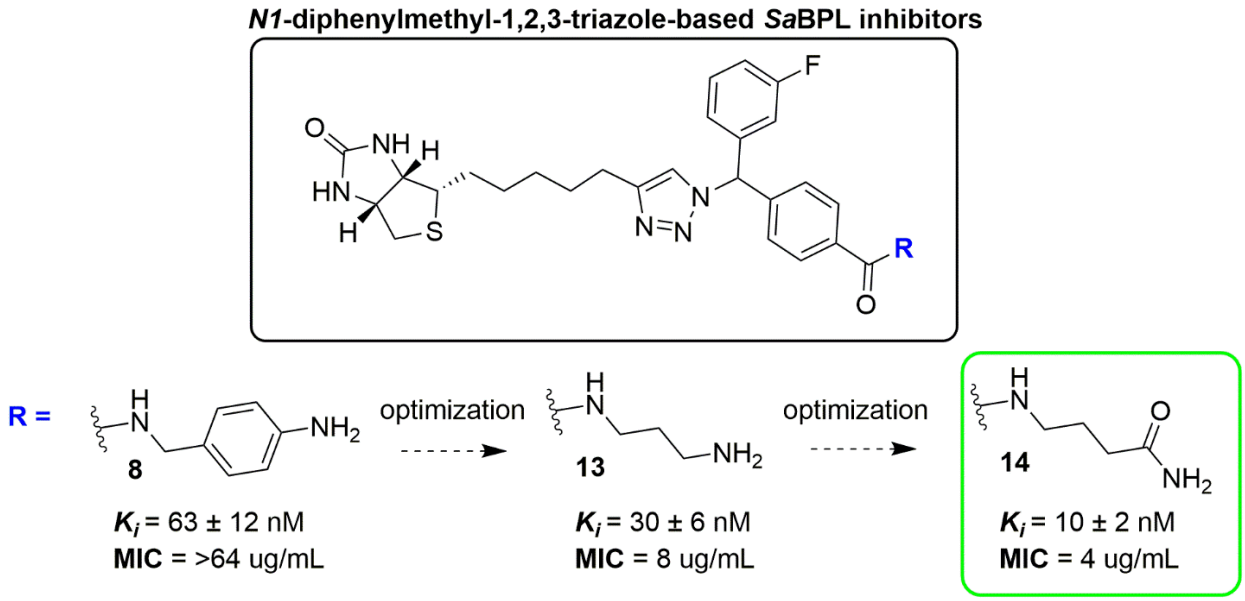

Optimization of a N^1-diphenylmethyl-triazole template as potent *Sa*BPL inhibitors.

3.2: Introduction

The Center for Disease Control (CDC) and Prevention reports that 23 thousand deaths are attributed to drug resistant bacterial infections annually in the USA alone,[1] with global figures predicted to be 10 million by the year 2050.[2] Alarmingly, a decline in antibiotic research has resulted in a shortage of new antibiotics that possess novel mechanisms of action, particularly against *Staphylococcus aureus* (*S. aureus*).[3,4] This bacterium is one of the deadly ESKAPE pathogens, with methicillin-resistant *S. aureus* (MRSA) associated with over 100,000 deaths globally in 2019 alone.[5–7] Biotin protein ligase (BPL) is a promising new drug target in this context, with potent BPL inhibitors reported for multiple pathogenic bacteria such as *S. aureus*, *Escherichia coli* and *Mycobacterium tuberculosis*.[8–12] Biotin protein ligase catalyses the post-translational attachment of biotin to biotin-dependent enzymes (biotinylation) via the natural intermediate biotinyl-5'-AMP **1**.[13,14] Critically, biotinylation of acetyl-CoA-carboxylase and pyruvate carboxylase, enzymes responsible for fatty acid biosynthesis and gluconeogenesis respectively, are essential for bacterial cell viability.[15–17]

Typically, BPL inhibitors have the labile phosphoanhydride linker of **1** replaced with a stable bioisostere, e.g. as in biotinol-5'-AMP **2** which inhibits *Sa*BPL with a K_i value of 0.03 ± 0.01 μM (see Figure 1).[18] However, **2** also inhibits the human homologue. Selectivity for *Sa*BPL has, however, been achieved by substituting the phosphodiester of **2** for a 1,2,3-triazole as in analogue **3** (K_i =1.17 ± 0.3 μM), introduced by Huisgen cycloaddition of biotin acetylene with a suitable azide.[18] X-ray crystallography of **3** bound to *Sa*BPL revealed key hydrogen bonds of the triazole *N2* and *N3* with Arg125 of *Sa*BPL, where the equivalent amino acid in human BPL is a non-conservative asparagine.[18] Triazole-based inhibitors are thus important scaffolds for further antibiotic development.[18–21]

It has also been shown that the adenosine group of **3**, can be replaced with a structurally simpler benzyl group,[19,20] improving potency ~5-fold, e.g. **4** and **5** have K_i values of 0.28 and 0.67 μM, respectively (see Figure 1).[19] An X-ray crystal structure of **5** in complex with *Sa*BPL reveals that its benzyl group occupies the adenosine binding pocket.[19] However, for triazole **4**, the position of the benzyl group was ill-defined in the active site of *Sa*BPL. *In silico* docking studies suggest that this group can not only bind the adenosine pocket, but also an alternative site adjacent to this pocket.[19] Our recently reported N^1-diphenylmethyl-1,2,3-triazole series addressed this finding by combining the aryl ring functionalities of both benzyl triazoles **4** and **5** into the one structure.[21] The two aryl groups then occupy both the adenosine binding pocket

and the adjacent binding site. Notably, substituting the *p*-carboxy acid of the aryl group of a N^1-diphenylmethyl-1,2,3-triazole with an imidazole or aminopyridine group, as in **6** and **7**, resulted in the most potent triazole-based *Sa*BPL inhibitors reported to date (K_i =6.01 ± 1.01 and 8.43 ± 0.73 nM, respectively).[21] Furthermore, triazoles **6** and **7** exhibited excellent whole cell activity against a clinical isolate strain of *S. aureus*, ATCC 49775 (MIC =1 and 8 µg/mL,[21] respectively), superior to previously reported triazole based inhibitors.[19] The nanomolar potency exhibited by triazoles **6** and **7** is likely associated with hydrogen bonding interactions between the respective imidazole/aminopyridine groups and Asn212/Ser128 in the adenine binding site of *Sa*BPL. Analogous interactions between Asn212/Ser128 and the adenine of the natural intermediate **1** are also apparent.[18,21] However, further work is required to investigate whether establishing interactions with Asn212 and Ser128 manifests in potent N^1-diphenylmethyl-1,2,3-triazole *Sa*BPL inhibitors.

Here we present a series of new N^1-diphenylmethyl-1,2,3-triazoles (**8-19**) designed to bind and probe these, and other interactions within the adenine binding site of *Sa*BPL (see Figure 2). 5-Fluorotriazoles **17-19** are presented to further diversify the N^1-diphenylmethyl-1,2,3-triazole series, as triazole fluorination has been shown to influence *Sa*BPL potency in previous work.[19] An *in silico* docking study is also reported to define the binding conformations of these analogues and interactions within the adenine binding site.

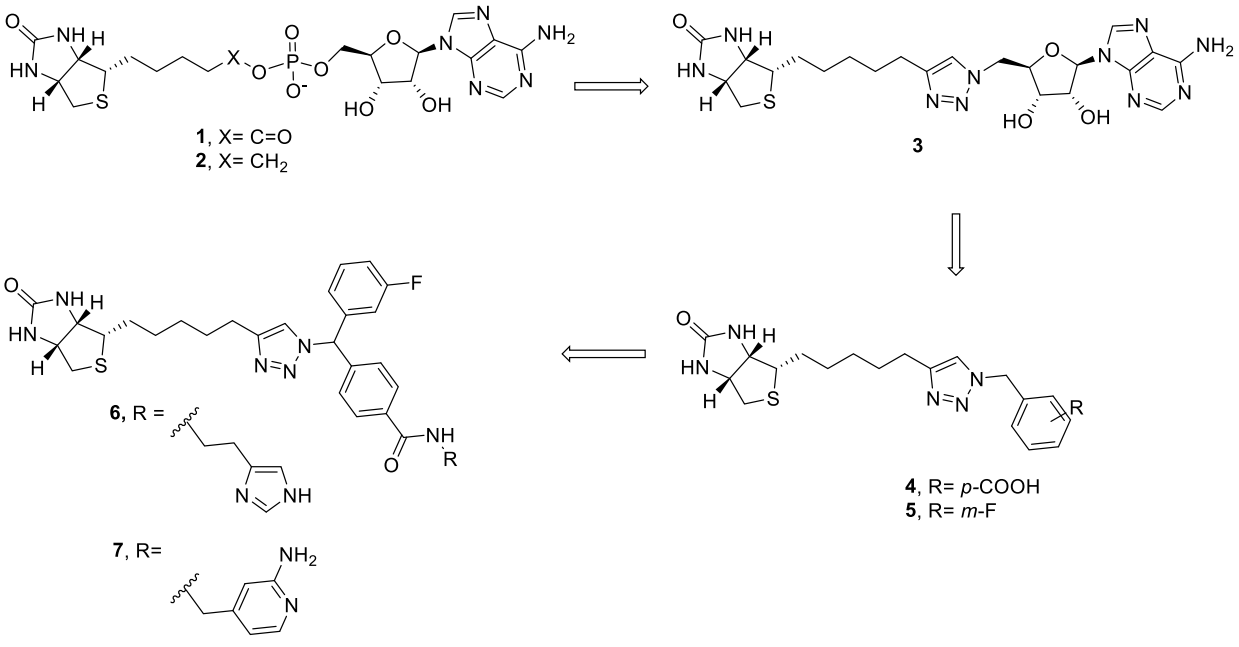

Figure 1: Reported inhibitors of *Sa*BPL.[15,18]

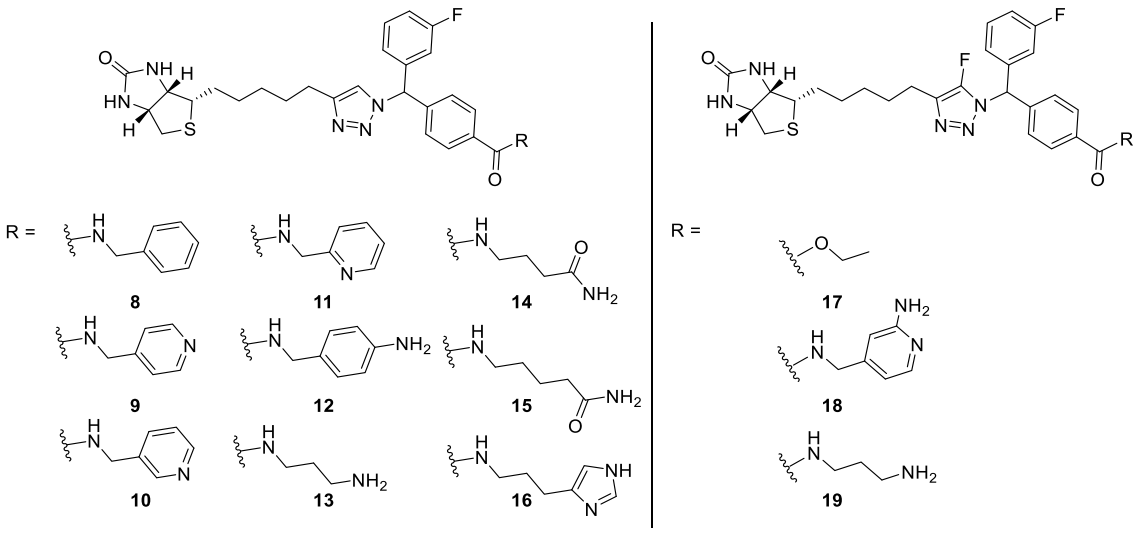

Figure 2: Proposed N^1-di-phenylmethyl 1,2,3-triazole *Sa*BPL inhibitors **8-19**.

3.3: Results and Discussion

In silico docking indicates the imidazole and aminopyridine groups of highly potent N^1-diphenylmethyl-triazoles **6** and **7** hydrogen bond with Asn212 and Ser128 in the adenine pocket of *Sa*BPL.[21] This suggests that replacing these groups with a range of other hydrogen bond donor (HBD) and acceptor (HBA) substituents warrants further investigation (see **9-19** in Figure 2). The triazoles **8-19** were docked *in silico* into the *Sa*BPL active site (PDB: 6APW[19]) using ICM-Pro in order to identify hydrogen bonding within the adenine binding site and the results are discussed below (see supporting information for docking protocol) The ammonium conjugate acids of triazoles **13** and **19** were docked, rather than the free amines, to better reflect physiological conditions. Additionally, discussion of the *in silico* docking study focuses on interactions established within the adenine binding region of *Sa*BPL.

The docking shows that the *N4*-pyridyl and *N3*-pyridyl groups of **9** and **10** respectively, interact closely with N212 of *Sa*BPL. Interestingly, the *N2*-pyridyl derivative **11** does not interact with either S128 or N212, highlighting the importance of the pyridyl nitrogen position. Triazole **8** provides a suitable negative control for the docking study, where its benzyl substituent does not interact with either N212 or S128.Docking of triazole **12** revealed a hydrogen bond between its 4-amino phenyl NH_2 and N212, which should reflect in enhanced binding affinity towards *Sa*BPL.

The conjugate acid of the propylamine substituent **13** forms two hydrogen bonds with Asn212. Importantly, the terminal butanamide substituent of triazole **14** hydrogen bonds both Asn212

and Ser128 as per the adenine of the natural intermediate, biotinyl-5'-AMP **1**. The pentanamide substituent of **15**, with an extra carbon in its butanamide alkyl chain, does not form a hydrogen bond with Asn212 (compare Figures S7 and S8). The propyl imidazole substituent of **16** does not interact with either Asn212 or Ser128, while the truncated ethyl chain of more potent **6** was predicted to do so.[21] As expected, the carboxy ethyl group of 5-fluorotriazole **17** occupies the adenine binding site without specific interactions. The aminopyridine substituents of both 5-fluorotriazole **18** and highly potent **7**[21] similarly hydrogen bond to Asn212 and Ser128. The propyl ammonium groups of 5-fluorotriazole **19** similarly hydrogen bonds N212, relative to 5-prototriazole **13**. These docking studies establish triazoles **8-19** as viable synthetic targets for subsequent assay.

3.3.1: Synthesis of Triazoles 8-19

The 5-prototriazoles **8-16** and 5-fluorotriazoles **17-19** were prepared as shown in Schemes 1 and 2, respectively. The key carboxylic acid **20**[21] was used as a diastereomeric mixture (see below for further detail) and was coupled with the appropriate amine, in the presence of DIPEA and HATU, to give the 5-prototriazoles **8-12**, **14-16** and **21** in yields ranging from 50-95 %, see Scheme 1. Preparation of triazole **13** required Boc deprotection of **21**, which was mediated by 1 M HCl in dioxane. Each of these triazoles was isolated as a mixture of diastereomers and used as such in subsequent assays.

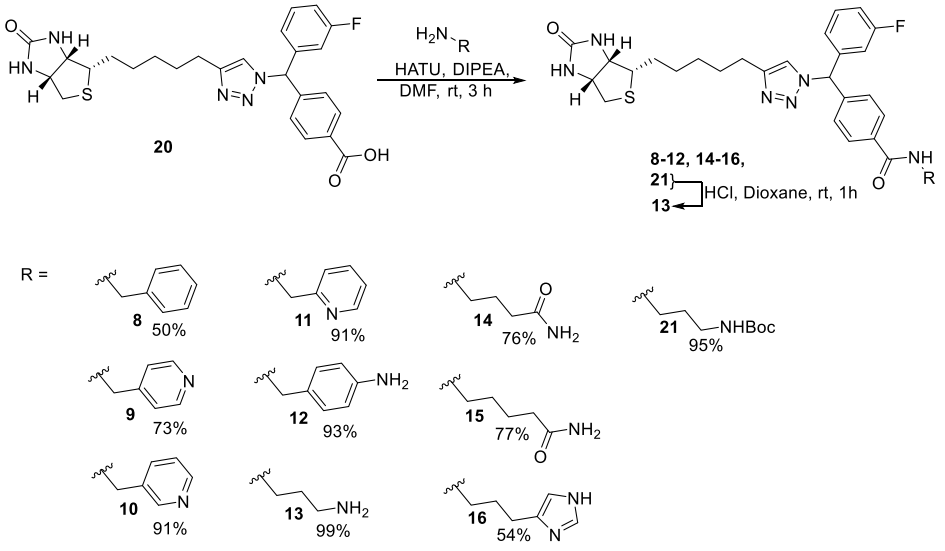

Scheme 1: Synthesis of triazoles **8-16** and intermediate **21**.

The synthesis of 5-fluorotriazole analogues **17-19** required preparation of the 5-iodotriazole **24**. Specifically, copper catalysed Huisgen cycloaddition of biotin acetylene **22**[18] and racemic di-phenylmethyl azide **23**,[21] in the presence of $Cu(ClO_4)_2$, LiI, TBTA and TEA, gave 5-iodotriazole **24** in 82% yield (see Scheme 2). Using adapted conditions from Paparella *et al*,[19] 5-iodo triazole **24** was reacted with KF in a microwave reactor to give 5-fluorotriazole **17** in 82%. Subsequent hydrolysis of the ethyl ester group with LiOH gave carboxylic acid triazole **25** in 95 % yield. This carboxylic acid was coupled with 4-(aminomethyl)pyridine-2-amine, in the presence of HATU and DIPEA, to give the corresponding amide **18** in good yield. Propylamine **19** was prepared in two steps from carboxylic acid triazole **25**, by initial HATU mediated amidation with *N*-3-Boc-propyldiamine and subsequent reaction with 1 M HCl in dioxane, 77 % yield over two-steps. The 5-fluorotriazoles were also isolated as mixtures of diastereomers and were used as such in subsequent assays. Interestingly, each diastereomer of **8-19** similarly docked with *Sa*BPL, see Figures S1-12 in the supporting information for binding conformations. There is no evidence of distereoisomers in the respective ^{1}H or ^{13}C NMR spectra of triazoles **8-19**, thus separation of isomers was not attempted. However, 1:1 ratio is assumed as the racemic azides **23**[21] were used to prepare key coupling precursors **20**[21] and **24**.

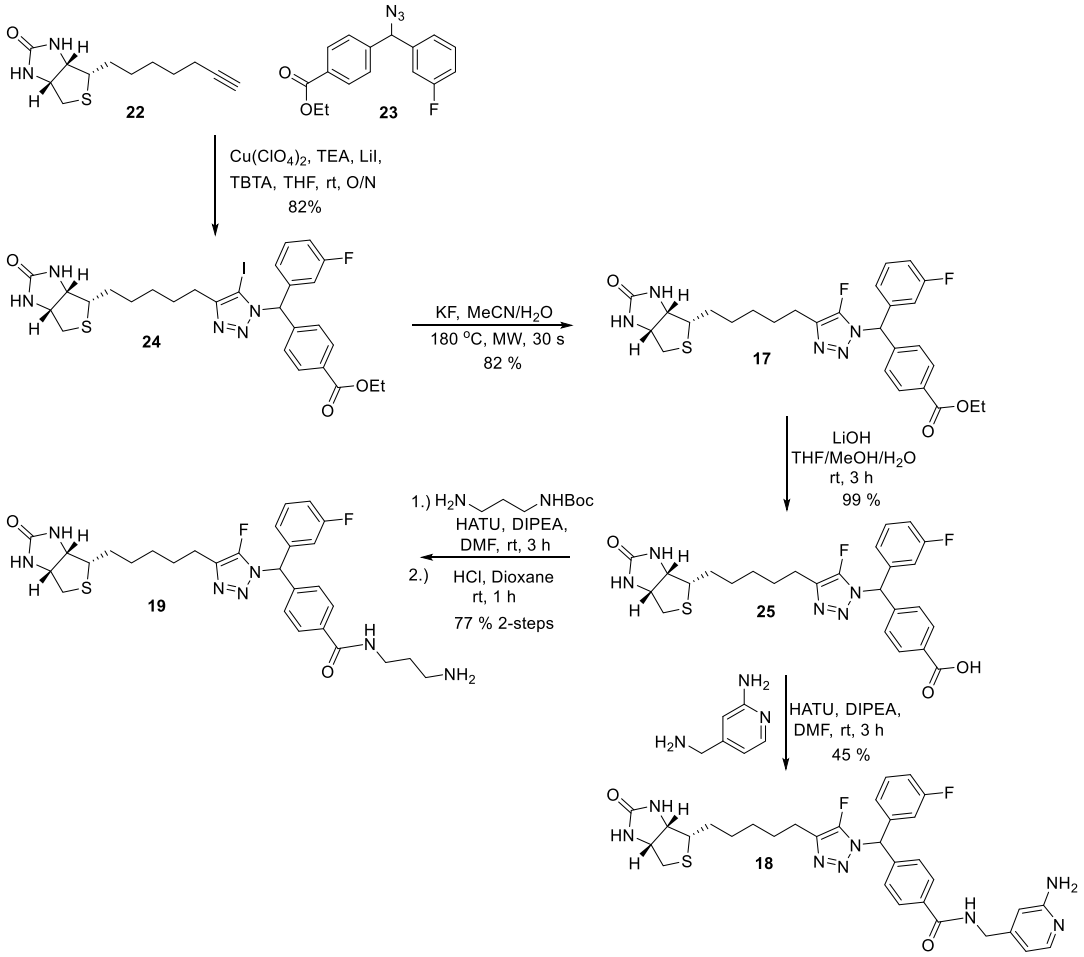

Scheme 2: Synthesis of triazoles **17-19**

3.4: Biochemical and Antimicrobial Assay of Triazoles 8-19

All triazoles (**8-19**) were evaluated for inhibitory activity *Sa*BPL using an established *in vitro* protein biotinylation assay,[21] with the results shown in Table 1. Triazole **9** with its *N4*-pyridyl substituent (K_i = 130 ± 20 nM), was significantly more potent than triazole **8** with its unsubstituted benzyl group (K_i = 867 ± 40 nM). This is consistent with docking, where the *N4*-pyridyl nitrogen of triazole **9** was predicted to interact with N212. Triazole **9** was more potent than the *2*- and *3*-pyridyl derivatives, **10** and **11** (K_i = 237 ± 56 and 544 ± 59 nM, respectively). This is also consistent with the docking study which indicated the *N4*-pyridiyl of **9** establishes the shortest hydrogen bond with the terminal amide of N212 of these three analogues (**9-11**). The 4-amino phenyl substituted triazole **12**, displayed enhanced potency with a K_i value of 62 ± 12 nM. This trend, where hydrogen bonding to Asn212 manifests in enhanced potency, was also apparent with the aminopropyl group of triazole **13** (K_i = of 30 ± 6 nM), which was shown to behave as both a HBA and HBD with Asn212. As expected, the butanamide substituted derivative **14** was the most potent of the series against *Sa*BPL (K_i = 10 ± 2 nM), where docking revealed hydrogen bonding with both Asn212 and Ser128 for this inhibitor. The potency exhibited by butanamide **14** is comparable to the most potent triazoles reported to date (**6**, K_i = 6.01 ± 1.01 and **7**, K_i = 8.43 ± 0.73 nM[21]). Crucially, triazoles **6** and **7** are also reported to potentially hydrogen bond both Asn212 and Ser128.[21] An approximate 25-fold loss in activity was apparent for pentanamide **15** when compared to the butanamide substituent of **14** (K_i = 246 ± 22 vs 10 ± 2 nM, respectively). This drop in potency is consistent with docking, where the pentanamide was predicted to interact only with Ser128. A 30-fold loss in potency was also apparent for propyl imidazole **16** relative to ethyl imidazole derivative **6** (K_i = 181 ± 11 vs 6.01 ± 1.01 nM, respectively). This too is consistent with docking, whereby **16** did not hydrogen bond either Asn212 or Ser128. These assay results for triazoles **8-16** present a clear correlation with the docking results, whereby hydrogen bonding to Asn212 and/or Ser128 within the adenine binding site gives rise to enhanced inhibitory activity against *Sa*BPL.

Interestingly, the 5-fluorotriazoles **18** and **19**, that each contain an aminopyridine and propylamine substituent respectively, demonstrated only modest potency against *Sa*BPL (K_i = 131 ± 17 and 268 ± 23 nM, respectively) despite being predicted to bind Asn212 and/or Ser128. This represents an approximately 10-fold loss in activity compared to the corresponding 5-prototriazole derivatives **7** and **13** (K_i = 8.43 ± 0.7[21] and 30 ± 6 nM, respectively) which were also predicted to hydrogen bond Asn212 and/or Ser128. This result is inconsistent with the observations presented above for each of triazoles **8-16**. Interestingly, literature reports

disparate K_i values for some 5-proto and 5-fluorotriazole-based *Sa*BPL inhibitors, particularly benzoxazolones **26** and **27** (K_i = 0.23 and 0.42 µM, respectively),[19] see Figure 3. Interestingly, the triazole nitrogens of **26** and **27** similarly hydrogen bond to R125 and R122 of *Sa*BPL,[19] suggesting fluorination of the triazole does not affect *Sa*BPL-triazole ring interactions Superimposing the separate co-crystal structures of *Sa*BPL in complex with **26** and **27** reveals structural differences within the adenine binding region (PDB: **26**-*Sa*BPL 3V7S[19] and **27**-*Sa*BPL 8ENI) with Ser128 and Trp127 residues shown to adopt different conformations, see Figure 4. The Trp127 residue is presumed to be orientated to accommodate the fluorine atom on the triazole ring of **27**, resulting in a tilted conformation of S128 and an overall increase in volume area of adenine binding site as previously reported.[19] Thus, 5-fluorotriazoles **18** and **19** were re-docked using the 5-fluorotriazole **27** cocrystal structure (PDB: 8ENI) to shed further light on the matter. This docking provides an improved representation of the *Sa*BPL active site when complexed with a 5-fluorotriazole based inhibitor. This reveals that the respective aminopyridine and propylamine substituents of **18** and **19** respectively, do not form hydrogen bonds to either N212 or S128 (see Figures S13 and S14). This more representative docking result for 5-fluorotriazoles **18** and **19** is now more consistent with the observations presented for the 5-prototriazoles **8**-**16**, where a lack of predicted hydrogen bonding to these amino acids results in only modest inhibition of *Sa*BPL.

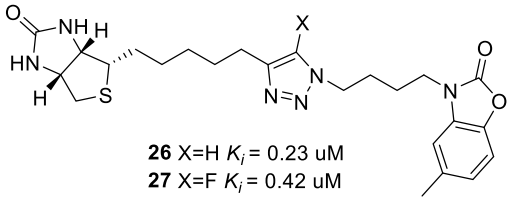

Figure 3: Chemical structure of 5-prototriazole **26** and 5-fluorotriazole **27**.

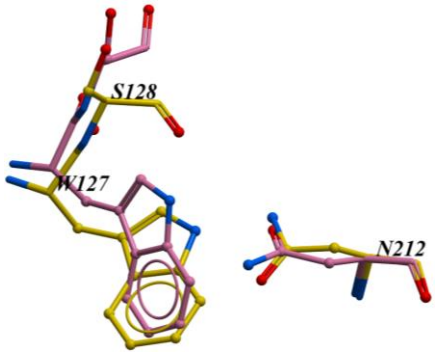

Figure 4: Comparison of cocrystal structures. The **26**-*Sa*BPL (yellow, PDB: 3V7S[19]) and **27**-*Sa*BPL (pink, PDB: 8ENI) complexes are superimposed, showing only the amino acids Trp127, Ser128 and Asn212 within the adenine binding site.

The antimicrobial activity of triazoles **8-19** was also assessed against a clinical isolate of *S. aureus* (ATCC 49775) using a broth microdilution assay, with the results summarized in Table 1. Triazoles **13** and **14**, with propyl amine and butanamide groups respectively, were particularly potent with corresponding MIC values of 8 and 4 μg/mL. These values are comparable to those recently reported for highly potent triazoles **6** and **7** (MIC = 1 and 8 μg/mL,[21] respectively). Notably, a clear correlation was found between the microbiological and biochemical data for these four structurally related N^1-diphenylmethyl triazole-based *Sa*BPL inhibitors (**6**, **7**, **13** and **14**).

Table 1: Biochemical and anti-staphylococcal properties of inhibitors **8-19**

ID	K_i *Sa*BPL nM[a]	MIC μg/mL[b]
8	867 ± 48	>64
9	130 ± 20	>64
10	237 ± 56	>64
11	544 ± 59	>64
12	63 ± 12	>64
13	30 ± 6	8
14	10 ± 2	4
15	246 ± 22	>64
16	181 ± 11	32
17	N/A[c]	N/A[c]
18	131 ± 17	>64
19	268 ± 23	>64

[a] Inhibition constants (K_i) for the competitive inhibitors were derived from the IC_{50} for triazoles **8-13**, **15-19** and the Morrison equation for **14**. See Supporting Information for further detail. [b] MIC values reported against *S. aureus*, ATCC 49775. [c] Insoluble under assay conditions

3.5: Conclusion

Triazole **13** and **14** with propylamine, and butanamide substituents respectively, were synthesized and shown to be particularly potent inhibitors of *Sa*BPL with K_i values of 30 ± 6 and 10 ± 2 nM respectively. The docking of these derivatives revealed that both the respective propylamine and butanamide substituents form hydrogen bonds with Asn212 / Ser128 within the adenine binding site of *Sa*BPL. Similar interactions are established by the adenine of biotinyl-5'-AMP **1**, suggesting the butanamide and propylamine substituents may mimic this natural interaction. Triazoles **13** and **14** also show excellent whole cell activity against a clinical

isolate of *S. aureus* (MIC = 8 and 4 µg/mL, respectively). These combined studies highlight N^1-diphenylmethyl-triazole **13** and **14** as important *Sa*BPL inhibitors, that are suitable for further preclinical development.

3.6: Acknowledgments

We would like to thank Prof. Grant Booker, Prof. Matthew Wilce, Dr. John Horsley, and Dr. Kwang Jun Lee for their helpful discussions regarding the work described in this paper.

3.7 Abbreviations

BPL, biotin protein ligase, **$Cu(ClO_4)_2$**, copper perchlorate, **DIPEA**, *N*,*N* – diisopropylethylamine, **DMF**, dimethylformamide, **ESKAPE**, *Enterococcus faecium*, *Staphylococcus aureus*, *Klebsiella pneumoniae*, *Acinetobacter baumannii*, *Pseudomonas aeruginosa*, and *Enterobacter* spp, **HATU**, hexafluorophosphate azabenzotriazole tetramethyl uranium, **HBA**, hydrogen bond acceptor, **HBD**, hydrogen bond donor, **HBTU**, hexafluorophosphate benzotriazole tetramethyl uranium, **HCl**, hydrochloric acid, **KF**, potassium fluoride, **K_i**, absolute inhibition constant, **LiI**, lithium iodide, **LiOH**, lithium hydroxide, **MeCN**, acetonitrile, **MeOH**, methanol, **MIC**, minimum inhibitory concentration, **MRSA**, methicillin resistant *S. aureus*, **mw**, microwave, **PDB**, protein data bank, ***Sa*BPL**, *S. aureus* biotin protein ligase, **TBTA**, tris(benzyltriazolylmethyl)amine, **TEA**, triethyl amine, **THF**, tetrahydrofuran

3.8: References for Chapter Three

(1) Penchovsky, R.; Traykovska, M. Designing Drugs That Overcome Antibacterial Resistance: Where Do We Stand and What Should We Do? *Expert Opin. Drug Discov.* **2015**, *10* (6), 631–650. https://doi.org/10.1517/17460441.2015.1048219.

(2) de Kraker, M. E. A.; Stewardson, A. J.; Harbarth, S. Will 10 Million People Die a Year Due to Antimicrobial Resistance by 2050? *PLoS Med.* **2016**, *13* (11), e1002184. https://doi.org/10.1371/journal.pmed.1002184.

(3) Cooper, M. A.; Shlaes, D. Fix the Antibiotics Pipeline. *Nature* **2011**, *472* (7341), 32. https://doi.org/10.1038/472032a.

(4) Butler, M. S.; Blaskovich, M. A.; Cooper, M. A. Antibiotics in the Clinical Pipeline at the End of 2015. *J. Antibiot. (Tokyo).* **2017**, *70* (1), 3–24. https://doi.org/10.1038/ja.2016.72.

(5) Yang, Y.; Hu, Z.; Shang, W.; Hu, Q.; Zhu, J.; Yang, J.; Peng, H.; Zhang, X.; Liu, H.; Cong, Y.; Li, S.; Hu, X.; Zhou, R.; Rao, X. Molecular and Phenotypic Characterization Revealed High Prevalence of Multidrug-Resistant Methicillin-Susceptible Staphylococcus Aureus in Chongqing, Southwestern China. *Microb. Drug Resist.* **2017**, *23* (2), 241–246. https://doi.org/10.1089/mdr.2016.0078.

(6) Dantes, R.; Mu, Y.; Belflower, R.; Aragon, D.; Dumyati, G.; Harrison, L. H.; Lessa, F. C.; Lynfield, R.; Nadle, J.; Petit, S.; Ray, S. M.; Schaffner, W.; Townes, J.; Fridkin, S. National Burden of Invasive Methicillin-Resistant Staphylococcus Aureus Infections, United States, 2011. *JAMA Intern. Med.* **2013**, *173* (21), 1970–1979. https://doi.org/10.1001/jamainternmed.2013.10423.

(7) Turner, N. A.; Sharma-Kuinkel, B. K.; Maskarinec, S. A.; Eichenberger, E. M.; Shah, P. P.; Carugati, M.; Holland, T. L.; Fowler, V. G. Methicillin-Resistant Staphylococcus Aureus: An Overview of Basic and Clinical Research. *Nat. Rev. Microbiol.* **2019**, *17* (4), 203–218. https://doi.org/10.1038/s41579-018-0147-4.

(8) Tieu, W.; Jarrad, A. M.; Paparella, A. S.; Keeling, K. A.; Soares Da Costa, T. P.; Wallace, J. C.; Booker, G. W.; Polyak, S. W.; Abell, A. D. Heterocyclic Acyl-Phosphate Bioisostere-Based Inhibitors of Staphylococcus Aureus Biotin Protein Ligase. *Bioorganic Med. Chem. Lett.* **2014**, *24* (19), 4689–4693. https://doi.org/10.1016/j.bmcl.2014.08.030.

(9) Tieu, W.; Polyak, S. W.; Paparella, A. S.; Yap, M. Y.; Soares Da Costa, T. P.; Ng, B.; Wang, G.; Lumb, R.; Bell, J. M.; Turnidge, J. D.; Wilce, M. C. J.; Booker, G. W.; Abell, A. D. Improved Synthesis of Biotinol-5′-AMP: Implications for Antibacterial Discovery. *ACS Med. Chem. Lett.* **2015**, *6* (2), 216–220. https://doi.org/10.1021/ml500475n.

(10) Brown, P. H.; Cronan, J. E.; Grøtli, M.; Beckett, D. The Biotin Repressor: Modulation of Allostery by Corepressor Analogs. *J. Mol. Biol.* **2004**, *337* (4), 857–869. https://doi.org/10.1016/j.jmb.2004.01.041.

(11) Duckworth, B. P.; Geders, T. W.; Tiwari, D.; Boshoff, H. I.; Sibbald, P. A.; Barry, C. E.; Schnappinger, D.; Finzel, B. C.; Aldrich, C. C. Bisubstrate Adenylation Inhibitors of Biotin Protein Ligase from Mycobacterium Tuberculosis. *Chem. Biol.* **2011**, *18* (11), 1432–1441. https://doi.org/10.1016/j.chembiol.2011.08.013.

(12) Bockman, M. R.; Kalinda, A. S.; Petrelli, R.; De La Mora-Rey, T.; Tiwari, D.; Liu, F.; Dawadi, S.; Nandakumar, M.; Rhee, K. Y.; Schnappinger, D.; Finzel, B. C.; Aldrich, C. C. Targeting Mycobacterium Tuberculosis Biotin Protein Ligase (MtBPL) with Nucleoside-Based Bisubstrate Adenylation Inhibitors. *J. Med. Chem.* **2015**, *58* (18), 7349–7369. https://doi.org/10.1021/acs.jmedchem.5b00719.

(13) Satiaputra, J.; Shearwin, K. E.; Booker, G. W.; Polyak, S. W. Mechanisms of Biotin-Regulated Gene Expression in Microbes. *Synth. Syst. Biotechnol.* **2016**, *1* (1), 17–24. https://doi.org/10.1016/j.synbio.2016.01.005.

(14) McMahon, R. J. Biotin in Metabolism and Molecular Biology. *Annu. Rev. Nutr.* **2002**, *22*, 221–239. https://doi.org/10.1146/annurev.nutr.22.121101.112819.

(15) Polyak, S. W.; Abell, A. D.; Wilce, M. C. J.; Zhang, L.; Booker, G. W. Structure, Function and Selective Inhibition of Bacterial Acetyl-Coa Carboxylase. *Appl. Microbiol. Biotechnol.* **2012**, *93* (3), 983–992. https://doi.org/10.1007/s00253-011-3796-z.

(16) Pendini, N. R.; Yap, M. Y.; Polyak, S. W.; Cowieson, N. P.; Abell, A.; Booker, G. W.; Wallace, J. C.; Wilce, J. A.; Wilce, M. C. J. Structural Characterization of Staphylococcus Aureus Biotin Protein Ligase and Interaction Partners: An Antibiotic Target. *Protein Sci.* **2013**, *22* (6), 762–773. https://doi.org/10.1002/pro.2262.

(17) Sternicki, L. M.; Wegener, K. L.; Bruning, J. B.; Booker, G. W.; Polyak, S. W. Mechanisms Governing Precise Protein Biotinylation. *Trends Biochem. Sci.* **2017**, *42* (5), 383–394. https://doi.org/10.1016/j.tibs.2017.02.001.

(18) Soares Da Costa, T. P.; Tieu, W.; Yap, M. Y.; Pendini, N. R.; Polyak, S. W.; Pedersen, D. S.; Morona, R.; Turnidge, J. D.; Wallace, J. C.; Wilce, M. C. J.; Booker, G. W.; Abell, A. D. Selective Inhibition of Biotin Protein Ligase from Staphylococcus Aureus. *J. Biol. Chem.* **2012**, *287* (21), 17823–17832. https://doi.org/10.1074/jbc.M112.356576.

(19) Paparella, A. S.; Lee, K. J.; Hayes, A. J.; Feng, J.; Feng, Z.; Cini, D.; Deshmukh, S.; Booker, G. W.; Wilce, M. C. J.; Polyak, S. W.; Abell, A. D. Halogenation of Biotin Protein Ligase Inhibitors Improves Whole Cell Activity against Staphylococcus Aureus. *ACS Infect. Dis.* **2018**, *4* (2), 175–184. https://doi.org/10.1021/acsinfecdis.7b00134.

(20) Feng, J.; Paparella, A. S.; Tieu, W.; Heim, D.; Clark, S.; Hayes, A.; Booker, G. W.; Polyak, S. W.; Abell, A. D. New Series of BPL Inhibitors To Probe the Ribose-Binding Pocket of Staphylococcus Aureus Biotin Protein Ligase. *ACS Med. Chem. Lett.* **2016**, *7* (12), 1068–1072. https://doi.org/10.1021/acsmedchemlett.6b00248.

(21) Stachura, D. L.; Nguyen, S.; Polyak, S. W.; Jovcevski, B.; Bruning, J. B.; Abell, A. D. A New 1,2,3-Triazole Scaffold with Improved Potency Against Staphylococcus Aureus Biotin Protein Ligase. **2022**, *8* (12), 2579–2585. https://doi.org/10.1021/acsinfecdis.2c00452.

SUPPORTING INFORMATION

S3.1: Biological Assay and Docking Protocols

***SaBPL Assay*:**

The inhibitory activity of compounds was determined by measuring *S. aureus* BPL (*Sa*BPL) activity in the presence of varying concentrations of compound (25.0, 5.0, 1.0, 0.2, 0.04 and 0.008 μM) using an *in vitro* biotinylation assay.[1] The expression and purification of *Sa*BPL for enzymatic assays was performed as described previously.[1] The absolute inhibition constants (K_i) for triazoles **8-13**, **15-19** were determined using from the respective IC_{50} against *Sa*BPL,[2] with the K_i for triazole **14** calculated using the Morrison equation,[3] as detailed previously[1].

***Antibacterial Activity Evaluation*:**

Antibacterial activity was determined by a microdilution broth method as recommended by the CLSI (Clinical and Laboratory Standards Institute, Document M07-A8, 2009, Wayne, PA) using cation adjusted Mueller-Hinton broth (Trek Diagnostics Systems, U.K.). Compounds were dissolved in DMSO. Serial 2-fold dilutions of each compound were made using DMSO as the diluent. Trays were inoculated with 5×10^4 CFU of each strain in a volume of 100 μL (final concentration of DMSO was 3.2% (v/v)) and incubated at 35 °C for 16−20 h. Growth of the bacterium was quantified by measuring the absorbance at 620 nm.

Docking Studies:

Docking experiments were performed using ICM software version 3.8−7c (Molsoft L.L.C., San Diego, CA, USA). Proteins for docking were retrieved from RCSB Protein Data Bank (PDB = 6APW[4], 8ENI). Then, formal charges were assigned; protonation states of histidines were adjusted, and hydrogens, histidine, glutamine, and asparagine were optimized using the protein preparation procedure implemented in ICM.[5] The original bound ligand and all water molecules were removed from the binding site before docking. The binding site was defined as the cavity delimited by residues with at least one nonhydrogen atom within a 4.0 Å cutoff radius from the ligand **4** or **27**. The pocket was represented by 0.5 Å grid maps accounting for hydrogen bonding, hydrophobic, van der Waals, and electrostatic interactions. The molecules were flexibly docked into the rigid binding site and scored based on the ICM scoring function.

S3.2: Figures S1 – S17

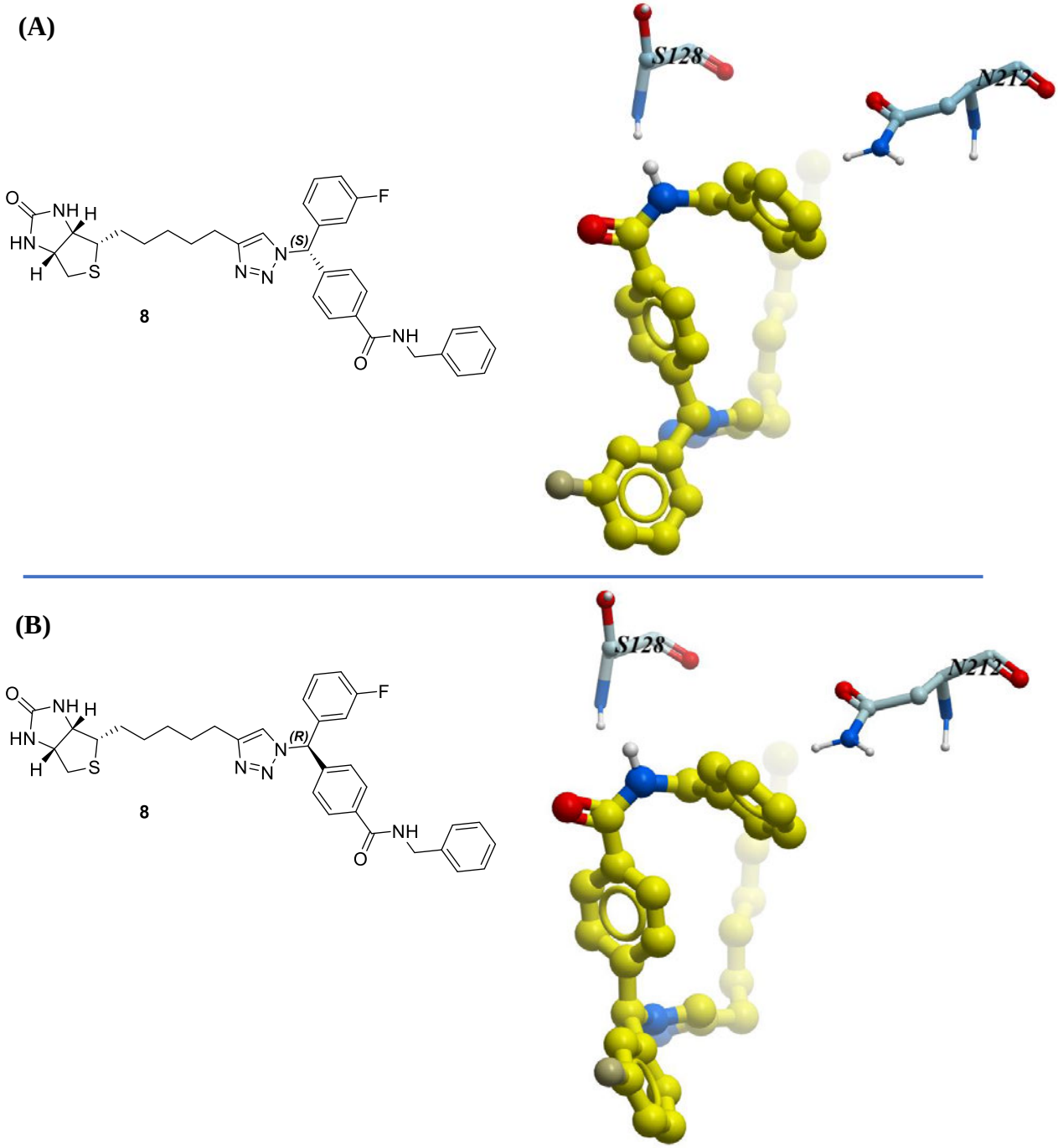

Figure S1: Predicted binding conformation of the *S* (**A**) and *R* (**B**) diastereomers of **8** within the adenine binding site of *Sa*BPL (PDB: 6APW[4]).

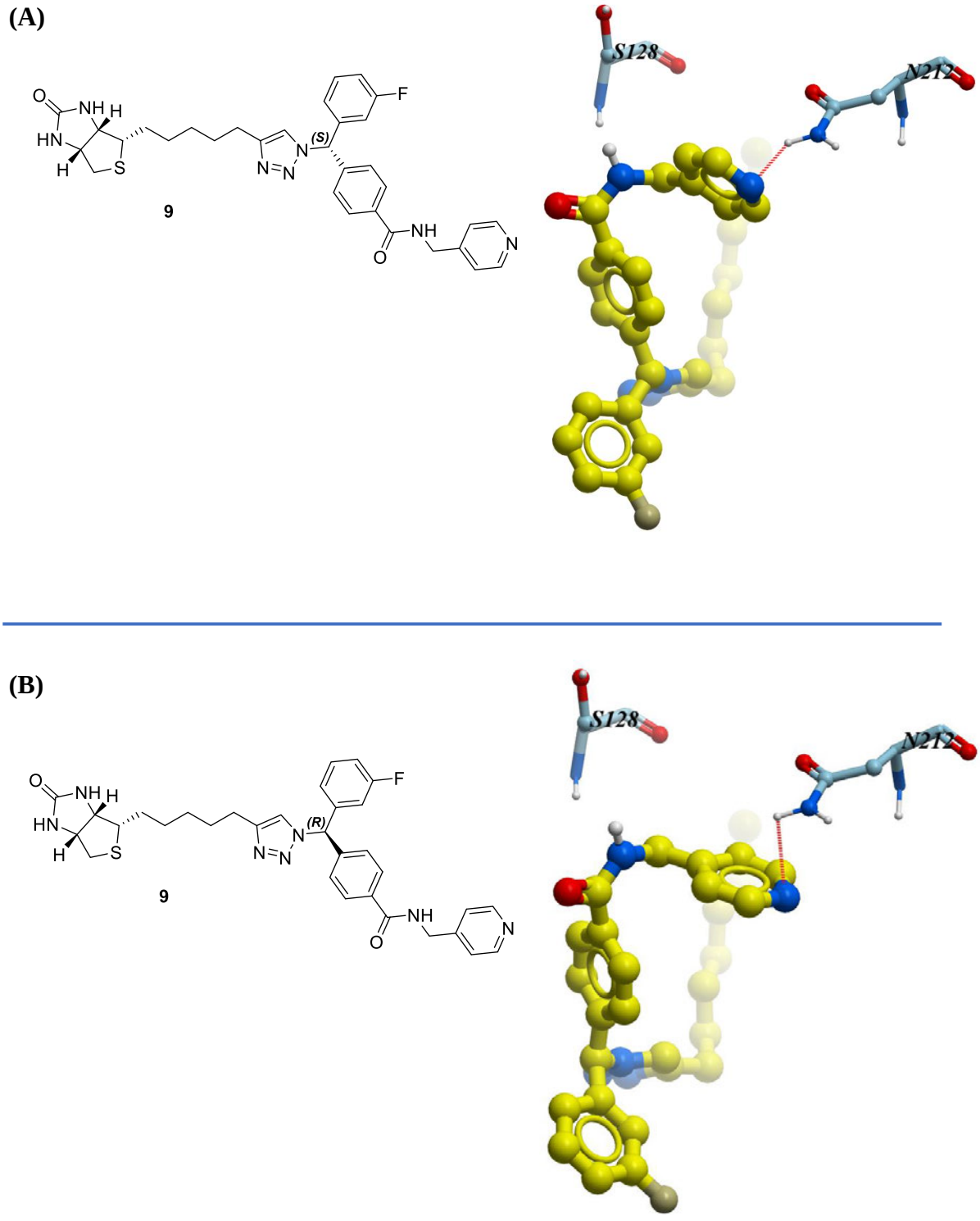

Figure S2: Predicted binding conformation of the *S* (**A**) and *R* (**B**) diastereomers of **9** within the adenine binding site of *Sa*BPL (PDB: 6APW[4]). Predicted interactions are highlighted as red-dashed lines.

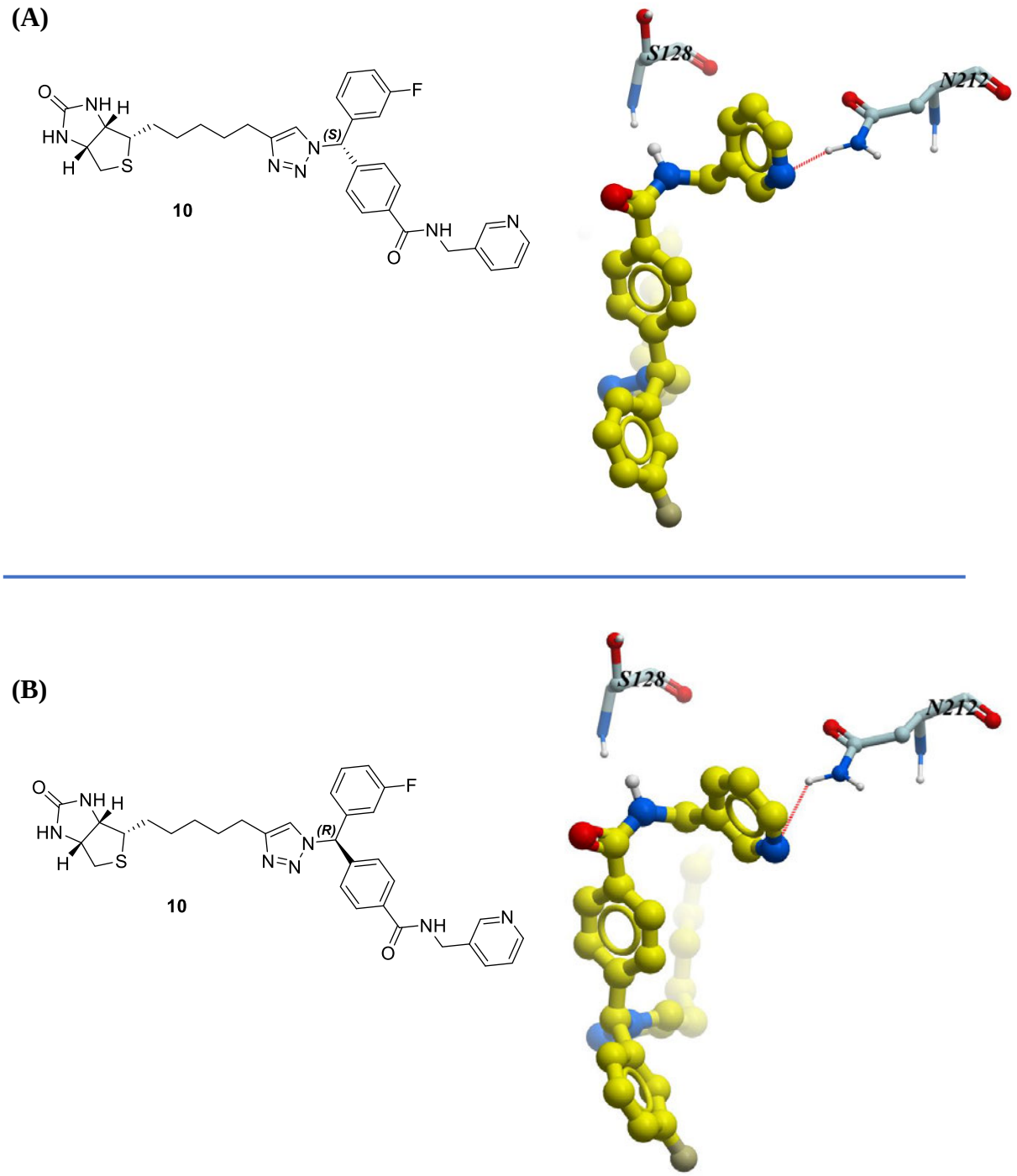

Figure S3: Predicted binding conformation of the *S* (**A**) and *R* (**B**) diastereomers of **10** within the adenine binding site of *Sa*BPL (PDB: 6APW[4]). Predicted interactions are highlighted as red-dashed lines.

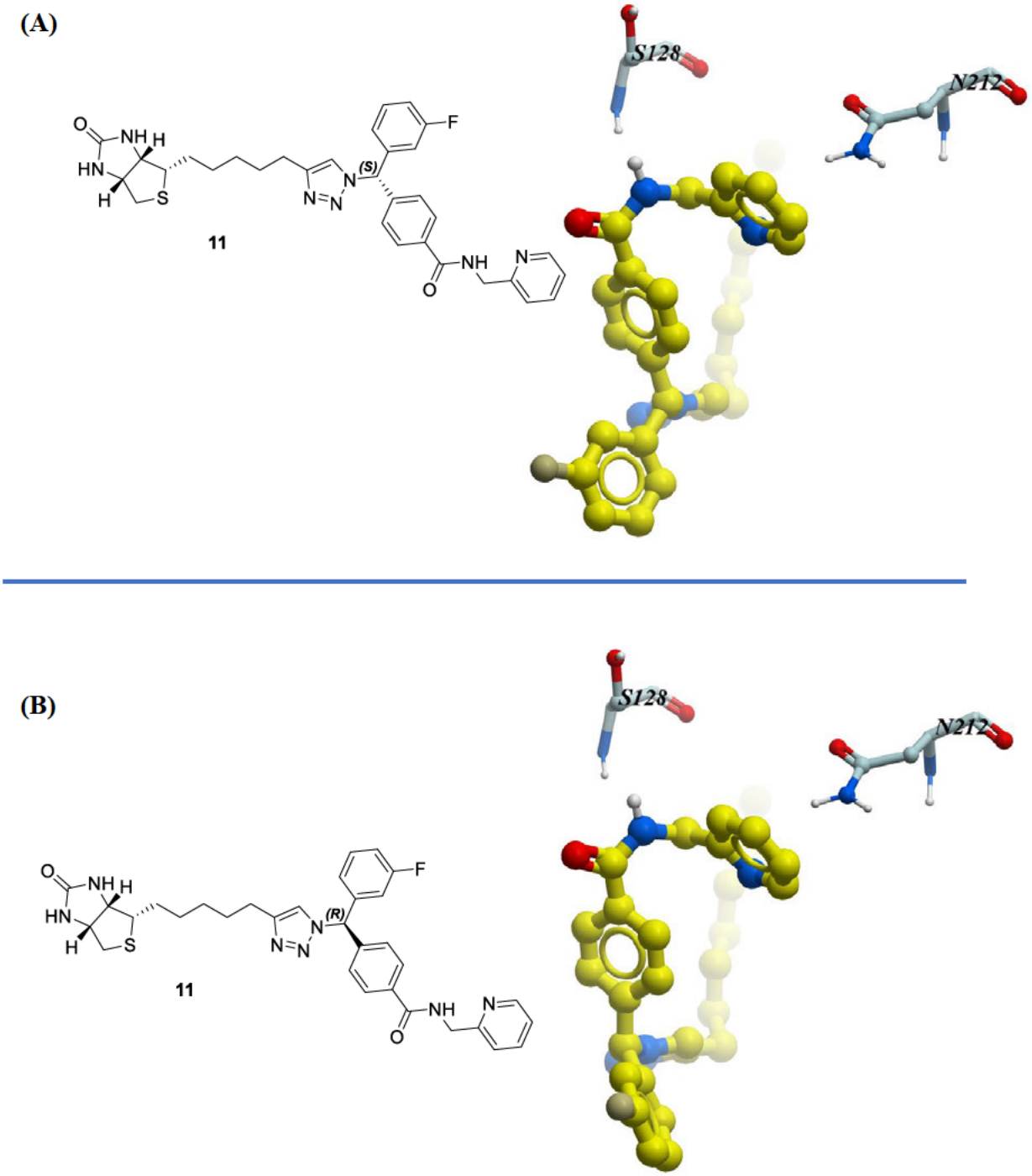

Figure S4: Predicted binding conformation of the *S* (**A**) and *R* (**B**) diastereomers of **11** within the adenine binding site of *Sa*BPL (PDB: 6APW[4]).

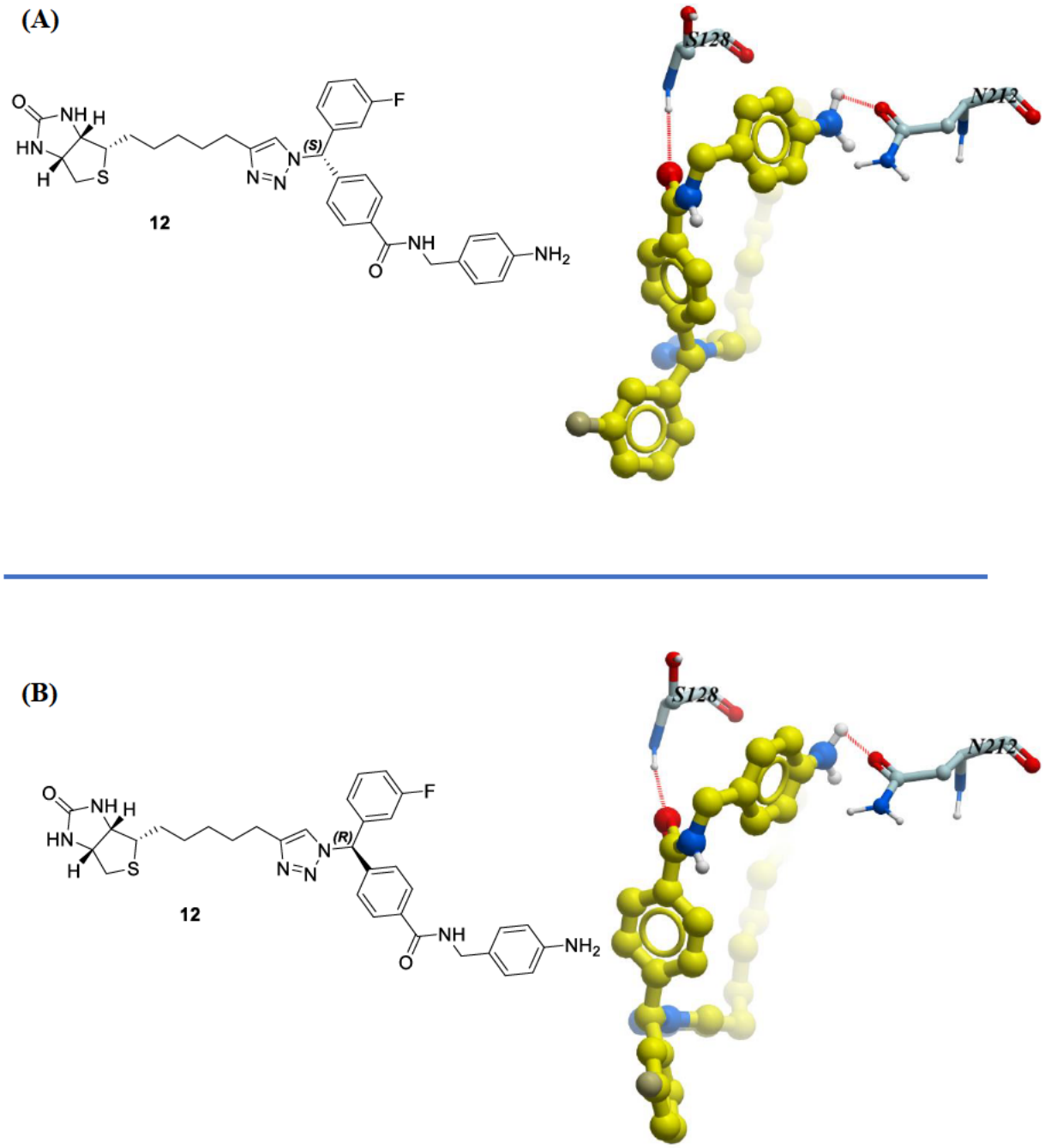

Figure S5: Predicted binding conformation of the *S* (**A**) and *R* (**B**) diastereomers of **12** within the adenine binding site of *Sa*BPL (PDB: 6APW[4]). Predicted hydrogen bonds are highlighted as red-dashed lines.

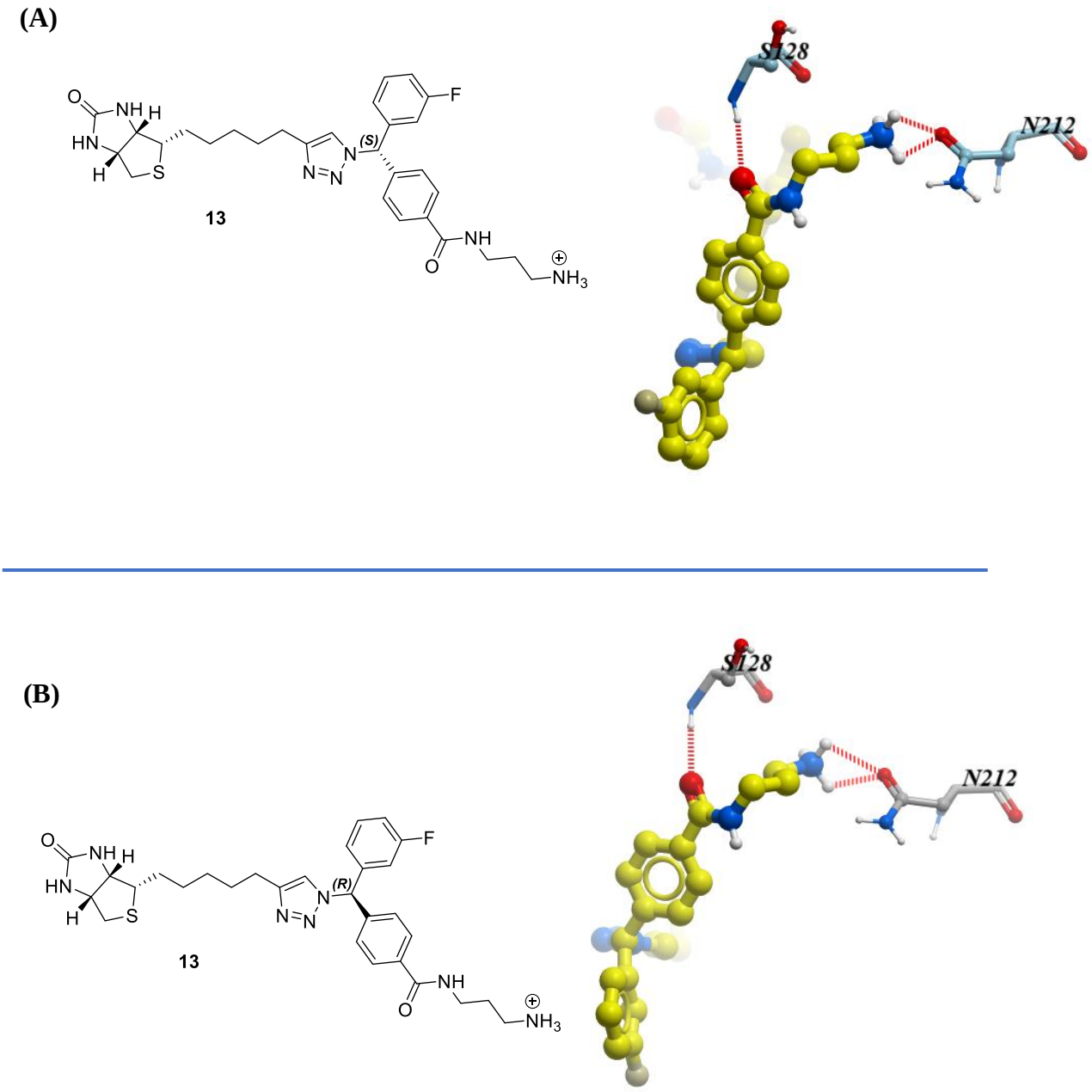

Figure S6: Predicted binding conformation of the *S* (**A**) and *R* (**B**) diastereomers of the ammonium form of **13** within the adenine binding site of *Sa*BPL (PDB: 6APW[4]). Predicted hydrogen bonds are highlighted as red-dashed lines.

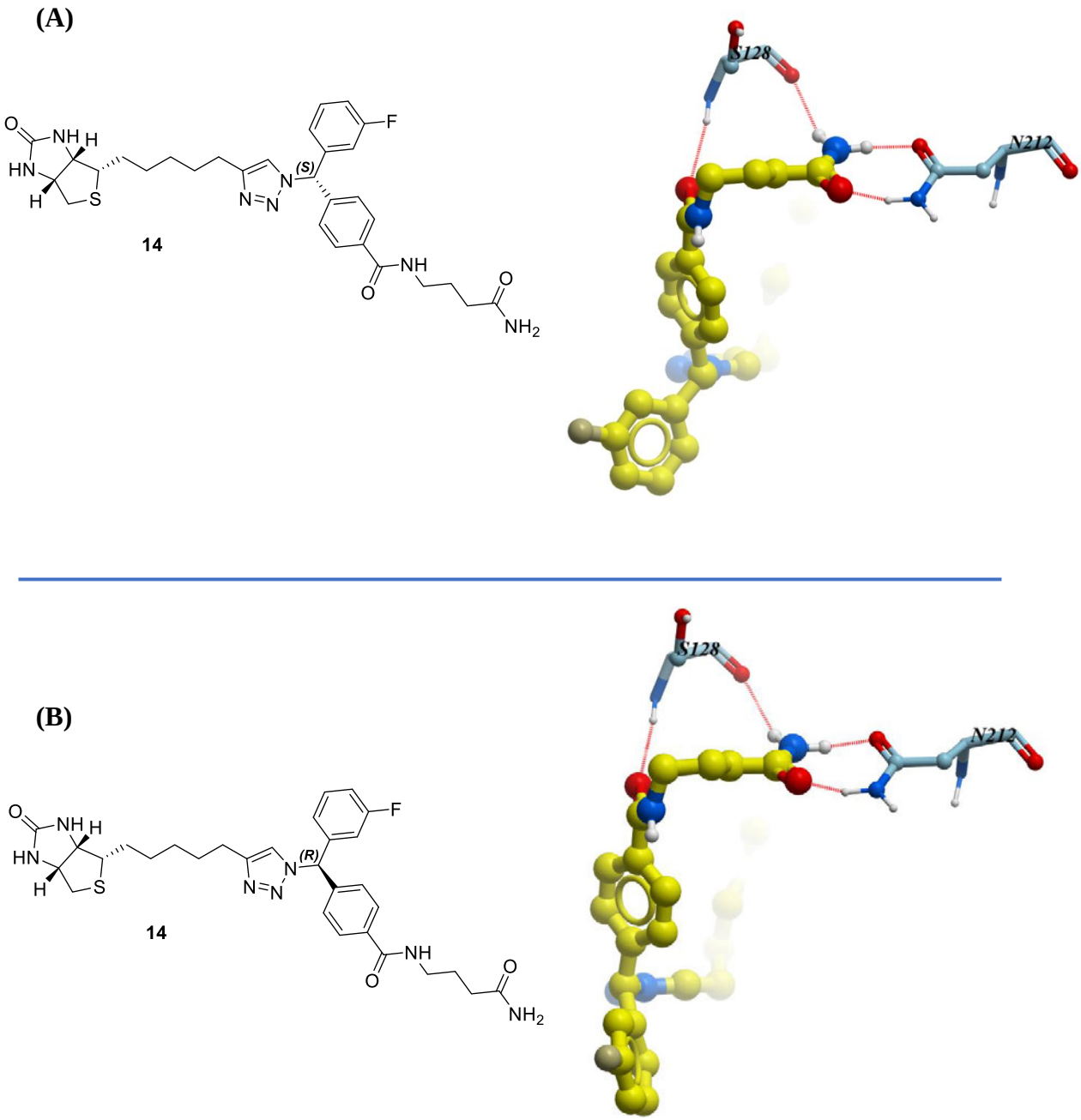

Figure S7: Predicted binding conformation of the *S* (**A**) and *R* (**B**) diastereomers of **14** within the adenine binding site of *Sa*BPL (PDB: 6APW[4]). Predicted hydrogen bonds are highlighted as red-dashed lines.

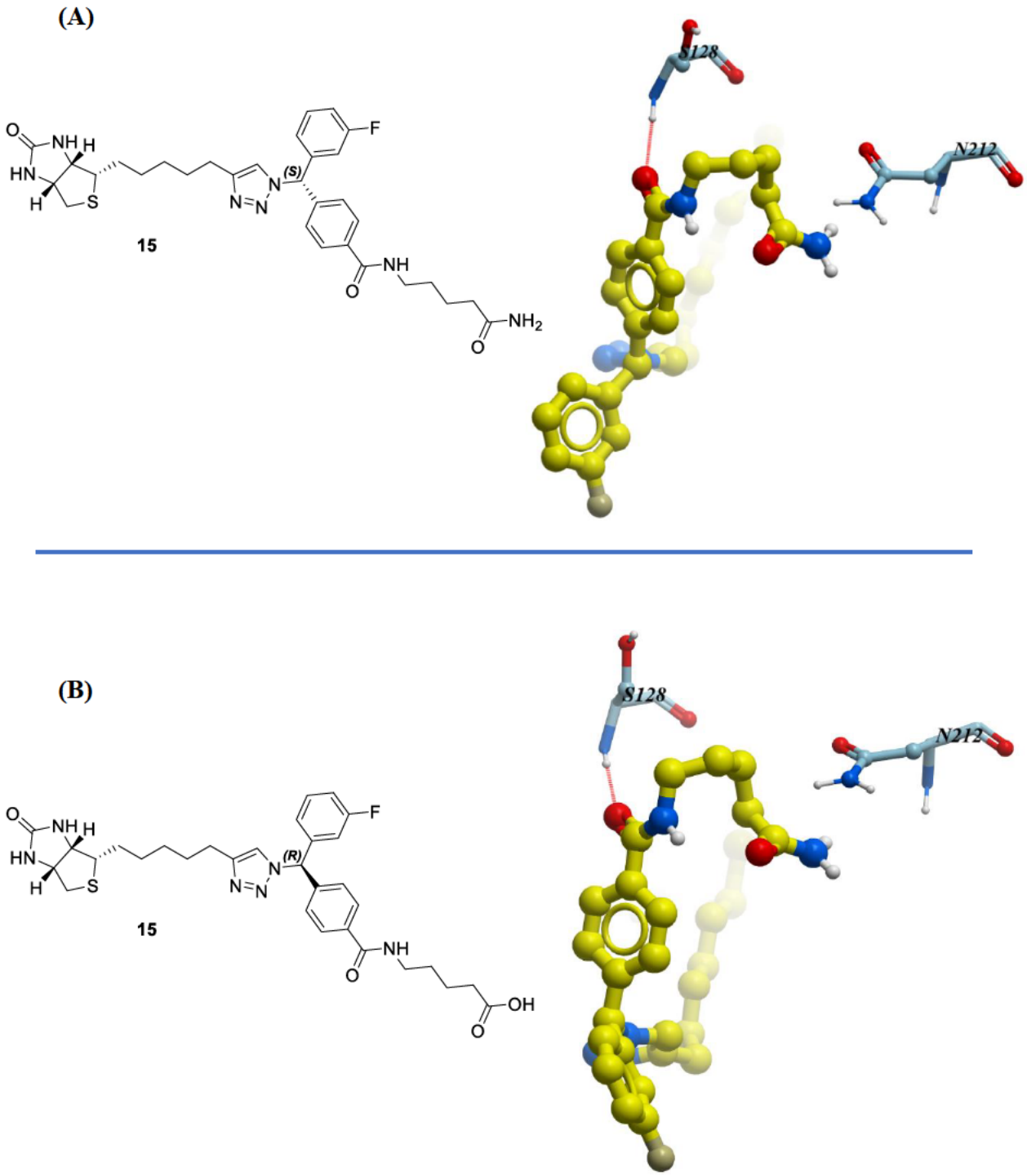

Figure S8: Predicted binding conformation of the *S* (**A**) and *R* (**B**) diastereomers of **15** within the adenine binding site of *Sa*BPL (PDB: 6APW[4]). Predicted hydrogen bonds are highlighted as red-dashed lines.

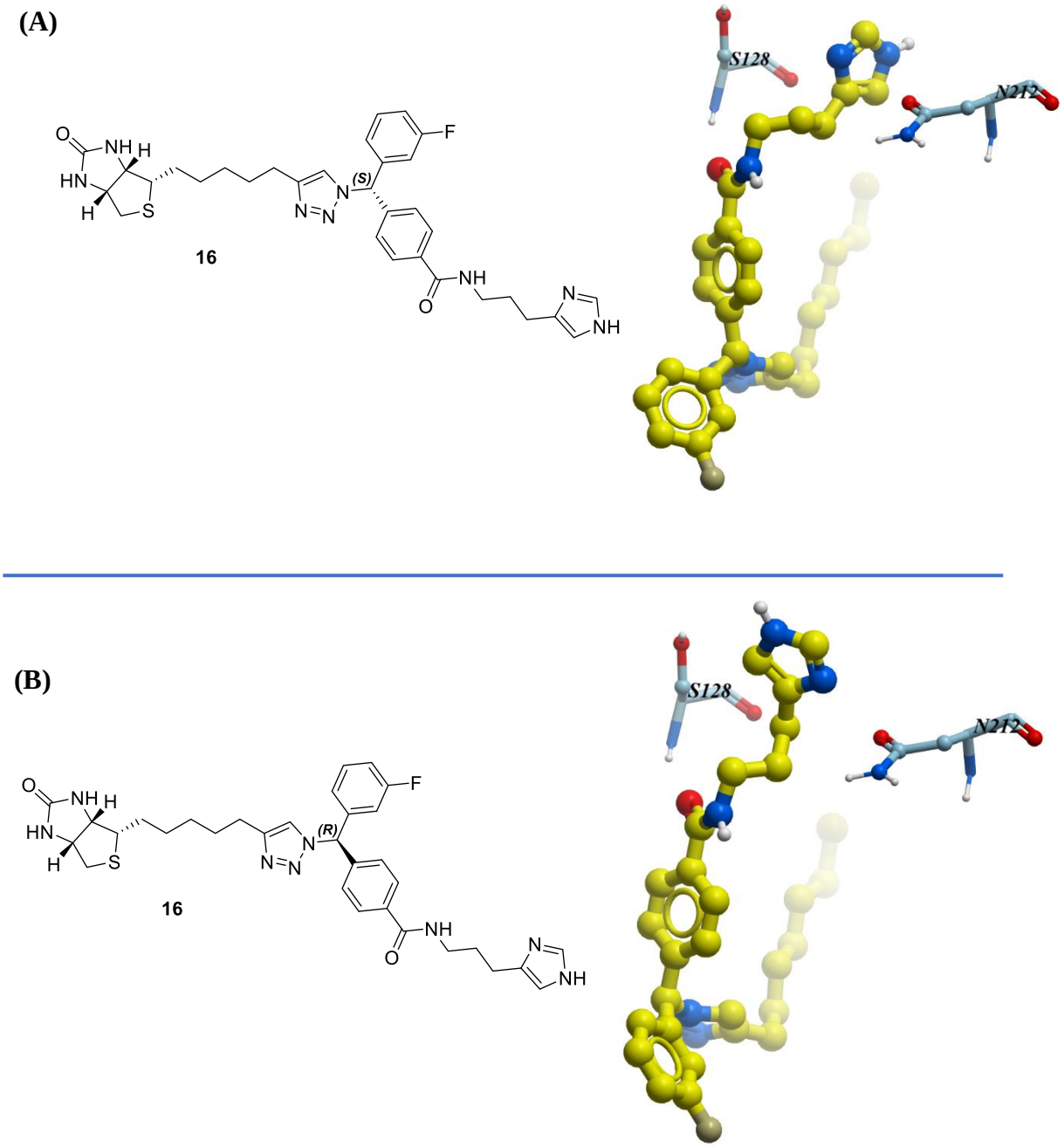

Figure S9: Predicted binding conformation of the *S* (**A**) and *R* (**B**) diastereomers of **16**within the adenine binding site of *Sa*BPL (PDB: 6APW[4]). Predicted hydrogen bonds are highlighted as red-dashed lines.

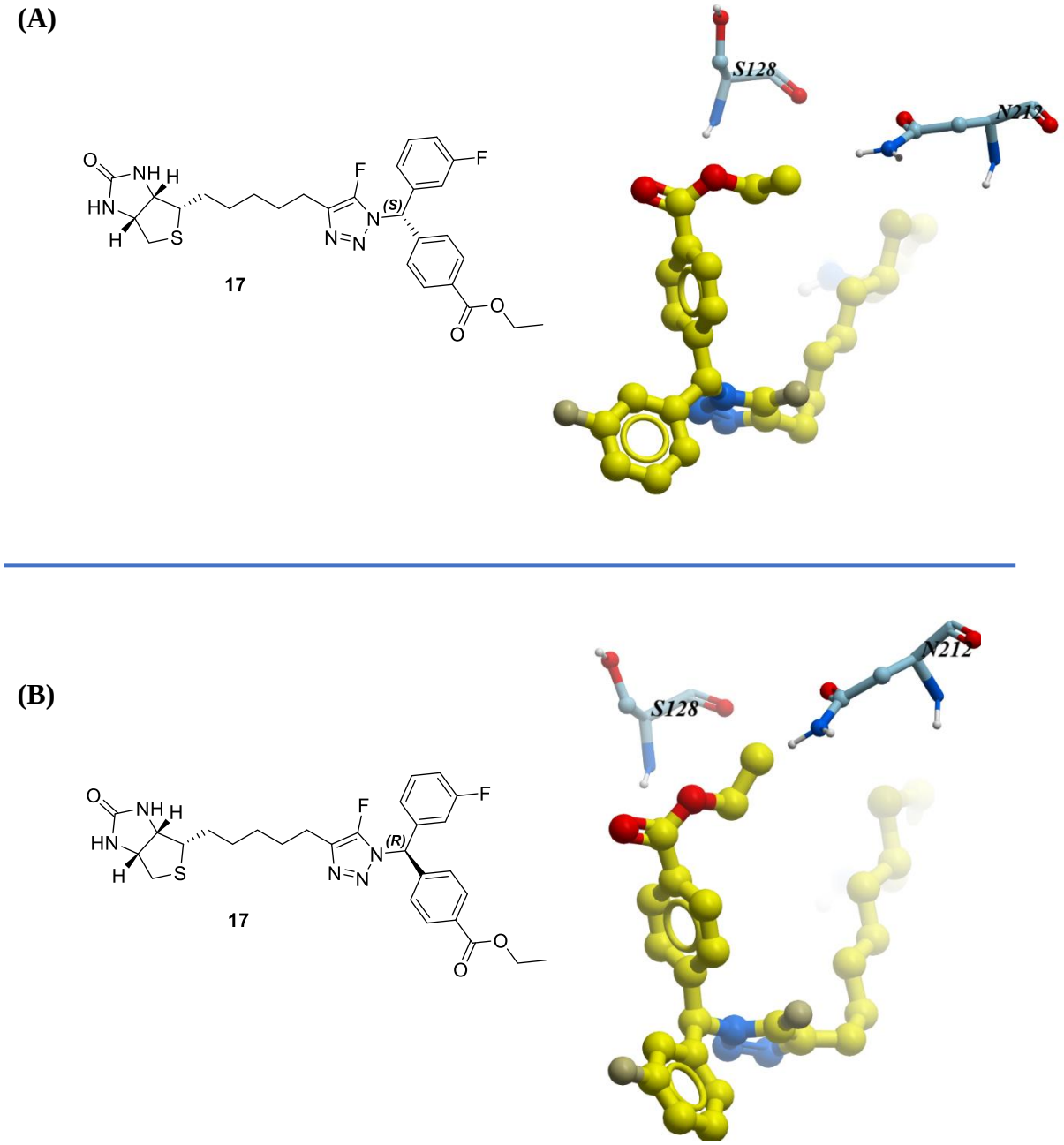

Figure S10: Predicted binding conformation of the *S* (**A**) and *R* (**B**) diastereomers of **17** within the adenine binding site of *Sa*BPL (PDB: 6APW[4]). Predicted hydrogen bonds are highlighted as red-dashed lines.

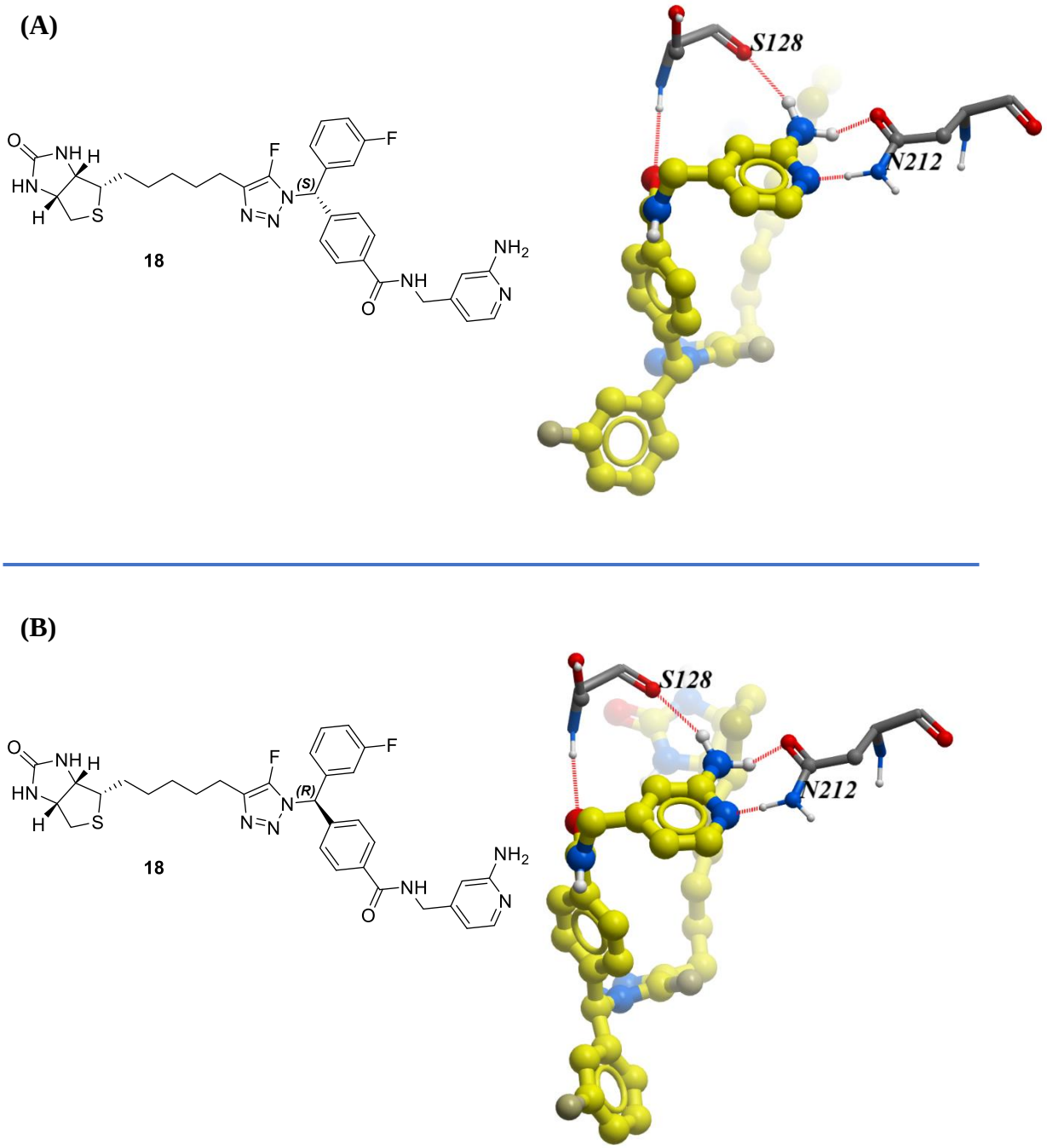

Figure S11: Predicted binding conformation of the *S* (**A**) and *R* (**B**) diastereomers of **18** within the adenine binding site of *Sa*BPL (**PDB: 6APW**[4]). Predicted hydrogen bonds are highlighted as red-dashed lines.

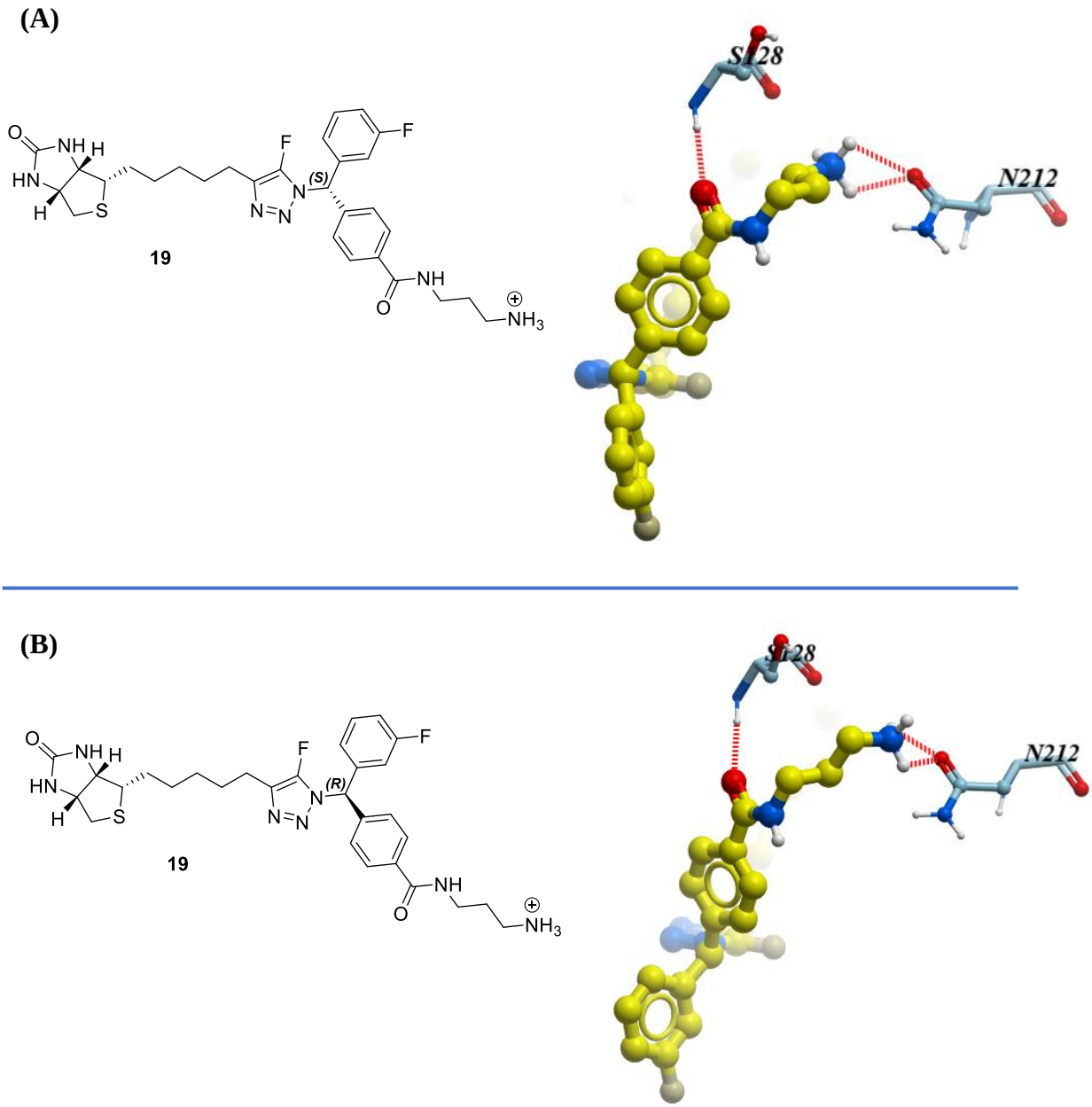

Figure S12: Predicted binding conformation of the *S* (**A**) and *R* (**B**) diastereomers of the ammonium form of **19** within the adenine binding site of *Sa*BPL (PDB: 6APW[4]). Predicted hydrogen bonds are highlighted as red-dashed lines.

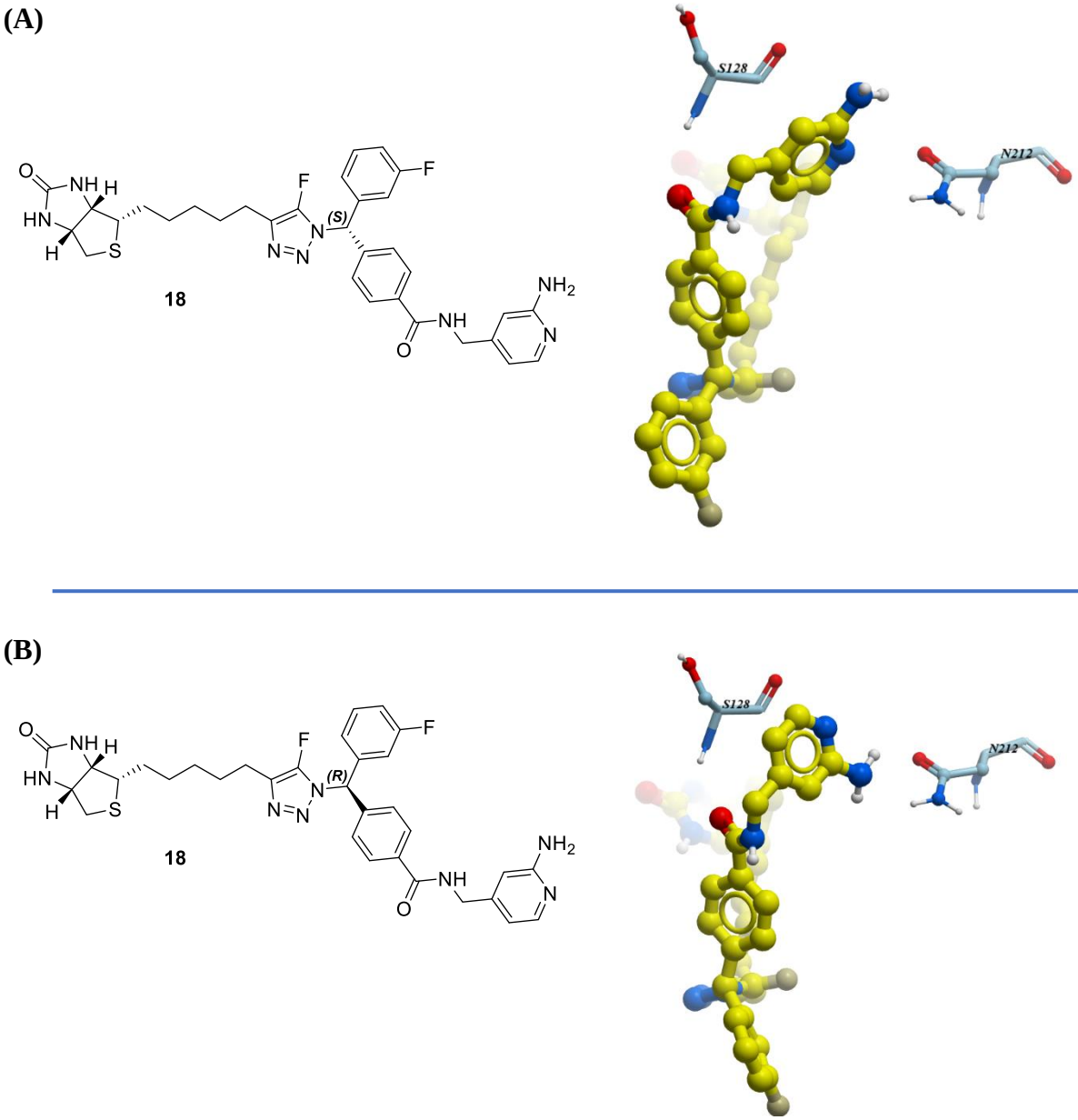

Figure S13: Predicted binding conformation of the *S* (**A**) and *R* (**B**) diastereomers of **18** within the adenine binding site of *Sa*BPL (**PDB: 8ENI**[4]).

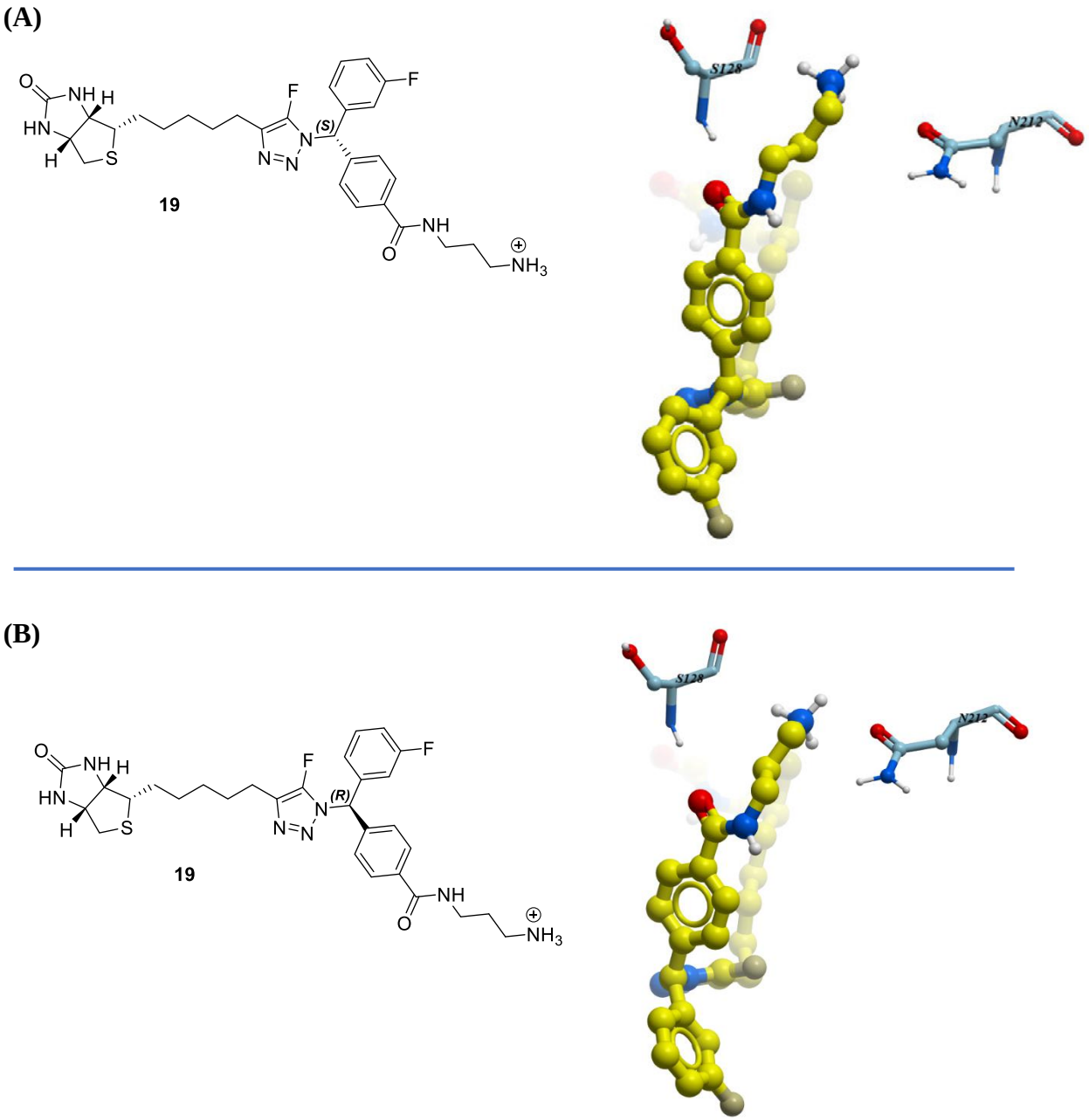

Figure S14: Predicted binding conformation of the *S* (**A**) and *R* (**B**) diastereomers of **19** within the adenine binding site of *Sa*BPL (**PDB: 8ENI**[4]).

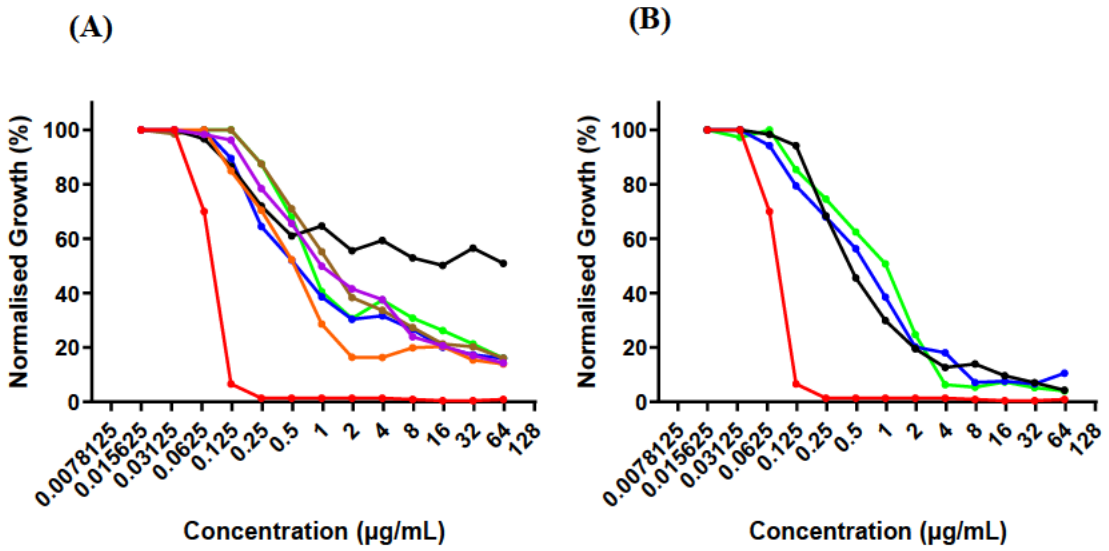

Figure S15: Inhibition growth of *S.aureus* growth *in vitro*. All compounds shown are from the same test plate and are divided into two plots for clarity. (**A**) Compounds **8** (black), **9** (green), **10** (blue), **11** (brown), **12** (purple) **15** (orange), and erythromycin (red) were tested against *S.aureus* ATCC 49775. (**B**) Compounds **13** (blue), **14** (green), **16** (black) and erythromycin (red) were tested against *S.aureus* ATCC 49775.

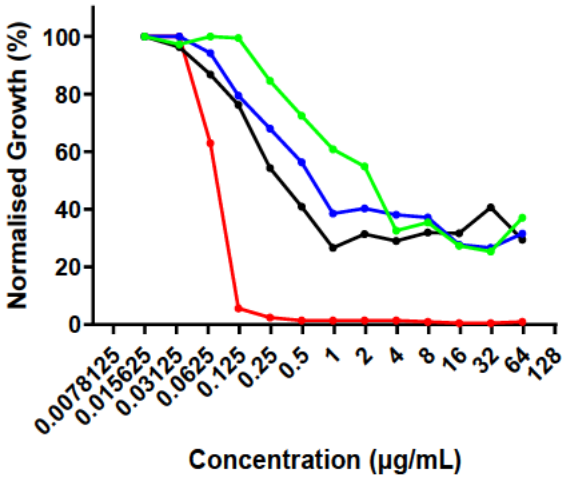

Figure S16: Inhibition growth of *S.aureus* growth *in vitro*. Compounds **17** (black), **18** (green), **19** (blue), and erythromycin (red) were tested against *S.aureus* ATCC 49775.

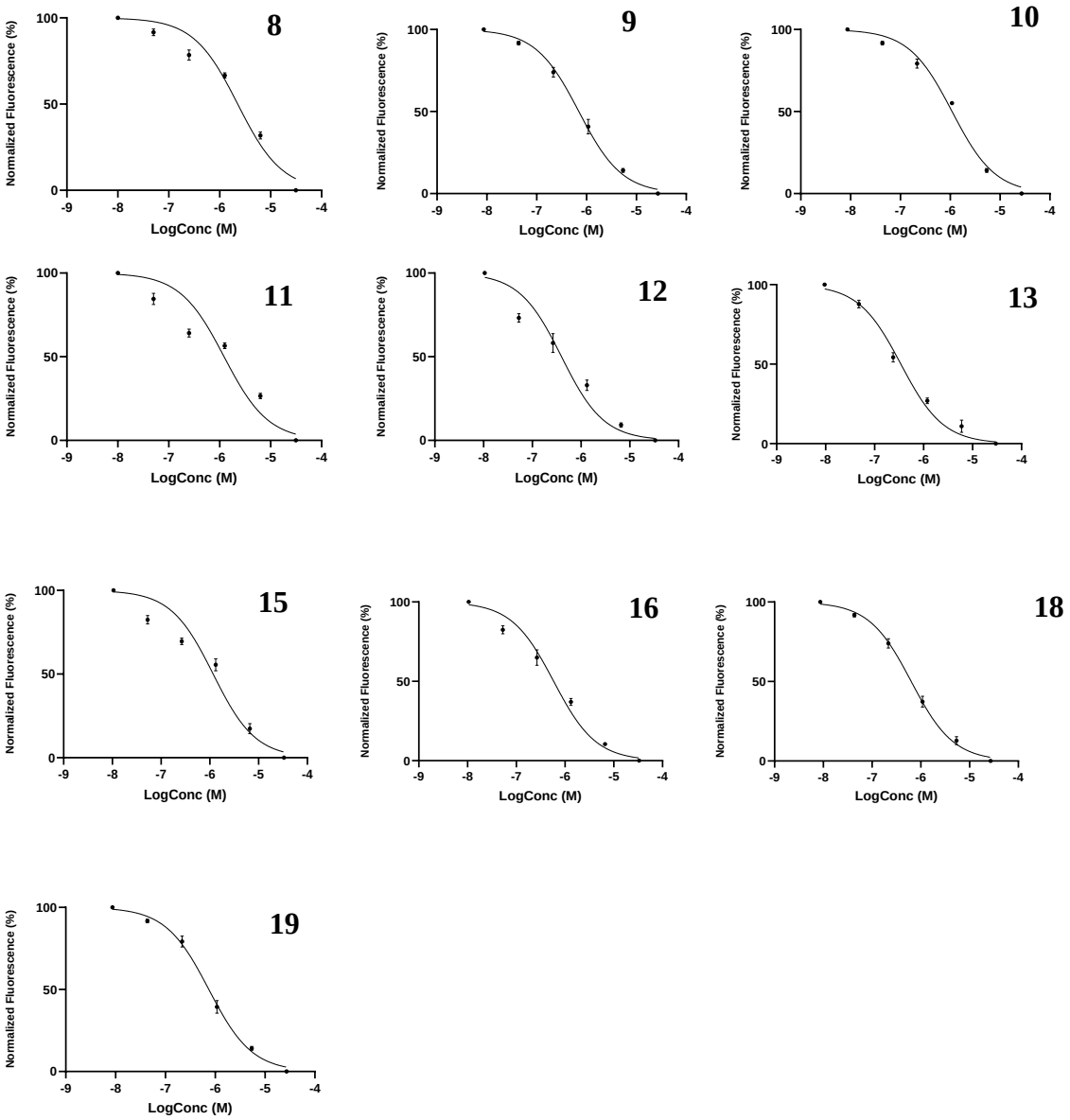

Figure S17: Normalized representative dose-response semi-log plots for triazoles **8 – 13**, **15**, **16**, **18** and **19** assayed against *Sa*BPL. Y axis = Normalized Fluorescence, X axis = LogConc (M).

S3.3: Synthetic Procedures

Chemistry: general Materials and Methods

All reagents were obtained from commercial sources and are of reagent grade or as specified. Solvents were also obtained from commercial sources, except for anhydrous THF and anhydrous DMF that were dried over solvent purifier (PS-Micro, Innovative Technology, USA). Reactions were monitored by TLC using precoated plates (silica gel 60 F254, 250 μm, Merck, Darmstadt, Germany), spots were visualised under ultraviolet light at 254 nm and with either sulfuric acid-vanillin spray, potassium permanganate dip or Hanessian's stain. Column chromatography was performed with silica gel (40-63 μm 60 Å, Davisil, Grace, Germany). ^{1}H and ^{13}C spectra were recorded on a Varian Inova 500 MHz or a Varian Inova 600 MHz. Chemical shifts are given in ppm (δ) relative to the residue signals, which in the case of DMSO-d_6 were 2.50 ppm for ^{1}H and 39.55 ppm for ^{13}C, and $CDCl_3$ were 7.26 ppm for ^{1}H and 77.23 ppm for ^{13}C. High-resolution mass spectra (HRMS) were recorded on an Agilent 6230 time of flight (TOF) liquid chromatography mass spectra (LC/MS) ($\Delta < 5$ ppm). All final compounds (**8**–**19**) used for biological assays were determined to be >95% pure by ^{1}H NMR. No unexpected or unusually high safety hazards were encountered.

General procedure 3A: *Amide linkage formation*: Amine (1 eq) was added to a solution of carboxylic acid (1 eq), HATU (1.1 eq), and DIPEA (4 eq) in DMF (1 mL per 1 eq of carboxylic acid), and the resultant reaction mixture was stirred for 16 h. The reaction mixture was diluted with conc. NH_4Cl (10 mL per 1 mL DMF), extracted with EtOAc, washed with water, brine, dried over Na_2SO_4, filtered, and concentrated *in vacuo*. See individual experiments for details

N-benzyl-4-((3-fluorophenyl)(4-(5-((3a*S*,4*S*,6a*R*)-2-oxohexahydro-1*H*-thieno[3,4-*d*]imidazol-4-yl)pentyl)-1*H*-1,2,3-triazol-1-yl)methyl)benzamide (**8**)

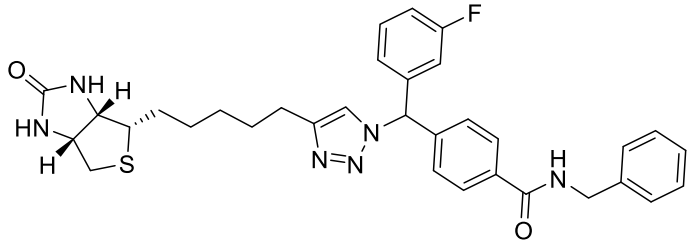

Benzylamine (0.005 g, 0.038 mmol) was reacted with carboxylic acid **20**[1] according to **general procedure 3A**, and was purified by flash chromatography on silica gel eluting with DCM/MeOH (v/v = 15:1) to give **8** as a white solid (0.012 g, 50 %); **^{1}H NMR** (500 MHz,

DMSO-d_6) δ 9.05 (t, *J* = 6.0 Hz, 1H), 7.92 – 7.89 (m, 3H), 7.46 (td, *J* = 8.0, 6.2 Hz, 1H), 7.33 (d, *J* = 8.8 Hz, 2H), 7.32 – 7.29 (m, 5H), 7.25 – 7.19 (m, 2H), 7.09 – 7.06 (m, 1H), 7.05 – 7.02 (m, 1H), 6.40 (s, 1H), 6.33 (s, 1H), 4.48 (d, *J* = 6.0 Hz, 2H), 4.31 – 4.26 (m, 1H), 4.14 – 4.08 (m, 1H), 3.12 – 3.04 (m, 1H), 2.80 (dd, *J* = 12.4, 5.1 Hz, 1H), 2.62 (t, *J* = 7.6 Hz, 2H), 2.57 (d, *J* = 12.5 Hz, 1H), 1.63 – 1.32 (m, 8H); **^{13}C NMR** (126 MHz, DMSO-d_6) δ 165.64, 163.07, 162.67, 161.12, 147.14, 141.37, 141.26, 141.20, 139.52, 134.24, 130.90, 130.83, 128.24, 127.89, 127.70, 127.13, 126.70, 124.21, 124.19, 122.13, 115.28, 115.12, 115.00, 114.82, 65.43, 61.03, 59.16, 55.49, 42.58, 39.78, 28.62, 28.57, 28.26, 28.17, 24.92; **HRMS** calcd. for (M + H^+) $C_{33}H_{36}FN_6O_2S^+$: requires 599.2599, found 599.2596.

4-((3-fluorophenyl)(4-(5-((3a*S*,4*S*,6a*R*)-2-oxohexahydro-1*H*-thieno[3,4-*d*]imidazol-4-yl)pentyl)-1*H*-1,2,3-triazol-1-yl)methyl)-*N*-(pyridin-4-ylmethyl)benzamide (**9**)

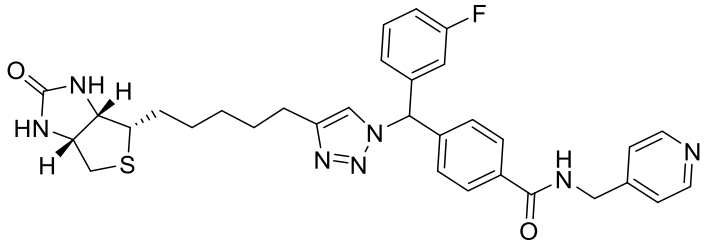

4-Picolyamine (0.005 g, 0.037 mmol) was reacted with carboxylic acid **20**[1] according to **general procedure 3A**, and was purified by flash chromatography on silica gel eluting with DCM/MeOH (v/v = 10:1) to give **9** as white solid (0.016 g, 73 %) **^{1}H NMR** (500 MHz, DMSO-d_6) δ 9.14 (t, *J* = 6.0 Hz, 1H), 8.51 – 8.46 (m, 2H), 7.95 – 7.89 (m, 3H), 7.46 (td, *J* = 8.0, 6.1 Hz, 1H), 7.36 – 7.26 (m, 4H), 7.26 – 7.18 (m, 1H), 7.08 (d, *J* = 8.0 Hz, 1H), 7.06 – 7.00 (m, 1H), 6.40 (s, 1H), 6.33 (s, 1H), 4.49 (d, *J* = 5.9 Hz, 2H), 4.32 – 4.26 (m, 1H), 4.13 – 4.10 (m, 1H), 3.12 – 3.05 (m, 1H), 2.80 (dd, *J* = 12.4, 5.1 Hz, 1H), 2.62 (t, *J* = 7.6 Hz, 2H), 2.57 (d, *J* = 12.4 Hz, 1H), 1.64 – 1.56 (m, 3H), 1.48 – 1.29 (m, 5H); **^{13}C NMR** (125 MHz, DMSO-d_6) δ 165.94, 163.07, 162.67, 161.13, 149.49, 148.44, 147.15, 141.59, 141.23, 141.17, 133.91, 130.91, 130.85, 127.96, 127.75, 124.23, 124.21, 122.14, 122.05, 115.30, 115.13, 115.01, 114.83, 65.43, 61.04, 59.16, 55.49, 54.87, 41.71, 39.78, 28.62, 28.57, 28.26, 28.17, 24.92; **HRMS** calcd. for (M + H^+) $C_{32}H_{35}FN_7O_2S^+$: requires 600.2551 found 600.2549.

4-((3-fluorophenyl)(4-(5-((3a*S*,4*S*,6a*R*)-2-oxohexahydro-1*H*-thieno[3,4-*d*]imidazol-4-yl)pentyl)-1*H*-1,2,3-triazol-1-yl)methyl)-*N*-(pyridin-3-ylmethyl)benzamide (**10**)

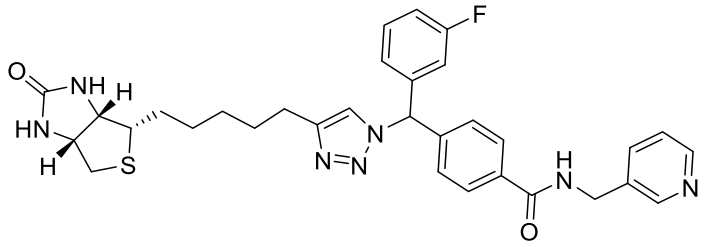

3-Picolyamine (0.005 g, 0.037 mmol) was reacted with carboxylic acid **20**[1] according to **general procedure 3A**, and was purified by flash chromatography on silica gel eluting with DCM/MeOH (v/v = 10:1) to give **10** as white solid (0.020 g, 91 %) **^{1}H NMR** (500 MHz, DMSO-d_6) δ 9.12 (t, *J* = 6.0 Hz, 1H), 8.56 – 8.52 (m, 1H), 8.47 – 8.43 (m, 1H), 7.92 (s, 1H), 7.90 (d, *J* = 8.4 Hz, 2H), 7.73 – 7.68 (m, 1H), 7.46 (td, *J* = 8.1, 6.1 Hz, 1H), 7.37 – 7.32 (m, 2H), 7.30 (d, *J* = 8.4 Hz, 2H), 7.22 (td, *J* = 8.6, 2.5 Hz, 1H), 7.09 – 7.05 (m, 1H), 7.05 – 7.00 (m, 1H), 6.42 (s, 1H), 6.35 (s, 1H), 4.49 (d, *J* = 5.9 Hz, 2H), 4.32 – 4.26 (m, 1H), 4.14 – 4.08 (m, 1H), 3.11 – 3.05 (m, 1H), 2.80 (dd, *J* = 12.4, 5.1 Hz, 1H), 2.62 (t, *J* = 7.6 Hz, 2H), 2.57 (d, *J* = 12.4 Hz, 1H), 1.61 – 1.58 (m, 3H), 1.48 – 1.28 (m, 5H); **^{13}C NMR** (125 MHz, DMSO-d_6) δ 165.83, 162.93, 162.71, 161.30, 148.79, 148.09, 147.17, 141.53, 141.25, 141.20, 135.08, 134.98, 134.02, 130.93, 130.88, 127.95, 127.75, 124.25, 124.24, 123.47, 122.17, 115.31, 115.18, 115.02, 114.87, 65.43, 61.05, 59.18, 55.53, 40.42, 28.65, 28.60, 28.30, 28.20, 24.95; **HRMS** calcd. for (M + H$^+$) $C_{32}H_{35}FN_7O_2S^+$: requires 600.2551 found 600.2550.

4-((3-fluorophenyl)(4-(5-((3a*S*,4*S*,6a*R*)-2-oxohexahydro-1*H*-thieno[3,4-*d*]imidazol-4-yl)pentyl)-1*H*-1,2,3-triazol-1-yl)methyl)-*N*-(pyridin-2-ylmethyl)benzamide (**11**)

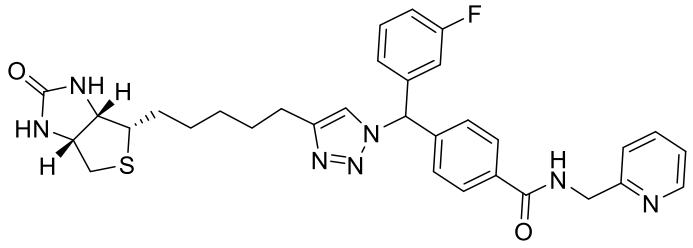

2-Picolyamine (0.005 g, 0.037 mmol) was reacted with carboxylic acid **20**[1]according to **general procedure 3A**, and was purified by flash chromatography on silica gel eluting with DCM/MeOH (v/v = 9:1) to give **11** as white solid (0.020 g, 91 %); **^{1}H NMR** (600 MHz, DMSO-d_6) δ 9.14 (t, *J* = 6.0 Hz, 1H), 8.52 – 8.48 (m, 1H), 7.96 – 7.91 (m, 3H), 7.74 (td, *J* = 7.7, 1.8

Hz, 1H), 7.47 (td, *J* = 8.0, 6.1 Hz, 1H), 7.35 (s, 1H), 7.34 – 7.28 (m, 3H), 7.28 – 7.23 (m, 1H), 7.26 – 7.19 (m, 1H), 7.10 – 7.06 (m, 1H), 7.06 – 7.01 (m, 1H), 6.42 (s, 1H), 6.35 (s, 1H), 4.56 (d, *J* = 5.9 Hz, 2H), 4.32 – 4.26 (m, 1H), 4.14 – 4.08 (m, 1H), 3.11 – 3.05 (m, 1H), 2.80 (dd, *J* = 12.5, 5.1 Hz, 1H), 2.62 (t, *J* = 7.6 Hz, 2H), 2.57 (d, *J* = 12.4 Hz, 1H), 1.65 – 1.55 (m, 2H), 1.49 – 1.29 (m, 6H); **^{13}C NMR** (150 MHz, DMSO-d_6) δ 165.82, 162.94, 162.71, 161.31, 158.67, 148.84, 147.18, 141.51, 141.27, 141.22, 136.70, 134.10, 130.94, 130.89, 127.96, 127.78, 124.26, 124.24, 122.18, 122.08, 120.88, 115.32, 115.18, 115.02, 114.87, 65.45, 65.44, 61.05, 59.18, 55.53, 44.69, 40.06, 28.65, 28.61, 28.30, 28.20, 24.95; **HRMS** calcd. for (M + H^+) $C_{32}H_{35}FN_7O_2S^+$: requires 600.2551 found 600.2554

N-(4-aminobenzyl)-4-((3-fluorophenyl)(4-(5-((3a*S*,4*S*,6a*R*)-2-oxohexahydro-1*H*-thieno[3,4-*d*]imidazol-4-yl)pentyl)-1*H*-1,2,3-triazol-1-yl)methyl)benzamide (**12**)

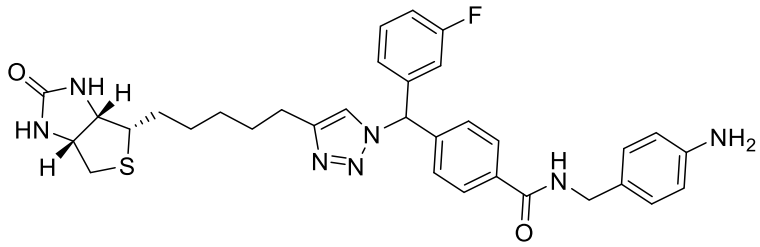

4-Aminobenzylamine hydrochloride (0.005 g, 0.041 mmol) was reacted with carboxylic acid **20**[1]according to **general procedure 3A**, and was purified by flash chromatography on silica gel eluting with DCM/MeOH (v/v = 9:1) to give **12** as a light-yellow solid (0.023 g, 93 %); **^{1}H NMR** (600 MHz, DMSO-d_6) δ 8.86 (t, *J* = 6.0 Hz, 1H), 7.91 (s, 1H), 7.88 (d, *J* = 8.5 Hz, 2H), 7.46 (td, *J* = 8.0, 6.1 Hz, 1H), 7.33 (s, 1H), 7.28 (d, *J* = 8.5 Hz, 2H), 7.22 (td, *J* = 8.6, 2.6 Hz, 1H), 7.09 – 7.05 (m, 1H), 7.05 – 7.00 (m, 1H), 6.96 (d, *J* = 8.3 Hz, 2H), 6.50 (d, *J* = 8.3 Hz, 2H), 6.42 (s, 1H), 6.35 (s, 1H), 4.93 (s, 2H), 4.32 – 4.27 (m, 3H), 4.14 – 4.08 (m, 1H), 3.11 – 3.05 (m, 1H), 2.80 (dd, *J* = 12.4, 5.1 Hz, 1H), 2.61 (t, *J* = 7.6 Hz, 2H), 2.57 (d, *J* = 12.4 Hz, 1H), 1.60 – 1.57 (m, 2H), 1.47 – 1.28 (m, 6H); **^{13}C NMR** (150 MHz, DMSO-d_6) δ 165.36, 162.93, 162.71, 161.30, 147.50, 147.17, 141.30, 141.25, 141.22, 134.51, 130.92, 130.87, 128.21, 127.85, 127.70, 126.41, 124.24, 124.22, 122.16, 115.30, 115.16, 115.01, 114.86, 113.67, 65.45, 65.44, 61.06, 59.18, 55.53, 54.92, 42.34, 28.65, 28.61, 28.30, 28.20, 24.95. ; **HRMS** calcd. for (M + H^+) $C_{33}H_{37}FN_7O_2S^+$: requires 614.2708 found 614.2712.

N-(3-aminopropyl)-4-((3-fluorophenyl)(4-(5-((3a*S*,4*S*,6a*R*)-2-oxohexahydro-1*H*-thieno[3,4-*d*]imidazol-4-yl)pentyl)-1*H*-1,2,3-triazol-1-yl)methyl)benzamide (**13**)

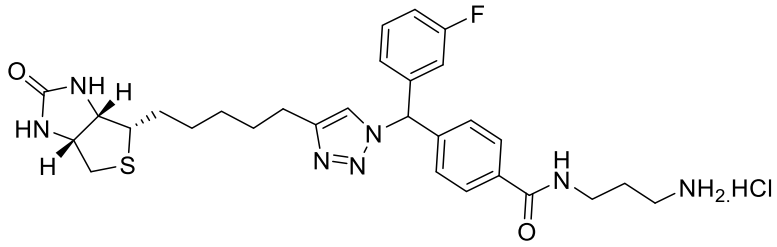

Triazole **21** (0.013 g, 0.019 mmol) was treated with 1 M HCl in dioxane (1 mL) for 1 h at rt. The solvent was removed *in vacuo* to afford **13** as a white solid, which was used without further purification (0.011 g, 99 %); ^{1}H NMR (500 MHz, D_2O) δ 7.76 (d, *J* = 7.9 Hz, 2H), 7.68 (s, 1H), 7.37 – 7.30 (m, 1H), 7.23 (d, *J* = 7.9 Hz, 2H), 7.18 (s, 1H), 7.10 – 7.03 (m, 1H), 7.00 – 6.95 (m, 1H), 6.92 – 6.86 (m, 1H), 4.52 – 4.48 (m, 1H), 4.28 – 4.25 (m, 1H), 3.50 (t, *J* = 6.7 Hz, 2H), 3.12 – 3.06 (m, 3H), 2.86 – 2.80 (m, 1H), 2.68 (d, *J* = 13.0 Hz, 1H), 2.64 – 2.60 (m, 2H), 2.04 – 1.98 (m, 2H), 1.62 – 1.38 (m, 5H), 1.29 – 1.16 (m, 3H); **^{13}C NMR** (126 MHz, d_2o) δ 172.28, 167.79, 164.28, 150.98, 143.72, 142.13, 136.33, 133.57, 133.51, 130.91, 130.39, 126.74, 126.00, 118.50, 118.31, 117.62, 69.45, 69.19, 64.69, 62.79, 58.04, 42.35, 39.75, 39.34, 32.24, 30.68, 30.46, 30.41, 29.44, 26.91; **HRMS** calcd. for (M + H^+) $C_{29}H_{37}FN_7O_2S^+$: requires 566.2708 found 566.2704.

N-(4-amino-4-oxobutyl)-4-((3-fluorophenyl)(4-(5-((3a*S*,4*S*,6a*R*)-2-oxohexahydro-1*H*-thieno[3,4-*d*]imidazol-4-yl)pentyl)-1*H*-1,2,3-triazol-1-yl)methyl)benzamide (**14**)

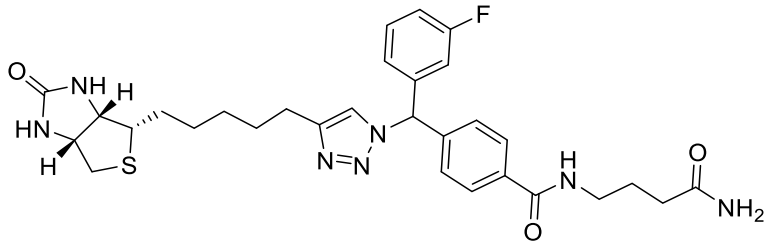

4-aminobutanamide hydrochloride (0.005 g, 0.036 mmol) was reacted with carboxylic acid **20**[1] according to **general procedure 3A**, and was purified by flash chromatography on silica gel eluting with DCM:MeOH (v/v = 6:1) to give **14** as white solid (0.016 g, 76%);**^{1}H NMR** (600 MHz, DMSO-d_6) δ 8.51 (t, *J* = 5.6 Hz, 1H), 7.92 (s, 1H), 7.84 (d, *J* = 8.4 Hz, 1H), 7.46 (td, *J* = 8.0, 6.1 Hz, 1H), 7.33 (s, 1H), 7.28 (d, *J* = 8.3 Hz, 3H), 7.22 (td, *J* = 8.6, 2.6 Hz, 1H), 7.07 (d, *J* = 8.7 Hz, 1H), 7.05 – 7.00 (m, 1H), 6.74 (s, 1H), 6.42 (s, 1H), 6.35 (s, 1H), 4.32 – 4.27 (m, 1H), 4.14 – 4.09 (m, 1H), 3.24 (q, *J* = 6.6 Hz, 2H), 3.13 – 3.05 (m, 1H), 2.80 (dd, *J* = 12.4, 5.1

Hz, 1H), 2.62 (t, *J* = 7.6 Hz, 2H), 2.57 (d, *J* = 12.4 Hz, 1H), 2.09 (t, *J* = 7.4 Hz, 2H), 1.72 (p, *J* = 7.3 Hz, 2H), 1.63 – 1.56 (m, 3H), 1.48 – 1.30 (m, 5H); **^{13}C NMR** (150 MHz, DMSO-d_6) δ 174.01, 165.61, 162.93, 162.71, 161.30, 147.17, 141.30, 141.25, 141.18, 134.58, 130.93, 130.87, 127.83, 127.62, 124.24, 124.22, 122.16, 115.30, 115.16, 115.00, 114.85, 65.45, 65.43, 61.06, 59.18, 55.53, 54.92, 32.62, 28.69, 28.66, 28.61, 28.30, 28.20, 25.06, 24.95; **HRMS** calcd. for (M + H^+) $C_{30}H_{36}FN_7O_3S^+$: requires 593.2579 found 594.2577.

N-(4-amino-4-oxopentyl)-4-((3-fluorophenyl)(4-(5-((3a*S*,4*S*,6a*R*)-2-oxohexahydro-1*H*-thieno[3,4-*d*]imidazol-4-yl)pentyl)-1*H*-1,2,3-triazol-1-yl)methyl)benzamide (**15**)

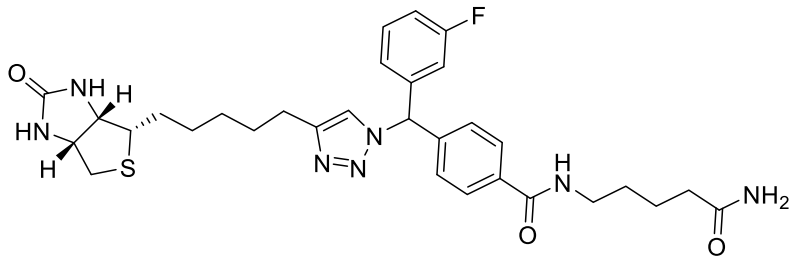

5-aminopentanamide hydrochloride (0.005 g, 0.036 mmol) was reacted with carboxylic acid **20**[1] according to **general procedure 3A**, and was purified by flash chromatography on silica gel eluting with DCM:MeOH (v/v = 8:1) to give **15** as white solid (0.018 g, 77 %);**^{1}H NMR** (600 MHz, DMSO-d_6) δ 8.48 (t, *J* = 5.7 Hz, 1H), 7.91 (s, 1H), 7.84 (d, *J* = 8.5 Hz, 2H), 7.46 (td, *J* = 8.0, 6.1 Hz, 1H), 7.33 (s, 1H), 7.28 (d, *J* = 8.4 Hz, 2H), 7.25 – 7.18 (m, 2H), 7.09 – 7.05 (m, 1H), 7.05 – 7.00 (m, 1H), 6.69 (s, 1H), 6.42 (s, 1H), 6.35 (s, 1H), 4.32 – 4.26 (m, 1H), 4.14 – 4.08 (m, 1H), 3.23 (q, *J* = 6.3 Hz, 2H), 3.11 – 3.05 (m, 1H), 2.80 (dd, *J* = 12.4, 5.1 Hz, 1H), 2.61 (t, *J* = 7.6 Hz, 2H), 2.57 (d, *J* = 12.4 Hz, 1H), 2.06 (t, *J* = 6.9 Hz, 2H), 1.62 – 1.57 (m, 3H), 1.52 – 1.46 (m, 5H), 1.41 – 1.29 (m, 4H); **^{13}C NMR** (150 MHz, DMSO-d_6) δ 174.18, 165.54, 162.93, 162.72, 161.31, 147.17, 141.31, 141.26, 141.15, 134.63, 130.93, 130.87, 127.83, 127.61, 124.25, 124.23, 122.16, 115.29, 115.16, 115.01, 114.86, 65.45, 61.06, 59.18, 55.53, 38.99, 34.77, 28.80, 28.65, 28.60, 28.30, 28.20, 24.95, 22.63; **HRMS** calcd. for (M + H^+) $C_{31}H_{39}FN_7O_3S^+$: requires 608.2814 found 608.2811

N-(3-(1*H*-imidazol-4-yl)propyl)-4-((3-fluorophenyl)(4-(5-((3a*S*,4*S*,6a*R*)-2-oxohexahydro-1*H*-thieno[3,4-*d*]imidazol-4-yl)pentyl)-1*H*-1,2,3-triazol-1-yl)methyl)benzamide (**16**)

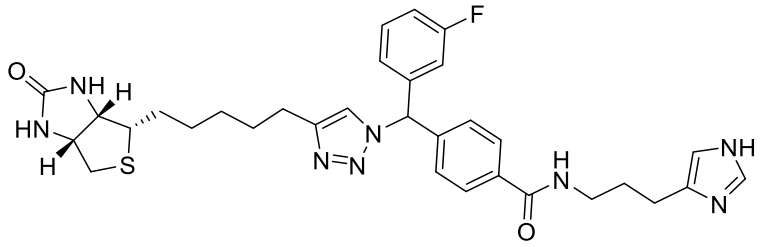

3(1*H*-imidazol-4-yl)propan-1-amine dihydrochloride (0.007 g, 0.035 mmol) was reacted with carboxylic acid **20**[1] according to **general procedure 3A**, and was purified by flash chromatography on silica gel eluting with DCM/MeOH (v/v = 5:1) to give **16** as white solid (0.012 g, 54 %); **^{1}H NMR** (600 MHz, DMSO-d_6) δ 8.58 (t, *J* = 5.6 Hz, 1H), 7.92 (s, 1H), 7.87 – 7.84 (m, 2H), 7.53 – 7.51 (m, 1H), 7.46 (td, *J* = 8.1, 6.1 Hz, 1H), 7.33 (s, 1H), 7.31 – 7.26 (m, 2H), 7.24 – 7.20 (m, 1H), 7.09 – 7.05 (m, 1H), 7.03 (dt, *J* = 9.9, 2.2 Hz, 1H), 6.76 (s, 1H), 6.42 (s, 1H), 6.36 (s, 1H), 4.32 – 4.27 (m, 1H), 4.12 – 4.09 (m, 1H), 3.30 – 3.25 (m, 2H), 3.10 – 3.06 (m, 1H), 2.80 (dd, *J* = 12.4, 5.1 Hz, 1H), 2.61 (t, *J* = 7.6 Hz, 2H), 2.57 (d, *J* = 12.4 Hz, 1H), 2.53 (t, *J* = 7.6 Hz, 2H), 1.79 (p, *J* = 7.3 Hz, 2H), 1.64 – 1.55 (m, 3H), 1.48 – 1.30 (m, 5H); **^{13}C NMR** (150 MHz, DMSO-d_6) δ 165.63, 162.93, 162.72, 161.30, 161.24, 147.16, 141.32, 141.27, 141.17, 134.61, 134.43, 130.93, 130.87, 127.84, 127.64, 124.25, 124.23, 122.17, 118.66, 115.29, 115.16, 115.01, 114.86, 110.36, 65.45, 65.44, 61.06, 59.18, 55.53, 54.92, 31.29, 28.99, 28.66, 28.60, 28.30, 28.20, 24.95, 22.09; **HRMS** calcd. for (M + H^+) $C_{32}H_{38}FN_8O_2S^+$: requires 617.2817 found 617.2823.

Ethyl-4-((5-fluoro-4-(5-((3a*S*,4*S*,6a*R*)-2-oxohexahydro-1*H*-thieno[3,4-*d*]imidazol-4-yl)pentyl)-1*H*-1,2,3-triazol-1-yl)(3-fluorophenyl)methyl)benzoate (**17**)

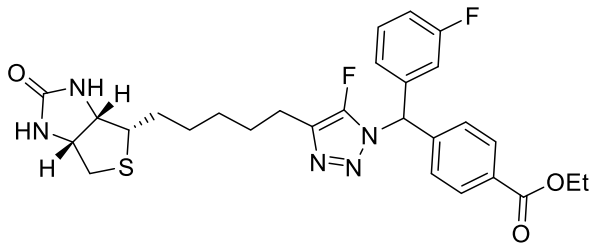

To a mixture of the 5-iodotriazole **24** (0.170 g, 0.34 mmol), and KF (0.074 g, 1.28 mmol) was added MeCN (1 mL), followed by water (1 mL). The reaction mixture was stirred for 60 s before being reacted in a microwave reactor (T = 180 °C, μλ = 300 W, P = 200 psi, t = 30 s). The resultant solution was extracted with EtOAc (4 x 5 mL), dried over Na_2SO_4, filtered,

concentrated *in vacuo*, and purified by silica gel flash chromatography eluting with DCM/MeOH (v/v = 20:1) to afford **17** as a white solid (0.105 g, 82 %); **^{1}H NMR** (500 MHz, $CDCl_3$) δ 8.06 (d, *J* = 8.1 Hz, 2H), 7.40 – 7.32 (m, 1H), 7.32 (d, *J* = 8.1 Hz, 2H), 7.11 – 7.04 (m, 1H), 7.05 – 6.98 (m, 1H), 6.97 – 6.92 (m, 1H), 6.78 (s, 1H), 5.36 (s, 1H), 5.04 (s, 1H), 4.52 – 4.45 (m, 1H), 4.38 (q, *J* = 7.0 Hz, 2H), 4.32 – 4.25 (m, 1H), 3.17 – 3.10 (m, 1H), 2.89 (dd, *J* = 12.8, 5.0 Hz, 1H), 2.71 (d, *J* = 12.7 Hz, 1H), 2.64 (t, *J* = 7.6 Hz, 2H), 1.76 – 1.58 (m, 4H), 1.50 – 1.35 (m, 7H); **^{13}C NMR** (126 MHz, $CDCl_3$) δ 165.99, 164.04, 163.44, 162.06, 151.38, 149.16, 141.15, 138.94, 138.88, 131.17, 130.78, 130.71, 130.30, 128.30, 128.28, 127.89, 127.81, 124.11, 124.08, 124.06, 116.19, 116.02, 115.76, 115.57, 64.86, 62.16, 61.37, 60.22, 55.75, 40.66, 29.17, 28.79, 28.67, 28.04, 23.67, 23.65, 14.43; **HRMS** calcd. for (M + H^+) $C_{28}H_{32}F_2N_5O_3S^+$: requires 556.2188 found 556.2191.

N-((2-aminopyridin-4-yl)methyl)-4-((5-fluoro-4-(5-((3a*S*,4*S*,6a*R*)-2-oxohexahydro-1*H*-thieno[3,4-*d*]imidazol-4-yl)pentyl)-1H-1,2,3-triazol-1-yl)(3-fluorophenyl)methyl)benzamide (**18**)

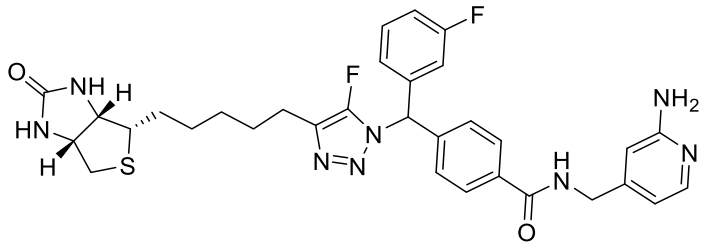

4-(aminomethyl)pyridine-2-amine hydrochloride (0.006 g, 0.049 mmol) was reacted with carboxylic acid **25** according to **general procedure 3A**, and was purified by flash chromatography on silica gel eluting with DCM/MeOH (v/v = 6:1) to give **18** as white solid (0.014 g, 45 %); **^{1}H NMR** (600 MHz, DMSO-d_6) δ 9.05 (t, *J* = 6.0 Hz, 1H), 7.93 (d, *J* = 8.5 Hz, 2H), 7.80 (d, *J* = 5.2 Hz, 1H), 7.48 (td, *J* = 7.7, 5.8 Hz, 1H), 7.37 (d, *J* = 8.4 Hz, 2H), 7.28 – 7.21 (m, 2H), 7.12 (d, *J* = 7.3 Hz, 1H), 6.43 – 6.41 (m, 1H), 6.41 – 6.39 (m, 1H), 6.35 (s, 1H), 6.32 (t, *J* = 1.2 Hz, 1H), 5.83 (s, 2H), 4.32 (d, *J* = 6.0 Hz, 2H), 4.32 – 4.26 (m, 1H), 4.14 – 4.08 (m, 1H), 3.11 – 3.05 (m, 1H), 2.80 (dd, *J* = 12.4, 5.1 Hz, 1H), 2.62 – 2.54 (m, 3H), 1.62 – 1.57 (m, 3H), 1.44 – 1.30 (m, 5H). **^{13}C NMR** (150 MHz, DMSO-d_6) δ 165.71, 162.90, 162.72, 161.27, 159.96, 150.76, 149.07, 148.91, 147.60, 140.05, 139.72, 139.67, 134.32, 131.01, 130.96, 128.03, 127.82, 126.86, 126.79, 124.33, 124.31, 115.59, 115.45, 115.23, 115.08, 110.63, 105.36, 62.79, 61.05, 59.18, 55.50, 54.92, 41.75, 40.06, 28.46, 28.21, 28.19, 27.59, 22.85, 22.83; **HRMS** calcd. for (M + H^+) $C_{32}H_{35}F_2N_8O_2S^+$: requires 633.2566 found 633.2574.

N-(3-aminopropyl)-4-((5-fluoro-4-(5-((3a*S*,4*S*,6a*R*)-2-oxohexahydro-1*H*-thieno[3,4-*d*]imidazol-4-yl)pentyl)-1*H*-1,2,3-triazol-1-yl)(3-fluorophenyl)methyl)benzamide (**19**)

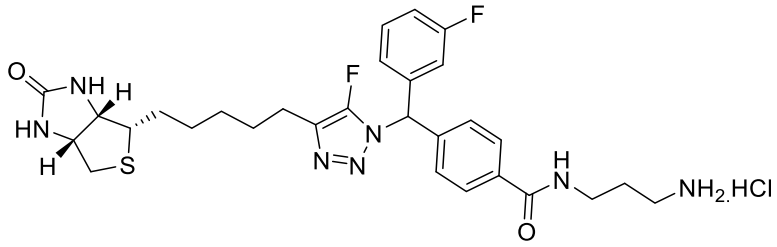

N-3-Boc-propyldiamine (0.006 g, 0.041 mmol) was reacted with carboxylic acid **25** according to **general procedure 3A** and was filtered through silica gel eluting with DCM:MeOH (v/v = 15:1). The filtrate was concentrated *in vacuo*, and the resulting solid was treated with 1M HCl in dioxane at rt for 1 h. The solvent was removed *in vacuo* to give **19** as a white solid (0.012 g, 77 % - 2 steps); **^{1}H NMR** (600 MHz, DMSO-d_6) δ 8.72 (t, *J* = 6.0, 3.0 Hz, 1H), 7.88 (d, *J* = 8.5 Hz, 2H), 7.86 – 7.82 (m, 3H), 7.48 (td, *J* = 8.2, 6.1 Hz, 1H), 7.35 (d, *J* = 8.4 Hz, 2H), 7.27 – 7.19 (m, 2H), 7.13 – 7.08 (m, 2H), 4.33 – 4.27 (m, 1H), 4.11 (dd, *J* = 7.7, 4.4 Hz, 1H), 3.33 (q, *J* = 6.5 Hz, 2H), 3.11 – 3.04 (m, 1H), 2.85 – 2.78 (m, 3H), 2.61 – 2.54 (m, 3H), 1.80 (p, *J* = 6.8 Hz, 2H), 1.66 – 1.55 (m, 3H), 1.48 – 1.39 (m, 1H), 1.39 – 1.26 (m, 4H); **^{13}C NMR** (150 MHz, DMSO-d_6) δ 166.01, 162.89, 162.74, 161.27, 150.76, 148.91, 139.97, 139.71, 139.66, 134.44, 131.00, 130.95, 127.96, 127.75, 126.85, 126.78, 124.35, 124.33, 115.59, 115.46, 115.24, 115.09, 72.17, 66.36, 62.78, 61.07, 59.20, 55.51, 43.62, 40.06, 36.80, 36.26, 34.14, 28.46, 28.22, 28.20, 27.58, 27.33, 22.84; **HRMS** calcd. for (M + H$^+$) $C_{29}H_{36}F_2N_7O_2S^+$: requires 584.2614 found 584.2620.

tert-butyl-(3-(4-((3-fluorophenyl)(4-(5-((3a*S*,4*S*,6a*R*)-2-oxohexahydro-1*H*-thieno[3,4-*d*]imidazol-4-yl)pentyl)-1*H*-1,2,3-triazol-1-yl)methyl)benzamido)propyl)carbamate (**21**)

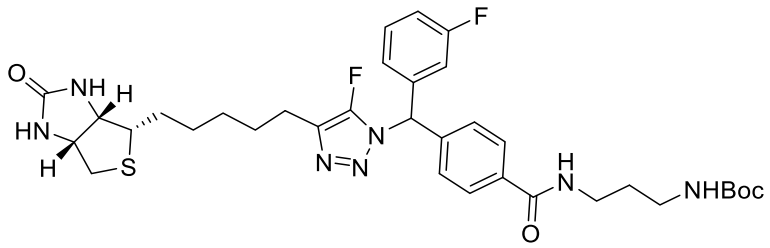

N-3-Boc-propyldiamine (0.032 g, 0.57 mmol) was reacted with carboxylic acid **20**[1] according to **general procedure 3A** and was purified by silica gel flash chromatography eluting with DCM/MeOH (v/v = 15:1) to give **21** as a white solid (0.039 g, 95 %); **^{1}H NMR** (600 MHz, DMSO-d_6) δ 8.45 (t, *J* = 5.7 Hz, 1H), 7.92 (s, 1H), 7.83 (d, *J* = 8.4 Hz, 2H), 7.46 (td, *J* = 8.1,

6.1 Hz, 1H), 7.33 (s, 1H), 7.28 (d, *J* = 8.4 Hz, 2H), 7.22 (td, *J* = 8.2, 2.2 Hz, 1H), 7.09 – 7.05 (m, 1H), 7.05 – 7.00 (m, 1H), 6.80 (t, *J* = 5.8 Hz, 1H), 6.42 (s, 1H), 6.35 (s, 1H), 4.32 – 4.26 (m, 1H), 4.14 – 4.08 (m, 1H), 3.24 (q, *J* = 6.7 Hz, 2H), 3.11 – 3.05 (m, 1H), 2.96 (q, *J* = 6.6 Hz, 2H), 2.80 (dd, *J* = 12.4, 5.1 Hz, 1H), 2.62 (t, *J* = 7.6 Hz, 2H), 2.57 (d, *J* = 12.4 Hz, 1H), 1.66 – 1.55 (m, *J* = 7.1 Hz, 6H), 1.49 – 1.40 (m, 1H), 1.36 (s, 9H), 1.35 – 1.28 (m, 3H); **^{13}C NMR** (150 MHz, DMSO-d_6) δ 165.62, 162.93, 162.71, 161.30, 155.58, 147.17, 141.30, 141.25, 141.22, 134.51, 130.92, 130.87, 127.86, 127.59, 124.24, 124.23, 122.15, 115.30, 115.16, 115.01, 114.86, 77.48, 65.44, 61.05, 59.18, 55.53, 54.91, 40.06, 37.70, 36.98, 29.54, 28.66, 28.61, 28.30, 28.25, 28.20, 24.95; **HRMS** calcd. for (M + H^+) $C_{34}H_{45}FN_7O_4S^+$: requires 666.3232 found 666.3227.

Ethyl-4-((3-fluorophenyl)(5-iodo-4-(5-((3a*S*,4*S*,6a*R*)-2-oxohexahydro-1*H*-thieno[3,4-*d*]imidazol-4-yl)pentyl)-1*H*-1,2,3-triazol-1-yl)methyl)benzoate (**24**)

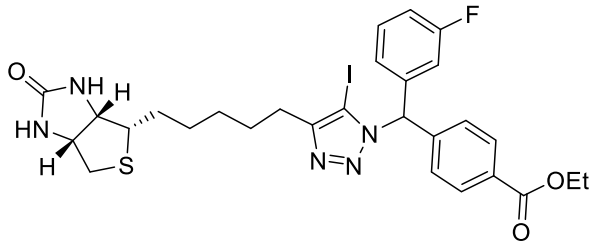

To a mixture of biotin acetylene **22**[1] (0.100 g, 0.42 mmol), LiI (0.224 g, 1.68 mmol), and $Cu(ClO_4)_2$ (0.389 g, 1.04 mmol) in anhydrous THF (6 mL) was added TEA (0.077 mL, 1.04 mmol). The mixture was stirred at rt for 45 min, then di-phenylmethyl azide **23**[1] was added (0.119 g, 0.42 mmol) followed by TBTA (0.022 g, 0.04 mmol). The resulting reaction mixture was stirred at rt for 16 h, then was quenched with 30% aqueous ammonia (10mL) and extracted with DCM (3 x 10 mL). The organic extracts were combined and was washed with 10% aqueous ammonia (3 x 10 mL), brine, water, dried over Na_2SO_4, filtered, concentrated *in vacuo*, and purified by silica gel flash chromatography eluting with DCM/MeOH (v/v =20:1) to afford **24** as a white solid (0.170 g, 82 %); **^{1}H NMR** (500 MHz, $CDCl_3$) δ 8.04 (d, *J* = 8.0 Hz, 2H), 7.37 – 7.31 (m, 1H), 7.29 – 7.26 (m, 2H), 7.09 – 7.01 (m, 1H), 7.01 – 6.96 (m, 1H), 6.94 – 6.89 (m, 1H), 6.85 (s, 1H), 5.10 (s, 1H), 4.85 (s, 1H), 4.52 – 4.46 (m, 1H), 4.37 (q, *J* = 7.1 Hz, 2H), 4.32 – 4.25 (m, 1H), 3.18 – 3.10 (m, 1H), 2.90 (dd, *J* = 12.8, 5.0 Hz, 1H), 2.74 – 2.65 (m, 3H), 1.76 – 1.63 (m, 4H), 1.52 – 1.40 (m, 4H), 1.38 (t, *J* = 7.1 Hz, 3H); **^{13}C NMR** (126 MHz, $CDCl_3$) δ 166.07, 163.98, 163.61, 162.01, 151.96, 141.97, 141.95, 139.68, 139.63, 130.95, 130.57, 130.51, 130.18, 128.59, 128.56, 124.44, 124.41, 124.40, 124.37, 116.09, 116.06, 115.97, 115.91, 115.88, 115.80, 79.99, 67.70, 62.17, 61.30, 60.23, 55.86, 40.66, 29.16, 28.78, 28.63,

28.53, 26.14, 14.43; **HRMS** calcd. for (M + H^+) $C_{28}H_{31}FIN_5O_3S^+$: requires 664.1249 found 664.1247.

4-((5-fluoro-4-(5-((3a*S*,4*S*,6a*R*)-2-oxohexahydro-1*H*-thieno[3,4-*d*]imidazol-4-yl)pentyl)-1*H*-1,2,3-triazol-1-yl)(3-fluorophenyl)methyl)benzoic acid (**25**)

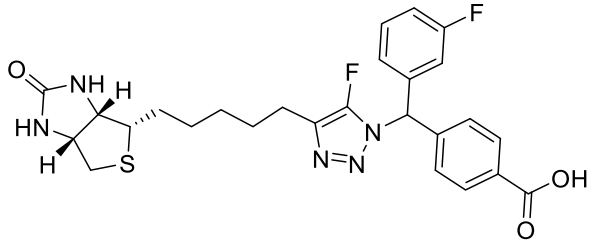

To a mixture of triazole **17** (0.100 g, 0.18 mmol) in THF, MeOH and water (v/v/v = 3:1:1) (5 mL) was added LiOH (0.010g, 0.41 mmol), and the resulting mixture was stirred at rt for 16 h. The reaction mixture was acidified to pH = 3 with 1.0 M aqueous HCl, then diluted with EtOAc (30 mL), washed with 0.5 M aqueous HCl, water and brine. The organic layer was dried over Na_2SO_4, filtered, and concentrated *in vacuo* to give **25** as a white (0.097 mg, 99 %); **^{1}H NMR** (500 MHz, DMSO-d_6) δ 13.03 (s, 1H), 7.97 (d, *J* = 8.4 Hz, 2H), 7.48 (td, *J* = 7.8, 5.9 Hz, 1H), 7.36 (d, *J* = 8.4 Hz, 2H), 7.28 (s, 1H), 7.27 – 7.20 (m, 1H), 7.16 – 7.09 (m, 2H), 6.41 (s, 1H), 6.34 (s, 1H), 4.32 – 4.26 (m, 1H), 4.14 – 4.08 (m, 1H), 3.11 – 3.04 (m, 1H), 2.80 (dd, *J* = 12.4, 5.1 Hz, 1H), 2.62 – 2.54 (m, 3H), 1.65 – 1.55 (m, 3H), 1.49 – 1.42 (m, 1H), 1.38 – 1.28 (m, 4H); **^{13}C NMR** (126 MHz, DMSO-d_6) δ 166.75, 163.03, 161.09, 150.93, 148.71, 141.53, 139.54, 139.48, 130.99, 130.92, 129.78, 128.17, 126.83, 126.75, 124.37, 124.35, 115.61, 115.45, 115.28, 115.10, 62.76, 61.03, 59.17, 55.46, 39.02, 28.42, 28.17, 28.15, 27.53, 22.83, 22.80; **HRMS** calcd. for (M + H^+) $C_{26}H_{28}F_2N_5O_3S^+$: requires 528.1875 found 528.1879.

S3.4: ^{1}H and ^{13}C NMR Spectra of 8 – 19, 21, 24, and 25

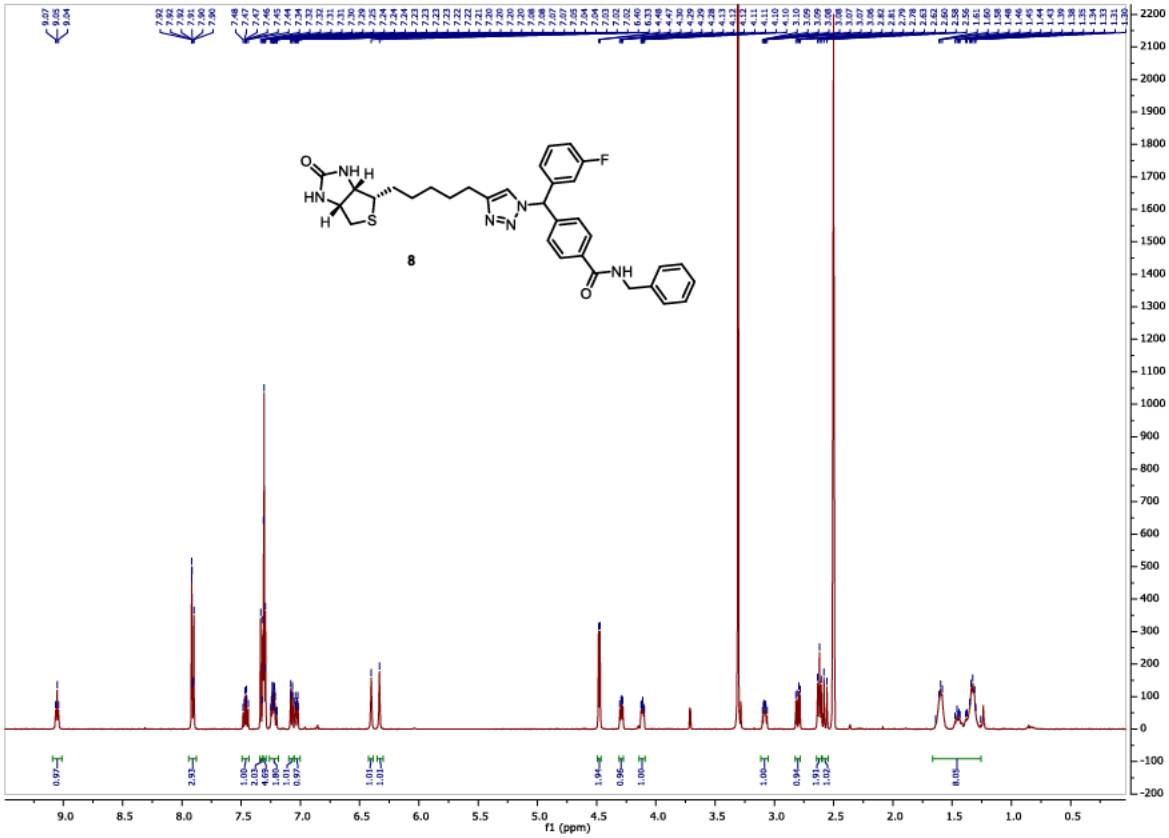

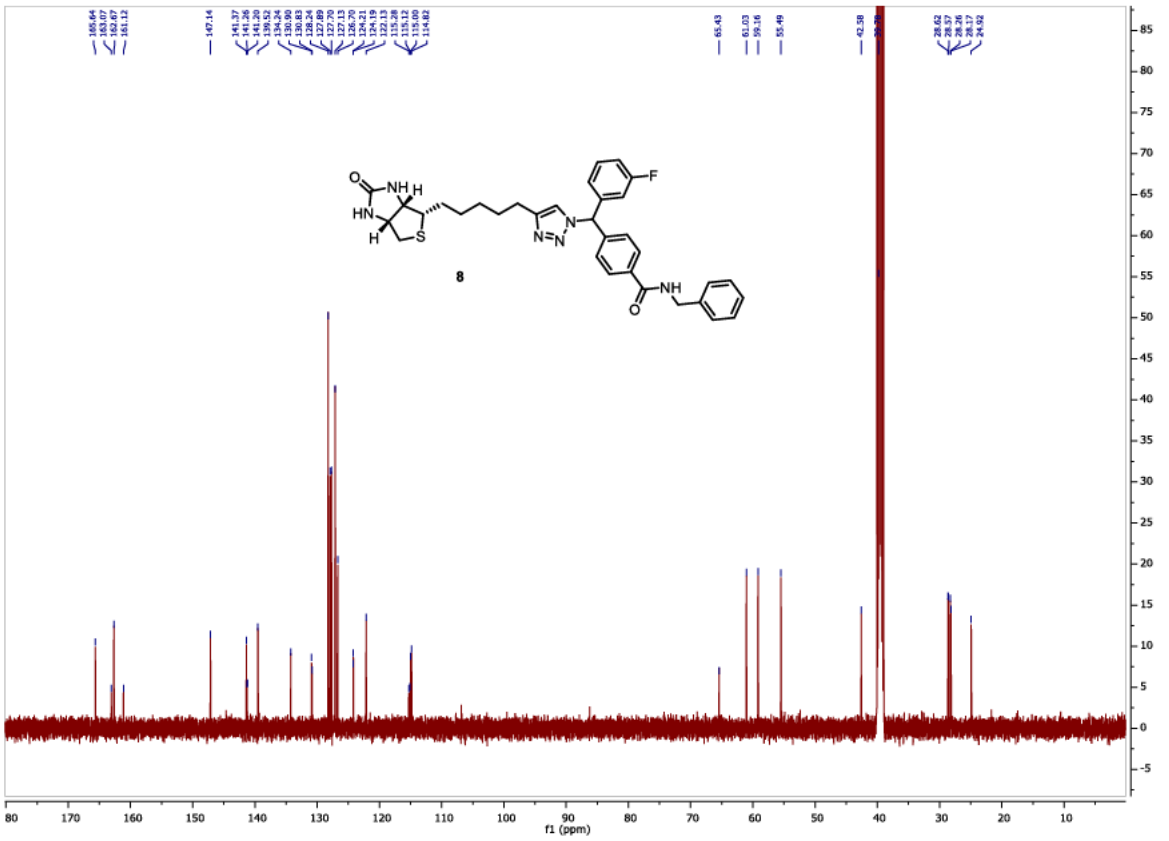

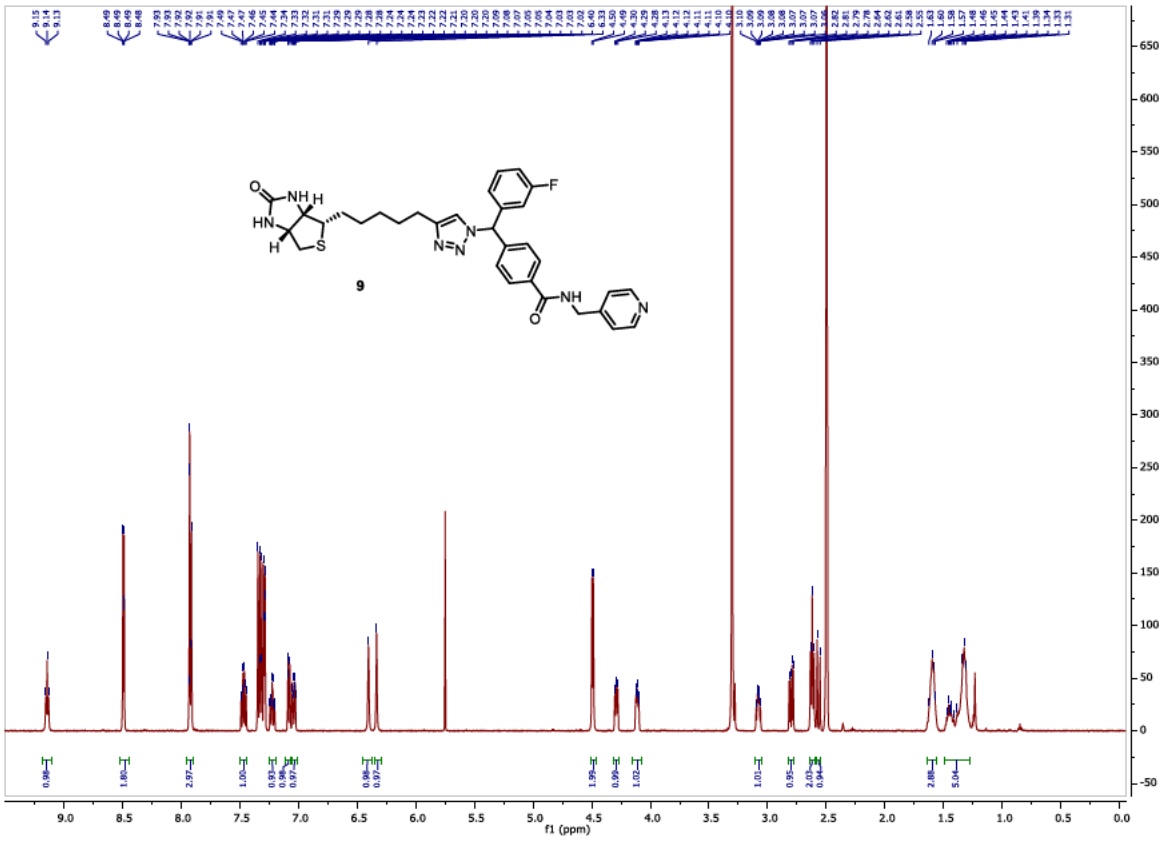
9
f1 (ppm)

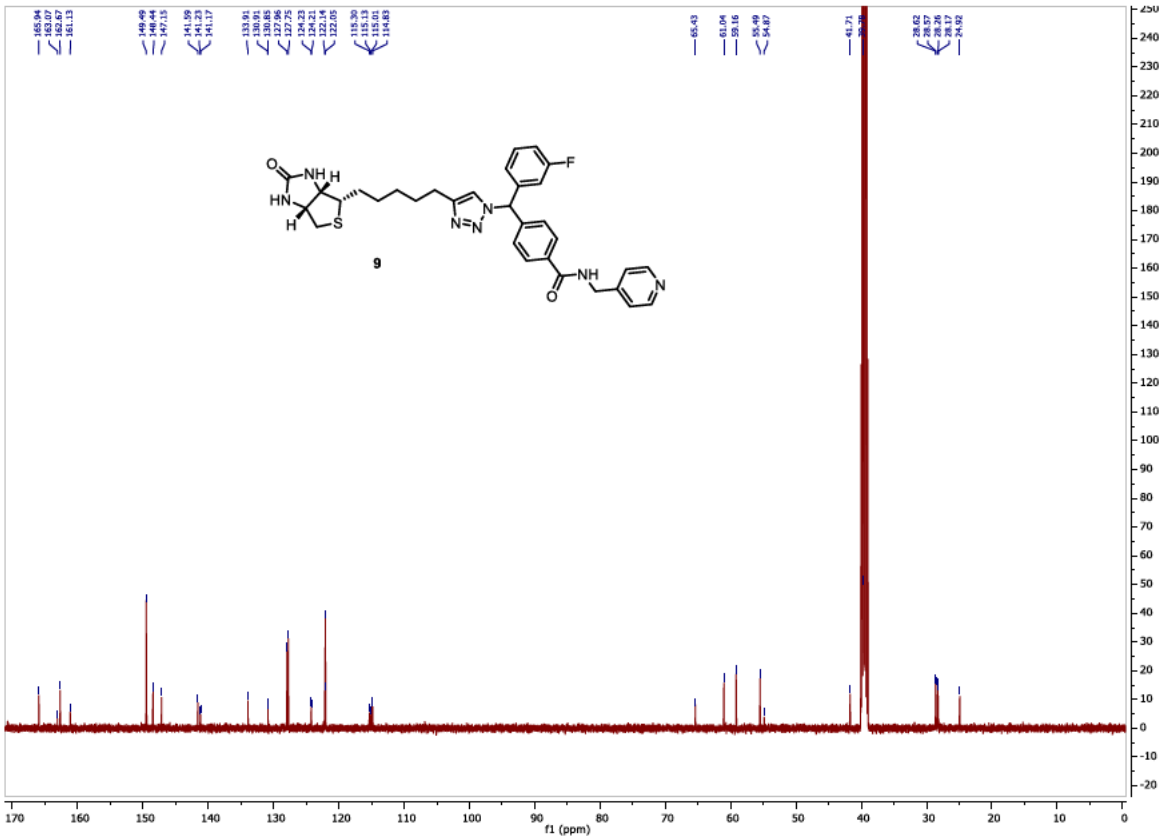
9
f1 (ppm)

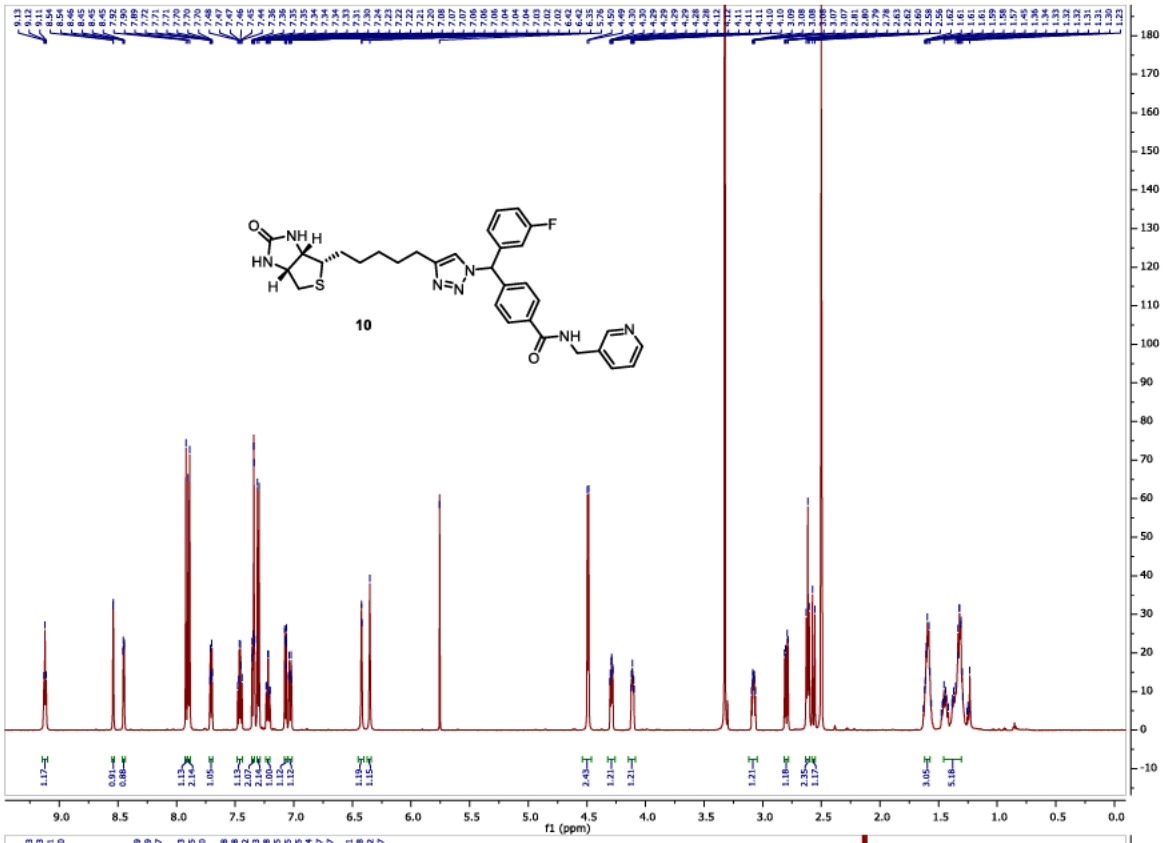
10
f1 (ppm)

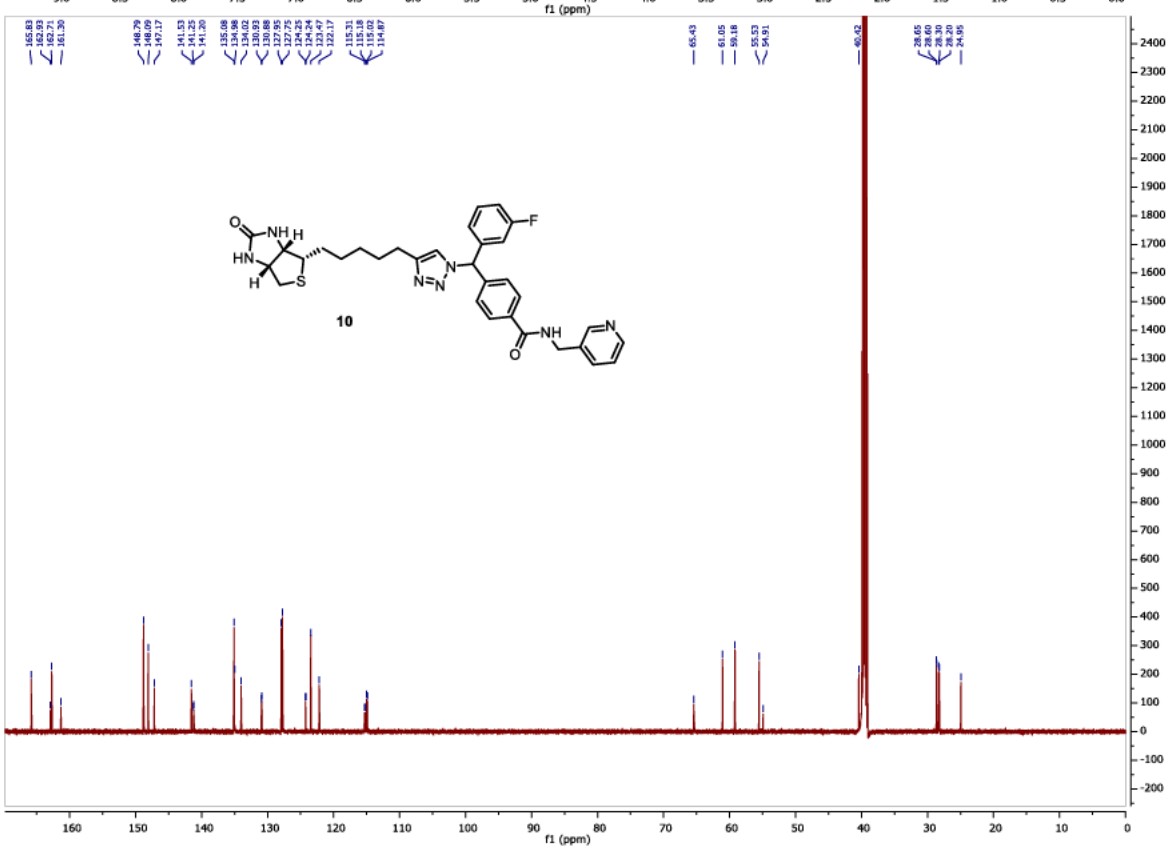
10
f1 (ppm)

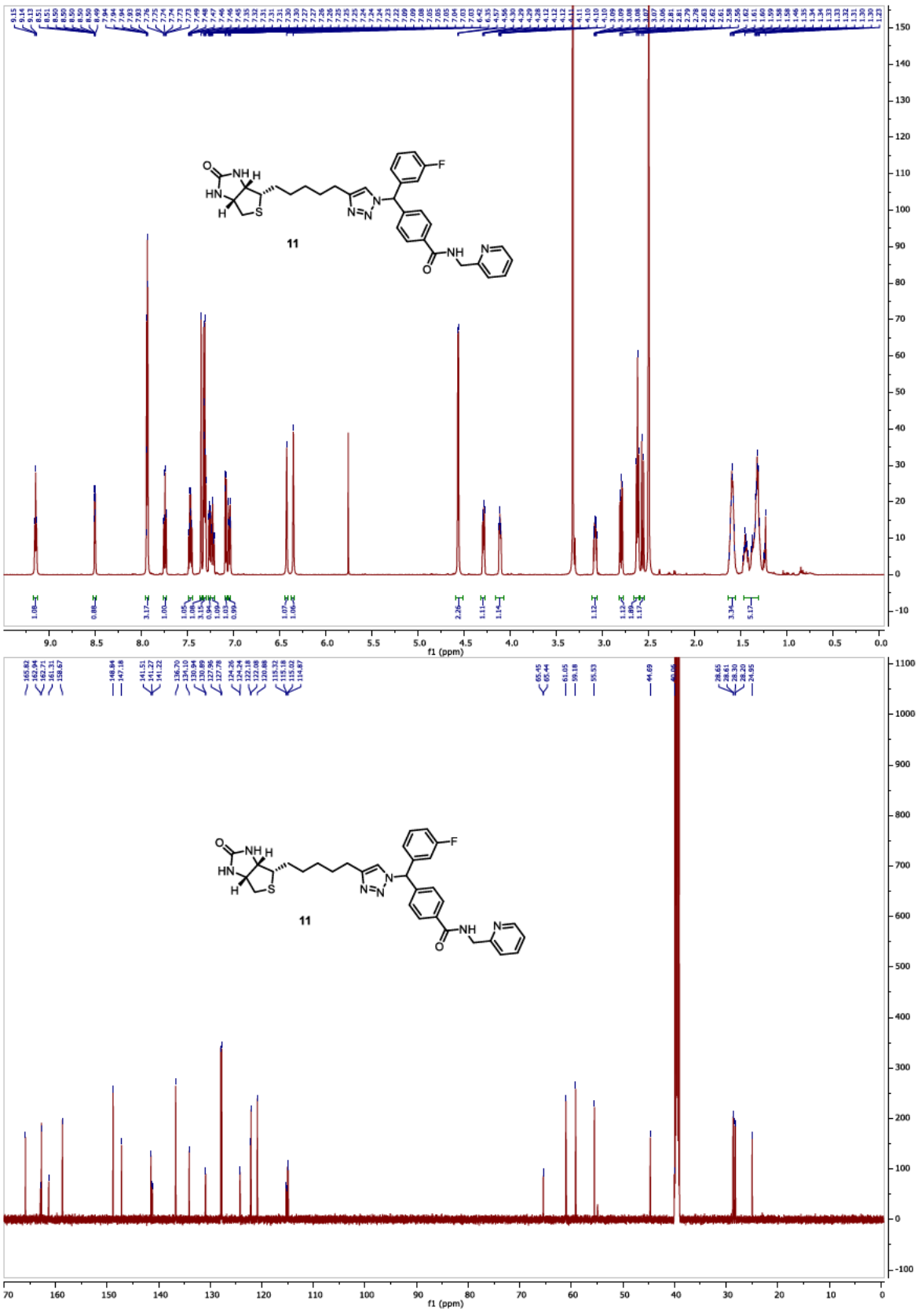
11
f1 (ppm)
11
f1 (ppm)

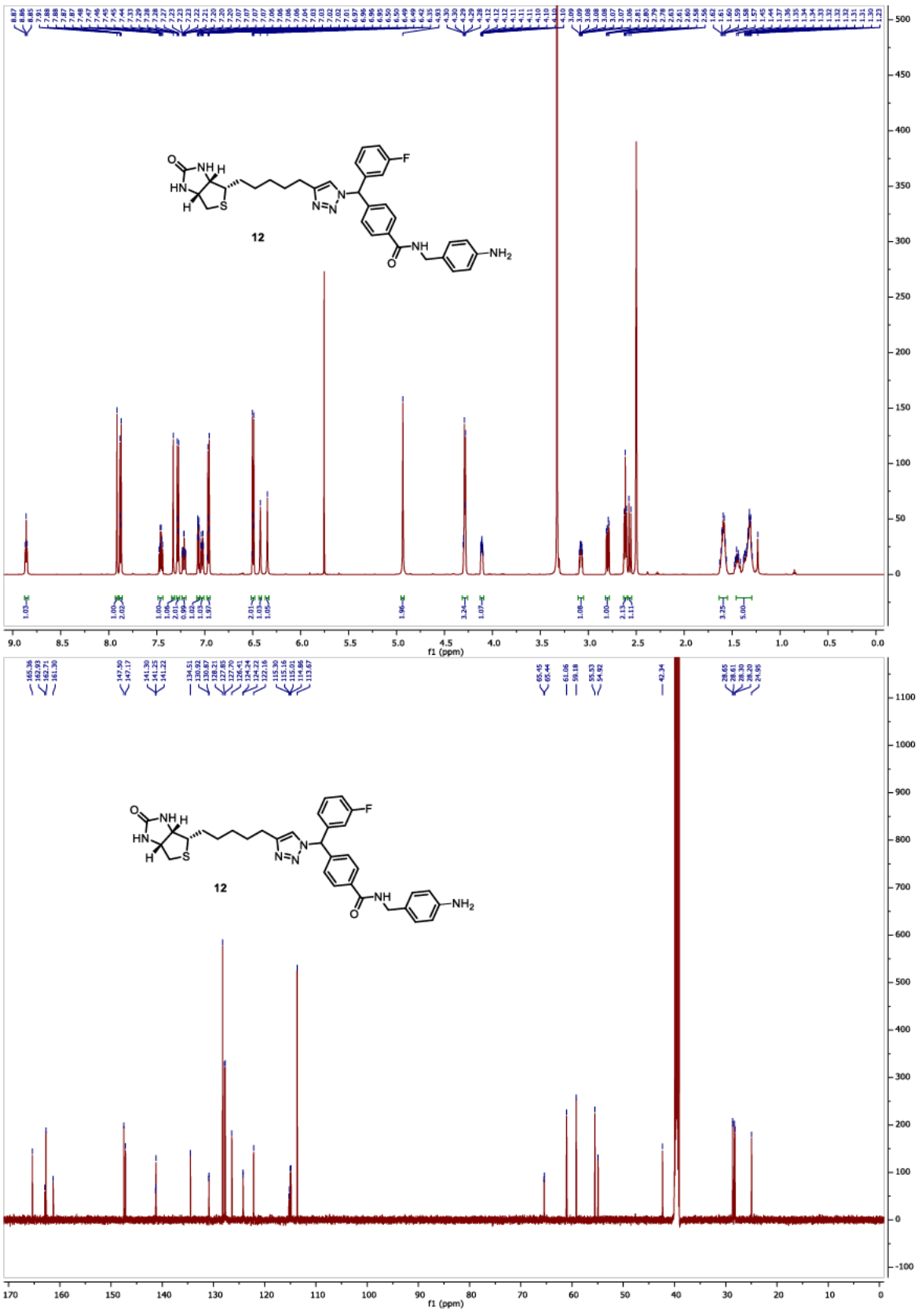
12
f1 (ppm)
12
f1 (ppm)

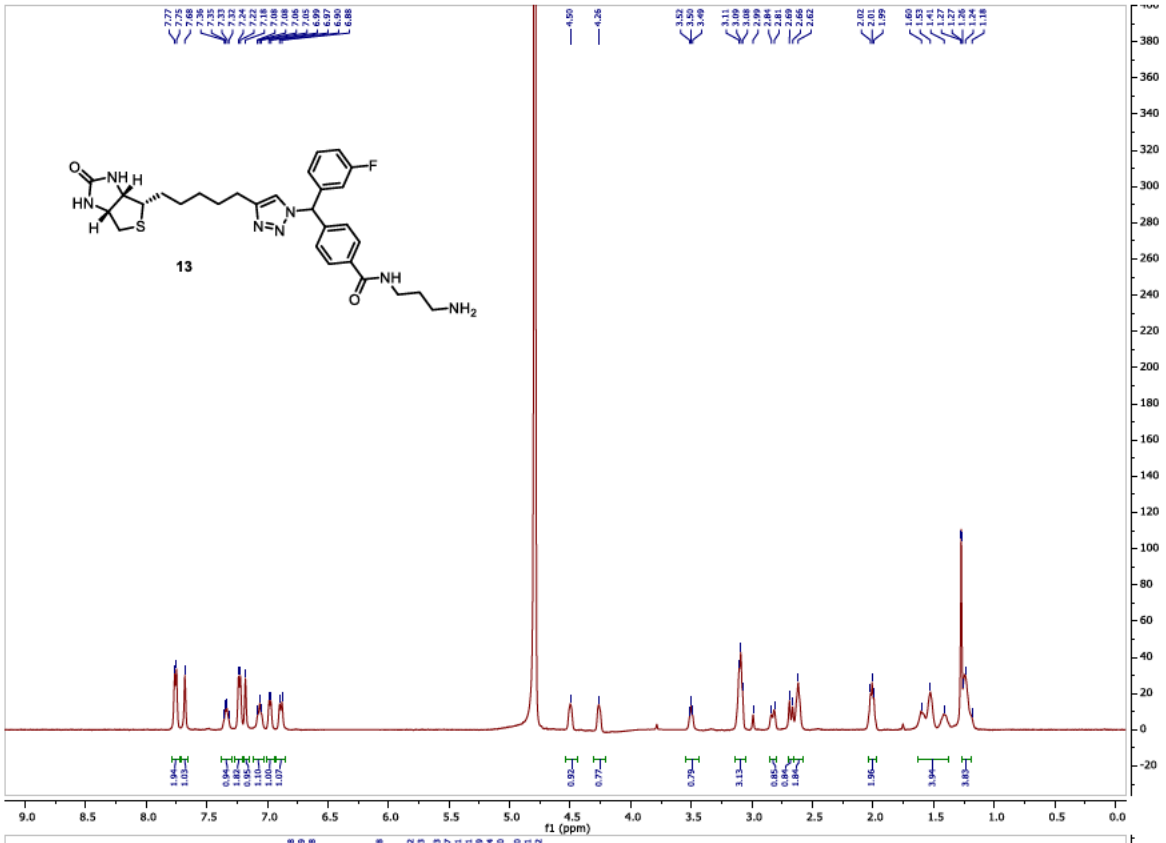
13
f1 (ppm)

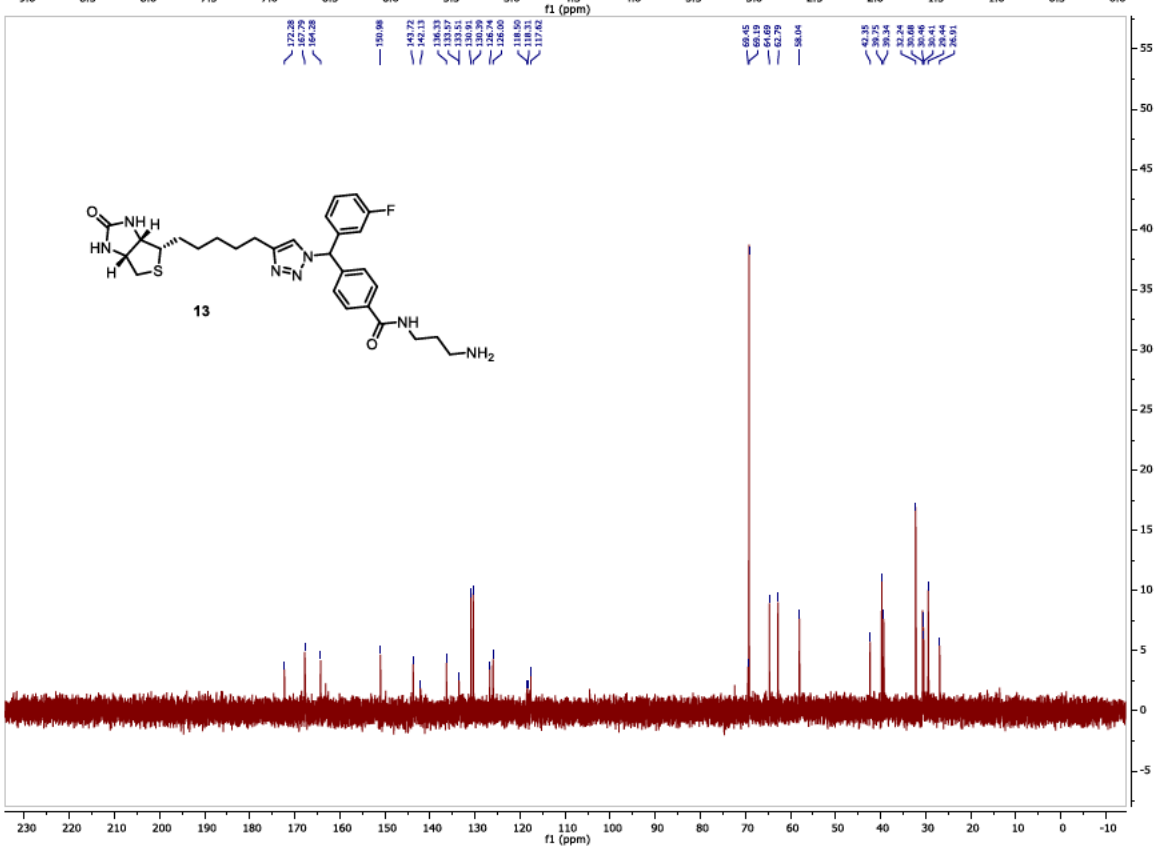
13
f1 (ppm)

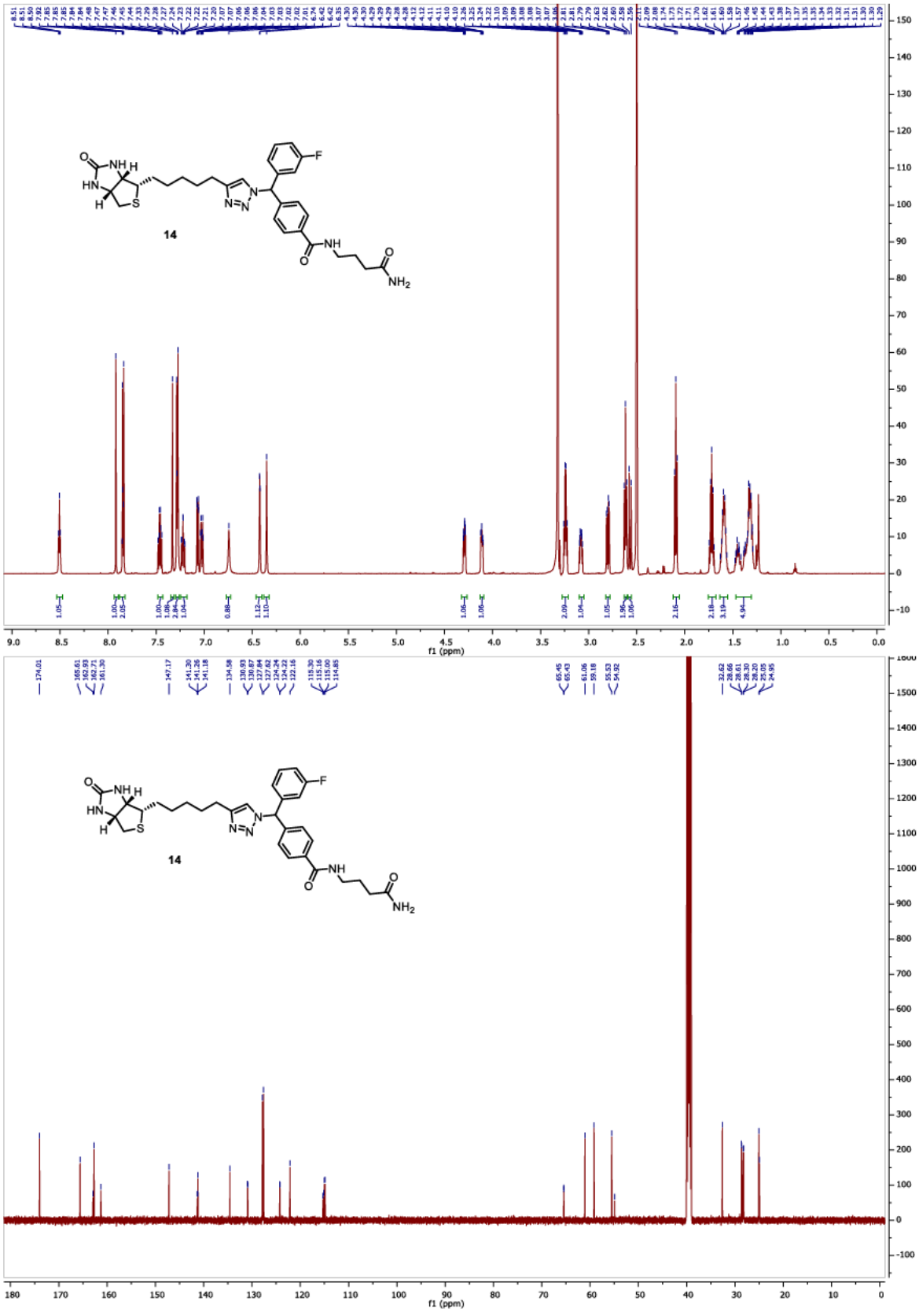
14
f1 (ppm)
14
f1 (ppm)

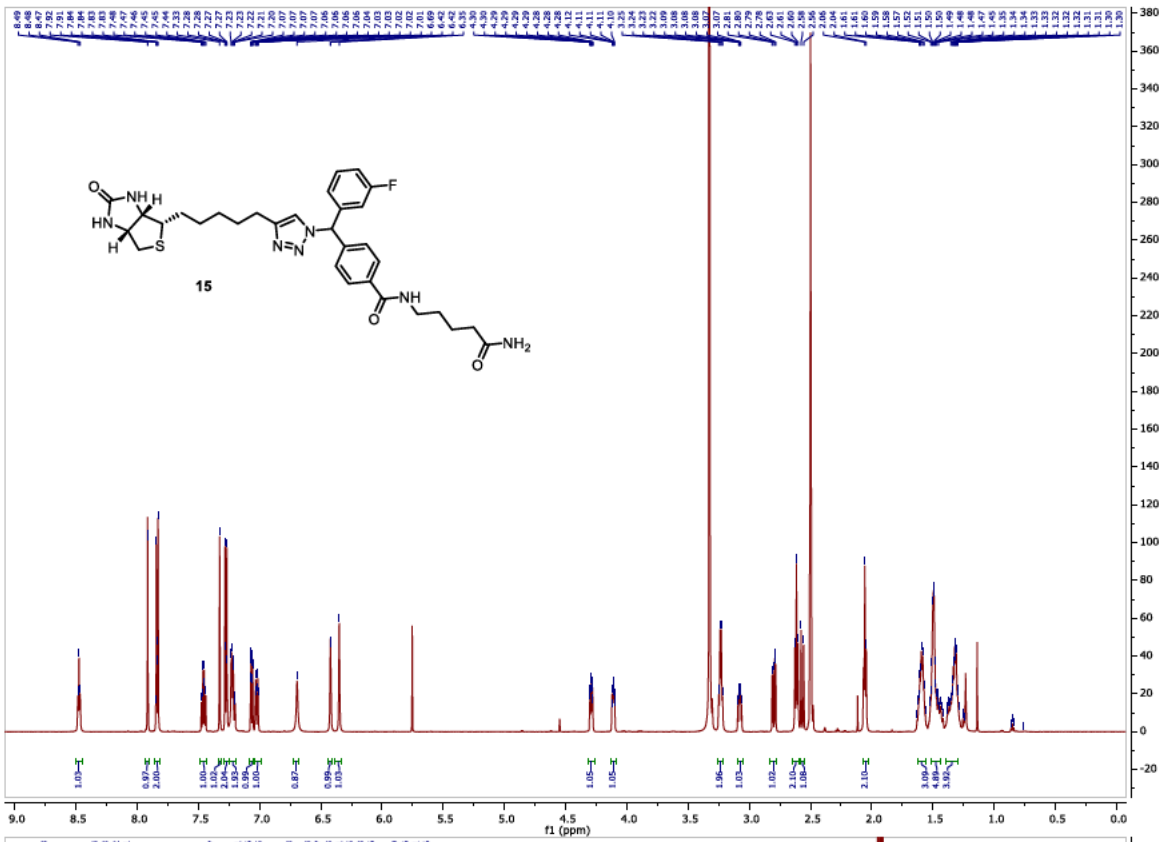
15
f1 (ppm)

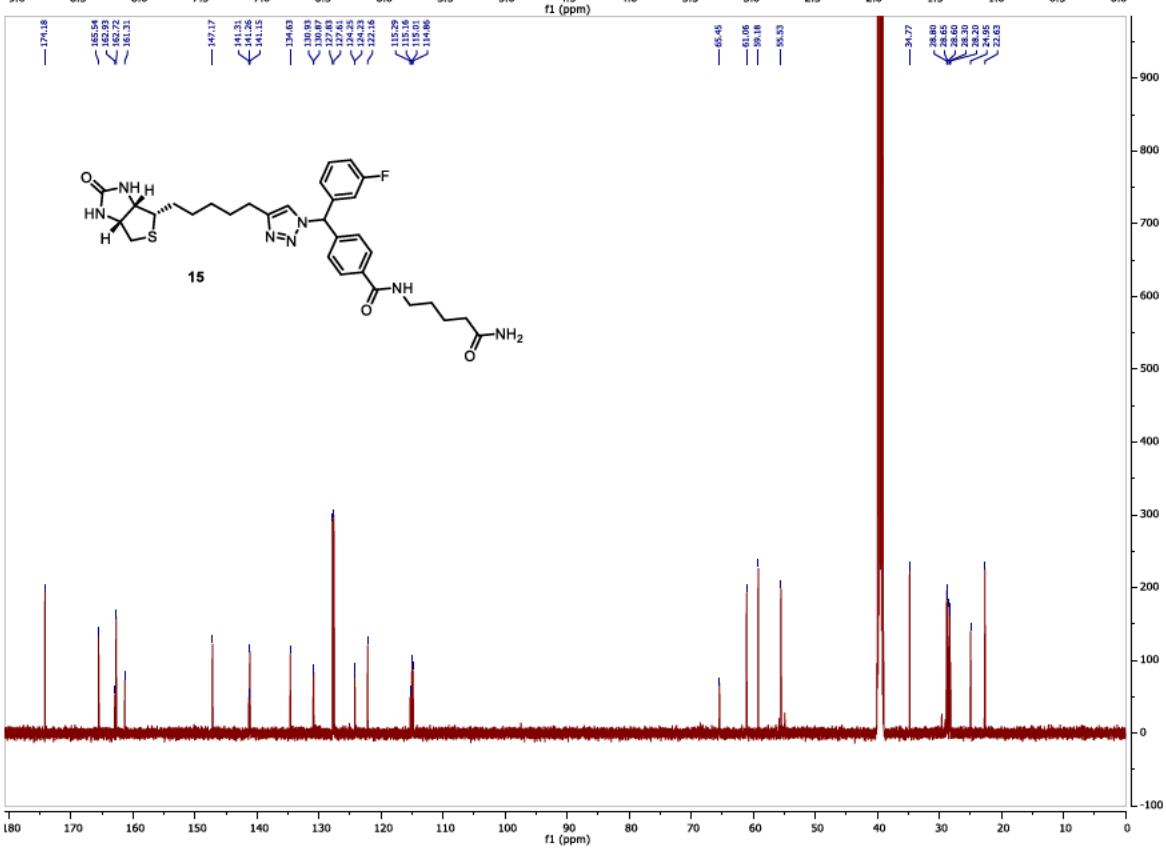
15
f1 (ppm)

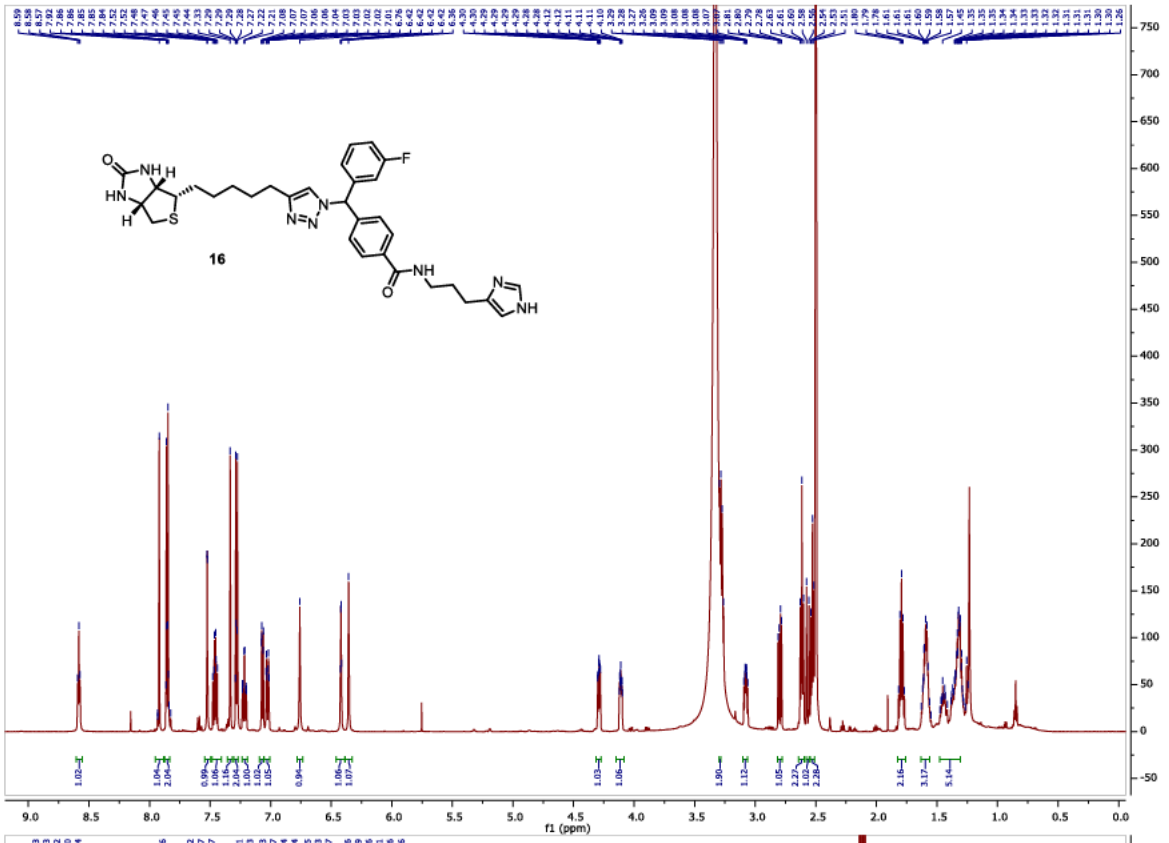
16
f1 (ppm)

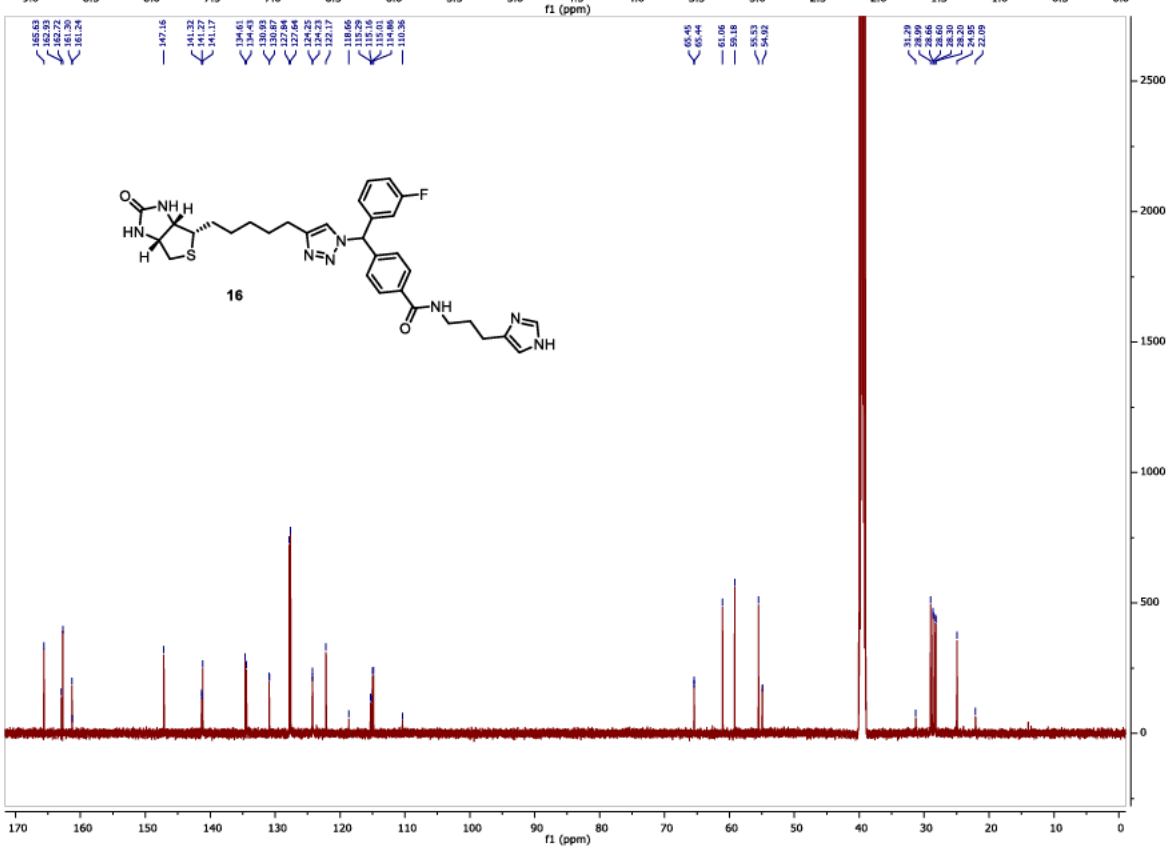
16
f1 (ppm)

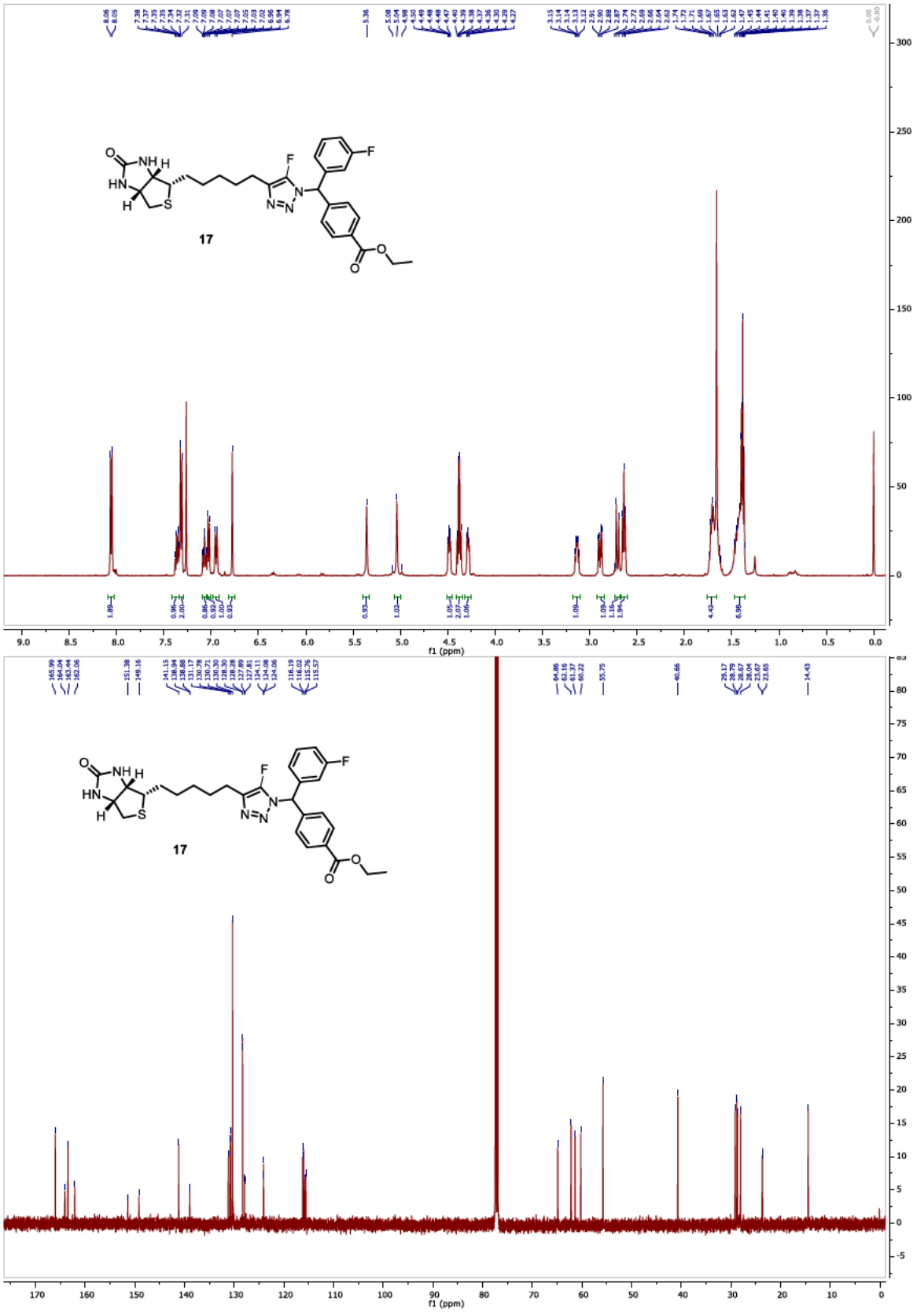
17
f1 (ppm)
17
f1 (ppm)

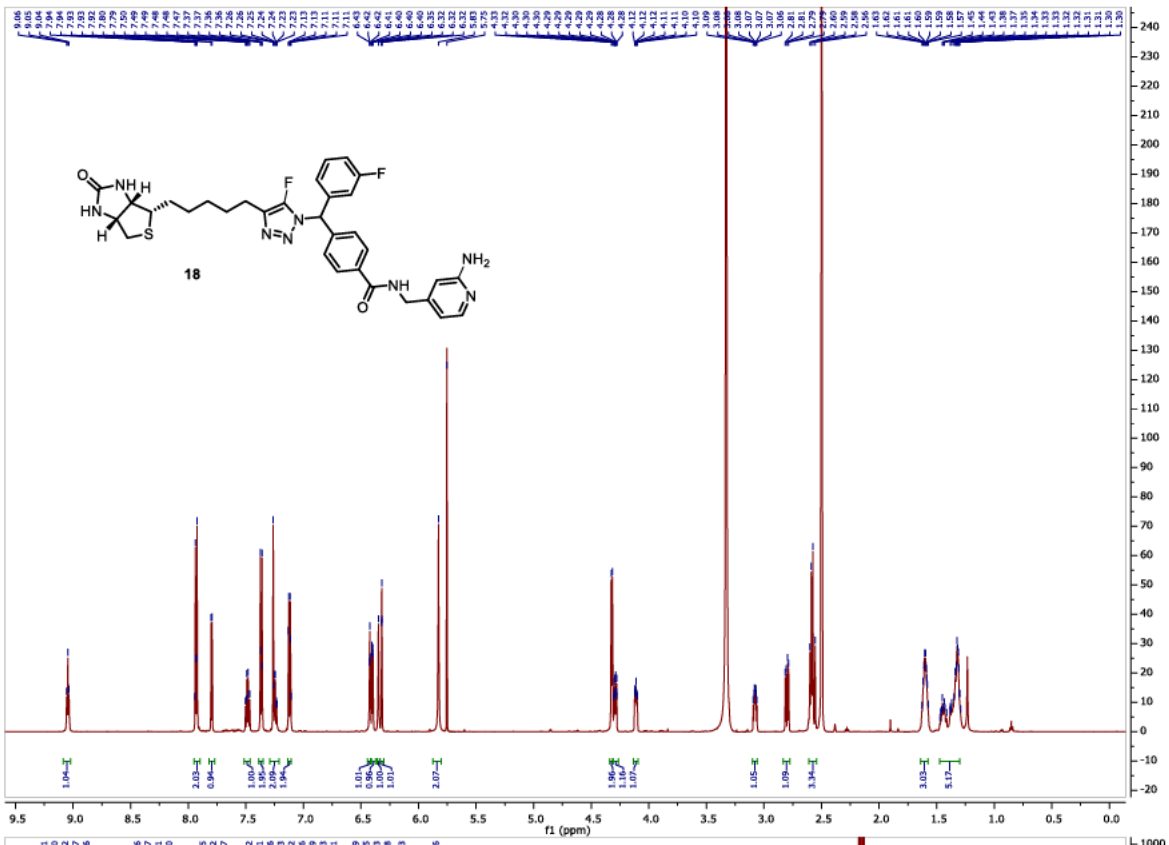
18
f1 (ppm)

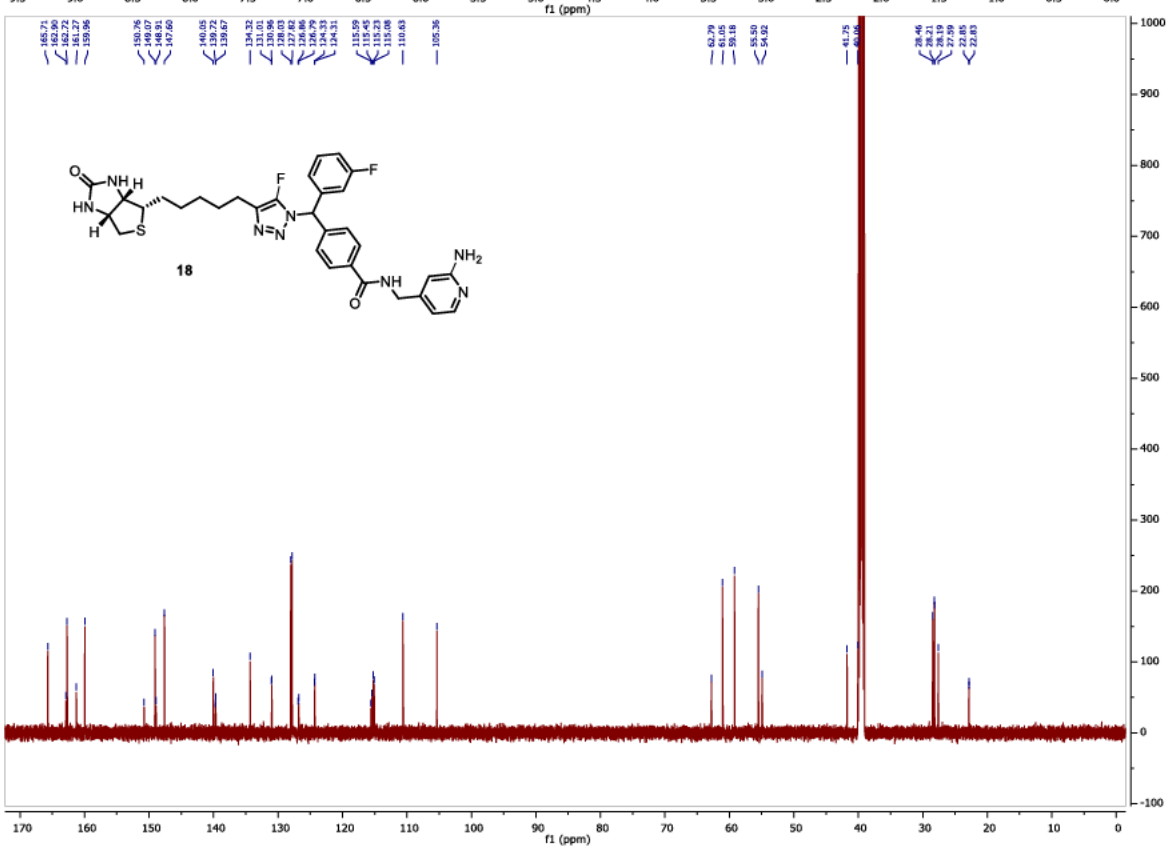
18
f1 (ppm)

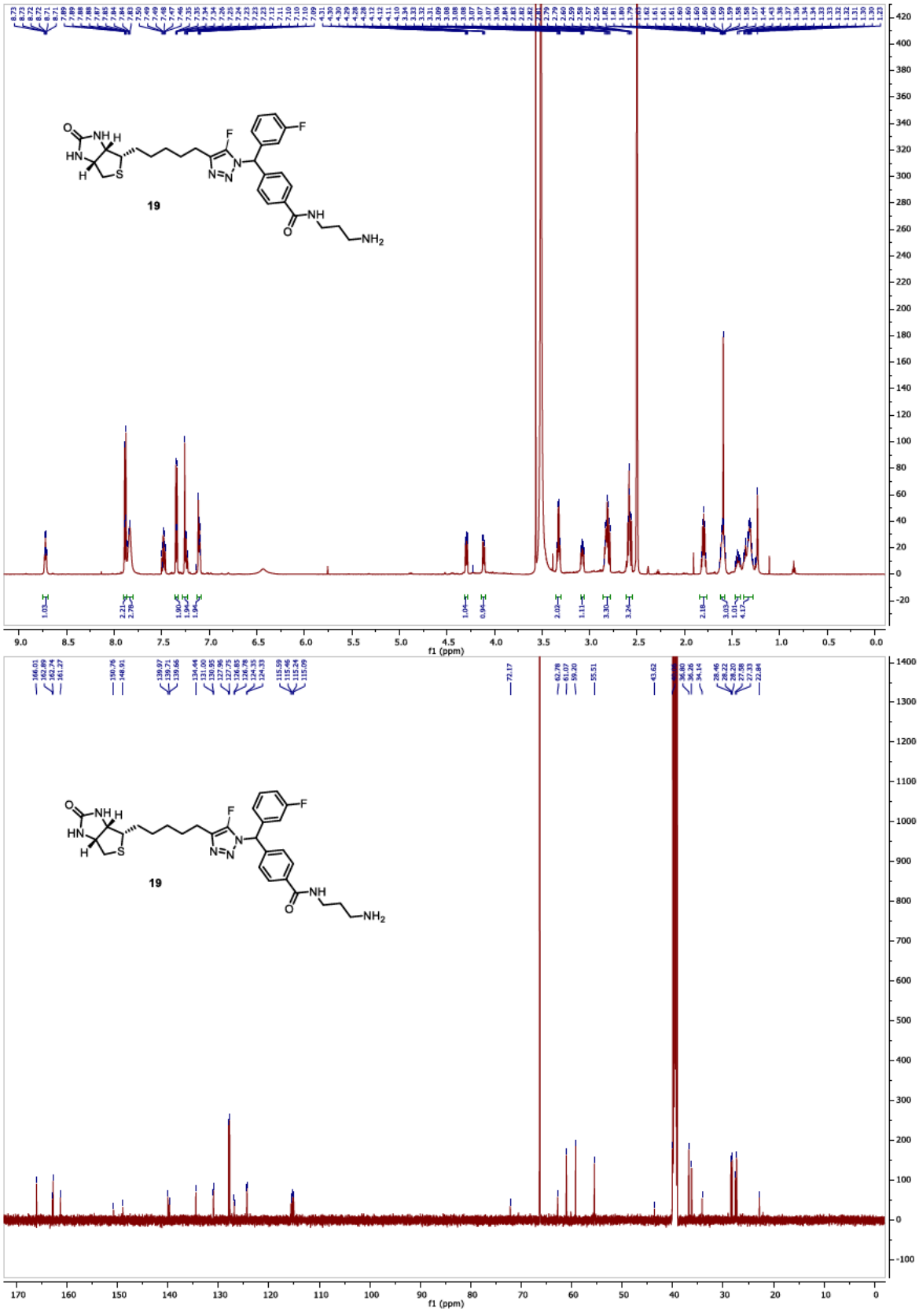
19
f1 (ppm)
19
f1 (ppm)

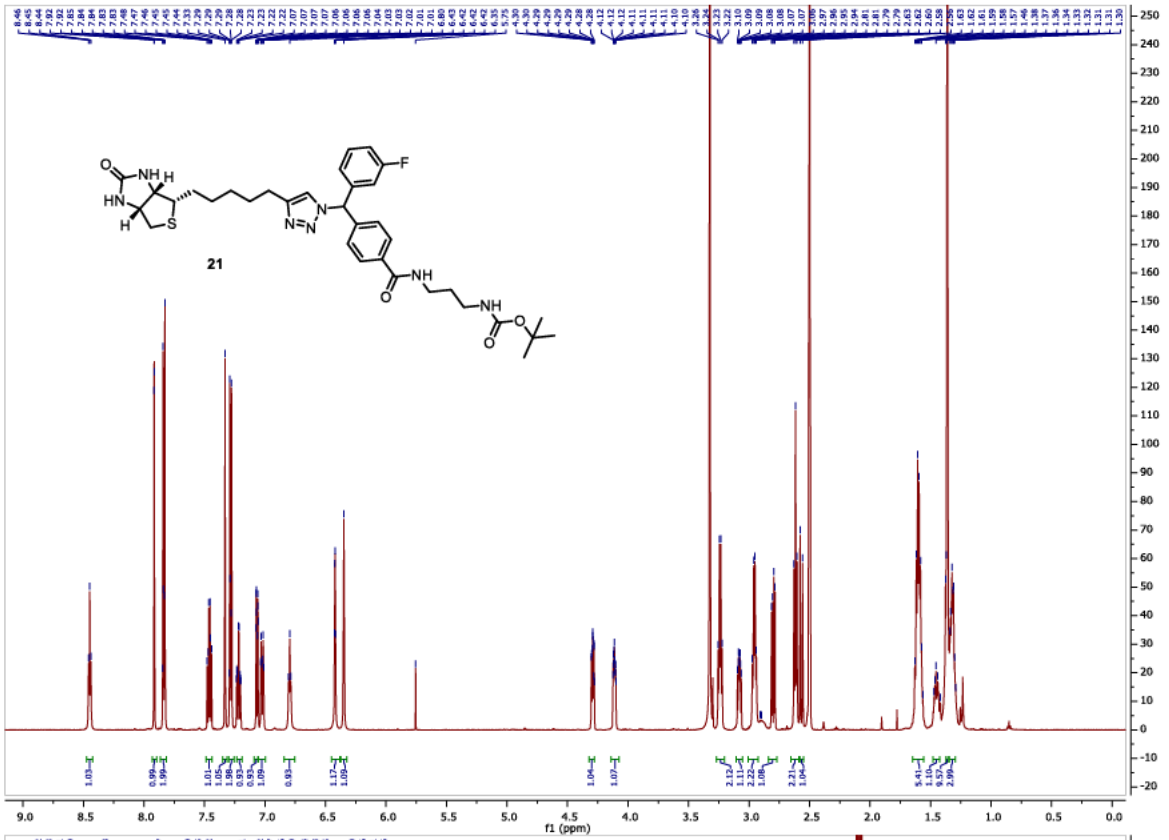
21
f1 (ppm)

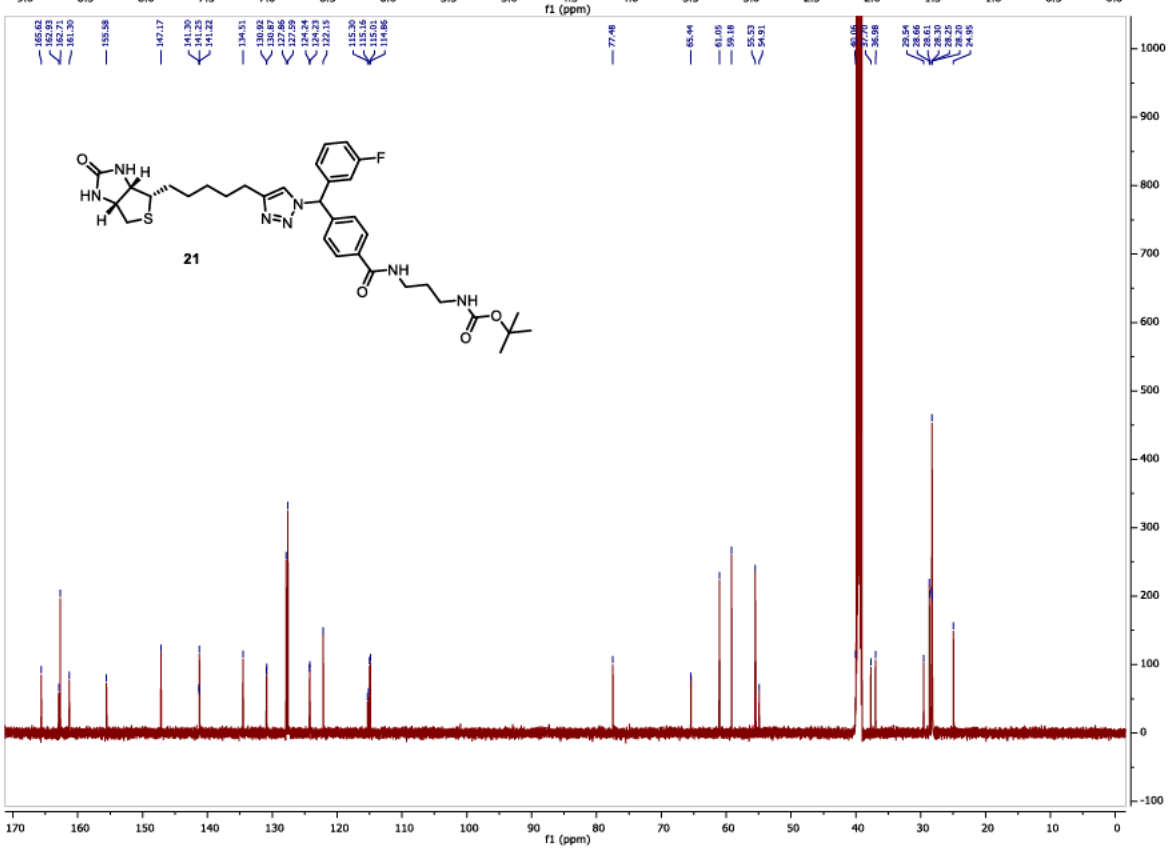
21
f1 (ppm)

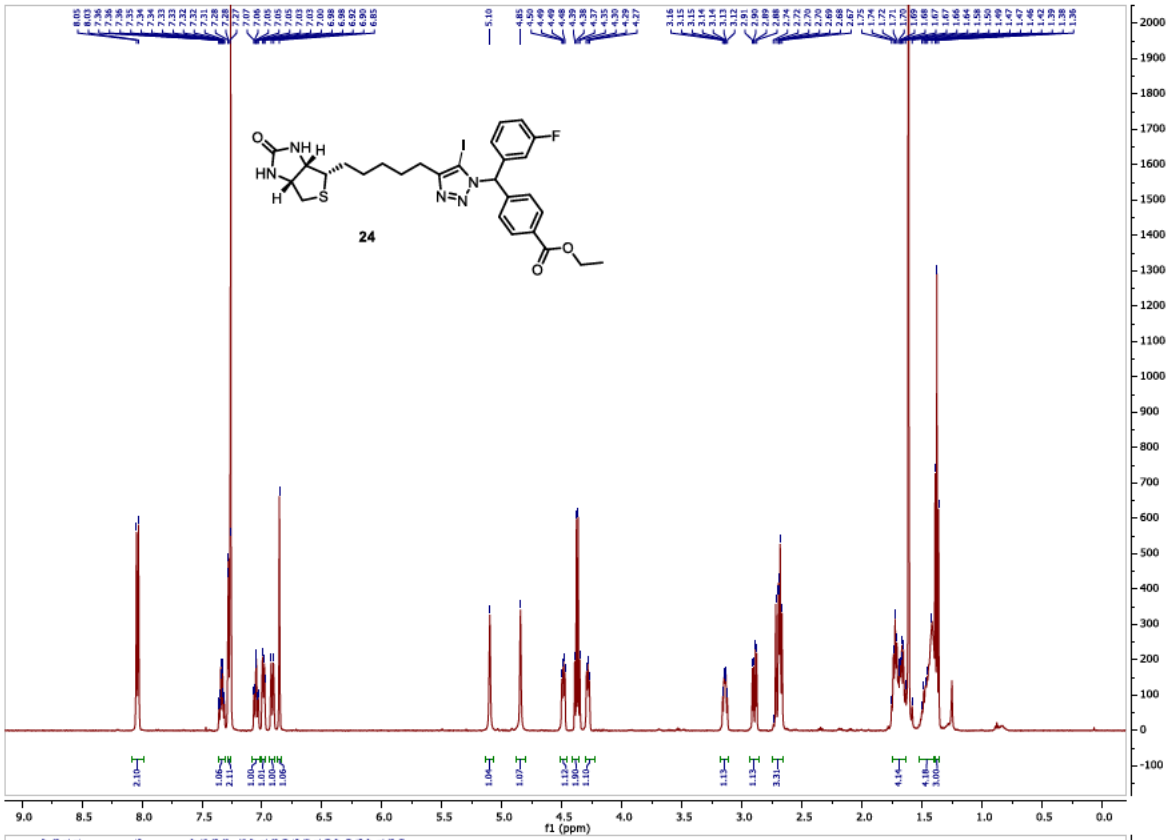
24
f1 (ppm)

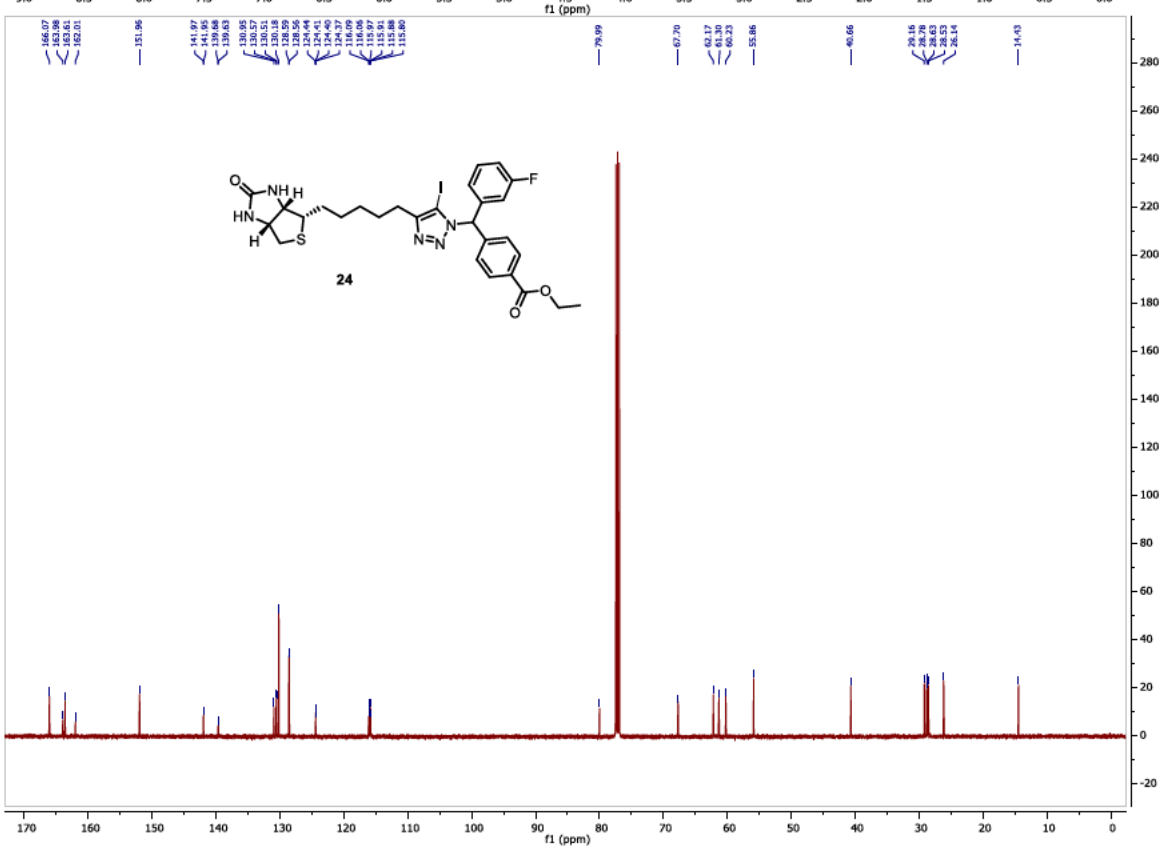
24
f1 (ppm)

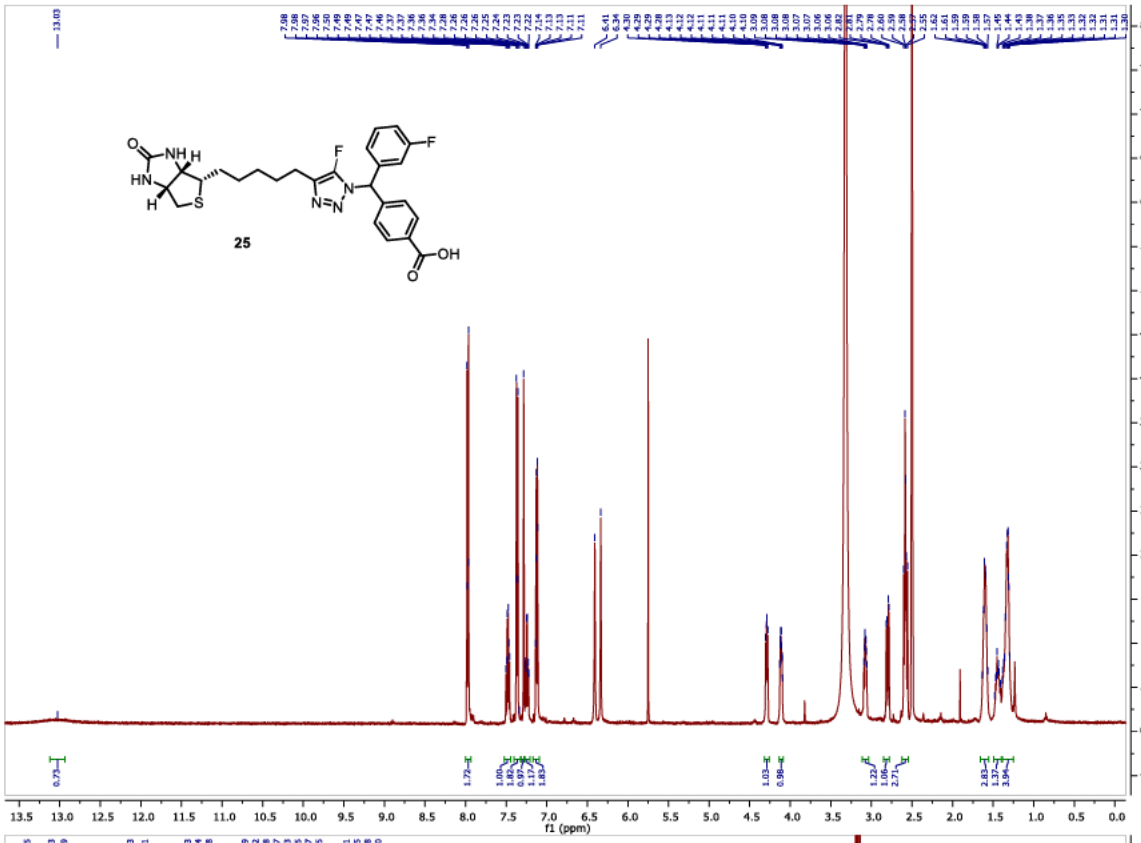
25
f1 (ppm)

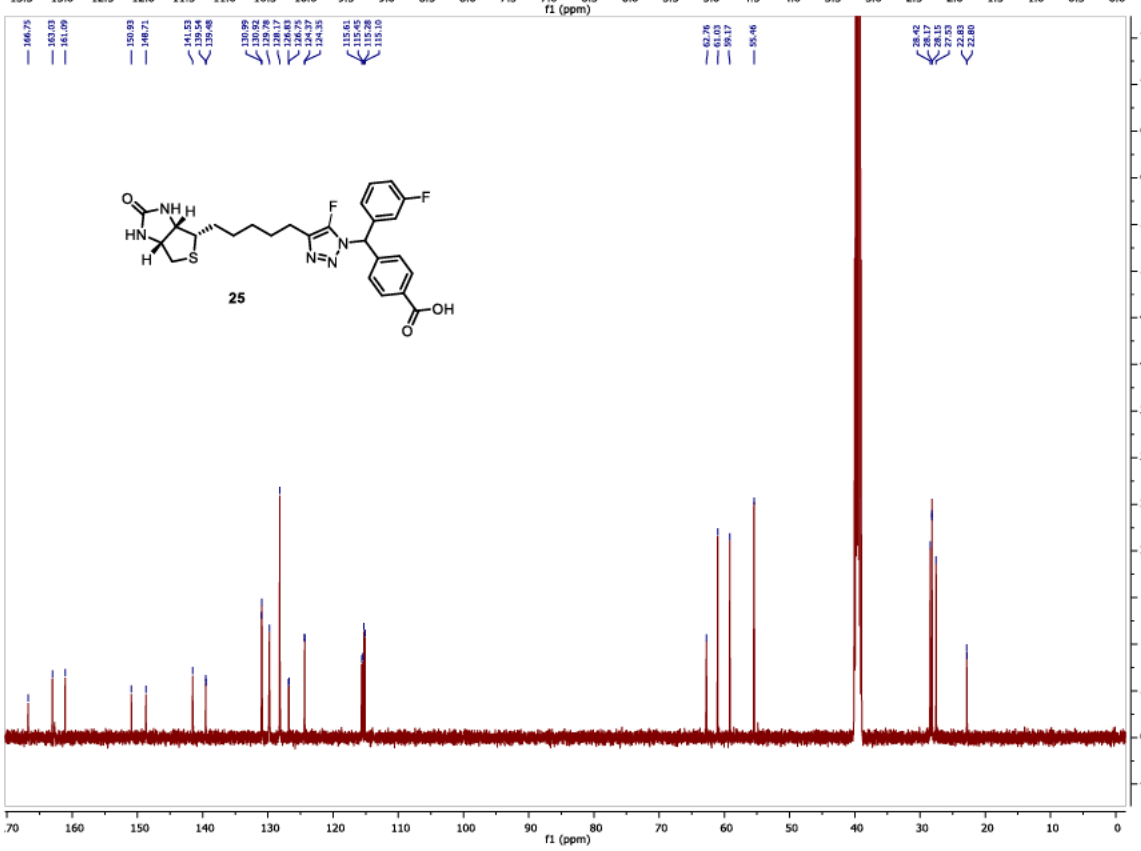
25
f1 (ppm)

3.5: Supplementary References

(1) Stachura, D. L.; Nguyen, S.; Polyak, S. W.; Jovcevski, B.; Bruning, J. B.; Abell, A. D. A New 1,2,3-Triazole Scaffold with Improved Potency Against Staphylococcus Aurues Biotin Protein Ligase. *ACS Infect. Dis*. **2022**, *8* (12), 2579–2585. https://doi.org/10.1021/acsinfecdis.2c00452.

(2) Yung-Chi, C.; Prusoff, W. H. Relationship between the Inhibition Constant (KI) and the Concentration of Inhibitor Which Causes 50 per Cent Inhibition (I50) of an Enzymatic Reaction. *Biochem. Pharmacol.* **1973**, *22* (23), 3099–3108. https://doi.org/10.1016/0006-2952(73)90196-2.

(3) Tonge, P. J. Quantifying the Interactions between Biomolecules: Guidelines for Assay Design and Data Analysis. *ACS Infect. Dis.* **2019**, *5* (6), 796–808. https://doi.org/10.1021/acsinfecdis.9b00012.

(4) Paparella, A. S.; Lee, K. J.; Hayes, A. J.; Feng, J.; Feng, Z.; Cini, D.; Deshmukh, S.; Booker, G. W.; Wilce, M. C. J.; Polyak, S. W.; Abell, A. D. Halogenation of Biotin Protein Ligase Inhibitors Improves Whole Cell Activity against Staphylococcus Aureus. *ACS Infect. Dis.* **2018**, *4* (2), 175–184. https://doi.org/10.1021/acsinfecdis.7b00134.

(5) Neves, M. A. C.; Totrov, M.; Abagyan, R. Docking and Scoring with ICM: The Benchmarking Results and Strategies for Improvement. *J. Comput. Aided. Mol. Des.* **2012**, *26* (6), 675–686. https://doi.org/10.1007/s10822-012-9547-0.

Chapter Four

The numbering of chemical structures in this chapter is designated by Ha**,** Hb**,** and Hc, rather than being based on chemical convention for clarity.

4.1: Introduction

As discussed in Chapter One, the phosphoryl linker of the natural intermediate biotinyl-5'-AMP **1.02** binds within the phosphate pocket of *Sa*BPL.[1] Replacing this linker with a 1,2,3-triazole, as in analogue **1.05**, results in potent and selective inhibitors of *Sa*BPL.[1] However, superimposing the X-ray co-crystal structures of **1.02**[1] and **1.05**[1] separately bound to *Sa*BPL, revealed good overlap of the key amino acid residues Arg122, Arg125 and Asp180, but not Lys187 (Figure 4.1). The phosphoryl linker of **1.02** forms hydrogen bonds with Arg122, Arg125, and Lys187, whereas the triazole of **1.05** only forms hydrogen bonds with the active site arginine residues. This suggests that the triazole linker of **1.05** does not fully exploit all possible hydrogen bond interactions within the phosphate pocket of *Sa*BPL. Related triazole-based inhibitor-*Sa*BPL cocrystal structures (e.g., *m*-F-benzyl triazole **1.07**) showed similar findings, with an absence of hydrogen bonding between Lys187 and the triazole linker.[2] Our recently reported sulfonamide-based inhibitors (**1.14** and **1.15**)[3] highlighted the importance of this residue, with hydrogen bonding of the sulfonyl linker to Lys187 associated with an increase in activity against *Sa*BPL, relative to **1.05**. Thus, further investigation is warranted to chemically modify the triazole linker, specifically at the C10 position, to enable key hydrogen bonding with Lys187. This would be expected to further enhance activity against *Sa*BPL and is discussed in detail below.

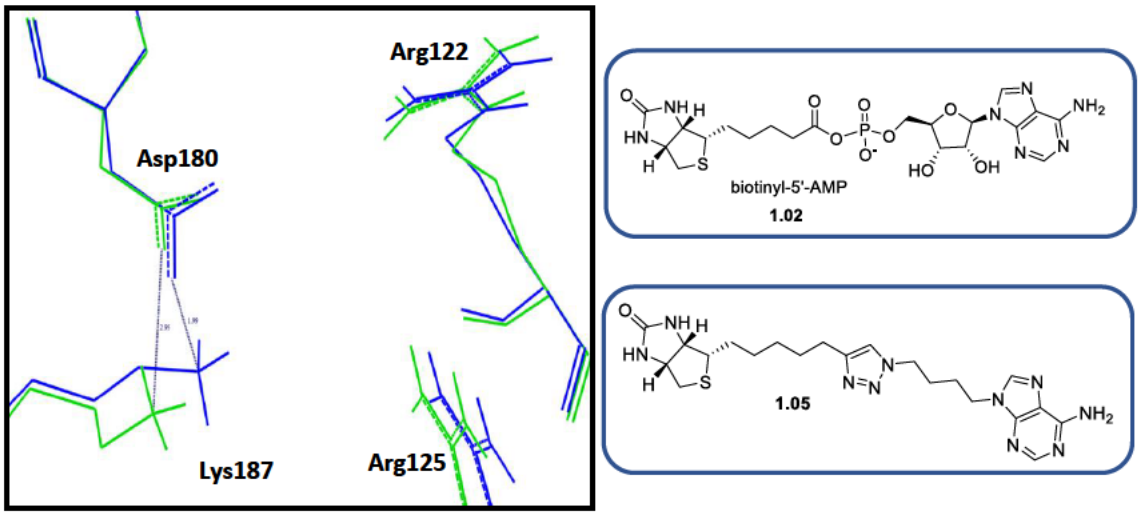

Figure 4.1: Superimposition of key amino acid residues in the phosphate binding domains for *Sa*BPL-**1.02** (blue) and *Sa*BPL-**1.05** (green) complexes. Bound ligands have been omitted for clarity. Hydrogen bond distances between Asp180 and Lys187 are highlighted (1.99 Å for *Sa*BPL-**1.02**, and 2.95 Å for *Sa*BPL-**1.05**).

4.2: Design and Synthesis of a C10-Carbonyl Analogue

Superimposing the published[1] X-ray structures of **1.02** and **1.05** bound separately to *Sa*BPL, revealed that the biotin C10 carbons of both compounds are similarly positioned, see Figure 4.2. Importantly, the phosphoryl linker of **1.02** is shown to form a hydrogen bond between Lys187 and the C10-carbonyl.[4] Thus, incorporation of a carbonyl group at the C10-position of triazole **1.05**, to give analogue **4.01**, should mimic this natural hydrogen bond interaction. This strategy also holds for the recently reported potent triazole-based inhibitor **1.07**,[2] which gives **4.02** when functionalised with a carbonyl group at the C10 position, see Figure 4.3. The subsequent docking study of **4.01** and **4.02** is detailed in Section 4.2.1.

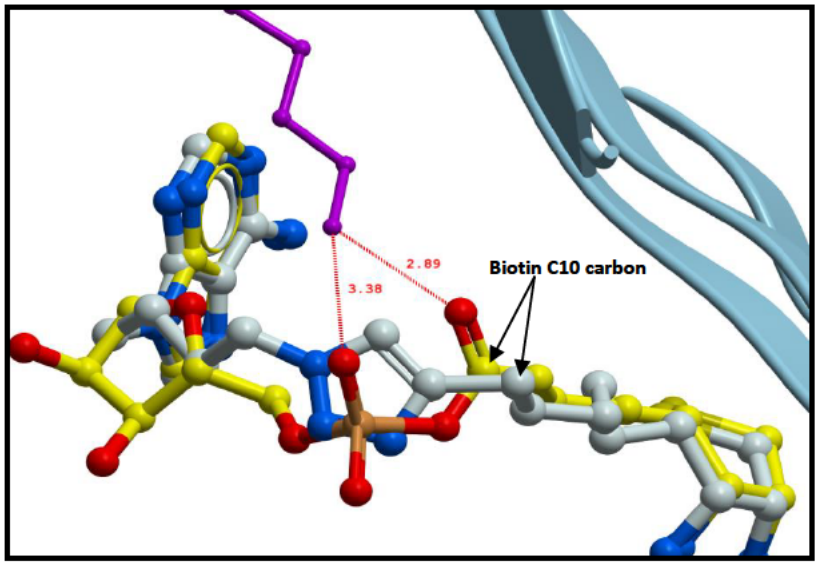

Figure 4.2: X-ray cocrystal structure of **1.02** (yellow,3V8L[1]) bound in the active site of *Sa*BPL, superimposed with triazole **1.05** (grey, 3V7R[1]). The *Sa*BPL amino acid residue Lys187 is highlighted in purple. Hydrogen bond distances between Lys187 and the phosphoryl oxygen and biotin carbonyl oxygen of **1.02** are highlighted (3.38 and 2.89 Å respectively). The triazole C10 carbon is labelled on **1.02** and **1.05**.

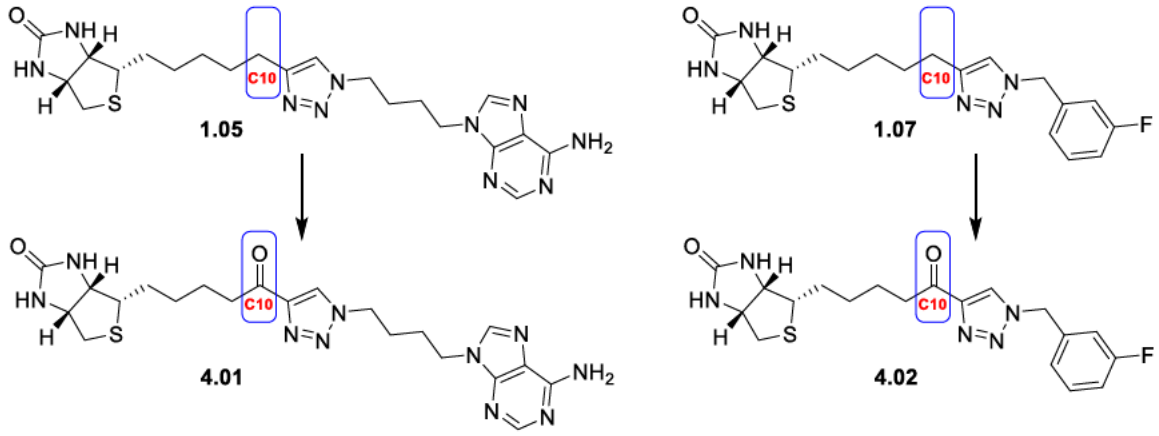

Figure 4.3: Proposed C10-carbonyl-triazole analogues **4.01** and **4.02**.

4.2.1: Docking of 4.01 and 4.02

Triazoles **4.01** and **4.02** were then docked *in silico* into *Sa*BPL to elucidate the potential interaction with Lys187. The active site of the *Sa*BPL-**1.02** complex (PDB: 3V8L[1]) was prepared for docking using the protein preparation procedure implemented in ICM-Pro version 3.8−7c.[5] The original bound ligand, **1.02**, and all water molecules, were removed from the binding site before docking of **4.01** or **4.02**. The active binding site was defined as the cavity enclosed by residues with at least one non-hydrogen atom within a 4.0 Å cut-off radius from the ligand **1.02**. The pocket was represented by 0.5 Å grid maps accounting for hydrogen bonding, hydrophobic, van der Waals, and electrostatic interactions. Compounds **4.01** and **4.02** were flexibly docked into the rigid binding site and scored based on the ICM scoring function.[5] The docking protocol was validated by removing the bound ligand **1.02** from its cocrystal structure with *Sa*BPL, followed by redocking into the vacated active site. The docking conformation and real ligand pose of **1.02** in the active site are similar, with an acceptable root-mean-square deviation (RMSD) of 0.47 Å, see Figure 4.4. Hence, this docking method was amenable for the docking study of **4.01** and **4.02**.

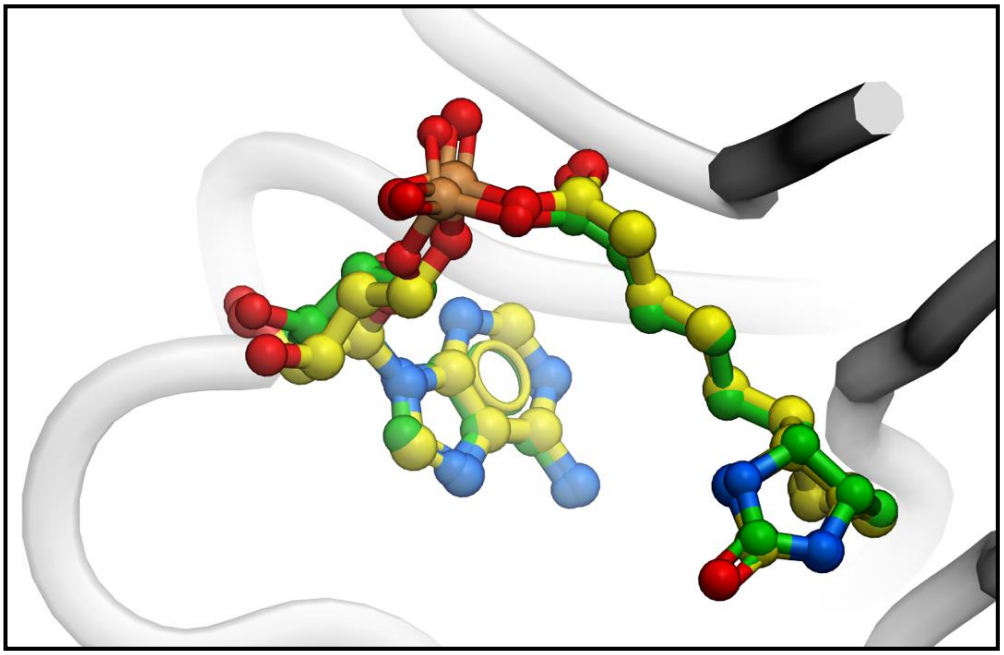

Figure 4.4: The superimposed image of the original ligand biotinyl-5'-AMP **1.02** binding conformation (green) with the predicted (yellow), where the RMSD = 0.47 Å.

The docking results for **4.01** and **4.02** reveal that both analogues can potentially form a hydrogen bond interaction between their respective C10-carbonyls and Lys187, see Figure 4.5. However, as the mono-benzyl triazole **1.07** exhibited greater potency than **1.05** (K_i = 0.66[1] vs

0.27[2] μM, respectively), and is substantially simpler to prepare, only analogue **4.02** was selected for subsequent synthesis and assay.

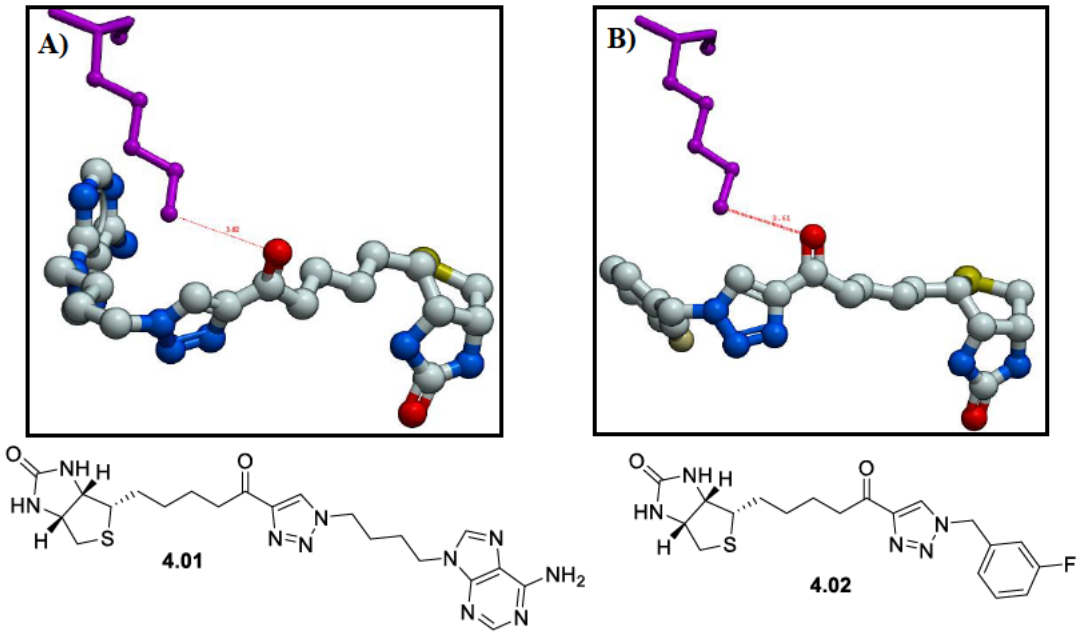

Figure 4.5: Predicted binding conformations of **4.01** (**A**) and **4.02** (**B**) within the active site of *Sa*BPL, as obtained by docking. Hydrogen bonding is highlighted by red dashes between Lys187 and the C10-carbonyl for both analogues (**A** = 3.62 Å, **B** = 3.61 Å).

4.2.2: Synthesis of biotin-ynone 4.04

A retrosynthesis of the target triazole **4.02** identified *m*-F benzyl azide **4.03**[2] and biotin-ynone **4.04** as suitable precursors, with **4.04** accessible from biotin **1.01**. The synthesis and detailed NMR characterisation of **4.04** is discussed in detail below.

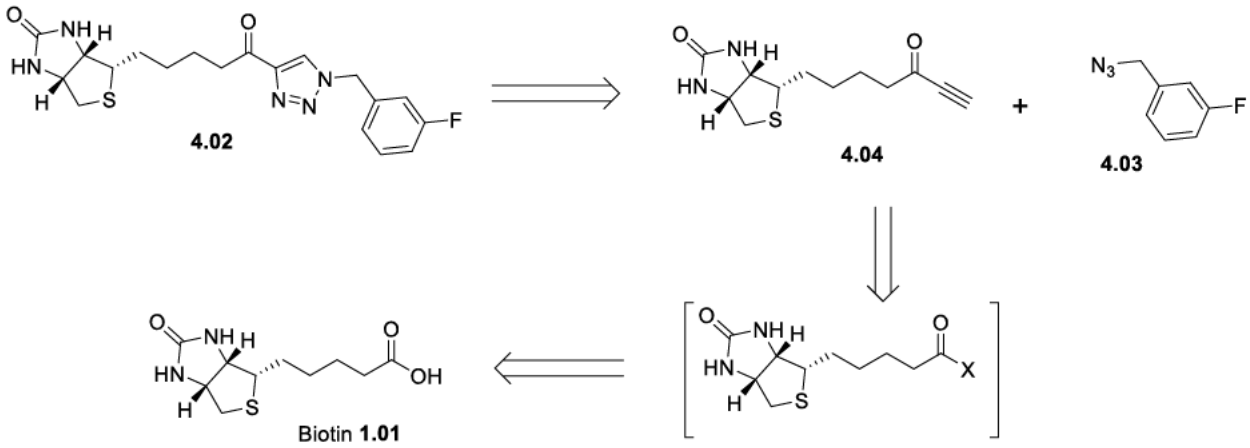

Figure 4.6: Retrosynthesis of triazole **4.02**.

The first attempted synthesis of biotin-ynone **4.04** from biotin-Weinreb amide **4.05** is shown in Scheme 4.1.[6] Coupling biotin **1.01** with *N,O*-dimethylhydroxyamide hydrochloride in the presence of EDCI and DIPEA, gave rise to 5% of **4.05** after purification by column chromatography.

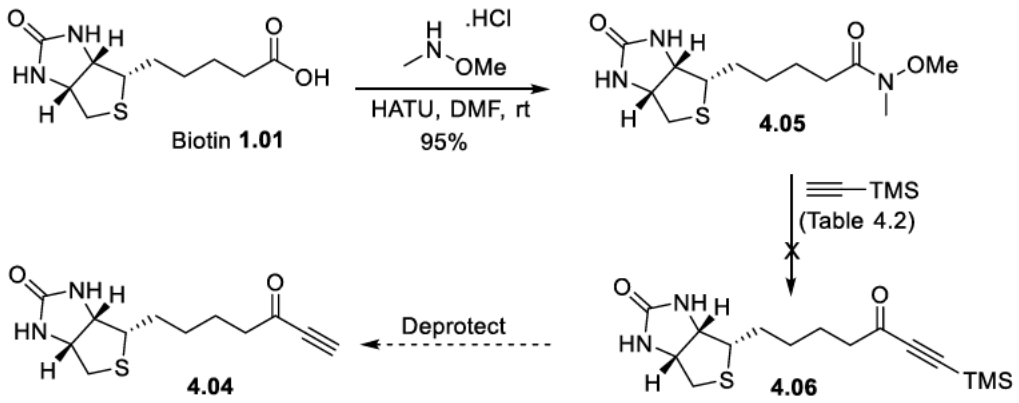

Scheme 4.1: Proposed synthetic pathway for biotin-ynone **4.04**

Further optimisation was attempted under the conditions outlined in Table 4.1. Coupling biotin **1.01** with 2.0 equivalents of EDCI as depicted in entry 2, gave returned starting material. This may reflect the relatively poor solubility of biotin **1.01** in DCM, which likely limits reactivity with EDCI. The use of DMF as the solvent considerably improved biotin **1.01** solubility and gave **4.05** in an improved yield (15 %), (entry 3). Replacing EDCI with HBTU or HATU (entries 4 and 5) further improved the yield to 53 and 95 % respectively.

Table 4.1: Optimisation of the Weinreb amide **4.05** synthesis.

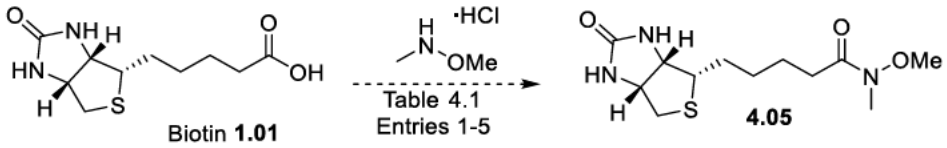

Entry	Coupling reagent / (Eq)	Base / (Eq)	Solvent	Yield (%)[a]
1	EDCI / 1.0	DIPEA / 3	DCM	5[b]
2	EDCI / 2.0	DIPEA / 3	DCM	0[c]
3	EDCI / 1.0	DIPEA / 3	DMF	15
4	HBTU / 1.0	DIPEA/ 3	DMF	53
5	HATU / 1.0	DIPEA / 3	DMF	95

[a] Isolated yield after flash chromatography. [b] Trace impurities still present according to ^{1}H NMR. [c] No product detected by TLC or ^{1}H NMR.

Weinreb amide **4.05** was then reacted with freshly prepared lithium TMS-acetylide in anhydrous THF at -78 °C,[6] however, only starting material was isolated. Optimisation of the reaction was attempted by increasing the equivalents of *n*-BuLi and TMS-acetylene (see Table 4.2, entries 2 – 4) to no avail. Solubility of **4.05** was thought to be an issue, so the reaction temperature was increased to -48 °C (entries 5 – 6) however, only starting material was isolated by column chromatography. The use of 5.0 equivalents of acetylide at -48 °C (entry 7) gave a complex mixture by TLC. Given the lack of success in preparing **4.06**, an alternate approach was devised.

Table 4.2: Attempted conditions to prepare TMS protected-ynone **4.06**.

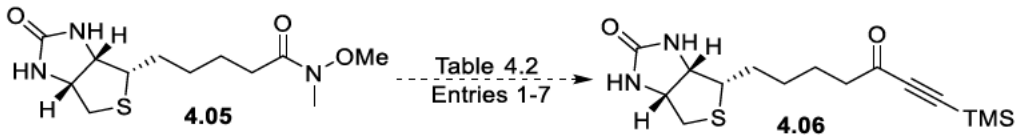

Entry	TMS-Acetylene (Eq)	*n*-BuLi (Eq)	Temperature (°C)	Yield (%)
1	1	1	-78	N/A
2	2	2	-78	N/A
3	5	5	-78	N/A
4	10	10	-78	N/A
5	1	1	-48	N/A
6	2	2	-48	N/A
7	5	5	-48	N/A[a]

[a] Complex organic mixture obtained as determined by TLC. No evidence of product found via LC-MS or ^{1}H NMR analysis.

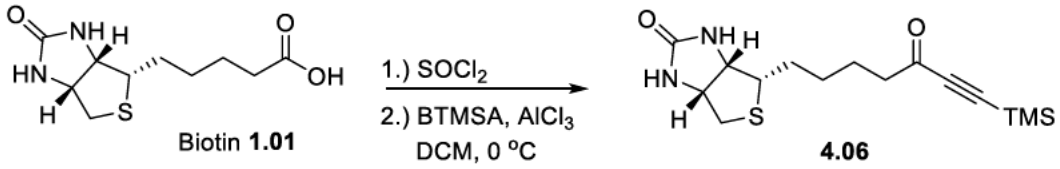

Scheme 4.2: Synthesis of TMS protected ynone **4.06**.

A second synthetic pathway to TMS-protected ynone **4.06** is outlined in Scheme 4.2,[7–11] with optimisation shown in Table 4.3. Biotin **1.01** was insoluble in neat $(COCl)_2$ (entry 1), which is reflected by the poor product yield of 2 %. Using a mixture of DCM/$(COCl)_2$ (entry 2) or DCM/DMF/$(COCl)_2$ (entry 3) enhanced the solubility of biotin **1.01** during acyl chloride formation, resulting in improved yields of 4 and 13 %, respectively. Replacing the $(COCl)_2$ for the more reactive $SOCl_2$ further improved the yield (entries 4 and 5). Increasing the equivalents

of BTMSA from 1.1 to 2.2 did not improve the yield (entry 6), however, increasing the amount of $AlCl_3$ from 1.0 to 2.0 equivalents (entry 7) gave **4.06** in 45 % yield. This additional equivalent of $AlCl_3$ was proposed to potentially accelerate the reaction rate of the Friedel-Crafts acylation between BTMSA and crude biotin acyl chloride. Increasing the equivalents of $AlCl_3$ further (entry 8), substantially reduced the yield of **4.06** (14 %) and resulted in a complex reaction mixture by TLC. Thus, entry 7 represents the optimised conditions for the preparation of TMS-protected ynone **4.06**.

Table 4.3: Optimization of TMS protected ynone **4.06**

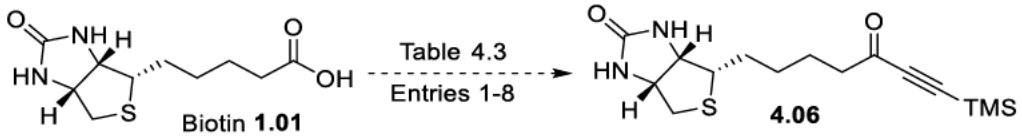

[b]Entry	Chlorinating Reagent	BTMSA (Eq)	$AlCl_3$ (Eq)	Step 1-Solvent (v/v)	Yield (%)[a]
1	$(COCl)_2$	1.1	1	N/A	2
2	$(COCl)_2$	1.1	1	DCM	7
3	$(COCl)_2$	1.1	1	DCM/DMF (20/1)	13
4	$SOCl_2$	1.1	1	N/A	15
5	$SOCl_2$	1.1	1	DCM/DMF (20/1)	32
6	$SOCl_2$	2.2	1	DCM/DMF (20/1)	30
7	$SOCl_2$	1.1	2	DCM/DMF (20/1)	45
8	$SOCl_2$	1.1	3	DCM/DMF (20/1)	14

[a] Isolated yield after flash chromatography. [b] All entries attempted on a 1 mmol scale of biotin **1.01**.

TMS-protected **4.06** was characterised by ^1H, ^{13}C and HMBC NMR. The ^1H NMR spectrum of **4.06** revealed a 9H singlet at 0.25 ppm that was assigned to the methyl protons of the TMS protecting group, see Figure 4.7 (A). The ^{13}C NMR spectrum showed a characteristic carbonyl resonance at 187 ppm, corresponding to the C10-carbonyl. Three additional resonances at 102, 98 and -0.71 ppm were assigned to the acetylene and TMS carbons respectively. A comparison of the ^{13}C NMR spectra of **4.06** and TMS-protected acetyl ynone **4.07**[10] revealed both compounds share these similar ^{13}C resonances at 187, 102, 98 and -0.71 ppm, see Figure 4.7.

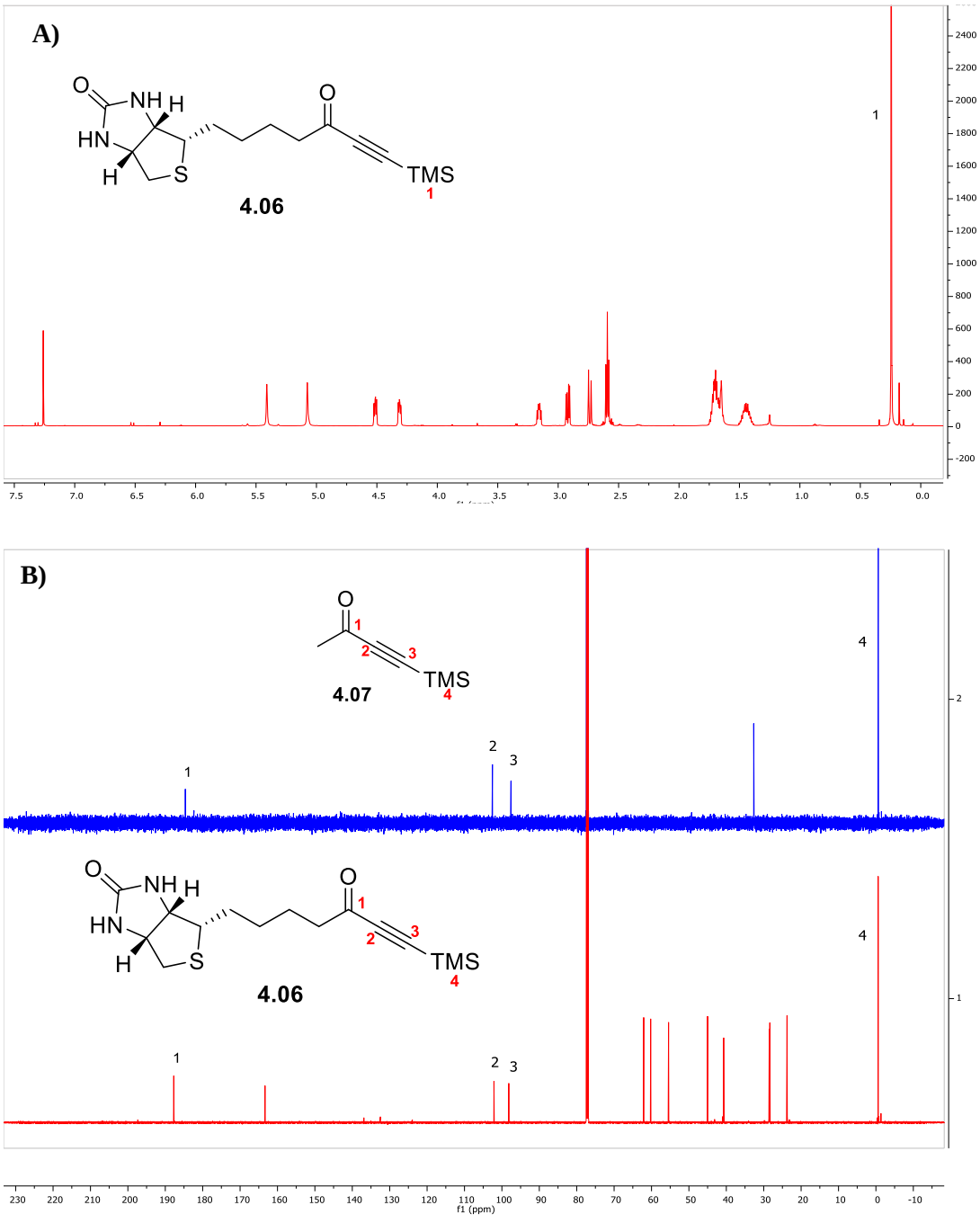

Figure 4.7: NMR spectra of ynone **4.06** and TMS-protected ynone **4.07**. (**A**) ^{1}H NMR spectrum of **4.06**. (**B**) Stacked ^{13}C NMR spectra of **4.06** and **4.07**.

The HMBC spectrum of **4.06** revealed a correlation between the *alpha*-C10 methylene protons (2.59 ppm) and the C10 carbonyl (187 ppm), and also to the acetylene carbon (102 ppm), see Figure 4.8 (A). The TMS protons (0.25 ppm) were observed to correlate only to the acetylene at 98 ppm carbon, see Figure 4.8 (B). These correlations confirm that the acetylene carbon assigned at 98 ppm is bonded to the TMS protecting group, while the 102 ppm resonance demonstrates that the acetylene carbon is bonded to the C10-carbonyl carbon at 187 ppm. Collectively, these data confirm the identity of the TMS-ynone substituent of **4.06**.

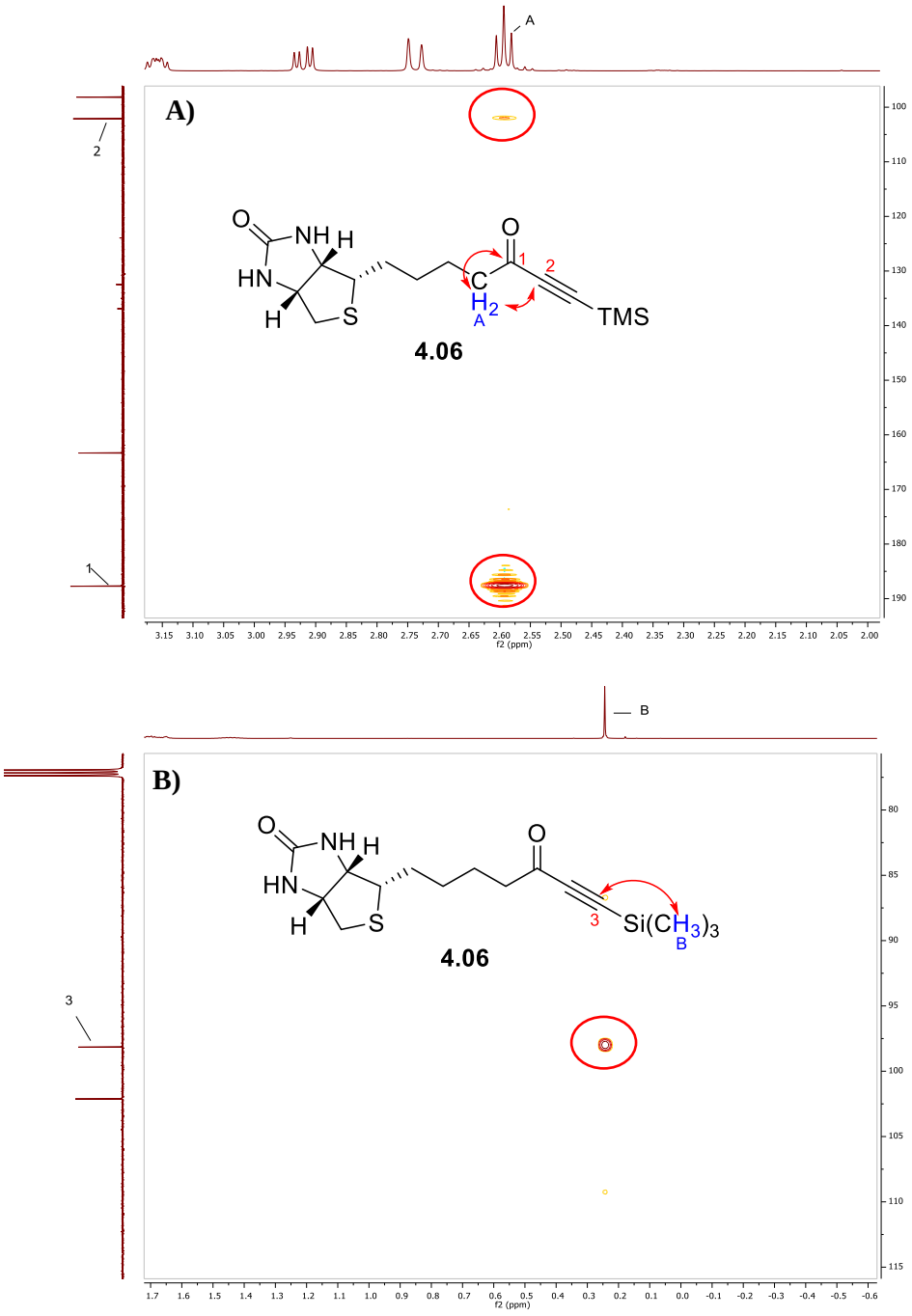

Figure 4.8: The partial HMBC spectrum of TMS-protected ynone **4.06**. (**A**) Coupling between the 2.59 ppm methylene protons and ynone carbons at 187 and 98 ppm. (**B**) Coupling between the 0.25 ppm TMS methyl protons and the ynone acetylene carbon at 102 ppm.

Subsequent TMS deprotection of **4.06**, to give target ynone **4.04**, was undertaken as outlined in Figure 4.9. For method 1,[12] addition of 1 M TBAF to **4.06** in THF gave a complex reaction mixture as indicated by TLC. An LC-MS trace of this mixture showed that the mass peak for **4.04** was not evident. Method 2,[13] involved reacting **4.06** with K_2CO_3 in MeOH, which gave a complex mixture with the mass of **4.04** also not detected by LC-MS. However, treating TMS-protected ynone **4.06** with an aqueous solution of KF, (method 3[14]) gave the desired biotin-

ynone **4.04** in a quantitative yield. A TLC analysis suggested **4.04** to be the sole compound formed under these conditions (See Chapter Six for method details).

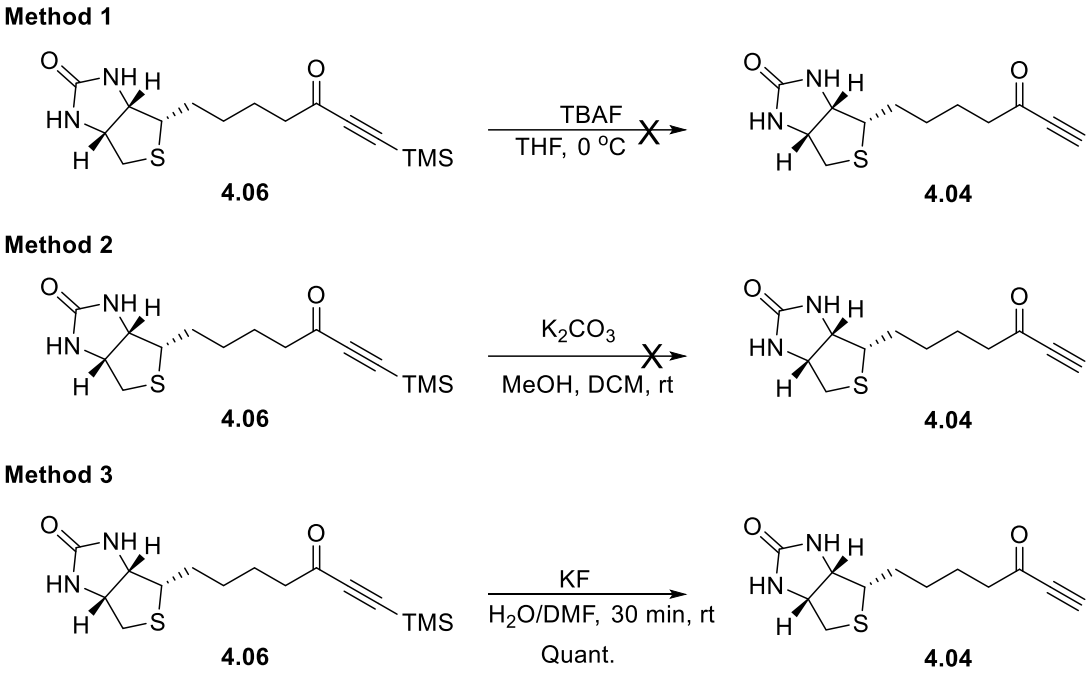

Figure 4.9: Synthetic schemes conducted for TMS deprotection of **4.06** to yield ynone **4.04**.

The ^{1}H NMR spectrum of **4.04** revealed a singlet at 3.22 ppm (assigned the ynone acetylene proton) together with the absence of the TMS resonance at 0.25 ppm, which indicated successful deprotection, see Figure 4.10. The absence of the TMS resonance from the ^{13}C NMR spectrum of **4.04** provided further evidence for the formation of the deprotected product, see Figure 4.11. Furthermore, the HMBC spectrum of **4.04** revealed that the acetylene proton (3.22 ppm) and *alpha* methylene protons (2.63 ppm) couple to the C10-carbonyl (187 ppm), confirming the presence of the ynone functionality in **4.04**, see Figure 4.12. As anticipated, all remaining resonances comprising the ^{1}H NMR and ^{13}C NMR spectra of **4.04** are consistent with the ureido-tetrahydrothiophene ring and aliphatic chain of biotin.[1]

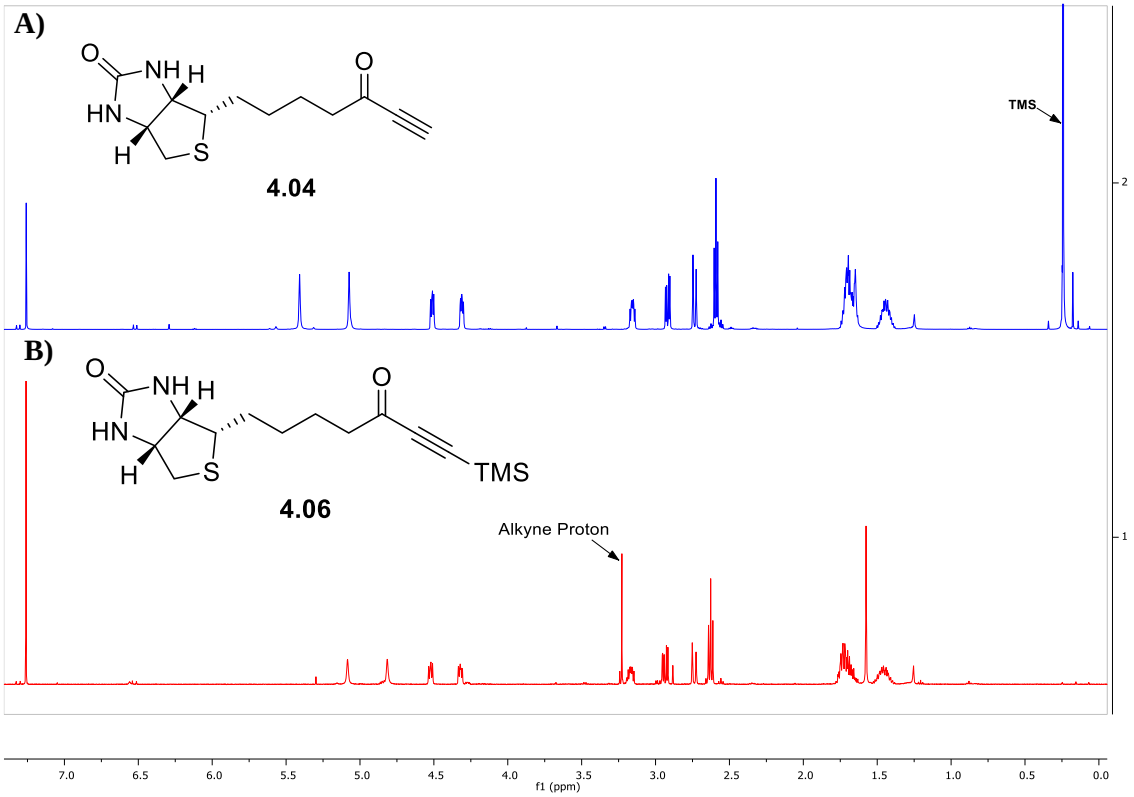

Figure 4.10: ^{1}H NMR spectra of TMS-protected ynone **4.06** (**A**) stacked against biotin-ynone **4.04** (**B**).

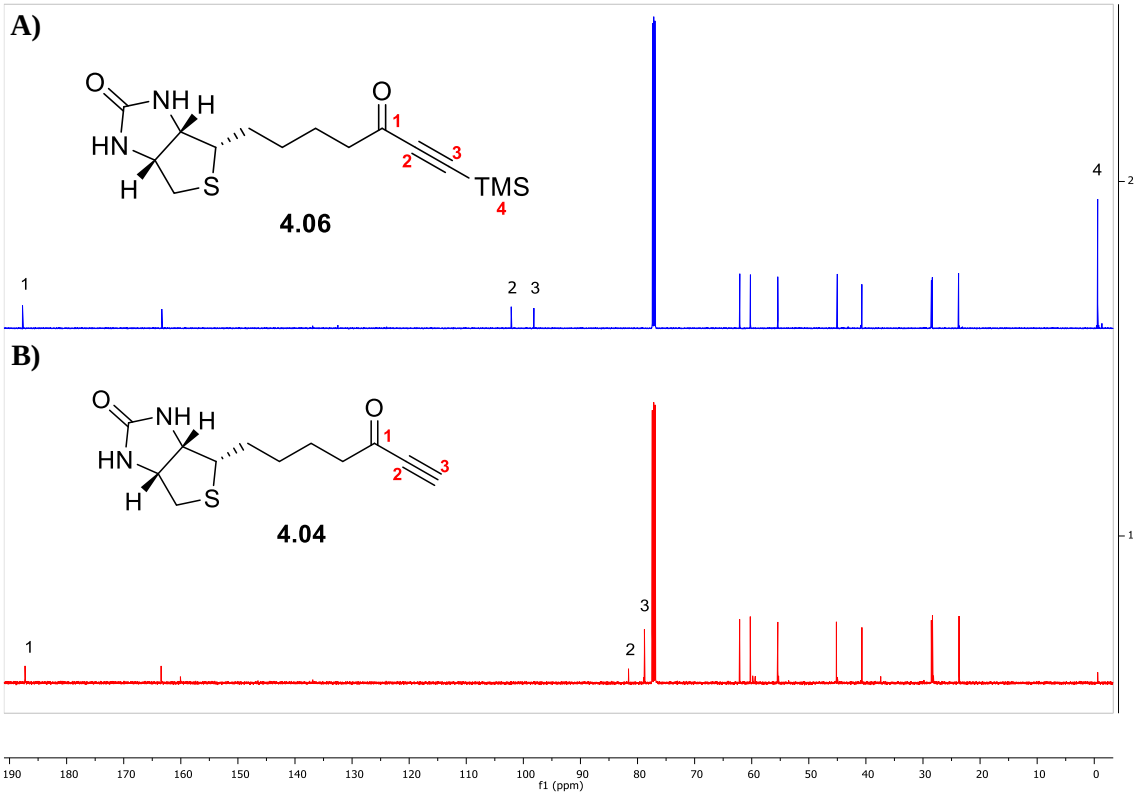

Figure 4.11: ^{13}C NMR spectra of TMS-protected ynone **4.06** (**A**) stacked against biotin-ynone **4.04** (**B**).

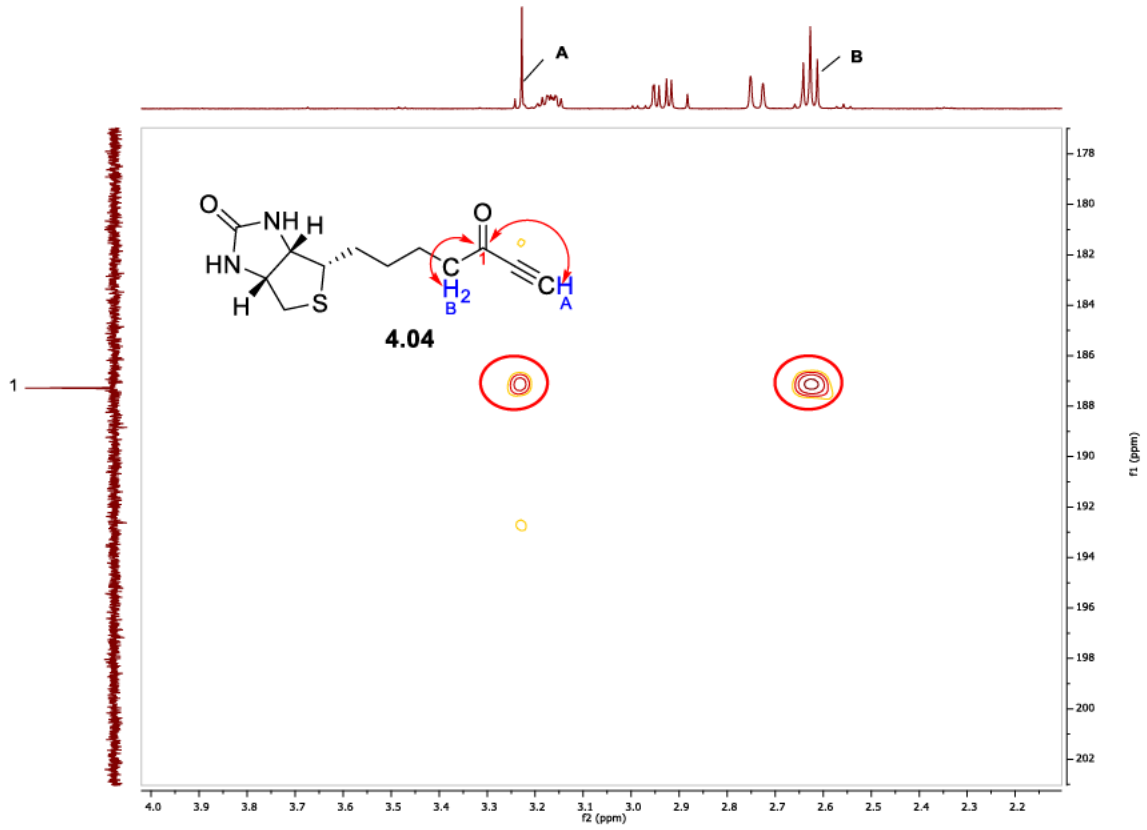

Figure 4.12: Partial HMBC spectrum of biotin-ynone **4.04**.

Despite the successful synthesis of biotin-ynone **4.04**, it was found to be unstable and decomposed after 20 min in $CDCl_3$, as evidenced by ^1H NMR. The corresponding decomposition products were not identifiable by ^1H NMR or LC-MS. The use of DMSO-d_6 instead of $CDCl_3$ also resulted in rapid decomposition of the ynone, as determined by ^1H NMR. Neutralising the $CDCl_3$ with K_2CO_3 to remove any residual D^+/H^+ prior to NMR analysis delayed decomposition by 2 h. Incidentally, TMS-protected ynone **4.06** was shown to be stable in untreated $CDCl_3$ even after 72 h as indicated by ^1H NMR. In light of these circumstances, the subsequent CuAAC reaction to synthesise analogue **4.02** (see section 4.2.3) was undertaken immediately following TMS deprotection of **4.06**.

4.2.3: Synthesis and Characterisation of Triazole 4.02

The synthesis of analogue **4.02** is outlined in Scheme 4.3. The *m*-F benzyl azide **4.03** was first prepared by reacting commercially sourced *m*-F benzyl chloride with NaN_3.[2] The CuAAC between this benzyl azide and freshly prepared biotin-ynone **4.04**, gave triazole **4.02** in good yield, 86 %.

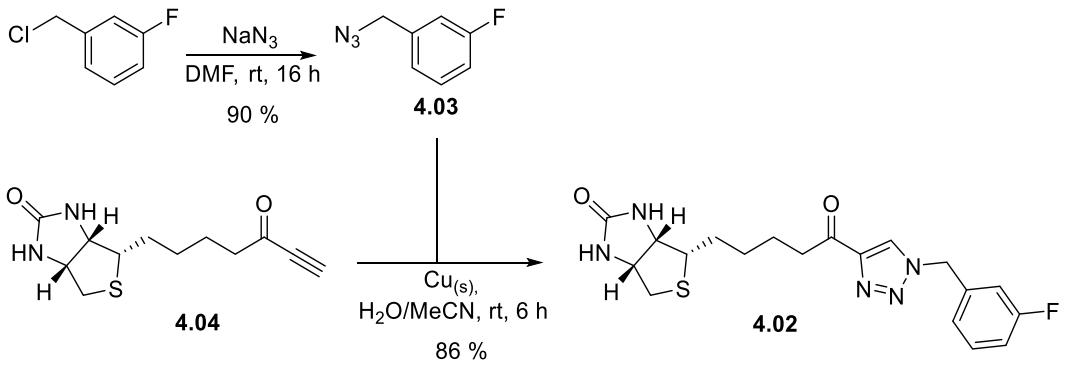

Scheme 4.3: Synthesis of triazole **4.02**.

Interestingly, this high yield of **4.02** was acquired after only 6 h of reaction time. This was unexpected as the equivalent CuAAC between biotin acetylene **4.08**,[1] which does not contain a carbonyl at the C10 position, and **4.03**, gave the corresponding triazole in 51 % over 12 h.[2] The rapid formation of **4.02** was attributed to the acidity of the ynone acetylene proton of **4.04**. Mechanistically, the CuAAC reaction ensues by first displacing the acetylene proton with Cu(I),[15,16] Thus, an acidic/labile acetylene proton would be expected to be more susceptible to displacement by this $Cu_{(I)}$ species. This is evident when comparing the acetylene proton resonances of **4.08** and **4.04**, where **4.08** is located significantly further upfield to **4.04** (1.95 ppm vs 3.22 ppm, respectively, see Figure 4.12). Hence, the improved CuAAC reaction rate for triazole **4.02**, relative to **1.07**, can be attributed to the acidity of the **4.04** ynone acetylene proton.

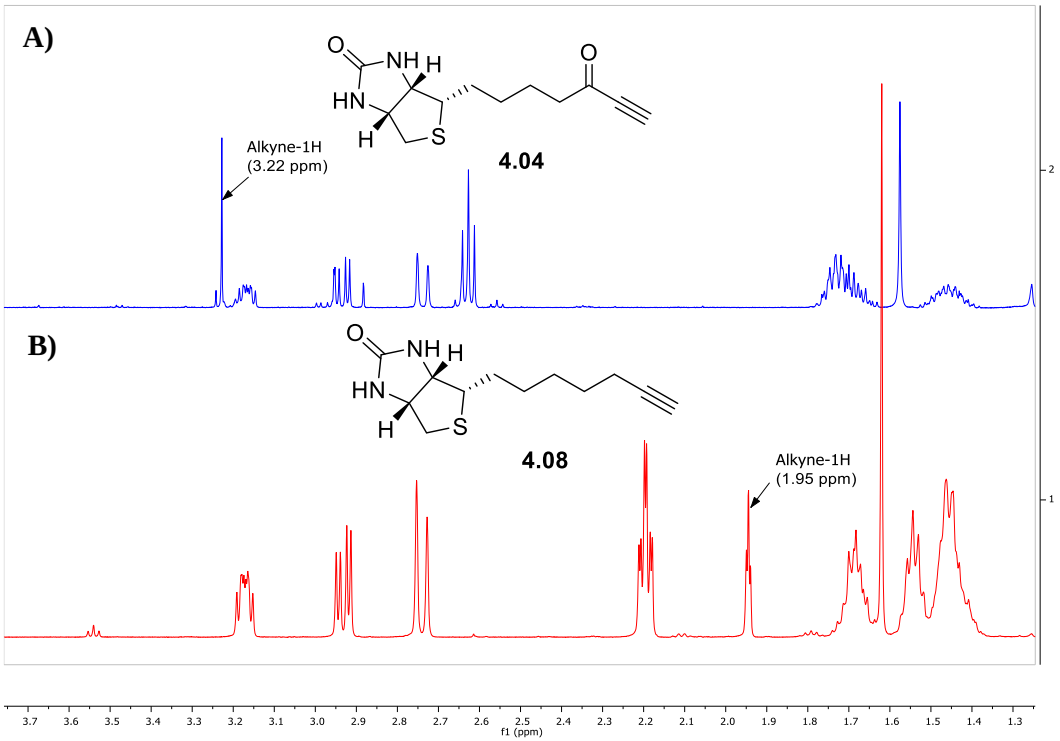

Figure 4.12: The stacked partial ^{1}H NMR spectra of biotin-ynone **4.04** (**A**) and biotin-acetylene **4.08** (**B**).

The C10-carbonyl-triazole linker of **4.02** was characterised unambiguously by ^{1}H, ^{13}C, HSQC, HMBC and NOESY NMR spectroscopy. The triazole proton (H_a), benzyl methylene protons (H_b), and methylene protons (H_c) were assigned resonances 8.00, 5.57 and 3.15 ppm respectively in the ^{1}H NMR spectrum of **4.02** (see Figure 4.13). The HSQC spectrum of **4.02** revealed that protons H_a, H_b, and H_c correlate to ^{13}C resonances 126, 54 and 39 ppm, respectively. The HMBC spectrum of **4.02** revealed that the H_c methylene protons (3.15 ppm) coupled to the C10-carbonyl carbon (195 ppm), the H_a triazole proton (8.00 ppm) coupled to the benzylic methylene carbon (54 ppm) and the H_b benzylic methylene protons (5.57 ppm) coupled to the triazole C5 carbon (126 ppm), see Figure 4.14.

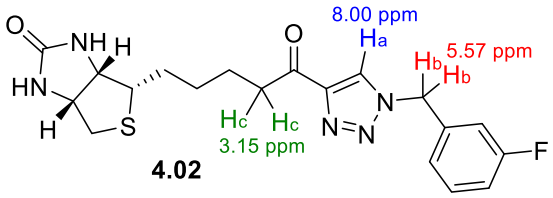

Figure 4.13: Diagnostic hydrogens with assigned chemical shifts for triazole **4.02**.

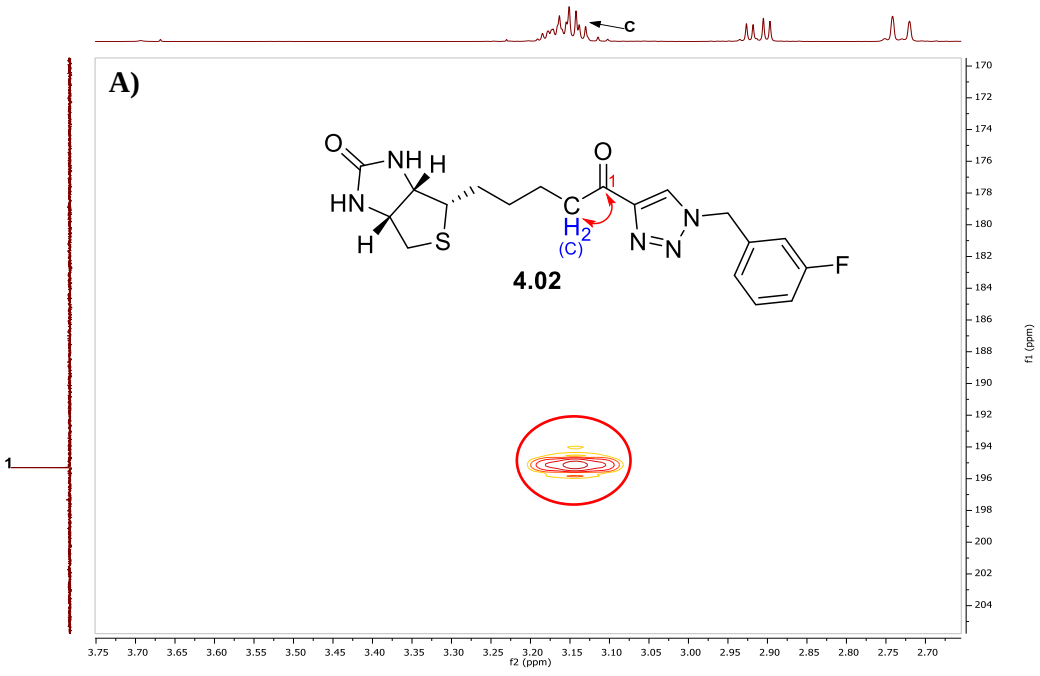

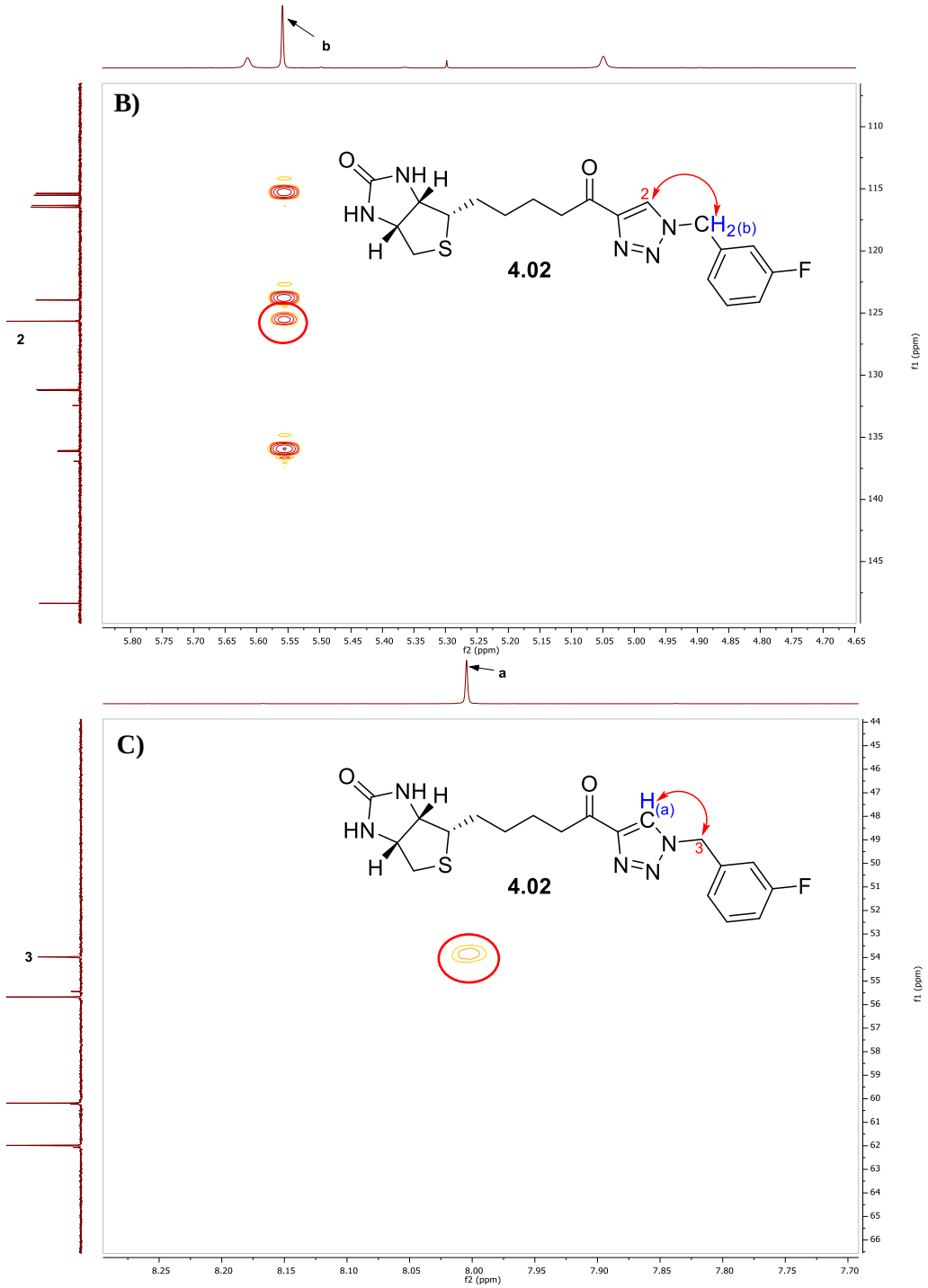

Figure 4.14: Partial HMBC spectrum of triazole **4.02**. (**A**) Coupling shown between the 3.15 ppm methylene protons and C10-carbonyl carbon at 195 ppm. (**B**) Coupling between the benzyl methylene protons at 5.57 ppm and the triazole carbon at 126 ppm. (**C**) Coupling shown between the triazole proton at 8.00 ppm and benzyl methylene carbon at 54 ppm.

The NOESY spectrum of triazole **4.02** revealed NOE correlations between the H_b benzyl methylene protons (5.57 ppm) and H_a triazole proton (8.00 ppm), see Figure 4.15(A). The H_a triazole proton (8.00 ppm) also correlated to the H_c methylene protons (3.15 ppm) *alpha* to the C10 carbonyl (Figure 4.15, B), suggesting free rotation occurs around the C10 – C4-triazole

bond. This indicates that the C10-carbonyl does not introduce rigidity into the triazole linker of **4.02** and should still permit flexible binding into the phosphate binding site of *Sa*BPL. Collectively, these data confirm the identity of the C10-carbonyl-containing triazole **4.02**.

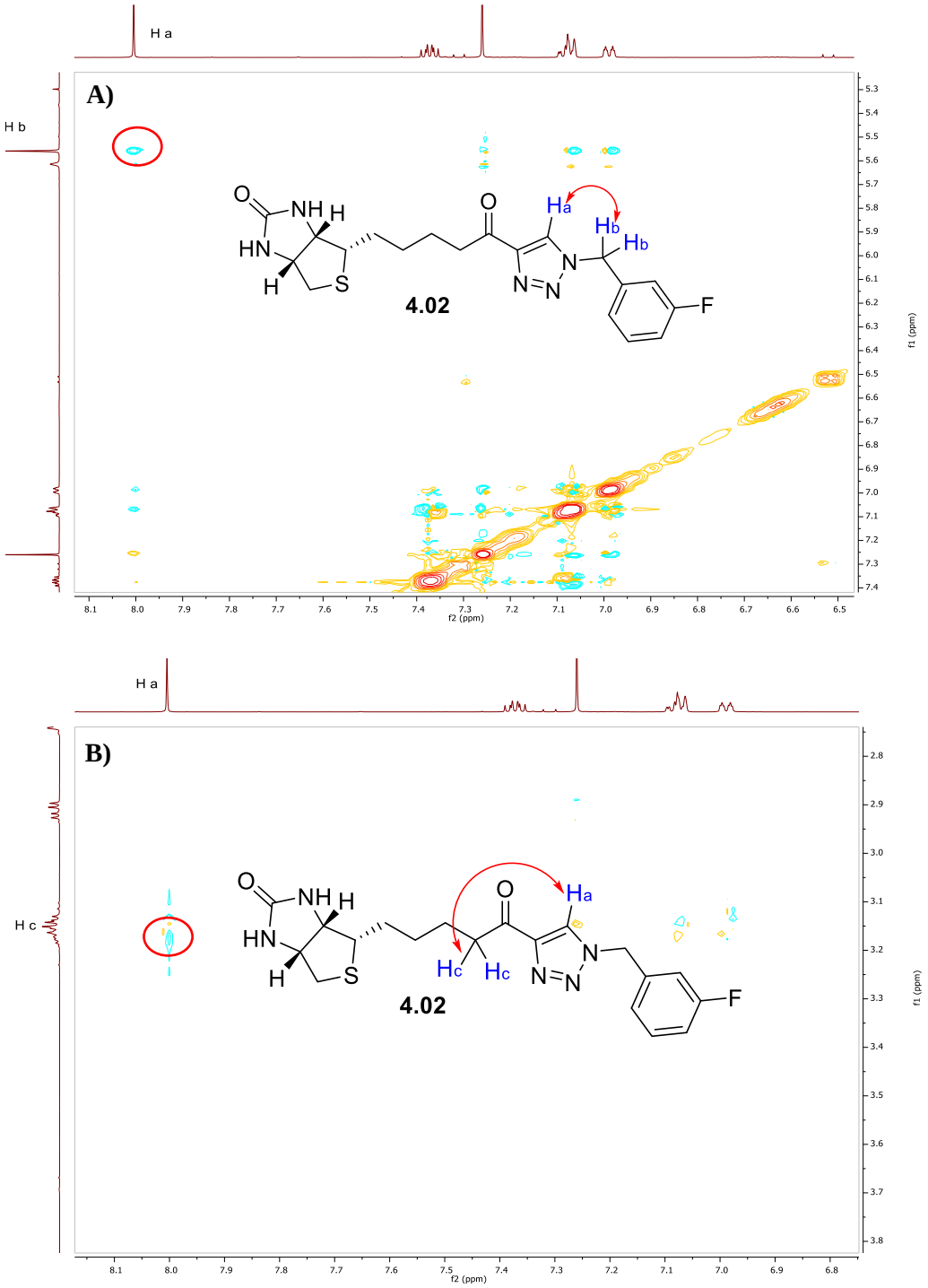

Figure 4.16: Partial NOESY spectrum of triazole **4.02**. NOE coupling between the triazole proton (H_a, 8.00 ppm) and methylene benzyl protons (H_b, 5.57 ppm) is highlighted (**A**) and coupling between the triazole proton (H_a, 8.00 ppm) and methylene protons (H_c, 3.15 ppm) (**B**).

4.3: Biochemical and Antimicrobial Assay of Triazole 4.02

Triazole **4.02** was assayed against *Sa*BPL using an *in vitro* biotinylation assay[17] (K_i values presented in Table 4.4). The whole cell activity of triazole **4.02** was also determined against a clinical isolate (ATCC 49775) and sensitive strain (RN4220) of *S. aureus* using an antibacterial susceptibility assay,[2] with minimum inhibitory concentrations (MIC, ≥ 90 % growth inhibited) shown in Table 4.4. The reported biochemical and antimicrobial data for **1.07**[2] is also presented here for direct comparison to **4.02**.

Table 4.4: Biochemical and anti-staphylococcal properties of Triazoles **4.02** and **1.07**.

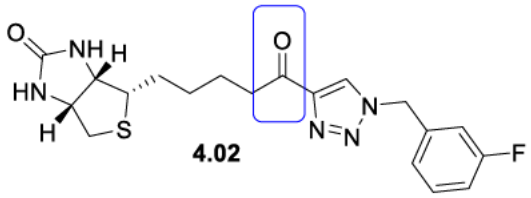

4.02

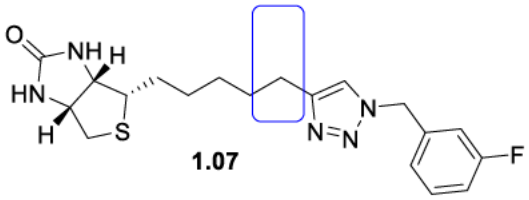

1.07

Compound	K_i *Sa*BPL (μM)	MIC RN4220 [a] (μg/mL)	MIC ATCC49775 [b] (μg/mL)
4.02	0.12 ± 0.01	32	>64 [c]
1.07[2]	0.25 ± 0.03	>64 [c]	>64 [c]

[a] Sensitive strain of *S. aureus*. [b] Clinical isolate of *S. aureus*. [c] MIC >64 μg/mL was reported for compounds where no MIC was attainable for 64 μg/mL (the highest concentration assayed in this study).

Triazole **4.02** provided a two-fold improvement in inhibitory activity against *Sa*BPL relative to **1.07** (K_i = 0.12 ± 0.01 vs 0.25 ± 0.03 μM, respectively). This result is consistent with docking, where the C10-carbonyl of **4.02** was predicted to form a hydrogen bond with Lys187. However, all attempts in obtaining an X-ray cocrystal structure of triazole **4.02** in complex with *Sa*BPL to confirm a hydrogen bond is formed between the C10-carbonyl of **4.02** and Lys187, were unsuccessful. Notably, **4.02** demonstrated comparable activity to recently reported potent N^1-diphenylmethyl triazole **10**[17] (K_i = 0.12 ± 0.01 vs 0.18 ± 0.03 μM, respectively). Mono-benzylic **4.02** suggests better atom economy relative to N^1-diphenylmethyl triazole **10**[17] and thus warrants further work to design new mono-benzyl-analogues bearing a C10-carbonyl moiety.

Both **4.02** and **1.07** showed poor whole cell activity against the clinical isolate ATCC 49775, however, **4.02** provided significant improvement in activity over **1.07** against the sensitive strain (MIC = 32 vs >64 μg/mL respectively). The combined biochemical and antimicrobial data confirm **4.02** as a superior inhibitor over **1.07** in both *Sa*BPL inhibition and anti-staphylococcal activity.

4.4: Conclusion

Triazole **4.02**, with its C10-carbonyl, was prepared by a CuAAC reaction and subsequently assayed against *Sa*BPL and *S. aureus* (RN4220 and ATCC49775). This compound was found to be significantly more potent against *Sa*BPL relative to the C10-methylene-triazole **1.07**[2] (K_i = 0.12 ± 0.01 vs 0.25 ± 0.03 µM, respectively). Furthermore, inhibitor **4.02** greatly improved whole cell activity against *S. aureus* RN4220 relative to **1.07** (32 vs ≥64 µg/mL). The 2-fold improvement against *Sa*BPL is consistent with findings from the docking study, which indicated a hydrogen bond interaction between the C10-carbonyl of **4.02** and Lys187 within the phosphate binding pocket. Collectively, these values reflect, that while we have previously established the triazole as an isostere of **1.02**, the incorporation of a carbonyl at the C10 position provides an even better mimic of the natural intermediate.

Potential future work for this C10-carbonyl-triazole linker would involve the following:

- First and foremost, obtaining an X-ray cocrystal structure of **4.02** in complex with *Sa*BPL. This would provide substantial evidence whether a hydrogen bond is formed between the C10 carbonyl of **4.02** and Lys187 of *Sa*BPL.
- Additional examples of mono-benzyl analogues should be prepared and assayed, to determine if affinity to *Sa*BPL can be further improved for the mono-benzyl-triazole-based inhibitors.
- Determine if the new C10-carbonyl-triazole pharmacophore does not inhibit *Hs*BPL.
- Prepare examples N^1-diphenylmethyl triazole-based inhibitors from Chapters Two. As Chapter Two highlighted, this particular chemotype is highly potent against *Sa*BPL, thus C10-carbonyl derivatives may procure highly potent inhibitors of *Sa*BPL. Examples of some potential analogues are presented below in Figure 4.16. Comparisons in activity could then be drawn between these analogues and the mono-benzyl derivatives.

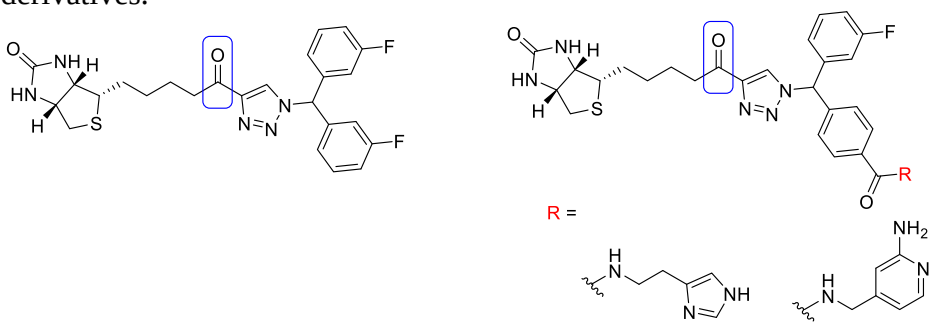

Figure 4.16: Future C10-triazole *Sa*BPL inhibitor analogues.

4.5: References for Chapter Four

(1) Soares Da Costa, T. P.; Tieu, W.; Yap, M. Y.; Pendini, N. R.; Polyak, S. W.; Pedersen, D. S.; Morona, R.; Turnidge, J. D.; Wallace, J. C.; Wilce, M. C. J.; Booker, G. W.; Abell, A. D. Selective Inhibition of Biotin Protein Ligase from Staphylococcus Aureus. *J. Biol. Chem.* **2012**, *287* (21), 17823–17832. https://doi.org/10.1074/jbc.M112.356576.

(2) Paparella, A. S.; Lee, K. J.; Hayes, A. J.; Feng, J.; Feng, Z.; Cini, D.; Deshmukh, S.; Booker, G. W.; Wilce, M. C. J.; Polyak, S. W.; Abell, A. D. Halogenation of Biotin Protein Ligase Inhibitors Improves Whole Cell Activity against Staphylococcus Aureus. *ACS Infect. Dis.* **2018**, *4* (2), 175–184. https://doi.org/10.1021/acsinfecdis.7b00134.

(3) Lee, K. J.; Tieu, W.; Blanco-Rodriguez, B.; Paparella, A. S.; Yu, J.; Hayes, A.; Feng, J.; Marshall, A. C.; Noll, B.; Milne, R.; Cini, D.; Wilce, M. C. J.; Booker, G. W.; Bruning, J. B.; Polyak, S. W.; Abell, A. D. Sulfonamide-Based Inhibitors of Biotin Protein Ligase as New Antibiotic Leads. *ACS Chem. Biol.* **2019**, *14* (9), 1990–1997. https://doi.org/10.1021/acschembio.9b00463.

(4) Soares Da Costa, T. P.; Tieu, W.; Yap, M. Y.; Pendini, N. R.; Polyak, S. W.; Pedersen, D. S.; Morona, R.; Turnidge, J. D.; Wallace, J. C.; Wilce, M. C. J.; Booker, G. W.; Abell, A. D. Selective Inhibition of Biotin Protein Ligase from Staphylococcus Aureus. *J. Biol. Chem.* **2012**, *287* (21), 17823–17832. https://doi.org/10.1074/jbc.M112.356576.

(5) Neves, M. A. C.; Totrov, M.; Abagyan, R. Docking and Scoring with ICM: The Benchmarking Results and Strategies for Improvement. *J. Comput. Aided. Mol. Des.* **2012**, *26* (6), 675–686. https://doi.org/10.1007/s10822-012-9547-0.

(6) Fedoseev, P.; Van Der Eycken, E. Temperature Switchable Brønsted Acid-Promoted Selective Syntheses of Spiro-Indolenines and Quinolines. *Chem. Commun.* **2017**, *53* (55), 7732–7735. https://doi.org/10.1039/c7cc02580g.

(7) Spantulescu, A.; Luu, T.; Yuming, Z.; McDonald, R.; Tykwinski, R. R. Synthesis and Characterization of Cyclic Alkyl Tetraynes. *Org. Lett.* **2008**, *10* (4), 609–612. https://doi.org/10.1021/ol702898a.

(8) Schwab, J. M.; Lin, D. C. T. Stereochemical Course of an Enzyme-Catalyzed Allene-Acetylene Isomerization. *J. Am. Chem. Soc.* **1985**, *107* (21), 6046–6052. https://doi.org/10.1021/ja00307a037.

(9) Earl, R. A.; Vollhardt, K. P. C. Cobalt-Catalyzed Cocyclizations of Isocyanatoalkynes: A Regiocontrolled Entry into 5-Indolizinones. Application to the Total Synthesis of Camptothecin. *J. Am. Chem. Soc.* **1983**, *105* (23), 6991–6993. https://doi.org/10.1021/ja00361a057.

(10) Heiss, C.; Laivenieks, M.; Zeikus, J. G.; Phillips, R. S. Mutation of Cysteine-295 to Alanine in Secondary Alcohol Dehydrogenase from Thermoanaerobacter Ethanolicus Affects the Enantioselectivity and Substrate Specificity of Ketone Reductions. *Bioorganic Med. Chem.* **2001**, *9* (7), 1659–1666. https://doi.org/10.1016/S0968-0896(01)00073-6.

(11) Walton, D. R. M.; Waugh, F. Friedel-Crafts Reactions of Bis(Trimethylsilyl)Polyynes with Acyl Chlorides; a Useful Route to Terminal-Alkynyl Ketones. *J. Organomet. Chem.* **1972**, *37* (1), 45–56. https://doi.org/10.1016/S0022-328X(00)89260-8.

(12) Liu, X.; Yu, L.; Luo, M.; Zhu, J.; Wei, W. Radical-Induced Metal-Free Alkynylation of Aldehydes by Direct C-H Activation. *Chem. - A Eur. J.* **2015**, *21* (24), 8745–8749. https://doi.org/10.1002/chem.201501094.

(13) Huxley, M. T.; Burgun, A.; Ghodrati, H.; Coghlan, C. J.; Lemieux, A.; Champness, N. R.; Huang, D. M.; Doonan, C. J.; Sumby, C. J. Protecting-Group-Free Site-Selective Reactions in a Metal-Organic Framework Reaction Vessel. *J. Am. Chem. Soc.* **2018**, *140* (20), 6416–6425. https://doi.org/10.1021/jacs.8b02896.

(14) Yamaguchi, J. Ichi; Sugiyama, S. Conjugate Addition of an Ynone Containing Azulene with a Tertiary Amine. *Tetrahedron Lett.* **2016**, *57* (41), 4514–4518. https://doi.org/10.1016/j.tetlet.2016.08.094.

(15) Seath, C. P.; Burley, G. A.; Watson, A. J. B. Determining the Origin of Rate-Independent Chemoselectivity in CuAAC Reactions: An Alkyne-Specific Shift in Rate-Determining Step. *Angew. Chemie - Int. Ed.* **2017**, *56* (12), 3314–3318. https://doi.org/10.1002/anie.201612288.

(16) Ben El Ayouchia, H.; Bahsis, L.; Anane, H.; Domingo, L. R.; Stiriba, S. E. Understanding the Mechanism and Regioselectivity of the Copper(i) Catalyzed [3 + 2] Cycloaddition Reaction between Azide and Alkyne: A Systematic DFT Study. *RSC Adv.* **2018**, *8* (14), 7670–7678. https://doi.org/10.1039/c7ra10653j.

(17) Stachura, D. L.; Nguyen, S.; Polyak, S. W.; Jovcevski, B.; Bruning, J. B.; Abell, A. D. A New 1,2,3-Triazole Scaffold with Improved Potency Against Staphylcoccus Aureus Biotin Protein Ligase. **2022**, *8* (12), 2579–2585. https://doi.org/10.1021/acsinfecdis.2c00452.

Chapter Five

5.1: Introduction

As presented in Chapter One, sulfonamide-based inhibitors of *S. aureus* BPL (*Sa*BPL) show promise as drug leads against this enzyme. For example, sulfamide **1.14** demonstrated high potency against *Sa*BPL (K_i = 7.00 ± 0.30 nM) and also a clinical isolate of *S. aureus*, ATCC 49775 (MIC = 0.25 μg/mL).[1] However, it has poor *in vivo* stability, where the sulfonyl linker rapidly hydrolyses (see Figure 5.1) when incubated in drug-free whole rat blood.[1]

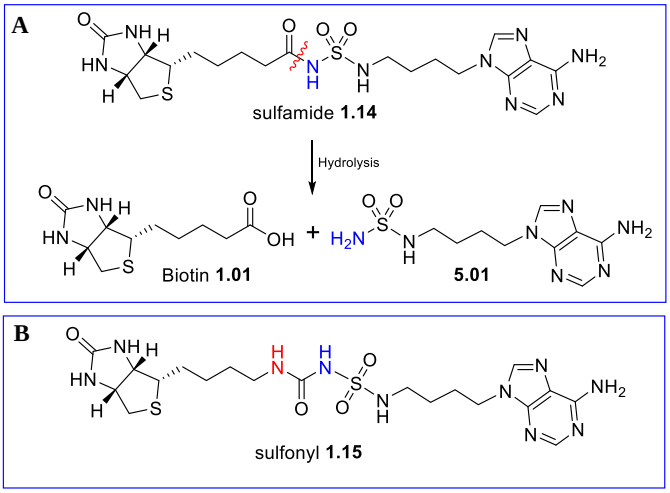

Figure 5.1: Reported sulfonamide-based inhibitors of *Sa*BPL.[1] (**A**) Proposed degradation of **1.14**, with subsequent products shown. (**B**) Chemical structure of sulfonylurea **1.15**. The central NH is highlighted in blue with the urea amine NH in red.

Recent work by Lee *et al* has demonstrated that replacing the sulfamide linker of **1.14** with an amino sulfonylurea, as in **1.15**, drastically improved *in vivo* stability.[1] However, this inhibitor (**1.15**, K_i = 65.0 ± 3.0 nM) was approximately 10-fold less active against *Sa*BPL, relative to **1.14** (K_i = 7.00 ± 0.30 nM).[1] It was proposed that this is linked to the relative acidity of the respective central NH (highlighted in blue, Figure 5.1) which may influence potency against *Sa*BPL. An X-ray crystal structure of sulfamide **1.14**, in complex with *Sa*BPL, suggested that the conjugate base of the sulfonamide/central NH forms an electrostatic interaction between Lys187 of *Sa*BPL (highlighted as blue Figure 5.1).[1] This interaction mimics the hydrogen bond formed between the phosphoryl linker of biotinyl-5'-AMP **1.02** and *Sa*BPL.[1] In contrast, sulfonylurea **1.15** in complex with *Sa*BPL, showed two distinct inhibitor binding conformations, with only the minor conformer (adopted by the conjugate base) reported to hydrogen bond with Lys187.[1] This limited interaction between Lys187 and *Sa*BPL-bound **1.15** suggests that the acidity of the central NH plays an important role in conferring potency. Indeed, the calculated pK_a values for the central NH of **1.14** and **1.15** are reported as 4.15 and 4.36

respectively,[1] which further supports this proposition. Thus, it is proposed that the relative acidity of the central NH can be influenced through chemical modification of the sulfonyl linker, to procure a series of potent sulfonamide-based *Sa*BPL inhibitors.

Work described in this Chapter highlights the design, synthesis, and biological evaluation of two types of sulfonamide-based analogues contingent on these observations. The first series has the sulfonyl amine NH of **1.15** replaced with electron withdrawing/poor groups (see compounds **5.01** – **5.03** section 5.3). The second series has the sulfonylurea of **1.15** replaced with a sulfonylcarbamate linker (see compounds **5.76 – 5.78** section 5.4). The central NH of these new sulfonyl linkers was expected to be more acidic relative to sulfonylurea **1.15** based on pK_a calculations (see Section 5.2), hence anticipated to provide improved binding affinity to *Sa*BPL. The design of these two series is discussed in detail below.

5.2: Designing Acidic Sulfonamide-based Analogues

The sulfonyl amine NH of **1.15** (highlighted in red, Figure 5.2) is superfluous to binding *Sa*BPL based on X-ray crystallography.[2,3] Thus, replacing this NH of **1.15** with a methylene (**5.02**), oxygen (**5.03**), or di-fluoro methylene (**5.04**), as outlined in Figure 5.3, should not adversely affect binding to *Sa*BPL. The calculated pK_a value of **5.02** (4.24) is lower than **1.15** (4.36), suggesting this analogue is slightly more acidic than **1.15**. Although the pK_a difference is small, (Δ = 0.12), it is still significant enough to warrant further investigation. Sulfamate **5.03** with its oxygen atom is even more acidic as reflected in its lower calculated pK_a (3.14) for the central NH. While di-fluoro methylene **5.04** (calculated pK_a = 3.35) was found to be slightly less acidic than **5.03**, it nevertheless offered enhanced stability as sulfamate-based analogues like **5.03** are reported to decompose intramolecularly.[4] Central NH acidity was predicted to be even lower for the sulfonylcarbamate series (**5.05** – **5.08**), as reflected by the calculated pK_a values, Figure 5.4. The synthesis and subsequent assay of these compounds was warranted given that each analogue from the two series (**5.02 – 5.08**) gave a calculated pK_a lower than amino sulfonylurea **1.15** (4.36[1]).

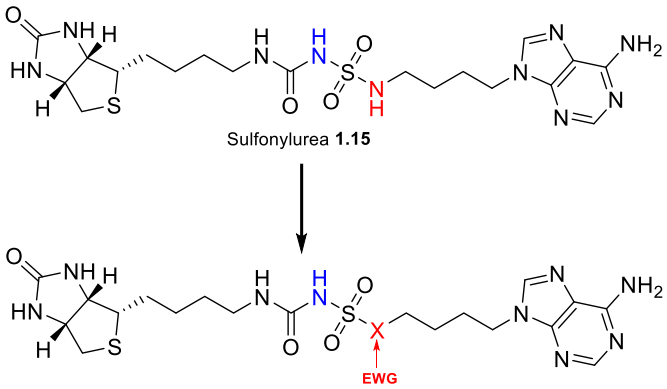

Figure 5.2: Sulfonylurea **1.15** and proposed site for chemical modification. The sulfonyl NH is highlighted in red, and the central NH in blue. EWG = electron withdrawing group

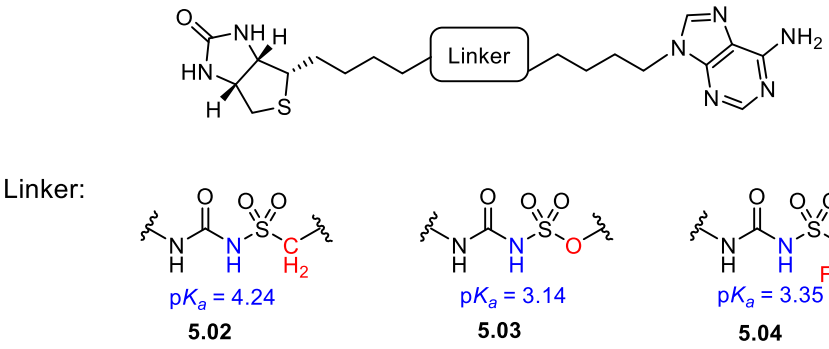

Figure 5.3: Proposed sulfonylurea analogues **5.02 – 5.04**. Calculated pK_a values for the central NH (blue) are shown. Calculated pK_a values were by Marvin from ChemAxon.[1]

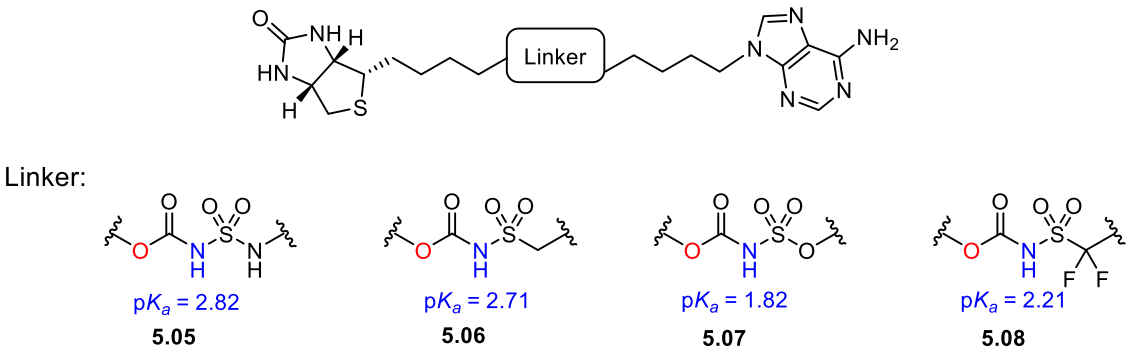

Figure 5.4: Proposed sulfonylcarbamate analogues **5.05 – 5.08**. Calculated pK_a values for the central NH (blue) are shown. Calculated pK_a values were by Marvin from ChemAxon.[1]

5.3: Synthesis of New Sulfonylurea Series

Literature reports that amino sulfonylurea **1.15** can be synthesised by coupling Bz-protected amino sulfonamide **5.10** to biotin carbamate **5.09** followed by removal of the Bz group with NH_4OH.[1] Analogues **5.02** – **5.04** were envisioned to be accessible by an analogous route, using sulfonamides **5.11** – **5.13** in place of **5.10** (see Figure 5.5).

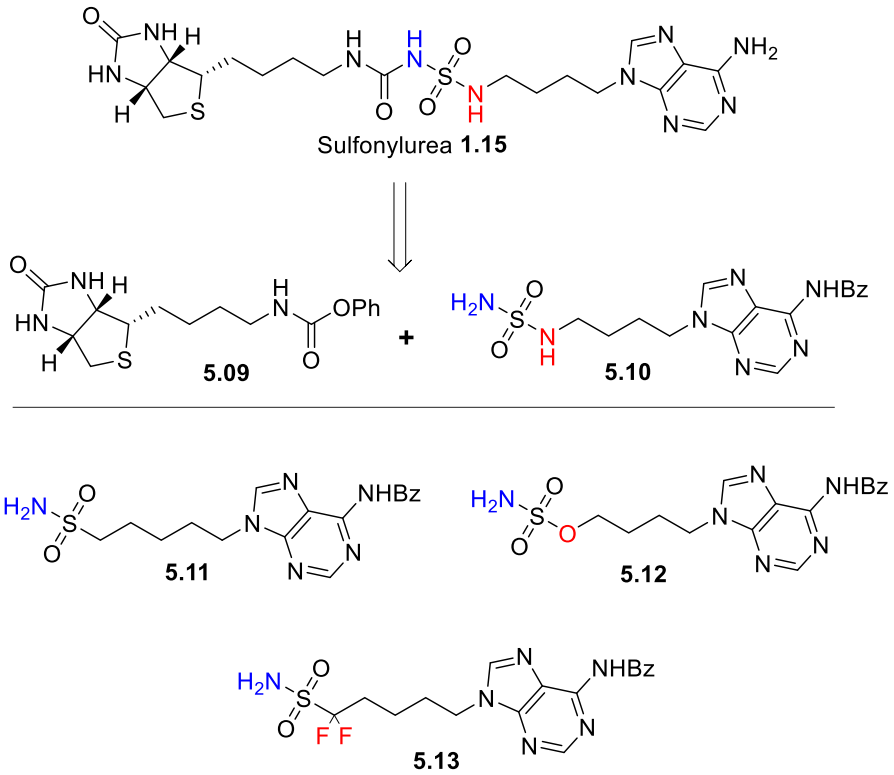

Figure 5.5: Synthetic intermediates used to prepare amino sulfonylurea **1.15**, and chemical structures of sulfonamides **5.11 – 5.13**.

5.3.1: Synthesis of Sulfonamide 5.11

Two routes to **5.11** were initially attempted as outlined in Scheme 5.1. Adenine **5.15** was alkylated with dibromopentane **5.14**[6], in the presence of Cs_2CO_3, to give **5.16** in, 77 % after column chromatography. Subsequent treatment of **5.16** with benzoyl chloride (BzCl) in pyridine (pyr) gave only the corresponding pyridinium salt **5.18**, as evidenced by ^{1}H NMR analysis. Similar observations have been reported for the reaction of alkyl halides under these described conditions.[7,8] Previous work demonstrated successful preparation of sulfonamides without Bz protection of the adenine aniline,[1] hence a second route that circumvented this step was investigated (see Scheme 5.1). The reaction of alkylated adenine **5.16** with aqueous Na_2SO_3 gave the corresponding sulfite **5.20** in an excellent yield of 96 %. However, successive

treatment of sulfite **5.20** with PPh_3, Br_2, and ammonia resulted in a complex mixture, with the desired product unable to be isolated by column chromatography.

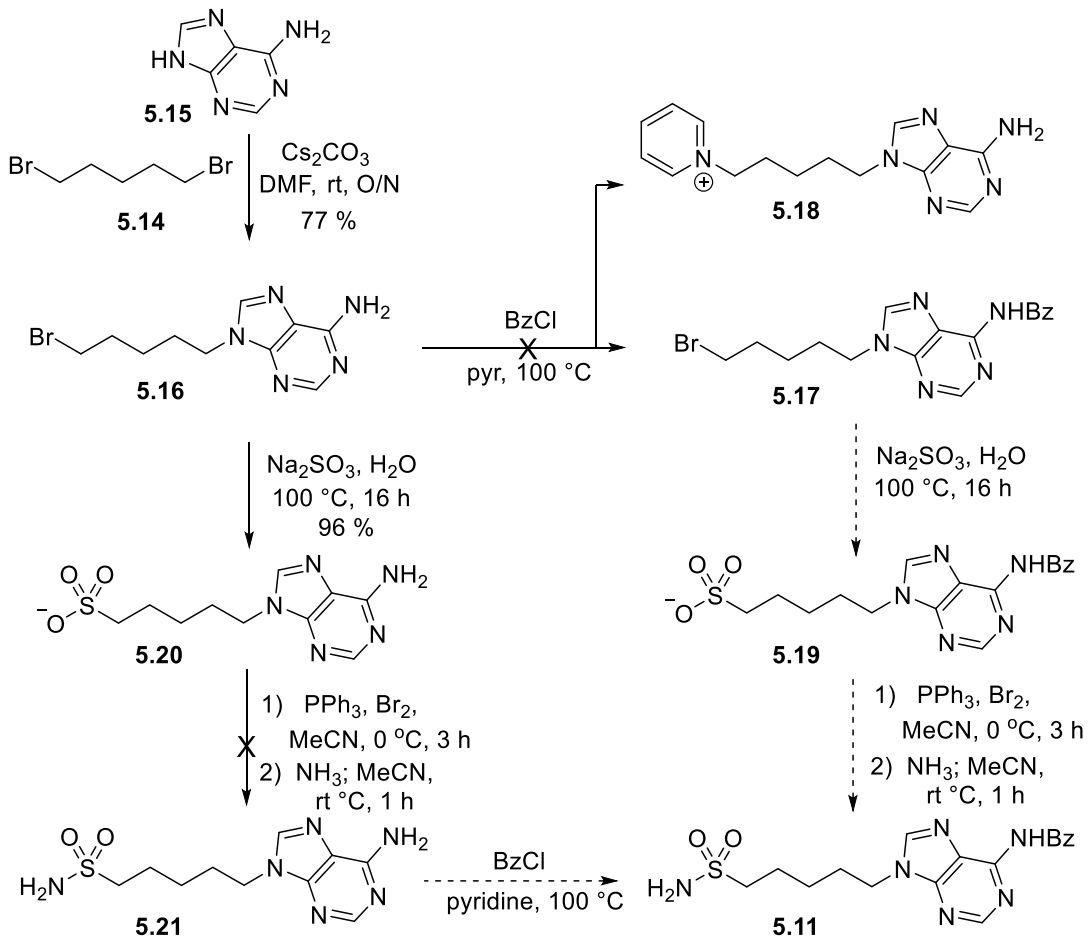

Scheme 5.1: Attempted synthesis of sulfonamide **5.11**.

Hence, an alternate synthetic pathway for **5.11** was devised, see Scheme 5.2. A Cs_2CO_3 mediated alkylation between dibromobutane **5.22**[6] and adenine **5.15** gave **5.23** in good yield, 72 %. Based on TLC, the subsequent reaction of **5.23** with Boc-protected methanesulfonamide **5.24** in the presence of *n*-BuLi, resulted in only starting material. Similar methanesulfonamide-alkylation conditions have been reported,[9] thus, optimisation of the reaction was attempted to procure **5.25** (see Table 5.1, all entries were undertaken on a 0.5 mmol scale of **5.23**). Increasing the equivalents of *n*-BuLi and **5.24** to 2.0 (entry 2) and 5.0 (entry 3) and reaction at -78 ℃ gave only starting material. Raising the reaction temperature to -30 ℃ did not improve reactivity between **5.23** and **5.24** (entry 4) again, with only starting material apparent by TLC. Increasing the equivalents of *n*-BuLi and **5.24** to 2.0 or 5.0 equivalents (entries 5 and 6), and reaction at -30 ℃ gave a complex reaction mixture, with the mass of **5.25** not evident in the LC-MS trace.

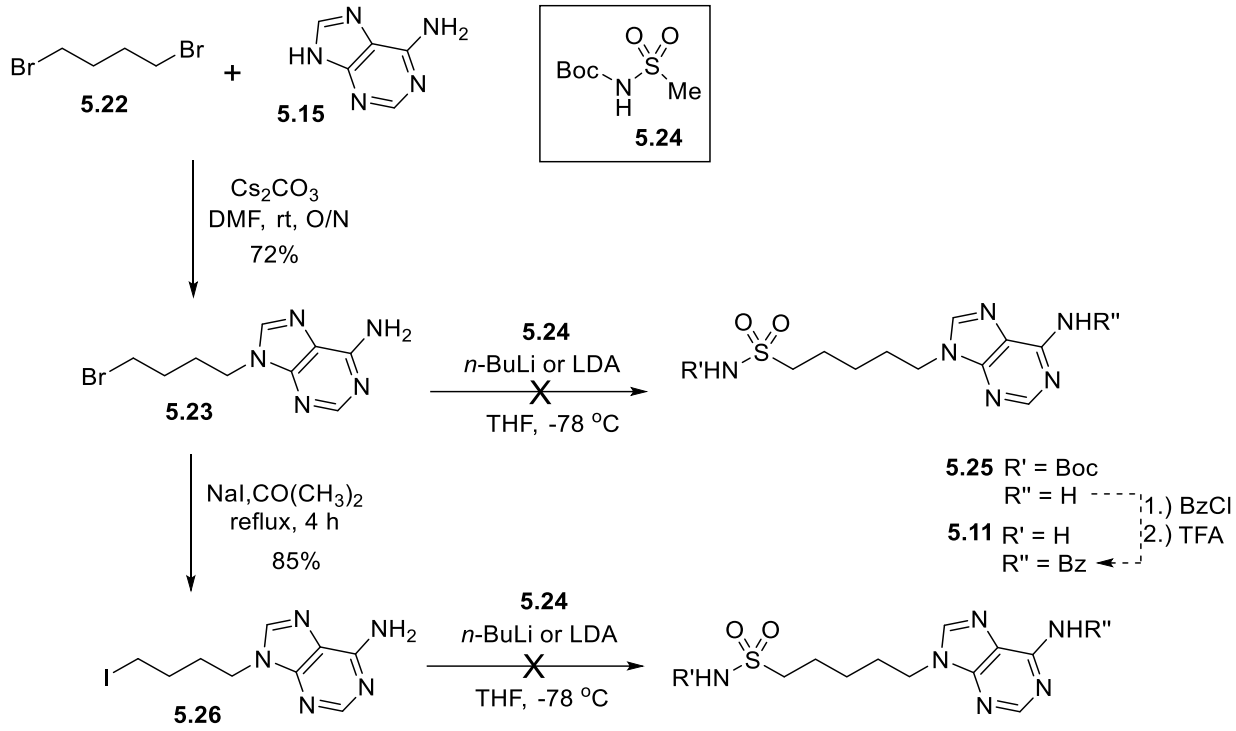

Scheme 5.2: Attempted synthesis of sulfonamide **5.11**.

The poor reactivity observed for entries 1 – 6 is likely due to preferential deprotonation of the labile carbamate NH of **5.24** by *n*-BuLi over the methyl proton. Thus, *n*-BuLi was replaced with the sterically hindered base LDA to account for this possibility, but this too gave only unreacted starting material (see entries 7 – 11). The alkyl bromide **5.23** was thought to be unreactive under the conditions depicted in Table 5.1, and a Finkelstein reaction of **5.23** was undertaken to give the more electrophilic alkyl iodide **5.26**, see Scheme 5.2. However, employing **5.26** as the electrophile and the conditions described for entries 1 and 7, gave complex mixtures based on TLC analysis. LC-MS analysis of these mixtures did not indicate a mass peak for **5.25**, thus no further attempts to prepare sulfonamide **5.11** via this route were investigated.

Table 5.1: Attempted optimisation for sulfonamide **5.25** synthesis.

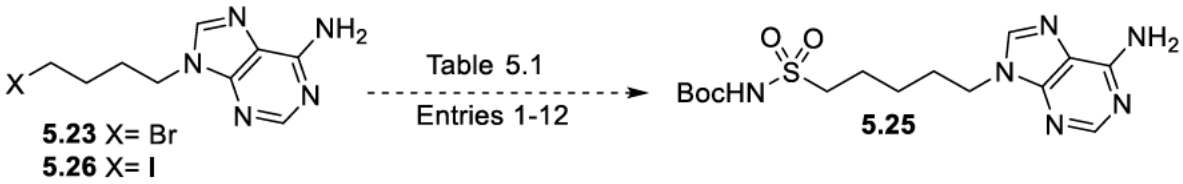

5.23 X= Br
5.26 X= I

5.25

Entry	Base / (Eq)	5.24 (Eq)	Temperature (°C)	Yield (%) [a]
1	*n*-BuLi / (1)	1.0	-78	N/A[b]
2	*n*-BuLi / (2)	2.0	-78	N/A[b]
3	*n*-BuLi / (5)	5.0	-78	N/A[b]
4	*n*-BuLi / (1)	1.0	-30	N/A[b]
5	*n*-BuLi / (2)	2.0	-30	N/A[c]
6	*n*-BuLi / (5)	5.0	-30	N/A[c]
7	LDA / (1)	1.0	-78	N/A[b]
8	LDA / (2)	2.0	-78	N/A[b]
9	LDA / (5)	5.0	-78	N/A[b]
10	LDA / (1)	1.0	-30	N/A[b]
11	LDA / (2)	2.0	-30	N/A[b]
12	LDA / (5)	5.0	-30	N/A[c]

[a] Isolated yield after flash chromatography. [b] Only starting material recovered. [c] Complex mixture obtained as determined by TLC and ^{1}H NMR.

Scheme 5.3 was devised given the lack of success in preparing sulfonamide **5.11**. This was inspired by recent work reported by Johnson *et al.*[10] In the first instance, adenine pentyl bromide **5.16** was alkylated with 2-mercaptopyrimidine, in the presence of Cs_2CO_3 to give the 2-pyrimidinyl thioether **5.27** in 99 % yield. Subsequent treatment of this thioether with BzCl gave the mono-Bz protected 2-pyrimidinyl thioether **5.28** in good yield, 62 %. Oxidation of **5.28** with *m*-CPBA gave the corresponding pyrimidinyl sulfone **5.29**, in 71 % after column chromatography. An excess of *m*-CPBA (3.5 equivalents), relative to the thioether **5.28**, was required for this reaction to proceed, otherwise the corresponding sulfoxide was isolated as the major product. De-arylation of pyrimidinyl sulfone **5.29** on treatment with 1.0 equivalent of NaOMe gave the crude sulfinate intermediate **5.30**, which was subsequently reacted with aqueous hydroxylamine-*O*-sulfonic acid (HOSA), to give sulfonamide **5.11** in 45 % yield over two steps.

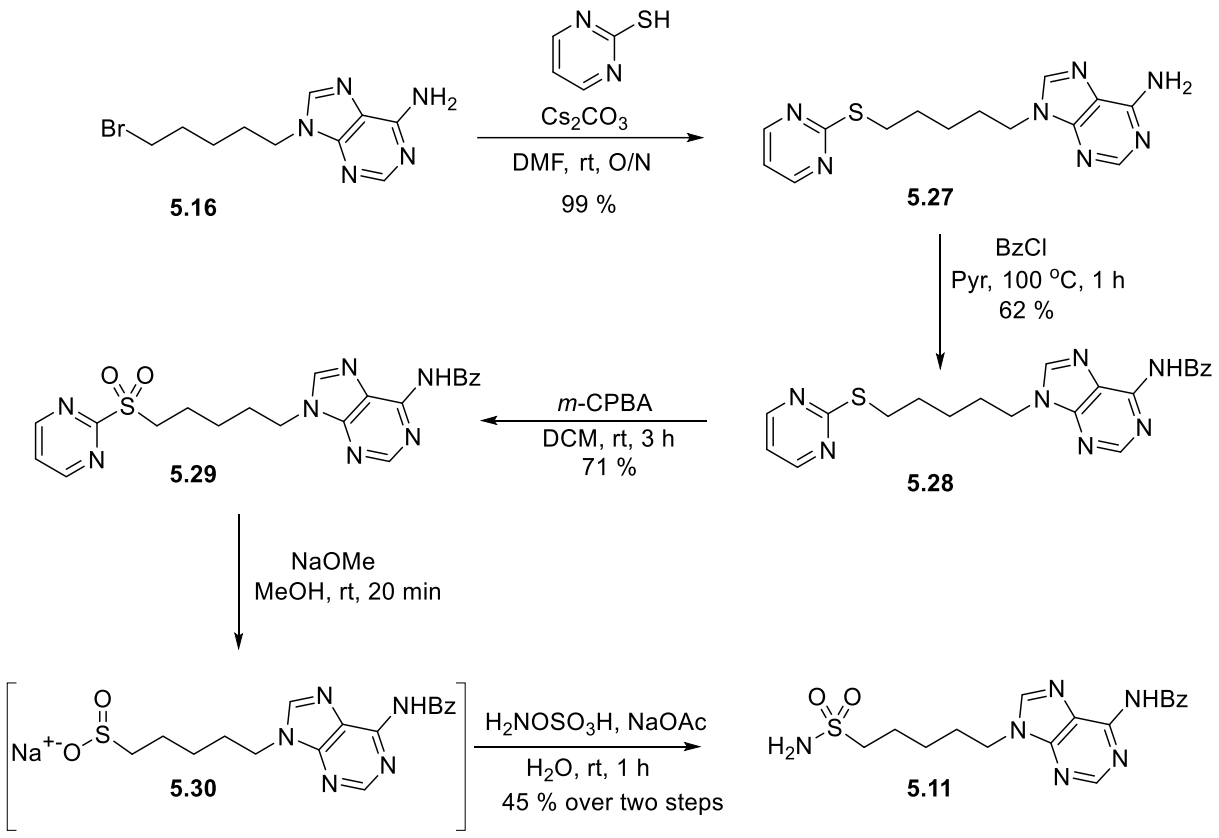

Scheme 5.3: Synthesis of sulfonamide **5.11.**

5.3.2: Synthesis of Sulfamate 5.12

The synthesis of sulfamate **5.12** is summarized in Scheme 5.4. A Cs_2CO_3 mediated alkylation between adenine **5.15** and methyl 4-bromobutyrate gave the methyl ester **5.31** in a quantitative yield. However, subsequent reduction to the alcohol **5.32** with $LiAlH_4$ gave a complex reaction mixture. Analysis of this mixture by LC-MS failed to reveal the product **5.32**. As such an alternative strategy was devised involving a Cs_2CO_3 mediated alkylation of adenine **5.15** with 4-bromobutyl acetate. This gave alkyl acetate **5.33** in 56 % yield following column chromatography. Hydrolysis of this acetate, with LiOH, gave the alcohol **5.32** in a quantitative yield. Subsequent Bz protection of the adenine moiety of **5.32** was achieved based on an optimised two-step reaction reported by D'Alonzo *et al*.[11] Alcohol **5.32** was first treated with an excess of TMSCl, and 1.0 equivalent of BzCl, and then reacted with NH_4OH to give the desired Bz-protected alcohol **5.34** in 56 % yield over two-steps.

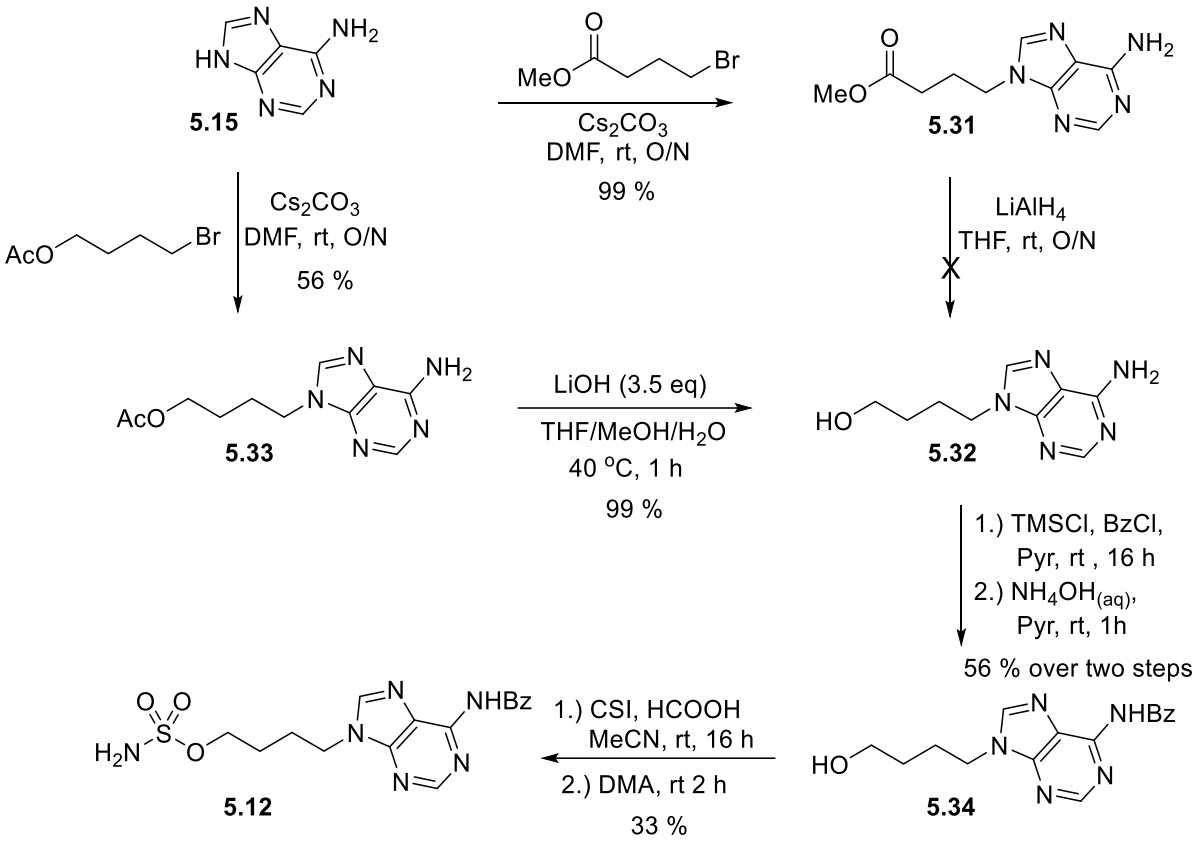

Scheme 5.4: Synthesis of sulfamate **5.12.**

Finally, the target sulfamate **5.12** was prepared by addition of the Bz-protected alcohol **5.34** to a solution of chlorosulfonyl isocyanate (CSI) in formic acid (33 % yield). The solution of CSI and formic acid gave the sulfonating reagent **5.35** *in situ*, which was subsequently reacted with **5.34** to give **5.12**, see Scheme 5.5.

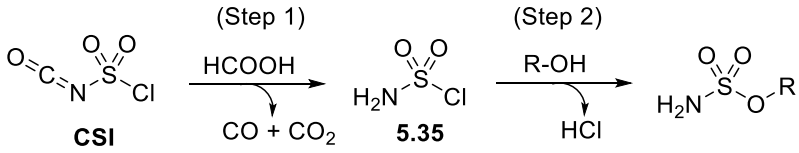

Scheme 5.5: Reaction between chlorosulfonyl isocyanate (CSI) and formic acid (Step 1), to generate the sulfonating reagent **5.35**. Subsequent addition of an alcohol (Step 2) is shown to give the corresponding sulfamate.

5.3.3: Attempted Synthesis of Sulfonamide 5.13

The synthetic pathway outlined in Scheme 5.6 was inspired by literature,[12] which reports the use of 2-(difluoromethylsulfonyl)pyridine (Hu's reagent) to give di-fluoro methylene sulfonamides. The alkyl bromide **5.23** was added to a solution of Hu's reagent, LiHMDS, and HMPA in anhydrous THF at -78 °C, however this gave a complex mixture as evidenced by TLC. The adenine NH_2 of **5.23** was suspected to participate in side-reactions under these conditions.

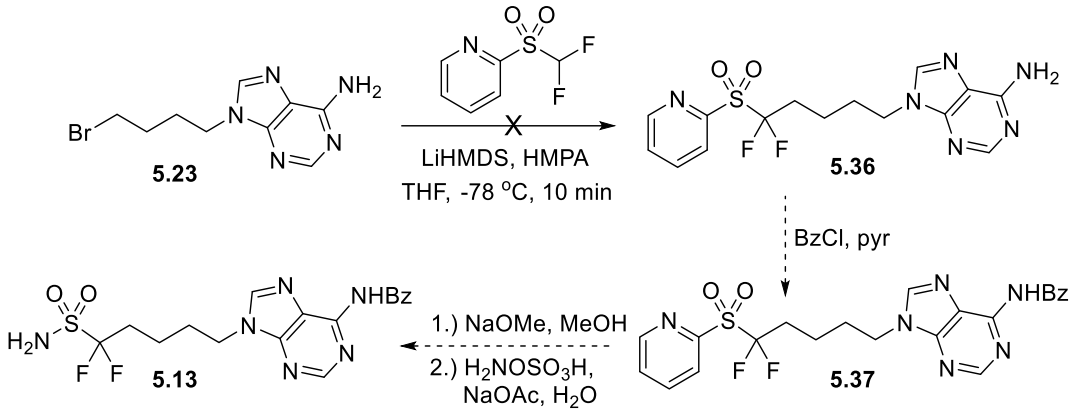

Scheme 5.6: Attempted synthesis of sulfonamide **5.13**.

Thus, a new synthetic route was conceived using benzyl 4-bromobutyl ether in place of the adenine alkyl **5.23**, see Scheme 5.7. However, treating this alkyl bromide with Hu's reagent resulted in only unreacted benzyl 4-bromobutyl ether after purification by column chromatography. This alkylation reaction was monitored by ^{1}H NMR at 10-min intervals to confirm degradation of Hu's reagent after approximately 40 min. In light of this, alkylation using Hu's reagent was not investigated further.

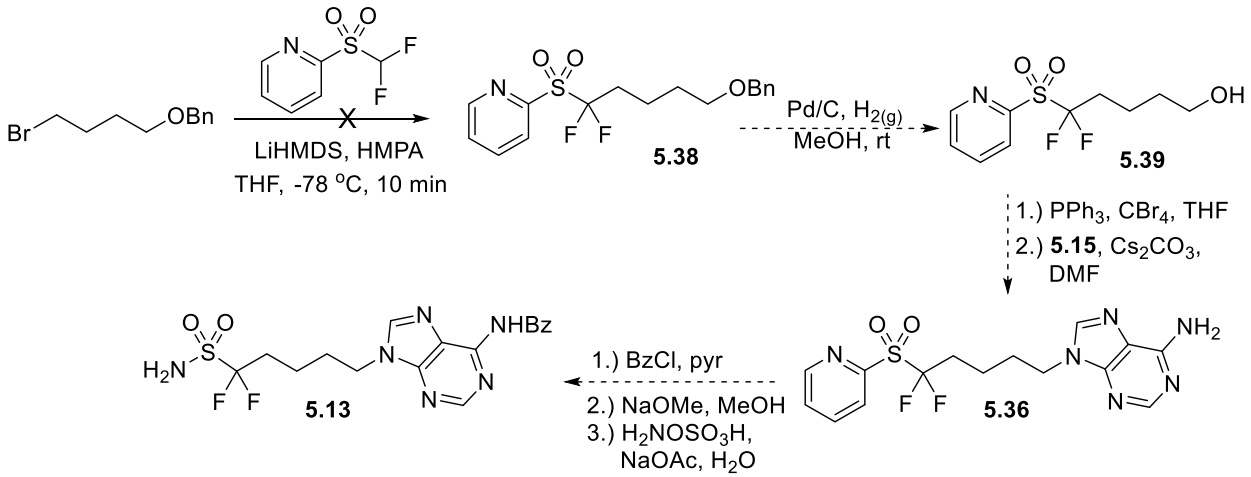

Scheme 5.7: Attempted synthesis of sulfonamide **5.13**.

Scheme 5.8 was conceived given that *N*-fluorobenzenesulfonimide (NFSi) is reported as a robust fluorinating reagent for the preparation of difluoro methylene sulfonamides.[13,14] In the first instance, sulfonamide **5.40** was prepared in two steps using a modified procedure by Zhong *et al*.[15] Commercial 5-bromopentyl ether was added to a solution of rongalite in DMSO, and subsequent treatment with aqueous HOSA and NaOAc gave sulfonamide **5.40** in 42 % yield over both steps. This sulfonamide was subsequently treated with *p*-methoxybenzyl chloride (PMBCl) in the presence of K_2CO_3 and potassium iodide (KI) in methyl ethyl ketone (MEK) to give the di-PMB protected sulfonamide **5.41** in 10 % yield after purification by column chromatography. The di-protected sulfonamide **5.41** was then treated with *n*-BuLi, followed by the addition of 2.5 equivalents of NFSi to give a complex mixture. An LC-MS analysis of this mixture indicated that **5.42** was not present. Given the limited success in preparing di-fluoro methylene **5.13**, alternative procedures were not investigated but might be considered in future studies as discussed in the Conclusion Section 5.7.

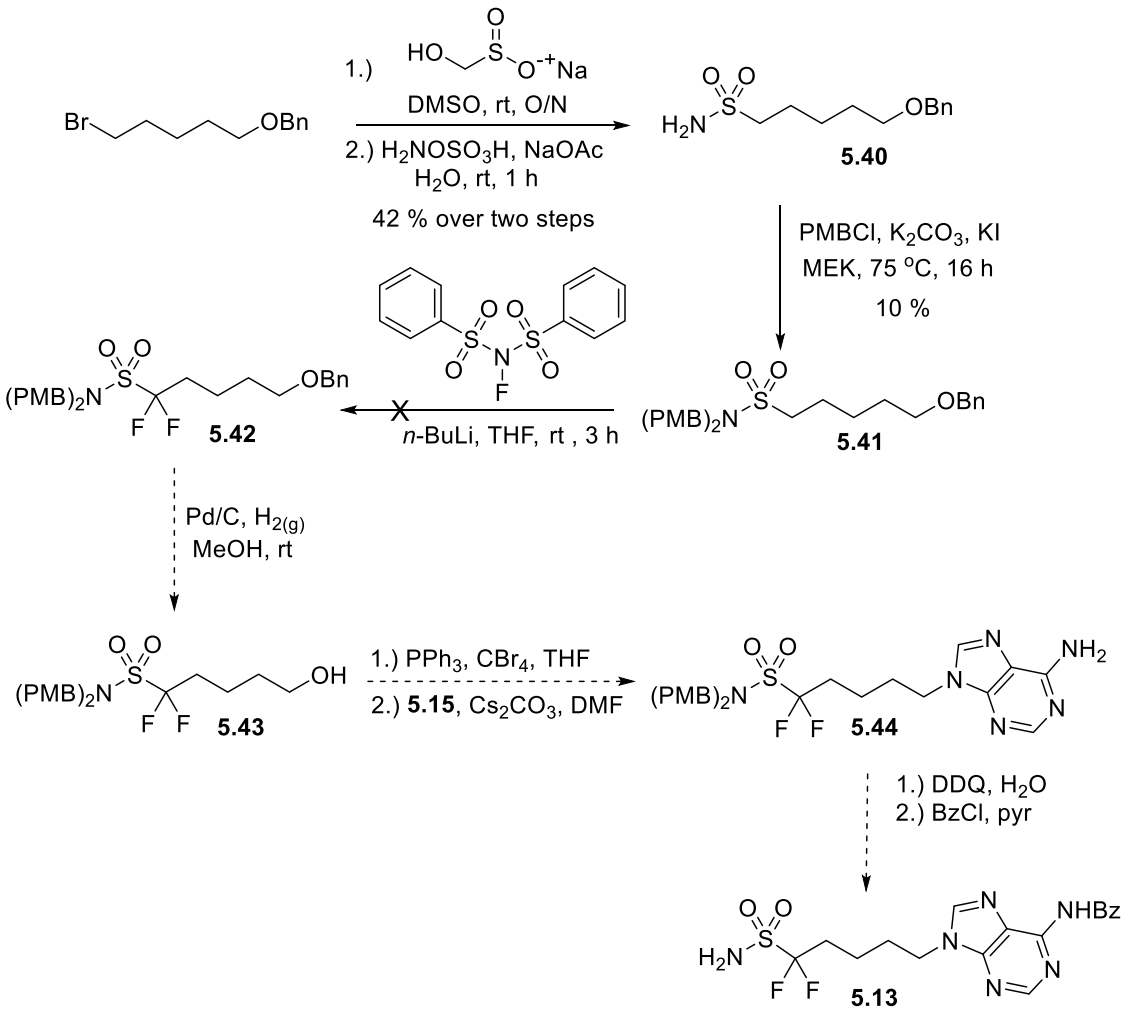

Scheme 5.8: Attempted synthesis of sulfonamide **5.13**.

5.3.4: Synthesis of Sulfonylurea Analogues 5.02 and 5.03.

The two sulfonylurea analogues, **5.02** and **5.03** were prepared based on conditions reported by Lee *et al*,[1] see Scheme 5.9. Samples of Biotin carbamate **5.09**[1] were separately reacted with sulfonamide **5.11** or sulfamate **5.12**, in the presence of DBU, to give Bz-protected sulfonylurea **5.45** and sulfamylurea **5.46**, respectively. These Bz-protected compounds were separately treated with NH_4OH in MeOH to give the corresponding sulfonylurea **5.02** and sulfamylurea **5.03** analogues, in 72 and 11 % respectively following column chromatography.

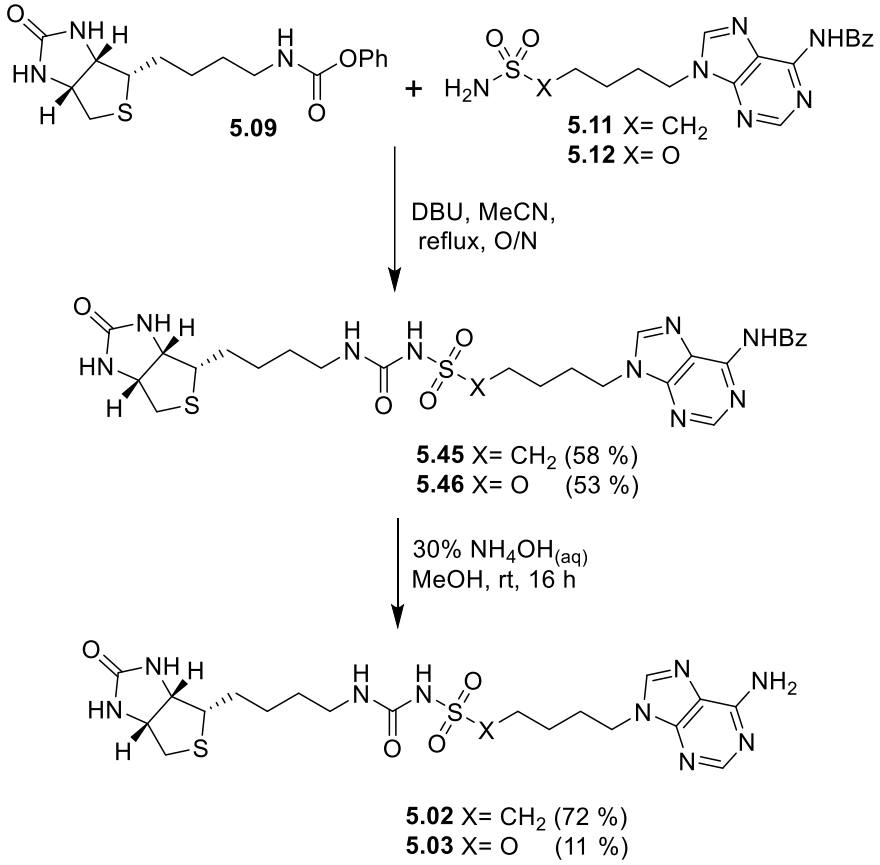

Scheme 5.9: Synthesis of analogues **5.02** and **5.03**

As expected, the sulfamylurea analogue **5.03** was unstable, and degraded after approx. 10 min by ^{1}H and ^{13}C NMR. Cleavage of the sulfamyl linker was likely occurring via an intramolecular cyclisation with the adenine moiety, analogous to sulfamate *Mt*BPL inhibitors reported by Duckwork *et al*.[16] Given the low yield of sulfamylurea **5.03** (11 %), further NMR analysis was not undertaken. Characterisation of **5.03** was thus limited to ^{1}H NMR, LC-MS and HRMS, which was deemed sufficient for the purpose of this study.

5.4: Synthesis of the Sulfonylcarbamate Series

Replacing the **5.09** carbamate for a carbonate, as in **5.47**, presents a new pathway for the preparation of sulfonylcarbamate-based analogues, see Figure 5.6. Retrosynthesis of biotin carbonate **5.47** identified norbiotinol **5.48** as a precursor. Two methods were formulated to prepare norbiotinol **5.48**, as discussed in detail below.

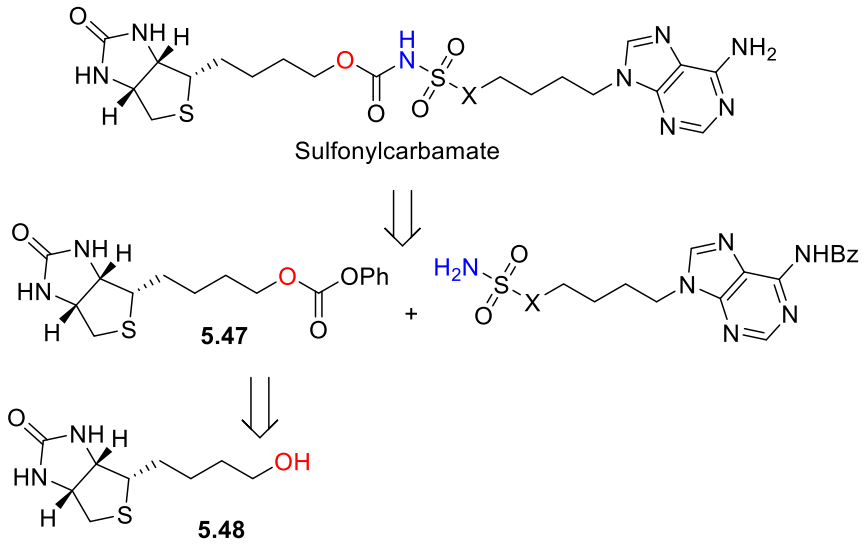

Figure 5.6: Retrosynthetic analysis of the sulfonylcarbamate analogue design. The retrosynthesis of biotin carbonate **5.47** identifies norbiotinol **5.48** as a direct precursor.

5.4.1: Attempted Synthesis of Norbiotinol 5.48

The synthesis depicted in Scheme 5.10 involved an initial Wolff rearrangement of biotin **1.01** to prepare biotin carbamate **5.09**,[1] followed by conversion of the terminal amine to an alcohol.[17] Thus, biotin **1.01** was reacted with diphenylphosporyl azide (DPPA) and *t*-BuOH to give **5.09**, which was subsequently reacted with aqueous 6 M HCl to give **5.49** as the hydrochloride salt. Subsequent treatment of **5.49**, with methyl dichloroacetate in the presence of TEA, gave biotin dichloroacetamide **5.50** in 32 % yield after column chromatography. Nitrosylation of **5.50** with $NaNO_2$, followed by heating at 40 °C, gave a complex reaction mixture by TLC. Nitrosylation of the biotin moiety ureido NHs was likely under these conditions, which is reflected by the complex intractable reaction mixture. Chemoselectivity issues associated with the route outlined in Scheme 5.10 suggested that a simpler alternative for the preparation of alcohol **5.48** was required.

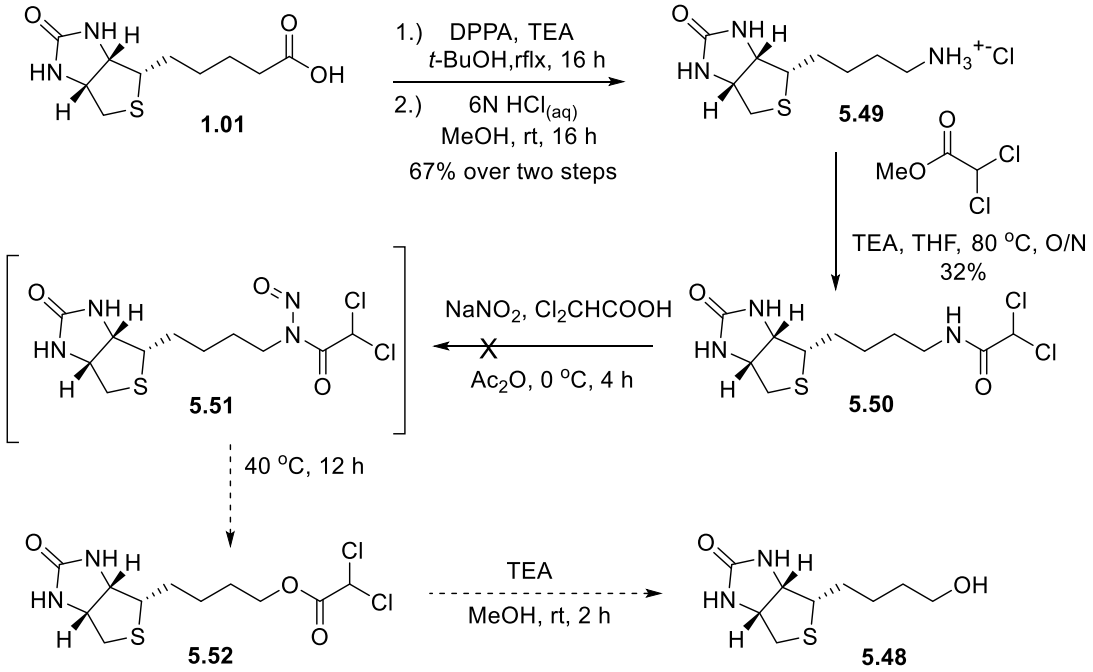

Scheme 5.10: Attempted synthesis of norbiotinol **5.48**.

A Baeyer-Villiger oxidation reaction to obtain norbiotinol **5.48** was proposed by a three-step synthesis starting from biotin Weinreb-amide **4.06**, see Scheme 5.11. Reaction of MeLi with biotin Weinreb-amide **4.06,** at -78 ℃, gave biotin methyl ketone **5.53**, in 47 % yield. An excess of MeLi (3.0 molar equivalents) was required for this reaction with 2.0 equivalents presumably consumed by deprotonation of the biotin ureido NHs. However, subsequent reaction of **5.53** with *m*-CPBA did not give the desired Baeyer-Villiger product **5.54**, and gave biotin sulfone **5.55** only, as determined by LC-MS. The use of an excess of *m*-CPBA (5.0 equivalents) with heating under reflux resulted in a quantitative yield of **5.55**. So too did the reaction between **5.53** and 10% H_2O_2, at rt. and 80 ℃. Hence, no further attempts were made to optimise this reaction to prepare norbiotinol **5.48**.

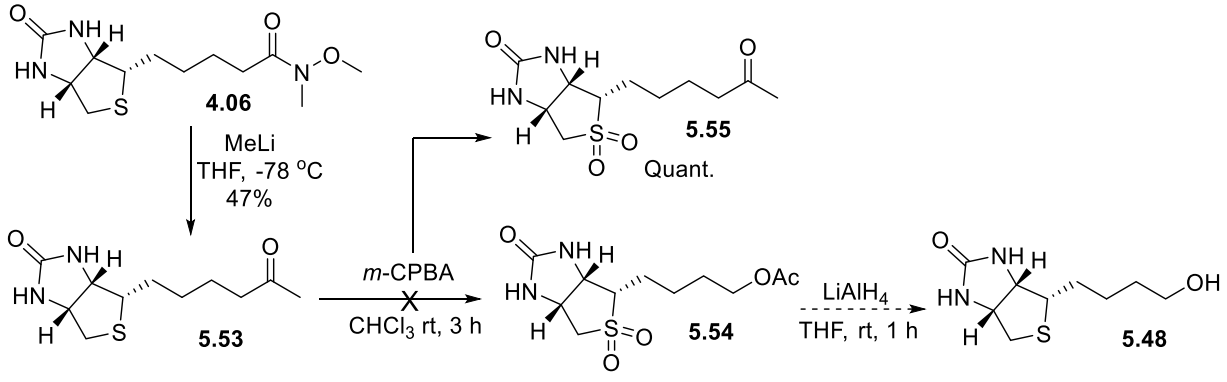

Scheme 5.11: Attempted synthesis of alcohol **5.48**.

5.4.2: Synthesis of Biotinol Carbonate 5.57

The lack of success in preparing norbiotinol **5.48** suggested revision of the sulfonylcarbamate linker design. Comparing the general structures of the sulfonylurea and sulfonylcarbamate inhibitor design revealed that both general structures are comprised of an eight-carbon chain tether, see Figure 5.7. Hence, by introducing an additional methylene to the biotin aliphatic chain and subsequently removing one from the adenine chain, a synthetically more accessible sulfonylcarbamate is envisioned (Figure 5.7, Design 2). This new design retained the eight-carbon tether, with a retrosynthetic analysis indicating that the biotin carbonate **5.56** precursor, to prepare the target sulfonylcarbamate, was accessible from biotinol **5.57**.

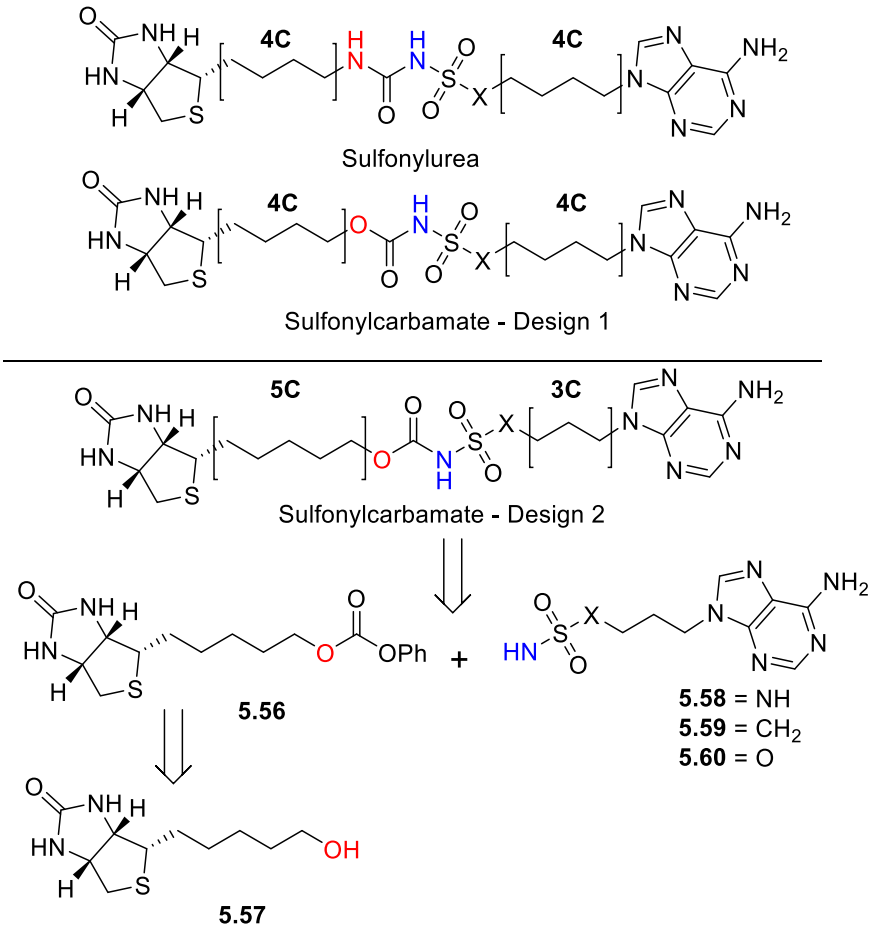

Figure 5.7: General structure of biotin sulfonylurea and sulfonylcarbamate analogues. Carbon chain lengths are highlighted. Retrosynthesis of the sulfonylcarbamate-design 2 shows biotin carbonate **5.56** as a precursor that can be prepared from biotinol **5.57**.

The preparation of biotinol **5.57** is well documented,[18] with the subsequent synthesis of biotin carbonate **5.56** from **5.57** outlined in Scheme 5.12. Biotin **1.01** was methylated in the presence of $SOCl_2$ and MeOH, with subsequent reduction by $LiAlH_4$ giving biotinol **5.57**.[19] Successive reaction of biotinol **5.57** with diphenyl carbonate in the presence of DBU, gave biotin carbonate **5.56** in good yield, 43 %.

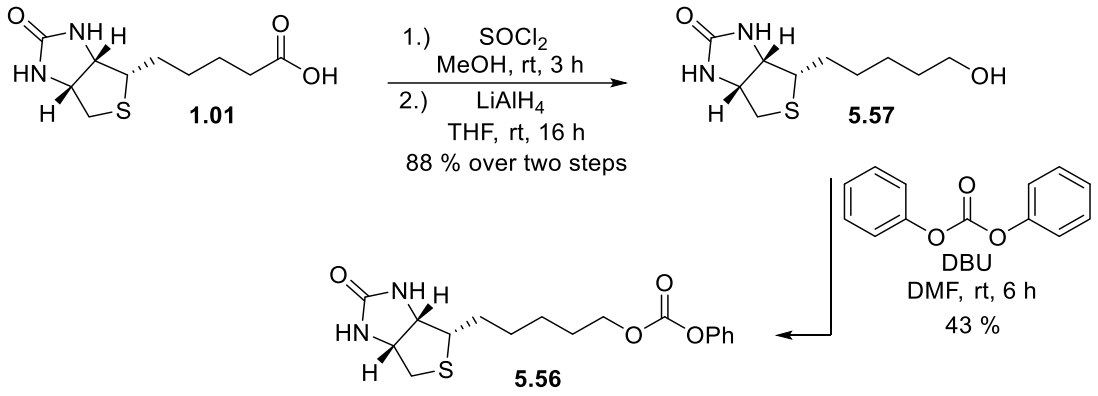

Scheme 5.12: Synthesis of biotin carbonate **5.56**

5.4.3: Synthesis of Sulfonamides 5.58 – 5.60

The successful preparation of biotin carbonate **5.56** justified the synthesis of sulfonamides **5.58 – 5.60** (structures highlighted in Figure 5.7). The reported synthesis of butyl amino sulfonamide **5.10**[1] (Figure 5.5) was adapted for the preparation of propyl amino sulfonamide **5.58**, as outlined in Scheme 5.13. The abovementioned conditions for the preparation of pentyl sulfonamide **5.11**, and butyl sulfamate **5.12** were repurposed for the synthesis of butyl sulfonamide **5.59** and propyl sulfamate **5.60**, see Schemes 5.14 and 5.15 respectively. The detailed synthesis of **5.58 – 5.60** is described below.

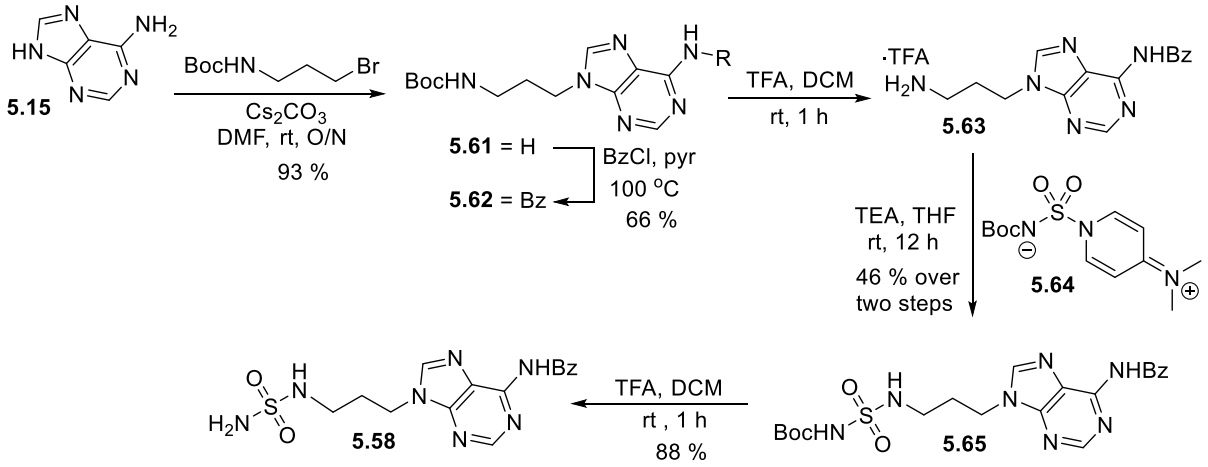

Scheme 5.13: Synthesis of amino sulfonamide **5.58**.

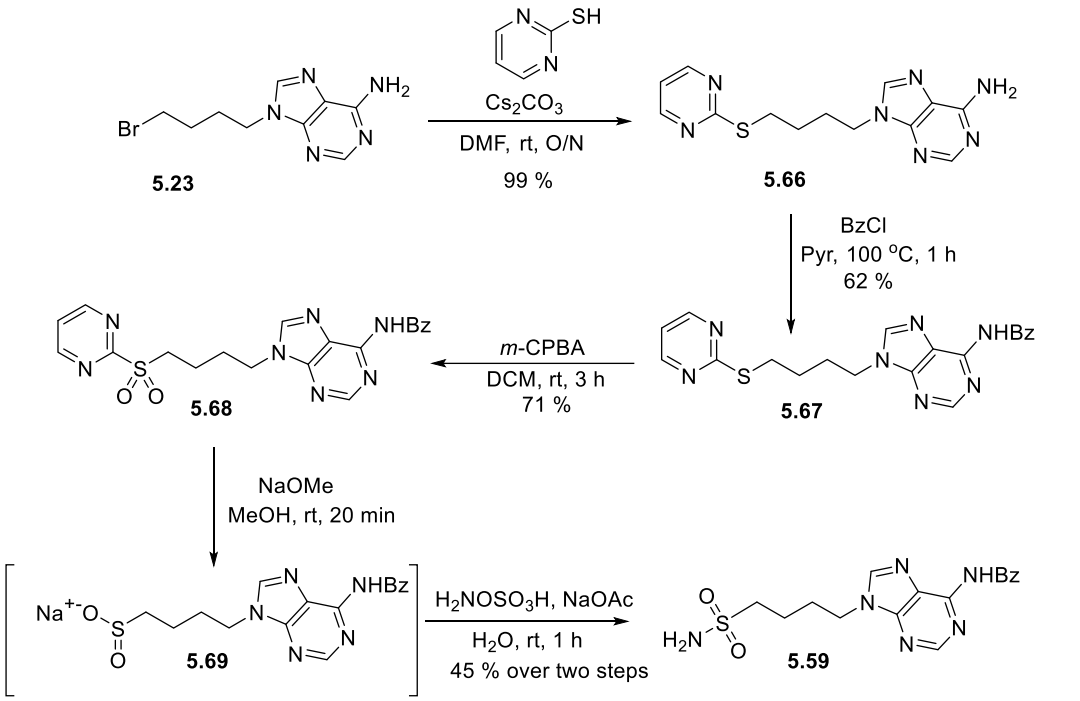

Scheme 5.14: Synthesis of sulfonamide **5.59**.

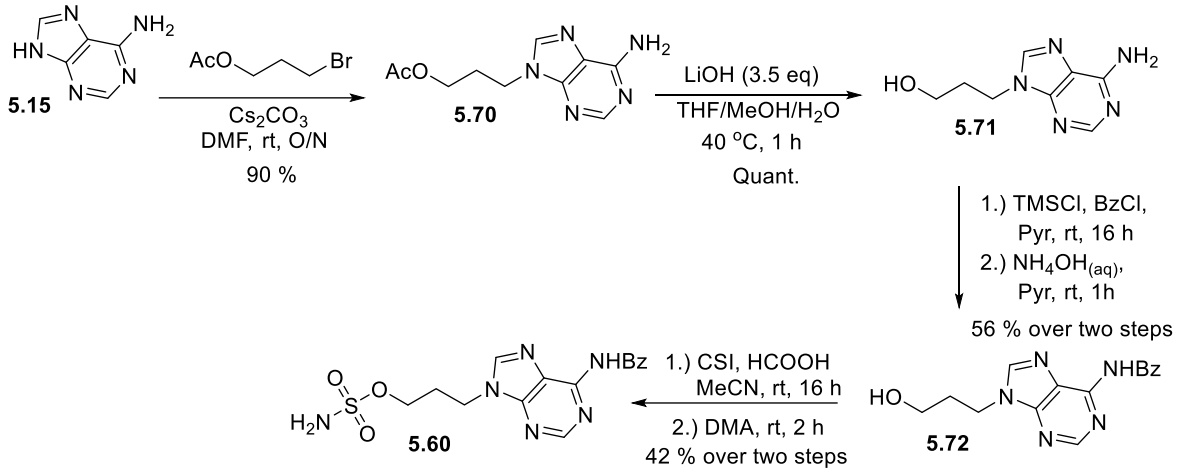

Scheme 5.15: Synthesis of sulfamate **5.60**.

Adenine **5.15** was alkylated with commercially sourced 3-(Boc-amino)propylbromide, in the presence of Cs_2CO_3, to give Boc-protected adenine amine **5.61** in an excellent yield of 93 %. Subsequent reaction of **5.61** with BzCl, in pyridine, gave **5.62** in 66 % after column chromatography. The Boc group of **5.62** was removed on treatment with TFA in DCM, and subsequent reaction with Boc-sulfonymating reagent **5.64**[20] gave the Boc-protected sulfamide **5.65**. Sequential Boc-deprotection with TFA gave sulfonamide **5.58**, in 88 % yield (see Scheme 5.13).

The 2-pyrimidinyl thioether **5.66** was prepared by a Cs_2CO_3 mediated alkylation between 2-mercaptopyrimidine and **5.23**. Subsequent reaction with BzCl in pyridine gave the Bz-protected thioether **5.67** in good yield, 62 %. Oxidation of the thioether with *m*-CPBA gave the corresponding pyrimidinyl sulfone **5.68** in 71 % yield. Finally, de-arylation of **5.68** with NaOMe, and amidation with an aqueous solution of HOSA, gave sulfonamide **5.59** in a 45 % yield over two steps (see Scheme 5.14).

Adenine **5.15** was reacted with 3-bromopropyl acetate, in the presence of Cs_2CO_3 to give **5.70** (90 %), the acetate of which was hydrolysed with LiOH to give **5.71**. The Bz-protected alcohol **5.72** was prepared by reacting adenine alcohol **5.71** with BzCl and TMSCl in pyridine, followed by reaction with NH_4OH. The Bz-protected alcohol was added to an ice-cooled solution of CSI and formic acid in MeCN to give the desired sulfamate **5.60** in 15 % yield after purification by column chromatography (see Scheme 5.15).

5.4.4: Synthesis of Sulfonylcarbamate Analogues 5.76 – 5.78

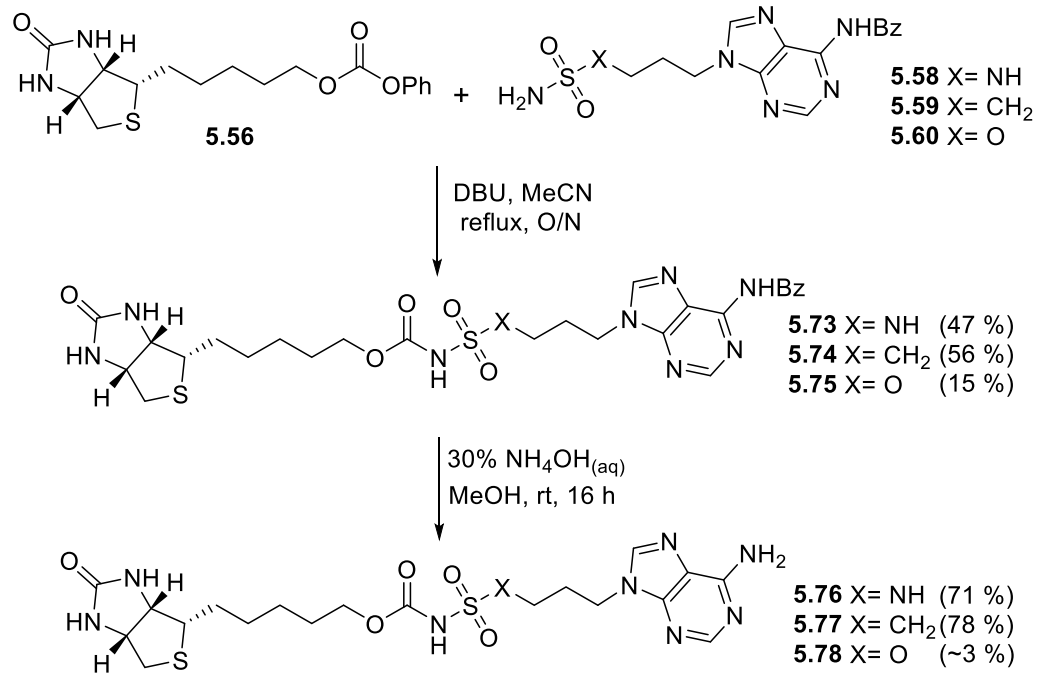

Scheme 5.16: Synthesis of sulfonylcarbamates **5.76 – 5.78**.

The synthesis of sulfonylcarbamate analogues **5.76** – **5.78** is depicted in Scheme 5.16. Samples of Biotin carbonate **5.56** were reacted separately with amino sulfonamide **5.58**, sulfonamide **5.59** and sulfamate **5.60** in the presence of DBU to give the respective Bz-protected sulfonylcarbamates **5.73**, **5.74**, and **5.75**, respectively. The Bz groups of **5.73**, **5.74**, and **5.75**

were removed on treatment with NH_4OH in MeOH, to give sulfonylcarbamates **5.76**, **5.77**, and **5.78**, in 71, 78 and 3 % yields, respectively. An ^{1}H NMR spectrum of **5.78** was not attained due to its rapid decomposition. The mass of **5.78** was however detected by HRMS but, due to poor stability and unknown purity, analogue **5.78** was excluded from subsequent biological assays.

The use of anhydrous biotinol carbonate **5.56** for the above coupling reactions with **5.58 – 5.60** was critical. Initial test reactions using **5.56** to prepare the Bz-protected sulfonylcarbamates **5.73**, **5.74**, and **5.75**, gave yields ranging from 4 – 8 %. A ^{1}H NMR spectrum of the biotinol carbonate **5.56** used for these test reactions, revealed the presence of phenol and biotinol **5.57**. Comparing the methylene quartet resonance at 3.38 ppm observed for **5.57** to the diagnostic methylene triplet at 4.20 ppm of biotin carbonate **5.56** in this ^{1}H NMR spectrum, suggested a 4:1 ratio respectively. Biotinol carbonate **5.56** was particularly hygroscopic, and its carbonate group likely hydrolysed on exposure to atmospheric water. The subsequent preparation and isolation of biotin carbonate **5.56** involved drying the compound under reduced pressure for 16 h and subsequent storage in a desiccator for future use. As depicted in Scheme 5.16, these additional steps resulted in a dramatically improved yield of the Bz-protected analogues.

5.5: Relative Central NH Acidity of Analogues 5.02, 5.03, 5.76 & 5.77.

The relative acidity of the central NH of **5.02**, **5.03**, **5.76** and **5.77** was evaluated by ^{1}H NMR, by comparing the chemical shift of this NH, against the equivalent NH of acyl sulfamide **1.15**[1] and sulfonylurea **1.14**[1] (see Table 5.2). The relative chemical shift of this labile proton presents a good indication on how susceptible it may be to deprotonation. The chemical shift for the central NH of **5.02** (10.04 ppm) and **5.03** (10.75 ppm) was revealed to be downfield relative to **1.15** (9.74 ppm).This downfield shift suggests the central NH of **5.02** and **5.03** are more acidic than the analogous NH of sulfonylurea **1.15**, however, still less acidic than acyl sulfamide **1.14** (central NH = 11.23 ppm). As expected, the central NH of sulfonylcarbamate analogues **5.76** and **5.77** was revealed to be significantly downfield relative to the sulfonylurea derivatives **5.02** and **5.03** (11.06 and 11.49 ppm vs 10.04 and 10.75 ppm respectively). This is consistent with the calculated pK_a values of these analogues, which suggested **5.76** and **5.77** to be more acidic than **5.02** and **5.03**. Importantly, the central NH resonance of sulfonylcarbamates **5.76** (11.06 ppm) and **5.77** (11.49 ppm) had comparable chemical shifts relative to the central NH resonance of acyl sulfamide **1.14** (11.23 ppm). Hence, it is anticipated that sulfonylcarbamates **5.76** and **5.77** are similarly acidic to acyl sulfamide **1.14**.

Table 5.2: ^{1}H NMR data comparison of the central NH for **1.14, 1.15, 5.02, 5.03, 5.76, 5.77**

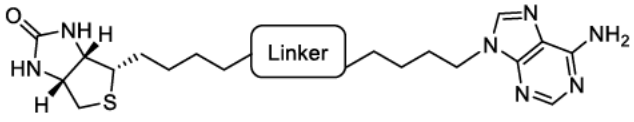

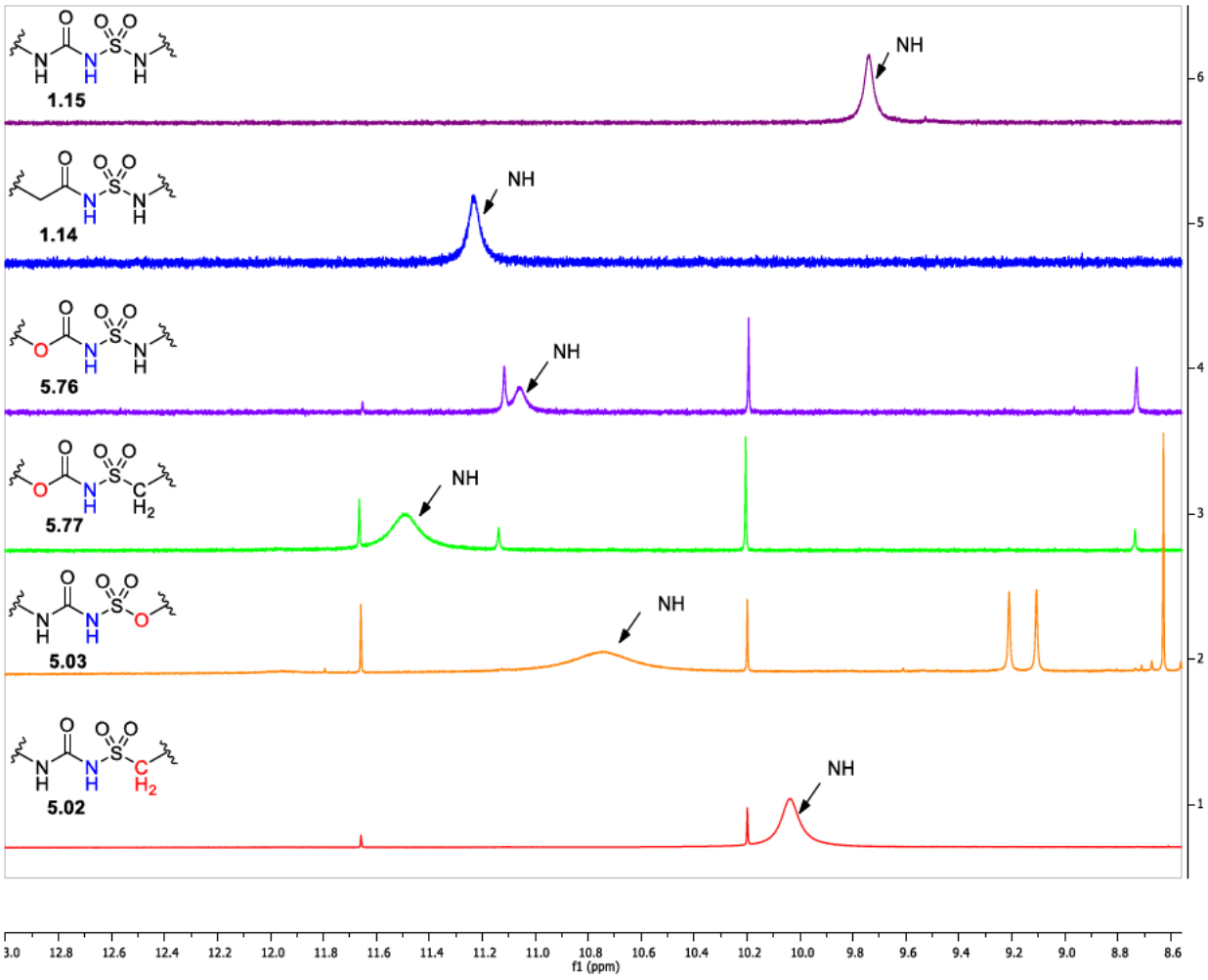

Compound	Central *NH* (ppm)	Δ1.14 *NH* (ppm)	Δ1.15 *NH* (ppm)
Acylsulfamide **1.14**	11.23	0	1.49
Sulfonylurea **1.15**	9.74	1.49	0
Analogue **5.76**	11.06	0.17	1.32
Analogue **5.77**	11.49	0.26	1.75
Analogue **5.03**	10.75	0.48	1.01
Analogue **5.02**	10.04	0.83	0.30

5.6: Biochemical and Antimicrobial Assay of 5.02, 5.03, 5.76 & 5.77

The sulfonamide analogues **5.02**, **5.03**, **5.76**, and **5.77** were assayed against *S. aureus* biotin *Sa*BPL using an *in vitro* biotinylation assay[21] (K_i values presented in Table 5.3). The whole cell activity of these analogues was also evaluated against a clinical isolate of *S. aureus* (ATCC 49775) using a published antibacterial susceptibility assay,[21] with the calculated minimum inhibitory concentrations (MIC, ≥ 90 % growth inhibited) presented in Table 5.3.

Table 5.3: Biochemical and anti-staphylococcal properties of **5.02, 5.03, 5.76** and **5.77**

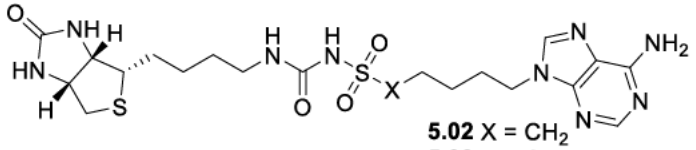

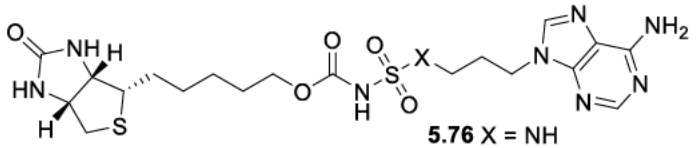

Compound	K_i *Sa*BPL (nM)	MIC *S. aureus* ATCC 49775 (μg/mL)
5.02	57.2 ± 6.5	4
5.03	35.3 ± 4.7	8
5.76	10.3 ± 3.8	>64 [a]
5.77	20.1 ± 5.2	>64 [a]

[a] MIC >64 μg/mL was reported for compounds where no MIC was attainable for 64 μg/mL (the highest concentration assayed in this study).

Methylene sulfonylurea **5.02** (K_i = 57.2 ± 6.5 nM) gave a similar K_i value against *Sa*BPL relative to amino sulfonylurea **1.15** (65.00 ± 3.00[1] nM), while the more acidic sulfamylurea **5.03** demonstrated a two-fold improvement (K_i = 35.3 ± 4.7 nM). This is consistent with the ^{1}H NMR data presented in Table 5.2 for these three analogues, where **5.02** (10.04 ppm) presented a similar chemical shift to **1.15** (9.74 ppm), whilst **5.03** was significantly further downfield (10.75 ppm). As discussed in Section 5.5, the chemical environment of the central NH in the ^{1}H NMR spectra, provided indication for relative acidity of this NH. Importantly, the sulfonylcarbamate analogues **5.76** (K_i = 10.3 ± 2.3 nM) and **5.77** (K_i = 20.1 ± 3.8 nM) were similarly potent to the reported acyl sulfamide **1.14** (K_i value of 7.00 ± 0.30[1] nM). This too is supported by the ^{1}H

NMR data presented in Table 5.3, where the chemical shifts of the central NH for **5.76** (11.06 ppm) and **5.77** (11.49 ppm) were comparable to **1.14** (11.23 ppm). The importance of the central NH acidity for effective *Sa*BPL inhibition is further evident when comparing the K_i values of methylene-sulfonylurea **5.02** and methylene-sulfonylcarbamate **5.76** (K_i = 40.24 ± 6.51 vs 20.12 ± 3.15 nM respectively). This approximate 2-fold improvement in activity is also consistent with the ^{1}H NMR data presented in Table 5.2, where the central NH resonance of **5.02** is upfield relative to **5.77** (10.75 and 11.49 ppm respectively). Thus, the K_i values obtained for inhibitors **5.02**, **5.03**, **5.76**, and **5.77** against *Sa*BPL each correlate with the chemical shift of the central sulfonyl NH, hence, correlate to the relative central NH acidity.

Sulfonylurea inhibitors **5.02** and **5.03** demonstrated good whole cell activity against a clinical isolate of *S. aureus* (MIC = 4 and 8 µg/mL, respectively), comparable to the activity exhibited by sulfonylurea **1.15** (MIC = 4 µg/mL[1]). In contrast, sulfonylcarbamates **5.76** and **5.77** inhibited clinical isolate growth by 20 and 30 % respectively, at 64 µg/mL. Analogues **5.76** and **5.77** demonstrated solubility issues during the antimicrobial assay, which may reflect the poor anti-staphylococcal activity of these compounds.

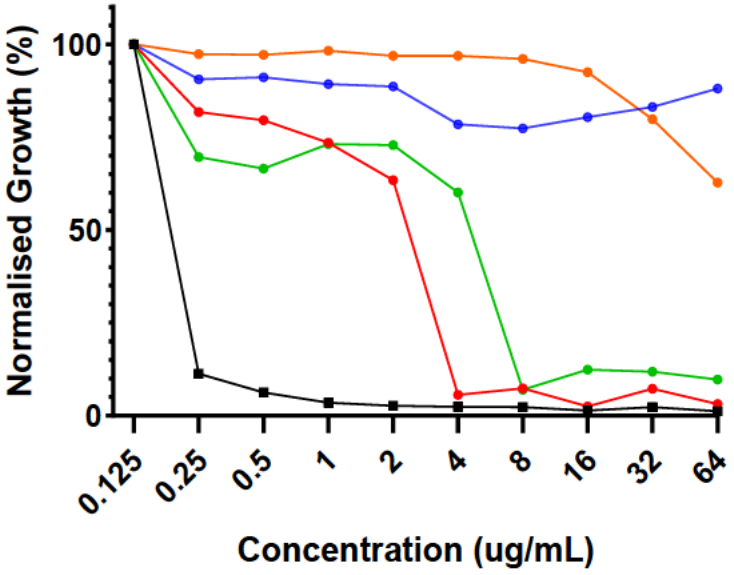

Figure 5.8: Inhibition growth of *S.aureus* growth *in vitro*. Compounds **5.02** (red), **5.03** (green), **5.76** (blue), **5.77** (orange) and erythromycin (black) were tested against *S.aureus* ATCC 49775.

5.7: Conclusion

Acidic sulfonylurea analogues (**5.02** and **5.03**) and sulfonylcarbamate analogues (**5.76** and **5.77**) were prepared and assayed against *Sa*BPL and a clinical isolate of *S. aureus* (ATCC 49755). The ^{1}H NMR spectra of analogues **5.02**, **5.03**, **5.76**, and **5.77** revealed that the sulfonyl central NH of these analogues can be inductively de-shielded by electron-poor substituents that flank the sulfonyl linker (e.g., CH_2, O), hence, making this labile NH more acidic. As anticipated, the K_i values obtained for **5.02**, **5.03**, **5.76**, and **5.77** against *Sa*BPL strongly correlated with this relative central NH acidity. In particular, sulfonylcarbamate **5.76** demonstrated comparable activity to the highly potent acyl sulfamide **1.14**[1] (K_i = 10.27 ± 2.34 vs 7.00 ± 1.00 nM), where both inhibitors share a similar central NH chemical environment (11.06 vs 11.23 ppm, respectively). Sulfonylurea analogues **5.02**, and **5.03** demonstrated good growth inhibition of *S. aureus* ATCC 49775 (MIC = 4 and 8 μg/mL respectively), similar to the recently reported sulfonylurea lead analogue **1.15**[1] (MIC = 4 μg/mL). These combined studies confirm that an acidic sulfonyl central NH translates in potent inhibitory activity against *Sa*BPL for the sulfonamide-based *Sa*BPL inhibitor chemotype.

The following continued future work is warranted:

- Experimentally determine the pK_a of the central NH for analogues **1.14**, **1.15**, **5.02**, **5.03**, **5.76**, and **5.77**. This can be potentially ascertained by ^{1}H NMR spectroscopy,[22] and should provide further evidence for the correlation between K_i and central NH acidity.
- Develop a synthetic route to prepare di-fluoro methylene sulfonamide **5.13** and subsequently prepare the corresponding di-fluoro methylene sulfonylurea analogue (**5.04**).[23] This analogue could further strengthen the K_i – central NH acidity correlation.
- An X-ray cocrystal structure of amino sulfonylcarbamate **5.76** complexed with *Sa*BPL should be acquired. This will confirm *a)* whether the sulfonylcarbamate linker binds the *Sa*BPL active site similarly to sulfonylurea **1.15**, and *b)* whether the protonated, de-protonated, or a mixture of both conformers of **5.76** bind the active site.
- Obtain *in vivo* biostability data for amino sulfonylcarbamate **5.76**. Determining if this potent inhibitor displays similar *in vivo* stability to sulfonylurea **1.15** is crucial to bring this chemotype closer to a preclinical space.
- Assay analogues **5.02**, **5.03**, **5.76** and **5.77** against other strains of *S. aureus* (e.g., RN4220, MRSA), to evaluate extent of anti-staphylococcal activity exhibited by these new analogues.

5.8: References for Chapter Five

(1) Lee, K. J.; Tieu, W.; Blanco-Rodriguez, B.; Paparella, A. S.; Yu, J.; Hayes, A.; Feng, J.; Marshall, A. C.; Noll, B.; Milne, R.; Cini, D.; Wilce, M. C. J.; Booker, G. W.; Bruning, J. B.; Polyak, S. W.; Abell, A. D. Sulfonamide-Based Inhibitors of Biotin Protein Ligase as New Antibiotic Leads. *ACS Chem. Biol.* **2019**, *14* (9), 1990–1997. https://doi.org/10.1021/acschembio.9b00463.

(2) Soares Da Costa, T. P.; Tieu, W.; Yap, M. Y.; Zvarec, O.; Bell, J. M.; Turnidge, J. D.; Wallace, J. C.; Booker, G. W.; Wilce, M. C. J.; Abell, A. D.; Polyak, S. W. Biotin Analogues with Antibacterial Activity Are Potent Inhibitors of Biotin Protein Ligase. *ACS Med. Chem. Lett.* **2012**, *3* (6), 509–514. https://doi.org/10.1021/ml300106p.

(3) Tieu, W.; Soares Da Costa, T. P.; Yap, M. Y.; Keeling, K. L.; Wilce, M. C. J.; Wallace, J. C.; Booker, G. W.; Polyak, S. W.; Abell, A. D. Optimising in Situ Click Chemistry: The Screening and Identification of Biotin Protein Ligase Inhibitors. *Chem. Sci.* **2013**, *4* (9), 3533–3537. https://doi.org/10.1039/c3sc51127h.

(4) Bockman, M. R.; Kalinda, A. S.; Petrelli, R.; De La Mora-Rey, T.; Tiwari, D.; Liu, F.; Dawadi, S.; Nandakumar, M.; Rhee, K. Y.; Schnappinger, D.; Finzel, B. C.; Aldrich, C. C. Targeting Mycobacterium Tuberculosis Biotin Protein Ligase (MtBPL) with Nucleoside-Based Bisubstrate Adenylation Inhibitors. *J. Med. Chem.* **2015**, *58* (18), 7349–7369. https://doi.org/10.1021/acs.jmedchem.5b00719.

(5) Tiwari, D.; Park, S. W.; Essawy, M. M.; Dawadi, S.; Mason, A.; Nandakumar, M.; Zimmerman, M.; Mina, M.; Ho, H. P.; Engelhart, C. A.; Ioerger, T.; Sacchettini, J. C.; Rhee, K.; Ehrt, S.; Aldrich, C. C.; Dartois, V.; Schnappinger, D. Targeting Protein Biotinylation Enhances Tuberculosis Chemotherapy. *Sci. Transl. Med.* **2018**, *10* (438). https://doi.org/10.1126/scitranslmed.aal1803.

(6) Billing, P.; Brinker, U. H. Mild One-Step Synthesis of Dibromo Compounds from Cyclic Ethers. *J. Org. Chem.* **2012**, *77* (24), 11227–11231. https://doi.org/10.1021/jo302360t.

(7) Zhu, Y.; Ching, C.; Carpenter, K.; Xu, R.; Selvaratnam, S.; Hosmane, N. S.; Maguire, J. A. Synthesis of the Novel Ionic Liquid [N-Pentylpyridinium]+ [Closo-CB11H12]- and Its Usage as a Reaction Medium in Catalytic Dehalogenation of Aromatic Halides. *Appl. Organomet. Chem.* **2003**, *17* (6–7), 346–350. https://doi.org/10.1002/aoc.407.

(8) Febriansyah, B.; Neo, C. S. D.; Giovanni, D.; Srivastava, S.; Lekina, Y.; Koh, T. M.; Li, Y.; Shen, Z. X.; Asta, M.; Sum, T. C.; Mathews, N.; England, J. Targeted Synthesis of Trimeric Organic-Bromoplumbate Hybrids That Display Intrinsic, Highly Stokes-Shifted, Broadband Emission. *Chem. Mater.* **2020**, *32* (11), 4431–4441. https://doi.org/10.1021/acs.chemmater.9b03925.

(9) Thompson, M. E. α, N-Alkanesulfonamide Dianions: Formation and Chemoselective C-Alkylation. *J. Org. Chem.* **1984**, *49* (10), 1700–1703. https://doi.org/10.1021/jo00184a006.

(10) Johnson, M. G.; Gribble, M. W.; Houze, J. B.; Paras, N. A. Convenient Route to Secondary Sulfinates: Application to the Stereospecific Synthesis of α- C -Chiral Sulfonamides. *Org. Lett.* **2014**, *16* (23), 6248–6251. https://doi.org/10.1021/ol503208z.

(11) D'Alonzo, D.; Van Aerschot, A.; Guaragna, A.; Palumbo, G.; Schepers, G.; Capone, S.; Rozenski, J.; Herdewijn, P. Synthesis and Base Pairing Properties of 1′,5′-Anhydro-l- Hexitol Nucleic Acids (L-HNA). *Chem. - A Eur. J.* **2009**, *15* (39), 10121–10131. https://doi.org/10.1002/chem.200901847.

(12) Prakash, G. K. S.; Ni, C.; Wang, F.; Hu, J.; Olah, G. A. From Difluoromethyl 2-Pyridyl Sulfone to Difluorinated Sulfonates: A Protocol for Nucleophilic Difluoro(Sulfonato)Methylation. *Angew. Chemie - Int. Ed.* **2011**, *50* (11), 2559–2563. https://doi.org/10.1002/anie.201007594.

(13) Hill, B.; Liu, Y.; Taylor, S. D. Synthesis of α-Fluorosulfonamides by Electrophilic Fluorination. *Org. Lett.* **2004**, *6* (23), 4285–4288. https://doi.org/10.1021/ol048249z.

(14) Baudoux, J. Electrophilic Fluorination with N-F Reagents. *Org. React. (Hoboken, NJ, United States)* **2007**, *69*, 347–672.

(15) Zhong, D.; Wu, D.; Zhang, Y.; Lu, Z.; Usman, M.; Liu, W.; Lu, X.; Liu, W. B. Synthesis of Sultams and Cyclic N-Sulfonyl Ketimines via Iron-Catalyzed Intramolecular Aliphatic C-H Amidation. *Org. Lett.* **2019**, *21* (15), 5808–5812. https://doi.org/10.1021/acs.orglett.9b01732.

(16) Duckworth, B. P.; Geders, T. W.; Tiwari, D.; Boshoff, H. I.; Sibbald, P. A.; Barry, C. E. 3rd; Schnappinger,

D.; Finzel, B. C.; Aldrich, C. C. Bisubstrate Adenylation Inhibitors of Biotin Protein Ligase from Mycobacterium Tuberculosis. *Chem. Biol.* **2011**, *18* (11), 1432–1441. https://doi.org/10.1016/j.chembiol.2011.08.013.

(17) MacArthur, N. S.; Wang, L.; McCarthy, B. G.; Jakobsche, C. E. Using N-Nitrosodichloroacetamides to Conveniently Convert Linear Primary Amines into Alcohols. *Synth. Commun.* **2015**, *45* (17), 2014–2021. https://doi.org/10.1080/00397911.2015.1061672.

(18) Tieu, W.; Polyak, S. W.; Paparella, A. S.; Yap, M. Y.; Soares Da Costa, T. P.; Ng, B.; Wang, G.; Lumb, R.; Bell, J. M.; Turnidge, J. D.; Wilce, M. C. J.; Booker, G. W.; Abell, A. D. Improved Synthesis of Biotinol-5′-AMP: Implications for Antibacterial Discovery. *ACS Med. Chem. Lett.* **2015**, *6* (2), 216–220. https://doi.org/10.1021/ml500475n.

(19) Soares Da Costa, T. P.; Tieu, W.; Yap, M. Y.; Pendini, N. R.; Polyak, S. W.; Pedersen, D. S.; Morona, R.; Turnidge, J. D.; Wallace, J. C.; Wilce, M. C. J.; Booker, G. W.; Abell, A. D. Selective Inhibition of Biotin Protein Ligase from Staphylococcus Aureus. *J. Biol. Chem.* **2012**, *287* (21), 17823–17832. https://doi.org/10.1074/jbc.M112.356576.

(20) Winum, J.-Y.; Toupet, L.; Barragan, V.; Dewynter, G.; Montero, J.-L. N -(Tert -Butoxycarbonyl)- N -[4-(Dimethylazaniumylidene)-1,4-Dihydropyridin-1-Ylsulfonyl] Azanide: A New Sulfamoylating Agent. Structure and Reactivity toward Amines . *Org. Lett.* **2001**, *3* (18), 2939–2939. https://doi.org/10.1021/ol010155r.

(21) Stachura, D. L.; Nguyen, S.; Polyak, S. W.; Jovcevski, B.; Bruning, J. B.; Abell, A. D. A New 1,2,3-Triazole Scaffold with Improved Potency against Staphylococcus Aureus Biotin Protein Ligase. *ACS Infect. Dis.* **2022**, *8* (12), 2579-2585. https://doi.org/10.1021/acsinfecdis.2c00452.

(22) Bezençon, J.; Wittwer, M. B.; Cutting, B.; Smieško, M.; Wagner, B.; Kansy, M.; Ernst, B. PKa Determination by 1H NMR Spectroscopy - An Old Methodology Revisited. *J. Pharm. Biomed. Anal.* **2014**, *93*, 147–155. https://doi.org/10.1016/j.jpba.2013.12.014.

(23) Gillis, E. P.; Eastman, K. J.; Hill, M. D.; Donnelly, D. J.; Meanwell, N. A. Applications of Fluorine in Medicinal Chemistry. *J. Med. Chem.* **2015**, *58* (21), 8315–8359. https://doi.org/10.1021/acs.jmedchem.5b00258.

Chapter Six

6.1: General Methods and Protocols

All reagents were obtained from commercial sources and are of reagent grade or as specified. Solvents were also obtained from commercial sources, except for anhydrous THF, anhydrous DCM and anhydrous DMF which were dried over a solvent purifier (PS-Micro, Innovative Technology, USA). Reactions were monitored by TLC using precoated plates (silica gel 60 F254, 250 μm, Merck, Darmstadt, Germany), spots were visualised under ultraviolet light at 254 nm and with either sulphuric acid-vanillin spray, potassium permanganate dip or Hanessian's stain. Flash column chromatography was performed with silica gel (40-63 μm 60 Å, Davisil, Grace, Germany). Microwave reactions were performed on a CEM Discovery SP with external IR temperature monitoring. Reactions were stirred for 5 min in a sealed container at ambient temperature, followed by 1 min stirring with increased microwave power until the prescribed temperature was reached. Both power and pressure were kept variable. ^{1}H, and ^{13}C spectra were recorded on a Varian Inova 500 MHz or a Varian Inova 600 MHz. Chemical shifts are given in ppm (δ) relative to the residual signals, which in the case of DMSO-d_6 were 2.50 ppm for ^{1}H and 39.55 ppm for ^{13}C, $CDCl_3$ were 7.26 ppm for ^{1}H and 77.23 ppm for ^{13}C and D_2O was 4.79 ppm for ^{1}H. Structural assignment was confirmed with COSY, NOESY, HSQC and HMBC. High-resolution mass spectra (HRMS) were recorded on an Agilent 6230 time of flight (TOF) liquid chromatography mass spectra (LC/MS) ($\Delta < 5$ ppm).

6.1.1: Expression and Purification of SaBPL and SaPC90-GST [1]

Recombinant *Sa*BPL fused to an *N*-terminal hexa-histidine tag, separated by a tobacco etch virus proteolytic cleavage site, was expressed in *Escherichia coli* BL21 (DE3-RIPL). Cells were cultured in Luria broth supplemented with Ampicillin (200 μg/mL) at 37 °C until an optical density of 0.7 was reached. Protein expression was then induced with IPTG (0.25 mM) for 16 h at 16 °C. Cells were collected via centrifugation, and the pellets were stored at −80 °C. Cells were lysed using a M110L microfluidizer processor, and the lysate was clarified by centrifugation. The cell lysate was loaded onto a 5 mL ZetaSep Nickel NTA column (EMP Biotech, Berlin, Germany) preequilibrated with buffer A (20 mM Tris pH 8.0, 500 mM NaCl, 10 mM imidazole, 2 mM β-mercaptoethanol). The column was then washed with 6 CV of 10% buffer B (20 mM Tris pH 8.0, 500 mM NaCl, 250 mM imidazole, 2 mM β-mercaptoethanol), and protein was eluted with an imidazole gradient from 10 to 250 mM. Fractions containing *Sa*BPL were then pooled and concentrated in an Amicon Ultra-15 Centrifugal Filter Unit (10 kDa MWCO) before loading onto a HiPrep 26/60 Sephacryl S-300 high-resolution size exclusion column preequilibrated in Storage Buffer (50 mM Tris pH 8.0, 0.5 mM

ethylenediamine tetraacetic acid (EDTA), 5% glycerol, 1 mM dithiothreitol (DTT)). Fractions containing *Sa*BPL were pooled, and protein purity was analyzed via sodium dodecyl sulfate poly(acrylamide) gel electrophoresis (SDS-PAGE). *Sa*BPL was concentrated to 1.7 mg/mL, flash-frozen in liquid nitrogen, and stored at −80 °C. Recombinant GST-*Sa*PC90 (a GST-tagged 90 amino acid fragment of *S. aureus* pyruvate carboxylase) was expressed and purified in *E. coli* BL21 (DE3) following methods described previously.[2]

6.1.2: SaBPL Inhibition Assay [1]

The inhibitory activity of compounds was determined by measuring *S. aureus* BPL (*Sa*BPL) activity in the presence of varying concentrations of compound (25.0, 5.0, 1.0, 0.2, 0.04 and 0.008 μM) using an *in vitro* biotinylation assay.[1] A reaction mixture was prepared containing 50 mM Tris HCl, pH 8.0, 3 mM adenosine triphosphate (ATP), 5 μM biotin, 5.5 mM $MgCl_2$, 100 mM KCl, 0.1 μM DTT, and 25 μM *Sa*PC90 fused to GST. Compounds for testing were dissolved in dimethyl sulfoxide (DMSO) and diluted into this reaction buffer to give a final concentration of 4% DMSO. The BPL reaction was initiated by the addition of *Sa*BPL at 37 °C (final [*Sa*BPL] = 6.25 nM). The BPL enzyme was stored in storage buffer prior to its addition (50 mM Tris pH 8.0, 0.5 nM EDTA, 5 % glycerol, 1mM DTT). The reaction was terminated after 20 min by addition of 180 μL of stop buffer (5.5 mM EDTA, 50 mM Tris pH 8.0), at 37 °C, and three 50 μL aliquots were added to each well of a white Lumitrac-600 96-well plate (Greiner) that had been precoated with a polyclonal anti-GST antibody (Sigma-Aldrich, 50 μL per well, 1:40 000 dilution) at 4 °C overnight, followed by blocking for 2 h (200 μL per well) with 1% bovine serum albumin (BSA) in TBS at 37 °C and incubated at 37 °C for 1 h. The plate was then washed five times (200 μL per well) with TBS containing 0.1% Tween-20. Europium labelled streptavidin (PerkinElmer) was diluted to 0.1 μg/mL in TBS containing 0.1% Tween-20. The streptavidin probe (50 μL per well) was incubated for 30 min at 37 °C, followed by washing five times with TBS containing 0.1% Tween-20. Enhancement solution (PerkinElmer, 50 μL) was added to each well and incubated for 10 min before reading the plate using a PerkinElmer Victor X5 multilabel reader (time-resolved fluorescence settings, 340 nm excitation, and 612 nm emission).[3] The IC_{50} value of each compound was obtained from a dose–response curve fitted in GraphPad Prism version 9 using a nonlinear fit of "log(inhibitor) vs normalized response," where the hillslope was constrained to −1. The absolute inhibition constants (K_i) for tested compounds were determined using equation 1.[4]

$$K_i = \frac{IC_{50}}{1+\frac{[S]}{K_M}} \qquad \textbf{(1)}$$

where [*S*] is the concentration of biotin (5 μM) and K_M is the affinity of the enzyme for biotin (1 μM [5]).

For compounds that produced a K_i value that approached [*Sa*BPL], required a re-calculation of the respective K_i value by fitting the inhibitory data of these compounds to the Morrison equation in GraphPad Prism version 9.

The standard error means were calculated for each averaged K_i value obtained. A minimal of three *Sa*BPL inhibition assays were undertaken for each compound presented throughout this thesis.

6.1.3: Antibacterial Activity Evaluation [1,6,7]

Antibacterial activity was determined by a microdilution broth method as recommended by the CLSI (Clinical and Laboratory Standards Institute, Document M07-A8, 2009, Wayne, PA) using cation adjusted Mueller-Hinton broth (Trek Diagnostics Systems, U.K.). Compounds were dissolved in DMSO. Serial 2-fold dilutions of each compound were made using DMSO as the diluent. Trays were inoculated with 5×10^4 CFU of each strain in a volume of 100 μL (final concentration of DMSO was 3.2% (v/v)) and incubated at 35 °C for 16−20 h. Growth of the bacterium was quantified by measuring the absorbance at 620 nm.

6.1.4: Detailed Docking Protocol and Method Validation [1,6]

Proteins (*Sa*BPL complexes) for docking were retrieved from the PDB. Formal charges were assigned, protonation states of histidines were adjusted, and hydrogens, histidine, glutamine, and asparagine were optimized using the protein preparation procedure implemented in ICM software version 3.8−7c (Molsoft L.L.C., San Diego, CA, USA).[8] The original bound ligand and all water molecules were removed from the binding site before docking. The binding site was defined as the cavity enclosed by residues with at least one non-hydrogen atom within a 4.0 Å cut-off radius from the ligand. The pocket was represented by 0.5 Å grid maps accounting for hydrogen bonding, hydrophobic, van der Waals, and electrostatic interactions. All molecules were flexibly docked into the rigid binding site and scored based on the ICM scoring function.

Docking protocol validation was undertaken prior to the docking of any analogues. Firstly, the bound ligand was removed from its co-crystal structure with *Sa*BPL, followed by redocking into the vacated enzyme. A root-mean-square deviation (RMSD) below 2 Å validates that the docking method is amenable to analogues desired for subsequent docking studies.

6.2 Experimental Work as Described in Chapter 4

(3a*S*,4*S*,6a*R*)-4-(5-(1-(3-fluorobenzyl)-1*H*-1,2,3-triazol-4-yl)-5-oxopentyl)tetrahydro-1*H*-thieno[3,4-*d*]imidazol-2(3*H*)-one (**4.02**)

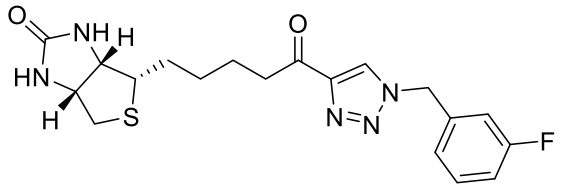

To a solution of biotin-ynone **4.04** (0.050 g, 0.20 mmol) and benzyl azide **4.03** (0.033 g, 0.22 mmol) in MeCN/H_2O (v/v = 2:1) (2 ml) was added copper nanopowder (0.003 g, 0.04 mmol). The reaction mixture was sonicated for 45 min, and the resulting reaction mixture was stirred for 6 h at rt. The suspension was filtered through celite, with the resulting filtrate concentrated under reduced pressure and purified by silica gel flash-column chromatography eluting with a mixture of 5 % MeOH in DCM to give triazole **4.02** as a white solid (0.068 g, 86 %).**^{1}H NMR** (600 MHz, $CDCl_3$) δ 8.00 (s, 1H), 7.41 – 7.35 (m, 1H), 7.11 – 7.06 (m, 2H), 7.01 – 6.97 (m, 1H), 5.61 (s, 1H), 5.56 (s, 2H), 5.05 (s, 1H), 4.54 – 4.49 (m, 1H), 4.35 – 4.31 (m, 1H), 3.21 – 3.10 (m, 3H), 2.91 (dd, *J* = 12.8, 5.0 Hz, 1H), 2.73 (d, *J* = 12.8 Hz, 1H), 1.83 – 1.77 (m, 3H), 1.73 – 1.67 (m, 1H), 1.58 – 1.46 (m, 2H); **^{13}C NMR** (150 MHz, $CDCl_3$) δ 195.30, 164.01, 163.35, 162.36, 148.37, 136.12, 136.07, 131.22, 131.17, 125.66, 123.97, 123.95, 115.52, 115.37, 61.98, 60.19, 55.68, 53.97, 40.74, 39.12, 28.43, 28.39, 23.89; **HRMS** calcd. for (M + H^+) $C_{19}H_{23}N_5O_2S^+$: requires 404.1551 found 404.1555

1-(azidomethyl)-3-fluorobenzene (**4.03**)

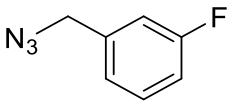

To a solution of *m*-F benzyl chloride (1.02 g, 6.92 mmol) in DMF (4 mL) was added NaN_3 (0.585 g, 8.99 mmol), and the resulting reaction mixture was stirred at rt for 16 h. The reaction mixture was poured onto water (100 mL) and extracted with diethyl ether. The organic extracts were combined, washed with water, brine, dried over Na_2SO_4, filtered, and concentrated under reduced pressure to give the benzyl azide **4.03** as a clear oil (0.959 g, 90 %). ^{1}H and ^{13}C NMR consistent with literature.[6]

(3a*S*,4*S*,6a*R*)-4-(5-oxohept-6-yn-1-yl)tetrahydro-1*H*-thieno[3,4-*d*]imidazol-2(3*H*)-one (**4.04**)

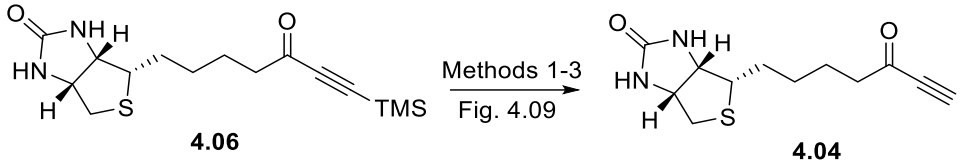

4.06 **4.04**

Method 1 (see Chapter 4, Figure 4.9): To a solution of **4.06** (0.020 g, 0.06 mmol) in THF (1.0 mL) at 0 °C was added TBAF (1.0 M in THF, 0.31 mL, 0.31 mmol). LC-MS of the subsequent reaction mixture indicated that **4.04** had not formed.

Method 2 (see Chapter 4, Figure 4.9): To a stirred solution of **4.06** (0.020 g, 0.06 mmol) in MeOH (1 mL) and DCM (1 mL), K_2CO_3 (0.009 g, 0.07 mmol) was added. The reaction mixture was sealed and stirred at rt for 2 h. LC-MS of the subsequent reaction mixture indicated that **4.04** had not formed.

Method 3 (see Chapter 4, Figure 4.9): To a solution of **4.06** (0.020 g, 0.06 mmol) in DMF (1 mL) was added an aqueous solution of KF (0.090 g, 1.54 mmol) in water (1.0 mL), and the reaction mixture was stirred for 30 min at rt. The reaction mixture was quenched with water and extracted with DCM. The organic extracts were combined, washed with brine, dried with Na_2SO_4, filtered, and concentrated under reduced pressure to give biotin-ynone **4.04** as a yellow solid (0.039 g, quant.). **^{1}H NMR** (500 MHz, $CDCl_3$) δ 5.53 (s, 1H), 5.14 (s, 1H), 4.57 – 4.48 (m, 1H), 4.35 – 4.30 (m, 1H), 3.23 (s, 1H), 3.20 – 3.12 (m, 1H), 2.92 (dd, *J* = 12.8, 5.0 Hz, 1H), 2.74 (d, *J* = 12.8 Hz, 1H), 2.62 (t, *J* = 7.4 Hz, 2H), 1.74 – 1.69 (m, 4H), 1.51 – 1.44 (m, 2H); **^{13}C NMR** (126 MHz, $CDCl_3$) δ 187.28, 163.45, 81.58, 78.79, 62.12, 60.25, 55.43, 45.16, 40.70, 28.54, 28.34, 23.69.

N-methoxy-*N*-methyl-5-((3a*S*,4*S*,6a*R*)-2-oxohexahydro-1*H*-thieno[3,4-*d*]imidazol-4-yl)pentanamide (**4.05**)

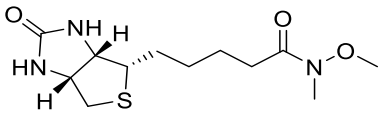

Method 1 (see Chapter 4 Table 4.1): To a suspension of biotin **1.01** (0.200 g, 0.82 mmol), and EDCI (0.140 g, 0.90 mmol) in DCM (10 mL) was added DIPEA (0.317 g, 2.46 mmol) followed by *N*,*O*-dimethylhydroxylamine hydrochloride (0.090 g, 1.47 mmol), and the resulting reaction

mixture stirred at rt for 16 h under a N_2 atmosphere. The reaction mixture was diluted with DCM (70 mL), washed with 0.5 M $HCl_{(aq)}$ (50 mL), sat. bicarb solution (50 mL), water (30 mL) and brine (30 mL), dried over Na_2SO_4, filtered, concentrated under reduced pressure, and purified by silica gel flash-chromatography eluting with 7% MeOH in DCM to give **4.05** as a light brown solid (0.011 g, 5%).

Method 2 (see Chapter 4 Table 4.1): To a suspension of biotin **1.01** (0.200 g, 0.82 mmol), and EDCI (0.254 g, 1.63 mmol) in DCM (10 mL) was added DIPEA (0.317 g, 2.46 mmol) followed by *N*,*O*-dimethylhydroxylamine hydrochloride (0.090 g, 1.47 mmol), and the resulting reaction mixture stirred at rt for 16 h under a N_2 atmosphere. Work up in accordance with method 1. No product was obtained.

Method 3 (see Chapter 4 Table 4.1): To a suspension of biotin **1.01** (0.200 g, 0.82 mmol), and EDCI (0.140 g, 0.90 mmol) in DMF (4 mL) was added DIPEA (0.317 g, 2.46 mmol) followed by *N*,*O*-dimethylhydroxylamine hydrochloride (0.090 g, 1.47 mmol), and the resulting reaction mixture stirred at rt for 16 h under a N_2 atmosphere. Work up in accordance with method 1, (0.035 g, 15%).

Method 4 (see Chapter 4 Table 4.1): A solution of biotin **1.01** (0.050 g, 0.20 mmol), DIPEA (0.143 mL, 0.60 mmol), and HBTU (0.077 g, 0.20 mmol) in DMF (1 mL) was stirred at rt for 15 min. To this solution was added *N*,*O*-hydroxylamine hydrochloride (0.022 g, 0.22 mmol), and the resulting reaction mixture was stirred for 3 h. The reaction mixture was diluted with sat. aqueous NH_4Cl (10 mL) and extracted with EtOAc. The organic extracts were combined and washed with brine, dried over Na_2SO_4, filtered, concentrated under reduced pressure, and purified by silica gel flash-column chromatography eluting with 7% MeOH in DCM to give **4.05** as a light brown solid (0.035 g, 53%).

Method 5 (see Chapter 4 Table 4.1): A solution of biotin **1.01** (0.050 g, 0.20 mmol), DIPEA (0.143 mL, 0.60 mmol), and HATU (0.077 g, 0.20 mmol) in DMF (1 mL) was stirred at rt for 15 min. To this solution was added *N*,*O*-hydroxylamine hydrochloride (0.022 g, 0.22 mmol), and the resulting reaction mixture was stirred for 3 h. Work up in accordance with method 4 (0.055 g, 95%).**^{1}H NMR** (600 MHz, DMSO-d_6) δ 6.43 (s, 1H), 6.35 (s, 1H), 4.35 – 4.27 (m, 1H), 4.16 – 4.11 (m, 1H), 3.65 (s, 3H), 3.15 – 3.02 (m, 4H), 2.82 (dd, J = 12.4, 5.1 Hz, 1H), 2.58 (d, J = 12.4 Hz, 1H), 2.41 – 2.31 (m, 2H), 1.66 – 1.58 (m, 1H), 1.55 – 1.44 (m, 3H), 1.40

– 1.28 (m, 2H); **^{13}C NMR** (150 MHz, DMSO-d_6) δ 162.71, 61.06, 59.18, 55.44, 40.06, 39.86, 31.73, 30.86, 28.28, 28.14, 24.18.

(3a*S*,4*S*,6a*R*)-4-(5-oxo-7-(trimethylsilyl)hept-6-yn-1-yl)tetrahydro-1*H*-thieno[3,4-*d*]imidazol-2(3*H*)-one(**4.06**)

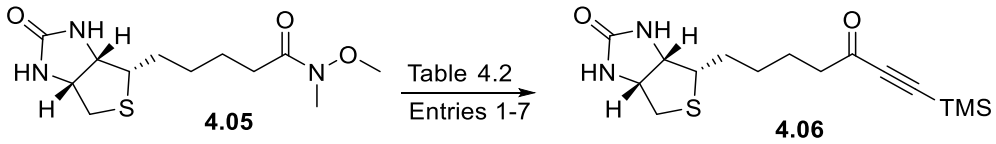

4.05 **4.06**

Method 1 (see Chapter 4 Table 4.2, Entry 1): A solution of *n*-BuLi in hexanes (2.5 M, 0.70 mL, 1.74 mmol) was added dropwise to a solution of TMS-acetylene (0.33 mL, 1.74 mmol) in anhydrous THF (5 mL) over 2 min at -78 ℃ under a N_2 atmosphere, and the resulting solution was stirred for 30 min. Biotin Weinreb amide **4.05** (0.050 g, 0.17 mmol) was added at -78 ℃ over 5 min and the resulting solution was stirred for 2 h. The reaction was quenched with sat. aqueous NH_4Cl (2 mL) and warmed to rt. The resulting mixture was concentrated under reduced pressure, and the resulting residue was extracted with EtOAc and concentrated to give a crude solid. This residue was purified by silica gel flash-column chromatography eluting with 5% MeOH in DCM to give unreacted starting material.

Method 2 (see Chapter 4 Table 4.2, Entry 2): Following the conditions described in method 1. However, the molar equivalents of *n*-BuLi and TMS-acetylene = 2 (3.48 mmol respectively). ^{1}H NMR of the crude residue solid confirmed only starting material was present.

Method 3 (see Chapter 4 Table 4.2, Entry 3): Following the conditions described in method 1. However, the molar equivalents of *n*-BuLi and TMS-acetylene = 5 (8.70 mmol respectively). ^{1}H NMR of the crude residue solid confirmed only starting was present.

Method 4 (see Chapter 4 Table 4.2, Entry 4): Following the conditions described in method 1. However, the molar equivalents of *n*-BuLi and TMS-acetylene = 10 (17.40 mmol respectively). ^{1}H NMR of the crude residue solid confirmed only starting material was present.

Method 5 (see Chapter 4 Table 4.2, Entry 5): Following the conditions described in method 1. However, However, the reaction was undertaken at -48 ℃. ^{1}H NMR of the crude residue solid confirmed only starting material was present.

Method 6 (see Chapter 4 Table 4.2, Entry 6): Following the conditions described in method 1. However, the reaction was undertaken at -48 ℃ and the molar equivalents of *n*-BuLi and TMS-acetylene = 2 (3.48 mmol respectively). ^{1}H NMR of the crude residue solid confirmed only starting material was present.

Method 7 (see Chapter 4 Table 4.2, Entry 7): Following the conditions described in method 1. However, the reaction was undertaken at -48 ℃ and the molar equivalents of *n*-BuLi and TMS-acetylene = 5 (8.70 mmol respectively). ^{1}H NMR and TLC confirmed the presence of a complex mixture. No evidence for product formation obtained.

1.01 **4.06**

Method 1 (see Chapter 4 Table 4.3, Entry 1): Biotin **1.01** (0.220 g, 1.00 mmol) was treated with $(COCl)_2$ (1 mL). The reaction mixture was stirred at for 1 h, concentrated under reduced pressure to give crude biotin acid chloride (1.00 mmol). Crude biotin acid chloride (1.00 mmol) and BTMSA (0.15 g, 0.90 mmol) in dry DCM (10 mL) was cooled to 0 ℃. To this chilled solution was added $AlCl_3$ (0.131 g, 0.98 mmol) portion-wise over 15 min, and the reaction mixture was stirred at 0 ℃for 2 h. The reaction mixture was allowed to warm up to rt, then to stirred for a further 2 h. The reaction mixture was then poured onto 1:1 aqueous 1M HCl and ice (50 mL) and extracted with DCM. The organic extracts were combined, dried over Na_2SO_4, concentrated under reduced pressure, and purified by silica gel flash-column chromatography eluting with 8% MeOH in DCM to give **4.06** as a yellow solid (0.007 g, 2 %).

Method 2 (see Chapter 4 Table 4.3, Entry 2): A suspension of biotin **1.01** (0.220 g, 1.00 mmol) in DCM (10 mL) was treated with $(COCl)_2$ (1 mL). The reaction mixture was stirred at for 1 h, concentrated under reduced pressure to give crude biotin acid chloride (1.00 mmol). Crude biotin acid chloride (1.00 mmol) and BTMSA (0.15 g, 0.90 mmol) in dry DCM (10 mL) was cooled to 0 ℃. To this chilled solution was added $AlCl_3$ (0.131 g, 0.98 mmol) portion-wise over 15 min, and the reaction mixture was stirred at 0 ℃for 2 h. The reaction mixture was allowed to warm up to rt, then to stirred for a further 2 h. The reaction mixture was then poured onto 1:1 1M $HCl_{(aq)}$ and ice (50 mL) and extracted with DCM. The organic extracts were combined, dried over Na_2SO_4, concentrated under reduced pressure, and purified by silica gel

flash-column chromatography eluting with 8% MeOH in DCM to give **4.06** as a yellow solid (0.019 g, 7%).

Method 3 (see Chapter 4 Table 4.3, Entry 3): Following the conditions, workup and purification described in method 2. However, the DCM solvent was replaced with DCM:DMF (v:v = 20:1) when preparing the crude biotin acid chloride. **4.06** isolated as a yellow solid (0.037 g, 13%).

Method 4 (see Chapter 4 Table 4.3, Entry 4): Following the conditions, workup and purification described in method 2. However, the ($COCl_2$) and DCM was replaced with neat $SOCl_2$ when preparing the crude biotin acid chloride. **4.06** isolated as a yellow solid (0.037 g, 15%).

Method 5 (see Chapter 4 Table 4.3, Entry 5): A suspension of *D*-Biotin **1.01** (0.200 g, 1.00 mmol) in DCM:DMF (v:v = 20:1, 10 mL) was treated with thionyl chloride (1 mL). The reaction mixture was stirred at for 1 h, concentrated under reduced pressure to give crude biotin acid chloride (1.00 mmol). Crude biotin acid chloride (1.00 mmol) and BTMSA (0.15 g, 0.90 mmol) in dry DCM (10 mL) was cooled to 0 ℃. To this chilled solution was added $AlCl_3$ (0.131 g, 0.98 mmol) portion-wise over 15 min, and the reaction mixture was stirred at 0 ℃ for 2 h. The reaction mixture was allowed to warm up to rt, then to stirred for a further 2 h. The reaction mixture was then poured onto 1:1 aqueous 1M $HCl_{(aq)}$ and ice (50 mL) and extracted with DCM. The organic extracts were combined, dried over Na_2SO_4 and concentrated under reduced pressure, and purified by silica gel flash-column chromatography eluting with 6% MeOH in DCM to give **4.06** as a yellow solid (0.085 g, 32%).

Method 6 (see Chapter 4 Table 4.3, Entry 6): Following the conditions described in method 5. However, the molar equivalents of BTMSA = 2.2 (1.80 mmol). **4.06** isolated as a yellow solid (0.081 g, 30%).

Method 7 (see Chapter 4 Table 4.3, Entry 7): Following the conditions described in method 5. However, the molar equivalents of $AlCl_3$ = 2 (1.96 mmol). **4.06** isolated as a yellow solid (0.119 g, 45%).

Method 8 (see Chapter 4 Table 4.3, Entry 8): Following the conditions described in method 5. However, the molar equivalents of $AlCl_3$ = 3 (2.94 mmol). **4.06** isolated as a yellow solid

(0.035 g, 14%). **^{1}H NMR** (600 MHz, $CDCl_3$) δ 5.41 (s, 1H), 5.08 (s, 1H), 4.56 – 4.48 (m, 1H), 4.36 – 4.28 (m, 1H), 3.25 – 3.10 (m, 1H), 2.92 (dd, *J* = 12.8, 5.0 Hz, 1H), 2.74 (d, *J* = 12.8 Hz, 1H), 2.59 (t, *J* = 7.3 Hz, 2H), 1.73 – 1.67 (m, 4H), 1.46 – 1.38 (m, 2H), 0.24 (s, 9H); **^{13}C NMR** (150 MHz, $CDCl_3$) δ 187.73, 163.33, 102.12, 98.16, 62.09, 60.22, 55.44, 45.01, 40.71, 28.52, 28.36, 23.77, -0.60.

6.3 Experimental Work as Described in Chapter 5

General procedure 5A: *Bz de-protection*: To a solution of Bz-protected sulfonylurea or Bz-protected sulfonyl carbamate in MeOH (1.6 mL per 0.10 mmol of Bz-protected sulfonylurea or Bz-protected sulfonyl carbamate) was added 30% $NH_4OH_{(aq)}$ (2.4 mL per 0.10 mmol of Bz-protected sulfonylurea or Bz-protected sulfonyl carbamate), and the resulting mixture was stirred for 16 h. The solvent was removed under reduced pressure, and the resulting residue purified by silica gel flash-column chromatography. See individual experiments for details.

General procedure 5B: *Synthesis of sulfonylurea*: DBU (1.2 eq) was added to a solution of biotin-carbamate **5.09**[7] (1.0 eq) and sulfonamide/sulfamide/sulfamate (0.8 eq) in MeCN (10 mL per 0.20 mmol of **5.09**), and the resulting mixture was heated under reflux for 16 h. The solvent was removed under reduced pressure, and the resulting residue purified by silica gel flash-column chromatography. See individual experiments for details.

General procedure 5C: *Synthesis of sulfonylcarbamate*: DBU (1.2 eq) was added to a solution of biotin-carbonate **5.56** (1.0 eq) and sulfonamide/sulfamide/sulfamate (0.8 eq) in MeCN (10 mL per 0.20 mmol of **5.56**), and the resulting mixture was heated under reflux for 16 h. The solvent was removed under reduced pressure, and the resulting residue purified by silica gel flash-column chromatography. See individual experiments for details.

5-(6-amino-9H-purin-9-yl)-N-((4-((3aS,4S,6aR)-2-oxohexahydro-1H-thieno[3,4-d]imidazol-4-yl)butyl)carbamoyl)pentane-1-sulfonamide (**5.02**)

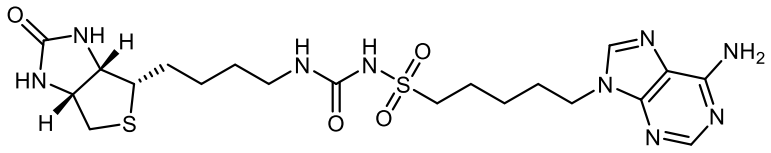

Bz-protected sulfonylurea **5.45** (0.050 g, 0.10 mmol) was de-protected according to **general procedure 5A**, and was purified by silica gel flash-column chromatography eluting with

DCM:MeOH (v/v = 5:1) to give **5.02** as a white solid (0.030 g, 72 %); **^{1}H NMR** (600 MHz, DMSO-d_6) δ 10.03 (s, 1H), 8.13 (s, 2H), 7.18 (s, 2H), 6.47 (s, 1H), 6.41 (t, *J* = 5.6 Hz, 1H), 6.36 (s, 1H), 4.33 – 4.26 (m, 1H), 4.14 – 4.09 (m, 3H), 3.10 – 3.05 (m, 1H), 3.01 (q, *J* = 6.6 Hz, 2H), 2.82 – 2.79 (m, 1H), 2.57 (d, *J* = 12.5 Hz, 1H), 1.82 (p, *J* = 7.2 Hz, 2H), 1.69 (q, *J* = 7.6 Hz, 2H), 1.64 – 1.56 (m, 1H), 1.49 – 1.23 (m, 8H); **^{13}C NMR** (150 MHz, DMSO-d_6) δ 162.72, 155.94, 152.35, 149.52, 140.75, 118.70, 61.02, 59.17, 55.49, 51.99, 42.54, 39.86, 29.30, 28.90, 27.97, 25.83, 24.43, 22.62; **HRMS** calcd. for (M + H^+) $C_{20}H_{32}N_9O_4S_2^+$: requires 526.2013 found 526.2016.

4-(6-amino-9*H*-purin-9-yl)butyl-((4-((3a*S*,4*S*,6a*R*)-2-oxohexahydro-1*H*-thieno[3,4-*d*]imidazol-4-yl)butyl)carbamoyl)sulfamate (**5.03**)

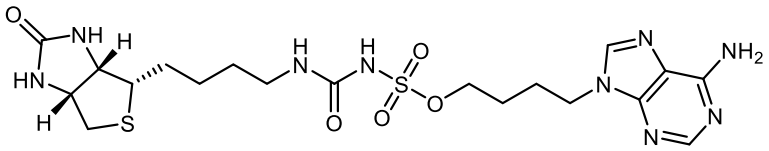

Bz-protected sulfonylurea **5.46** (0.020 g, 0.03 mmol) was de-protected according to **general procedure 5A** and was purified by silica gel flash-column chromatography eluting with DCM/MeOH (v/v = 5:1) to give **5.03** as a white solid (0.006 g, 11%). **^{1}H NMR** (600 MHz, DMSO-d_6) δ 10.74 (s, 1H), 8.14 (s, 2H), 7.19 (s, 2H), 6.54 (s, 1H), 6.41 (s, 1H), 6.37 (s, 1H), 4.56 – 4.51 (m, 1H), 4.46 – 4.43 (m, 1H), 4.32 – 4.27 (m, 2H), 4.11 – 4.08 (m, 2H), 3.09 – 3.05 (m, 1H), 2.81 – 2.77 (m, 1H), 2.57 (d, *J* = 12.5 Hz, 2H), 1.87 – 1.85 (m, 2H), 1.62 – 1.59 (m, 4H), 1.46 – 1.24 (m, 6H); **HRMS** calcd. for (M + H^+) $C_{19}H_{30}N_9O_5S_2^+$: requires 528.1806 found 528.1803.

N-(9-(5-sulfamoylpentyl)-9*H*-purin-6-yl)benzamide (**5.11**)

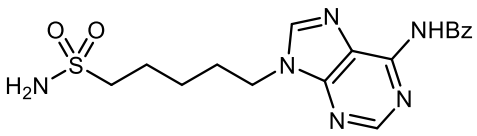

A solution of pyrimidinyl sulfone **5.29** (0.514 g, 1.14 mmol) in MeOH (8 mL) was cooled to 0 ℃, to which NaOMe, 25 wt. % solution in methanol (0.317 mL, 1.14 mmol) was added dropwise in one portion. The mixture was stirred at 0-5 ℃ for 20 min and then concentrated under reduced pressure, to give a crude residue of sulfinate **5.30**. This resulting residue was dissolved into a solution of NaOAc (0.117 g, 1.43 mmol) in H_2O (5 ml). To this solution was added a solution of HOSA (0.155 g, 1.37 mmol) in water (1 mL), and the resulting reaction

mixture was stirred for 1 h at rt, concentrated under reduced pressure and purified by silica gel flash-column chromatography eluting with 10% MeOH in DCM to give sulfonamide **5.11** as a white solid (0.204 g, 45% over 2-steps). **^{1}H NMR** (600 MHz, DMSO-d_6) δ 11.12 (s, 1H), 8.73 (s, 1H), 8.50 (s, 1H), 8.04 (d, *J* = 7.9, 1.5 Hz, 2H), 7.66 – 7.63 (m, 1H), 7.59 – 7.51 (m, 2H), 6.73 (s, 2H), 4.28 (t, *J* = 7.1 Hz, 2H), 2.98 – 2.93 (m, 2H), 1.91 (q, *J* = 7.5 Hz, 2H), 1.77 – 1.71 (m, 2H), 1.47 – 1.35 (m, 2H); **^{13}C NMR** (150 MHz, DMSO-d_6) δ 165.55, 152.47, 151.37, 150.05, 144.72, 133.44, 132.39, 128.46, 128.43, 125.40, 54.14, 43.03, 28.83, 24.74, 23.09; **HRMS** calcd. for (M + H$^+$) $C_{17}H_{21}N_6O_3S^+$: requires 389.1390 found 389.1393.

4-(6-benzamido-9H-purin-9-yl)butyl sulfamate (**5.12**)

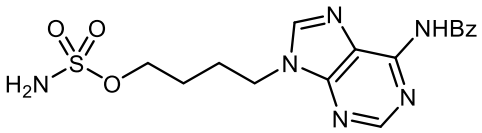

Formic acid (0.040 mL, 1.06 mmol) was added to neat CSI (0.090 mL, 1.06 mmol) at 0 ℃ under a N_2 atmosphere. The reaction mixture was stirred at 0 ℃ until a white solid appeared, then anhydrous MeCN (2 mL) was added, and the resulting mixture was stirred at rt O/N. The reaction mixture now containing sulfonating reagent **5.35** was cooled to 0 ℃, and a suspension of Bz-protected alcohol **5.34** (0.102 g, 0.48 mmol) in DMA (2 mL) was added dropwise. The resulting reaction mixture was stirred at 0 ℃ for 1.5 h, then warmed to rt and stirred for a further 2 h. The reaction mixture was quenched with water (1 mL), concentrated under reduced pressure, and purified by silica gel flash-column chromatography to give Bz-protected sulfamate **5.12** as a crystalline solid (0.041 g, 33 %). **^{1}H NMR** (600 MHz, DMSO-d_6) δ 11.13 (s, 1H), 8.74 (s, 1H), 8.51 (s, 1H), 8.04 (d, *J* = 7.6 Hz, 2H), 7.64 (t, *J* = 7.4 Hz, 1H), 7.55 (t, *J* = 7.6 Hz, 2H), 7.42 (s, 2H), 4.32 (t, *J* = 7.1 Hz, 2H), 4.07 (t, *J* = 6.3 Hz, 2H), 2.00 – 1.92 (m, 2H), 1.65 (p, *J* = 6.6 Hz, 2H); **^{13}C NMR** (150 MHz, DMSO-d_6) δ 165.55, 152.47, 151.41, 150.08, 144.72, 133.42, 132.39, 128.46, 128.44, 125.39, 68.38, 42.79, 39.94, 25.78, 25.67; **HRMS** calcd. for (M + H$^+$) $C_{16}H_{19}N_6O_4S^+$: requires 391.1183 found 389.1179.

9-(5-bromopentyl)-9H-purin-6-amine (**5.16**)

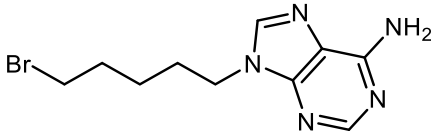

Adenine **5.15** (3.0 g, 22.20 mmol) was alkylated with 1,5-dibromopentane **5.14** (6.08 mL, 44.40 mmol) in DMF (20 mL) in the presence of Cs_2CO_3 (10.85 g, 33.30 mmol). The solution was stirred at rt O/N. The reaction mixture was diluted into H_2O (200 mL), extracted with EtOAc, washed with water, brine, dried over Na_2SO_4, filtered, concentrated under reduced pressure, and purified via silica gel flash-column chromatography eluting with DCM/MeOH (v/v: 10:1) to give adenine alkyl bromide **5.16** as a white solid (4.85 g, 77 %).**^{1}H NMR** (500 MHz, DMSO-d_6) δ 8.14 (s, 1H), 8.13 (s, 1H), 7.17 (s, 2H), 4.14 (t, J = 7.1 Hz, 2H), 3.50 (t, J = 6.7 Hz, 2H), 1.87 – 1.79 (m, 4H), 1.40 – 1.32 (m, 2H). **^{13}C NMR** (126 MHz, DMSO-d_6) δ 155.83, 152.21, 149.51, 140.82, 118.71, 42.61, 34.86, 31.55, 28.42, 24.54; **HRMS** calcd. for (M + H^+) $C_{10}H_{15}BrN_5^+$: requires 284.0505 found 284.0507.

5-(6-amino-9H-purin-9-yl)pentane-1-sulfonate (**5.20**)

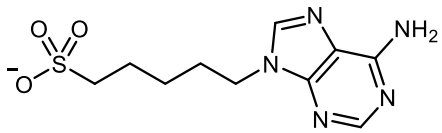

A solution of adenine alkyl bromide **5.16** (1.25 g, 4.40 mmol) and sodium sulphite (0.665 g, 5.28 mmol) in water (25 mL) was refluxed overnight. After cooling to rt, the reaction solution was concentrated under reduced pressure, and purified by silica gel flash-column chromatography eluting with 20 % MeOH in DCM to give sulfonate **5.20** as a white solid (1.29 g, 96 %).**^{1}H NMR** (600 MHz, DMSO-d_6) δ 8.14 (s, 1H), 8.13 (s, 1H), 7.16 (s, 2H), 4.11 (t, J = 7.3 Hz, 2H), 2.43 – 2.35 (m, 2H), 1.78 (p, J = 7.3 Hz, 2H), 1.59 (p, J = 8.0 Hz, 2H), 1.29 (p, J = 7.7 Hz, 2H); **^{13}C NMR** (151 MHz, DMSO-d_6) δ 155.91, 152.35, 152.29, 149.52, 140.90, 140.85, 118.72, 51.25, 42.84, 29.30, 25.47, 24.70; **HRMS** calcd. for (M + H^+) $C_{10}H_{15}N_5O_3S^+$: requires 285.0896 found 285.0897.

5-(6-amino-9H-purin-9-yl)pentane-1-sulfonamide (**5.21**)

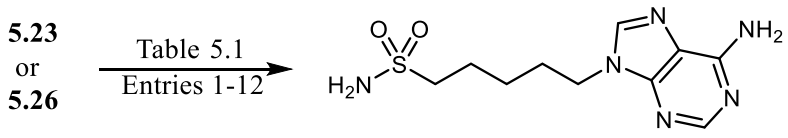

Method 1 (see Chapter 5 Table 5.1, Entry 1): To a solution of Boc-protected methanesulfonamide **5.24** (0.100 g, 0.51 mmol) in anhydrous THF (5 mL) under a N_2

atmosphere was added a solution of *n*-BuLi (2.5 M in hexane, 1 equiv, 0.50 mmol, 0.20 mL) at -78 ℃. The reaction mixture was allowed to warm to r.t. over a period of 30 min and then was cooled to -78 ℃. Adenine alkyl bromide **5.23** or adenine alkyl iodide **5.26** (0.130 g, 0.50 mmol) was added and the reaction mixture was stirred for 3 h, then warmed to rt and stirred O/N. The mixture was quenched with a solution of sat. aqueous NH_4Cl and extracted with EtOAc. The organic extracts were combined, washed with brine, dried over Na_2SO_4, filtered, concentrated under reduced pressure purified by silica gel flash-column chromatography to give back unreacted starting material (adenine alkyl bromide **5.23** /iodide **5.26** and Boc-protected methanesulfonamide **5.24**).

Method 2 (see Chapter 5 Table 5.1, Entry 2): Following the conditions described in method 1. However, the molar equivalents of *n*-BuLi and Boc-protected methanesulfonamide = 2 (0.96 mmol respectively). Only adenine alkyl bromide **5.23** and Boc-protected methanesulfonamide **5.24** were isolated.

Method 3 (see Chapter 5 Table 5.1, Entry 3): Following the conditions described in method 1. However, the molar equivalents of *n*-BuLi and Boc-protected methanesulfonamide = 5 (2.40 mmol respectively). Only adenine alkyl bromide **5.23** and Boc-protected methanesulfonamide **5.24** were isolated.

Method 4 (see Chapter 5 Table 5.1, Entry 4): Following the conditions described in method 1. However, the reaction temperature was increased to -30 ℃. Only adenine alkyl bromide **5.23** and Boc-protected methanesulfonamide **5.24** were isolated.

Method 5 (see Chapter 5 Table 5.1, Entry 5): Following the conditions described in method 1. However, the reaction temperature was increased to -30 ℃ and the molar equivalents of *n*-BuLi and Boc-protected methanesulfonamide = 2 (1.44 mmol respectively) A TLC and ^{1}H NMR of the crude residue solid confirmed the presence of a complex mixture and starting material respectively. LC-MS showed no mass for the product.

Method 6 (see Chapter 5 Table 5.1, Entry 6): Following the conditions described in method 1. However, the reaction temperature was increased to -30 ℃ and the molar equivalents of *n*-BuLi and Boc-protected methanesulfonamide = 5 (2.40 mmol respectively) A TLC and ^{1}H NMR of the crude residue solid confirmed the presence of a complex mixture, and LC-MS analysis showed no mass for the product.

Method 7 (see Chapter 5 Table 5.1, Entry 7): Following the conditions described in method 1. However, *n*-BuLi was replaced for LDA. Only adenine alkyl bromide **5.23/** iodide **5.26** and Boc-protected methanesulfonamide **5.24** were isolated.

Method 8 (see Chapter 5 Table 5.1, Entry 8): Following the conditions described in method 1. However, *n*-BuLi was replaced for LDA, and the molar equivalents of LDA and Boc-protected methanesulfonamide = 2 (1.44 mmol respectively). Only adenine alkyl bromide **5.23** and Boc-protected methanesulfonamide **5.24** were isolated.

Method 9 (see Chapter 5 Table 5.1, Entry 9): Following the conditions described in method 1. However, *n*-BuLi was replaced for LDA, and the molar equivalents of LDA and Boc-protected methanesulfonamide = 5 (2.40 mmol respectively). Only adenine alkyl bromide **5.23** and Boc-protected methanesulfonamide **5.24** were isolated.

Method 10 (see Chapter 5 Table 5.1, Entry 10): Following the conditions described in method 1. However, *n*-BuLi was replaced for LDA, and the reaction temperature was increased to -30 ℃. Only adenine alkyl bromide **5.23** and Boc-protected methanesulfonamide **5.24** were isolated.

Method 11 (see Chapter 5 Table 5.1, Entry 11): Following the conditions described in method 1. However, *n*-BuLi was replaced for LDA, the reaction temperature was increased to -30 ℃, and the molar equivalents of LDA and Boc-protected methanesulfonamide = 2 (1.44 mmol respectively). Only adenine alkyl bromide **5.23** and Boc-protected methanesulfonamide **5.24** were isolated.

Method 12 (see Chapter 5 Table 5.1, Entry 12): Following the conditions described in method 1. However, *n*-BuLi was replaced for LDA, the reaction temperature was increased to -30 ℃ and the molar equivalents of LDA and Boc-protected methanesulfonamide = 5 (2.40 mmol respectively). A TLC and ^{1}H NMR of the crude residue solid confirmed the presence of a complex mixture, and LC-MS analysis showed no mass for the product.

9-(4-bromobutyl)-9*H*-purin-6-amine (**5.23**)

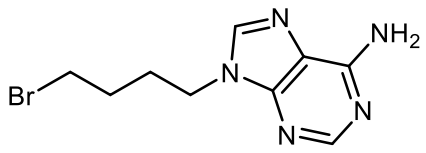

Adenine **5.15** (3.0 g, 22.20 mmol) was alkylated with 1,4-dibromobutane **5.22** (5.33 mL, 44.40 mmol) in DMF (17 mL) in the presence of Cs_2CO_3 (10.85 g, 33.30 mmol). The solution was stirred at rt O/N. The reaction mixture was diluted into H_2O (150 mL), extracted with EtOAc, washed with water, brine, dried over Na_2SO_4, filtered, concentrated under reduced pressure, and purified via silica gel flash-column chromatography eluting with DCM/MeOH (v/v 10:1) to give adenine alkyl bromide **5.23** as a white solid (2.58 g, 41 %). **^{1}H NMR** (500 MHz, DMSO-d_6) δ 8.15 (s, 1H), 8.13 (s, 1H), 7.19 (s, 2H), 4.17 (t, *J* = 6.9 Hz, 3H), 3.55 (t, *J* = 6.7 Hz, 3H), 1.93 (p, *J* = 7.0 Hz, 2H), 1.79 – 1.71 (m, 2H); **^{13}C NMR** (126 MHz, DMSO-d_6) δ 155.94, 152.39, 149.55, 147.86, 143.03, 140.82, 118.72, 42.01, 34.28, 29.36, 28.13; **HRMS** calcd. for (M + H^+) $C_9H_{13}BrN_5^+$: requires 270.0349 found 270.0352.

9-(4-iodobutyl)-9*H*-purin-6-amine (**5.26**)

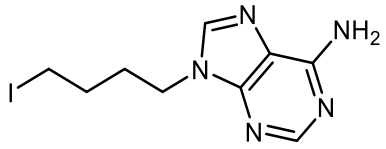

To a mixture of adenine alkyl bromide **5.23** (1.00 g, 3.70 mmol) in anhydrous acetone (50 mL) was added NaI (1.39 g, 9.30 mmol), and the resulting reaction mixture was heated under reflux for 4 h. The reaction mixture was filtered and concentrated under reduced pressure. The residue was suspended in a solution of sodium metabisulfite, and extracted with EtOAc, washed with brine, dried over Na_2SO_4, filtered, and concentrated under reduced pressure to afford adenine alkyl iodide **5.26** as a yellow solid (0.998 g, 85 %) **^{1}H NMR** (500 MHz, DMSO-d_6) δ 8.15 (s, 1H), 8.13 (s, 1H), 7.19 (s, 2H), 4.17 (t, *J* = 6.9 Hz, 3H), 3.15 (t, *J* = 6.7 Hz, 3H), 1.93 (p, *J* = 7.0 Hz, 2H), 1.79 – 1.71 (m, 2H); **^{13}C NMR** (126 MHz, DMSO-d_6) δ 155.94, 152.39, 149.55, 147.86, 143.03, 140.82, 118.72, 42.01, 29.36, 28.13, 8.32; **HRMS** calcd. for (M + H^+) $C_9H_{13}IN_5^+$: requires 318.0210 found 318.0211.

9-(5-(pyrimidin-2-ylthio)pentyl)-9*H*-purin-6-amine (**5.27**)

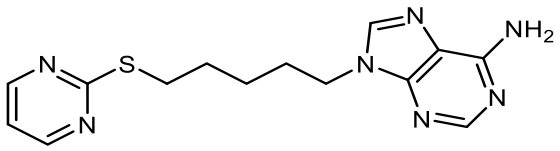

Adenine alkyl bromide **5.16** (1.00 g, 3.52 mmol) was alkylated with 2-mercaptopyrimidine (0.434 g, 3.87 mmol) in DMF (17 mL) in the presence of Cs_2CO_3 (1.72 g, 5.27 mmol), and the reaction suspension was stirred at rt O/N. The reaction mixture was diluted into H_2O (150 mL), extracted with DCM, washed with water, brine, dried over Na_2SO_4, filtered, concentrated under reduced pressure to give 2-pyrimidinyl thioether **5.27** as a yellow crystalline solid, which was used without further purification (1.09 g, quant.) **^{1}H NMR** (600 MHz, DMSO-d_6) δ 8.60 (d, J = 4.8 Hz, 2H), 8.13 (s, 1H), 8.11 (s, 1H), 7.18 (t, J = 4.8 Hz, 1H), 7.16 (s, 2H), 4.14 (t, J = 7.1 Hz, 2H), 3.13 – 3.06 (m, 2H), 1.84 (p, J = 7.3 Hz, 2H), 1.68 (p, J = 7.6 Hz, 1H), 1.40 – 1.33 (m, 2H). **^{13}C NMR** (150 MHz DMSO-d_6) δ 171.04, 157.71, 155.93, 152.33, 149.53, 140.81, 118.72, 117.09, 42.68, 29.71, 28.91, 28.27, 25.22; **HRMS** calcd. for (M + H^+) $C_{14}H_{18}N_7S^+$: requires 316.1339 found 316.1336.

N-(9-(5-(pyrimidin-2-ylthio)pentyl)-9*H*-purin-6-yl)benzamide (**5.28**)

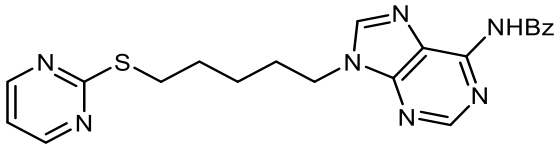

To a mixture of 2-pyrimidinyl thioether **5.27** (0.900 g, 2.84 mmol) in pyridine (5 mL) was slowly added BzCl (0.365 mL, 3.13 mmol) and the mixture was stirred at 100 °C for 1 h. The reaction mixture was concentrated under reduced pressure and the residue was purified by silica gel flash-column chromatography eluting with 5 % MeOH in DCM to yield Bz-protected 2-pyrimidinyl thioether **5.28** as a white solid (0.740 g, 67 %).**^{1}H NMR** (600 MHz, DMSO-d_6) δ 11.12 (s, 1H), 8.71 (s, 1H), 8.61 (d, J = 4.8 Hz, 2H), 8.50 (s, 1H), 8.04 (d, J = 6.8 Hz, 1H), 7.68 – 7.61 (m, 1H), 7.59 – 7.52 (m, 1H), 7.19 (t, J = 4.8 Hz, 1H), 4.29 (t, J = 7.1 Hz, 2H), 3.09 (t, J = 7.3 Hz, 2H), 1.91 (p, J = 7.3 Hz, 2H), 1.72 (p, J = 7.6 Hz, 2H), 1.44 – 1.36 (m, 2H); **HRMS** calcd. for (M + H^+) $C_{21}H_{22}N_7OS^+$: requires 420.1601 found 420.1602.

N-(9-(5-(pyrimidin-2-ylsulfonyl)pentyl)-9*H*-purin-6-yl)benzamide (**5.29**)

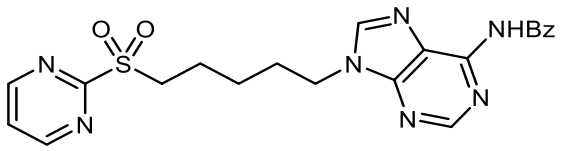

A solution of Bz-protected 2-pyrimidinyl thioether **5.28** (0.720 g, 1.72 mmol) in DCM (10 mL) at 0 °C was treated with *m*-CPBA (1.04 g, 6.01 mmol) and the resulting mixture was allowed to warm to rt and stirred for 3 h. The reaction mixture was concentrated under reduced pressure, and purified by silica gel flash column chromatography eluting with 6 % MeOH in DCM to the pyrimidinyl sulfone **5.29** as a white solid (0.551 g, 71 %) **^{1}H NMR** (600 MHz, DMSO-d_6) δ 11.12 (s, 1H), 9.08 (d, J = 4.9 Hz, 1H), 8.72 (s, 1H), 8.48 (s, 1H), 8.04 (d, J = 7.8, 1.5 Hz, 2H), 7.85 (t, J = 4.9 Hz, 1H), 7.66 – 7.63 (m, 1H), 7.58 – 7.53 (m, 2H), 4.26 (t, J = 7.0 Hz, 2H), 3.67 – 3.58 (m, 2H), 1.93 – 1.86 (m, 2H), 1.78 – 1.71 (m, 2H), 1.43 – 1.36 (m, 2H). **^{13}C NMR** (151 MHz, DMSO-d_6) δ 165.54, 164.94, 159.19, 152.46, 151.36, 150.02, 144.70, 133.44, 132.38, 128.46, 128.43, 125.37, 124.67, 54.92, 50.08, 42.84, 28.60, 24.69, 21.38; **HRMS** calcd. for (M + H^+) $C_{21}H_{22}N_7OS^+$: requires 452.1499 found 452.1496.

methyl 4-(6-amino-9H-purin-9-yl)butanoate (**5.31**)

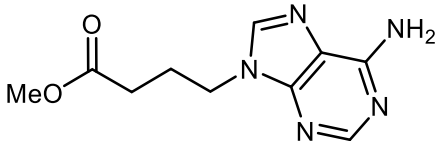

Adenine **5.15** (0.380 g, 2.81 mmol) was alkylated with methyl 4-bromobutyrate (0.560 g, 3.10 mmol) in DMF (5 mL) in the presence of Cs_2CO_3 (1.37 g, 4.22 mmol), and the reaction mixture was stirred at rt O/N. The reaction mixture was diluted with water (80 mL), extracted with DCM, washed with water, brine, dried over Na_2SO_4, filtered, and concentrated under reduced pressure to give methyl ester **5.31** as an off white solid which was used in subsequent steps without further purification (0.662 g, 99 %) **^{1}H NMR** (500 MHz, DMSO-d_6) δ 8.13 (s, 1H), 8.11 (s, 1H), 7.16 (s, 2H), 4.17 (t, J = 6.9 Hz, 2H), 3.54 (s, 3H), 2.31 (t, J = 7.4 Hz, 2H), 2.07 (p, J = 7.1 Hz, 2H).) **^{13}C NMR** (126 MHz, DMSO-d_6) δ 172.52, 155.93, 152.36, 149.56, 140.77, 118.72, 51.30, 42.19, 30.40, 24.81; **HRMS** calcd. for (M + H^+) $C_{10}H_{13}N_5O_2^+$: requires 235.1069 found 235.1073.

4-(6-amino-9*H*-purin-9-yl)butan-1-ol (**5.32**)

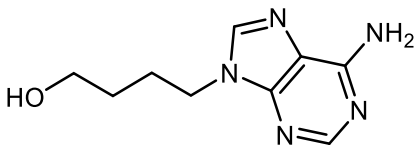

Method 1 (See Chapter 5, Scheme 5.04):A solution of methyl ester **5.31** (0.050 g, 0.21 mmol) in anhydrous THF (3 mL) was added to a suspension of $LiAlH_4$ (0.032 g, 0.85 mmol) in anhydrous THF (2 mL), and the resulting reaction mixture was stirred at rt O/N, quenched with water (0.160 mL), 15 % aqueous NaOH (0.160 mL), water (0.400 mL) successively. The ppt. that resulted was filtered off and washed with THF (5 mL). The washing and filtrate were combined and concentrated under reduced pressure. A ^{1}H NMR of the crude sample suggested a complex reaction mixture, with LC-MS analysis showing no mass peak for **5.32**.

Method 2 (See Chapter 5, Scheme 5.04):To a solution of alkyl acetate **5.33** (0.500 g, 2.00 mmol) in THF/MeOH/H_2O (3/1/1 = 5 mL) was added LiOH (0.144 g, 6.01 mmol), and the reaction mixture was stirred at 40 ℃ for 2 h, concentrated under reduced pressure and purified by silica gel flash column chromatography eluting with 17 % MeOH in DCM to give alcohol **5.32** as a white solid (0.410 g, 99 %). **^{1}H NMR** (600 MHz, DMSO-d_6) δ 8.14 (s, 1H), 8.12 (s, 1H), 7.17 (s, 2H), 4.47 (t, J = 5.2 Hz, 1H), 4.14 (t, J = 7.1 Hz, 2H), 3.41 – 3.37 (m, 2H), 1.85 – 1.79 (m, 2H), 1.40 – 1.33 (m, 2H); **^{13}C NMR** (150 MHz, DMSO-d_6) δ 155.93, 152.32, 149.54, 140.86, 118.74, 60.10, 42.83, 29.49, 26.29.

4-(6-amino-9*H*-purin-9-yl)butyl acetate (**5.33**)

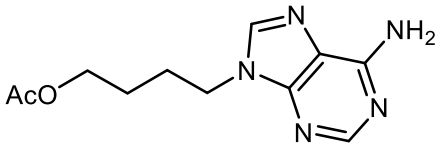

Adenine **5.15** (1.03 g, 7.6 mmol) was alkylated with 4-bromobutyl acetate (1.64 g, 8.40 mmol) in DMF (10 mL) in the presence of Cs_2CO_3 (3.73 g, 11.43 mmol), and the resulting suspension was stirred at rt O/N The reaction mixture was diluted with water (80 mL), extracted with DCM, washed with water, brine, dried over Na_2SO_4, filtered, concentrated and purified by silica gel flash column chromatography eluting with 10 % MeOH in DCM to give alkyl acetate **5.33** as a white solid (1.05 g, 56 %).**^{1}H NMR** (600 MHz, DMSO-d_6) δ 8.14 (s, 1H), 8.13 (s, 1H), 7.17 (s,

2H), 4.16 (t, *J* = 7.0 Hz, 2H), 4.00 (t, *J* = 6.6 Hz, 2H), 1.98 (s, 3H), 1.89 – 1.81 (m, 2H), 1.56 – 1.49 (m, 2H); **^{13}C NMR** (150 MHz, DMSO-d_6) δ 170.37, 155.95, 152.37, 149.54, 140.80, 118.72, 63.22, 42.46, 26.03, 25.30, 20.69; **HRMS** calcd. for (M + H^+) $C_{11}H_{15}N_5O_2^+$: requires 250.1229 found 250.1229.

N-(9-(4-hydroxybutyl)-9*H*-purin-6-yl)benzamide (**5.34**)

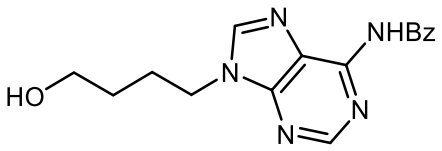

To a stirring solution of alcohol **5.32** (0.810 g, 3.96 mmol) in anhydrous pyridine (25 mL) was added TMSCl (4.94 mL, 39.09 mmol) under a N_2 atmosphere. After 30 min, BzCl (0.50 mL, 4.30 mmol) was added at 0 ℃. The resulting reaction mixture was warmed to rt and further stirred for 16 h. Then aqueous NH_4OH (10 mL) was added at 0 ℃, and the resulting reaction mixture was stirred at rt for 1 h; the solvent was removed under reduced pressure, and the resulting residue purified via silica gel flash column chromatography eluting with 10 % MeOH in DCM to give Bz-protected alcohol **5.34** (0.681 g, 56 %). **^{1}H NMR** (600 MHz, DMSO-d_6) δ 11.12 (s, 1H), 8.73 (s, 1H), 8.50 (s, 1H), 8.04 (d, *J* = 7.0 Hz, 1H), 7.68 – 7.61 (m, 1H), 7.55 (t, *J* = 7.8 Hz, 2H), 4.46 (t, *J* = 5.2 Hz, 1H), 4.29 (t, *J* = 7.1 Hz, 2H), 3.42 (td, *J* = 6.4, 5.1 Hz, 2H), 1.90 (p, *J* = 7.2 Hz, 2H), 1.45 – 1.38 (m, 2H); **^{13}C NMR** (150 MHz, DMSO-d_6) δ 165.54, 152.45, 151.32, 150.04, 144.76, 133.47, 132.37, 128.46, 128.43, 125.41, 60.09, 43.24, 29.52, 26.14; **HRMS** calcd. for (M + H^+) $C_{16}H_{18}N_5O_2^+$: requires 312.1455 found 312.1457.

9-(5,5-difluoro-5-(pyridin-2-ylsulfonyl)pentyl)-9*H*-purin-6-amine (**5.36**)

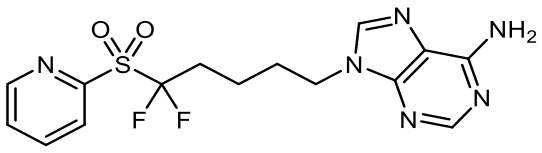

A solution of adenine alky bromide **5.23** (0.559 g, 2.07 mmol) and Hu's Reagent (0.200 g, 1.04 mmol) in anhydrous HMPA/THF (v/v = 1/3, 1 mL) was cooled to -78 ℃. Freshly prepared LiHMDS (0.111 mL, 1.50 mmol) was added dropwise to this solution, and the resulting reaction was stirred for 10 min before being quenched by addition of sat. aqueous NH_4Cl (1 mL). The mixture was extracted with EtOAc, dried over Na_2SO_4, filtered, concentrated under reduced

pressure. A ^{1}H NMR of the crude sample suggested a complex reaction mixture, with LC-MS analysis showing no mass peak for **5.36**.

2-((5-(benzyloxy)-1,1-difluoropentyl)sulfonyl)pyridine (**5.38**)

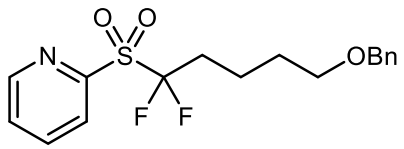

As described for the attempted synthesis of **5.36**. However, adenine alky bromide **5.23** was replaced for benzyl 4-bromobutyl ether (2.07 mmol). A repeat of the reaction replaced adenine alky bromide **5.23** for benzyl 4-bromobutyl ether (2.07 mmol), and the reaction temperature was set to -40 °C. In both instances, ^{1}H NMR of the crude sample suggested a complex reaction mixture, with LC-MS analysis showing no mass peak for **5.38**.

5-(benzyloxy)pentane-1-sulfonamide (**5.40**)

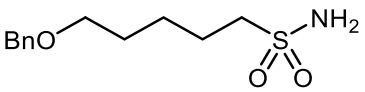

A suspension of Rongalite (1.26 g, 8.23 mmol) in DMSO (15 mL) was stirred at rt for 30 min, prior to the addition of 5-bromopentyl ether (1.00 g, 4.11 mmol). The resulting reaction mixture was stirred at rt O/N, diluted with H_2O (20 mL)and brine (15 mL), and extracted with EtOAc. The combined organic extracts were washed with brine, dried over Na_2SO_4, filtered, concentrated under reduced pressure, and purified by silica gel flash column chromatography eluting with 50 % EtOAc in hexane to give sulfonamide **5.40** as a white solid (0.420 g, 42 % 2-steps). **^{1}H NMR** (500 MHz, $CDCl_3$) δ 7.38 – 7.28 (m, 5H), 4.50 (s, 2H), 3.52 (td, *J* = 6.0, 0.9 Hz, 2H), 3.19 – 3.12 (m, 2H), 1.99 (p, *J* = 7.7 Hz, 2H), 1.78 (dt, *J* = 8.5, 6.4 Hz, 2H), 1.61-1.59 (m, 2H); **^{13}C NMR** (126 MHz, $CDCl_3$) δ 138.37, 128.61, 127.87, 127.85, 73.25, 69.47, 55.21, 28.36, 21.43, 19.45.

5-(benzyloxy)-N,N-bis(4-methoxybenzyl)pentane-1-sulfonamide (**5.41**)

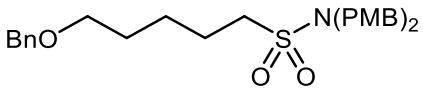

A solution of sulfonamide **5.40** (0.070 g, 0.29 mmol), PMBCl (0.08 mL, 0.60 mmol), anhydrous K_2CO_3 (0.199, 1.44 mmol) and KI (0.004 g, 0.03 mmol, 0.1 equiv.) in anhydrous MEK (10 mL) was stirred at 75˚C O/N. The resulting mixture was cooled to rt and filtered. The resulting filtrate was concentrated under reduced pressure and purified by silica gel flash column chromatography eluting with 50 % EtOAc in hexane to give the di-PMB protected benzyl ether **5.41** as a resin (0.014 g, 10 %).**^{1}H NMR** (500 MHz, $CDCl_3$) δ 7.40 – 7.28 (m, 5H), 7.20 (d, *J* = 8.1 Hz, 4H), 6.86 (d, *J* = 7.4 Hz, 4H), 4.25 (s, 4H), 3.80 (d, *J* = 1.4 Hz, 6H), 3.45 (t, *J* = 6.1 Hz, 2H), 2.93 – 2.85 (m, 2H), 2.34 – 2.15 (m, 2H), 1.90 (p, *J* = 7.6 Hz, 2H), 1.68 (p, *J* = 6.9 Hz, 2H); **^{13}C NMR** (126 MHz, $CDCl_3$) δ 159.45, 130.18, 128.57, 128.05, 127.77, 127.75, 114.19, 73.12, 69.57, 55.45, 53.55, 49.44, 28.54, 20.82, 18.43. **HRMS** calcd. for ($M + H^+$) $C_{28}H_{36}NO_5S^+$: requires 498.2309 found 498.2311.

5-(benzyloxy)-1,1-difluoro-*N*,*N*-bis(4-methoxybenzyl)pentane-1-sulfonamide (**5.42**)

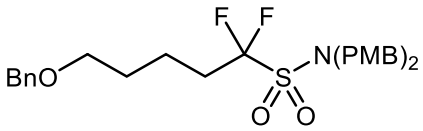

Di-PMB protected benzyl ether **5.41** (0.050 mg, 0.10 mmol) was dissolved in anhydrous THF (1 mL) and the resulting mixture was added to a solution of LDA (1M in THF, 0.20 mL, 0.21 mmol) in THF (1 mL) at -78 ℃. The resulting reaction mixture was stirred at -78 ℃ for 30 min, followed by dropwise addition of NFSI (0.03 g, 0.09 mmol) in anhydrous THF (1 mL) and the resulting mixture was stirred O/N at rt. A solution of sat. aqueous NH_4Cl was added to the reaction mixture, and the mixture extracted with EtOAc. A ^{1}H NMR of the crude sample suggested a complex reaction mixture, with LC-MS analysis showing no mass peak for **5.42**.

N-(9-(5-(*N*-((4-((3a*S*,4*S*,6a*R*)-2-oxohexahydro-1*H*-thieno[3,4-*d*]imidazol-4-yl)butyl)carbamoyl) sulfamoyl)pentyl)-9*H*-purin-6-yl)benzamide (**5.45**)

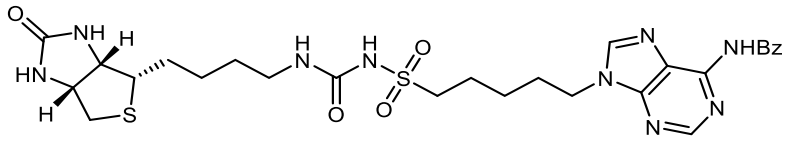

Biotin carbamate **5.09**[7] (0.070 g, 0.21 mmol) and Bz-protected sulfonamide **5.11** (0.065 g, 0.17 mmol) was reacted according to **general procedure 5B**, and purified by silica gel flash-column chromatography eluting DCM/MeOH (v/v = 9/1) to give **5.45** as a white solid (0.076 g, 58 %). **^{1}H NMR** (600 MHz, DMSO-d_6) δ 11.13 (s, 1H), 10.04 (s, 1H), 8.73 (s, 1H), 8.49 (s, 1H), 8.04 (d, *J* = 7.1 Hz, 2H), 7.64 (t, *J* = 7.4 Hz, 1H), 7.55 (t, *J* = 7.8 Hz, 2H), 6.47 – 6.39 (m, 2H), 6.35 (s, 1H), 4.31 – 4.26 (m, 3H), 4.16 – 4.08 (m, 1H), 3.38 – 3.34 (m, 2H), 3.10 – 3.06 (m, 1H), 3.02 (q, *J* = 6.7 Hz, 2H), 2.80 (dd, *J* = 12.4, 5.1 Hz, 1H), 2.56 (d, *J* = 12.4 Hz, 1H), 1.93 – 1.86 (m, 2H), 1.71 (p, *J* = 7.7 Hz, 2H), 1.64 – 1.58 (m, 1H), 1.49 – 1.36 (m, 5H), 1.34 – 1.26 (m, 2H); **^{13}C NMR** (150 MHz, DMSO-d_6) δ 165.54, 162.69, 152.46, 152.20, 151.36, 150.04, 144.68, 133.44, 132.38, 128.45, 128.44, 125.36, 60.98, 59.18, 55.48, 54.92, 52.05, 42.93, 39.84, 29.27, 28.74, 27.95, 25.81, 24.49, 22.59; **HRMS** calcd. for (M + H^+) $C_{27}H_{36}N_9O_5S_2^+$: requires 630.2275 found 630.2276.

4-(6-benzamido-9*H*-purin-9-yl)butyl-((4-((3a*S*,4*S*,6a*R*)-2-oxohexahydro-1*H*-thieno[3,4-*d*]imidazol-4-yl)butyl)carbamoyl)sulfamate (**5.46**)

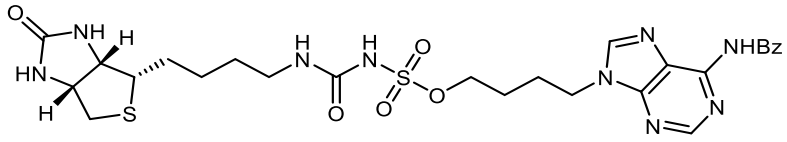

Biotin carbamate **5.09**[7] (0.024 g, 0.07 mmol) and with Bz-protected sulfamate **5.12** (0.022 g, 0.06 mmol) was reacted according to **general procedure 5B**, and purified by silica gel flash-column chromatography eluting DCM/MeOH (v/v = 1/4) to give **5.45** as a white solid (0.023 g, 53 %). **^{1}H NMR** (600 MHz, DMSO-d_6) δ 11.13 (s, 1H), 10.72 (s, 1H), 8.73 (s, 1H), 8.51 (s, 1H), 8.04 (d, *J* = 7.7 Hz, 2H), 7.64 (t, *J* = 7.4 Hz, 1H), 7.55 (t, *J* = 7.6 Hz, 2H), 6.44 (s, 1H), 6.39 – 6.32 (m, 2H), 4.31 (t, *J* = 7.1 Hz, 2H), 4.29 – 4.22 (m, 1H), 4.17 – 4.12 (m, 2H), 4.12 – 4.02 (m, 1H), 3.09 – 3.04 (m, 1H), 3.01 – 2.94 (m, 2H), 2.78 (dd, *J* = 12.4, 5.1 Hz, 1H), 2.55 (d, *J* = 12.3 Hz, 1H), 1.94 (p, *J* = 7.2 Hz, 2H), 1.68 – 1.57 (m, 3H), 1.47 – 1.35 (m, 3H), 1.33 –

1.24 (m, 2H); **^{13}C NMR** (150 MHz, DMSO-d_6, selected resonances due to signs of decomposition) δ 205.39, 168.64, 165.81, 157.90, 155.57, 154.50, 153.16, 147.80, 136.54, 135.49, 131.56, 64.09, 62.27, 58.61, 58.02, 42.98, 41.83, 32.85, 31.05, 29.00, 25.12; **HRMS** calcd. for (M + H^+) $C_{26}H_{34}N_9O_6S_2^+$: requires 632.2068 found 632.2073.

(3aS,4S,6aR)-4-(4-aminobutyl)tetrahydro-1H-thieno[3,4-d]imidazol-2(3H)-one-hydrochloride (**5.49**)

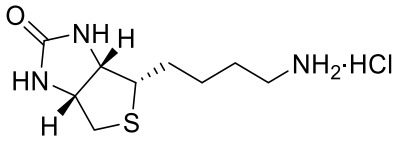

To a suspension of *D*-biotin (5.00 g, 20.47 mmol) in *t*-BuOH (100 mL) was added DPPA (4.84 mL, 22.51 mmol) and TEA (3.14 mL, 22.51 mmol), and the resulting reaction mixture was heated under reflux for 18 h. The mixture was concentrated under reduced pressure, and the residue was dissolved into THF (70 mL), and treated with aqueous 1 M $LiOH_{(aq)}$ (40 mL) for 5 min. The mixture was diluted with sat. NH_4Cl (50 mL) and extracted with EtOAc. The combined organic extracts were washed with sat. aqueos $NaHCO_3$, brine, dried over Na_2SO_4, filtered, concentrated under reduced pressure, and purified by silica gel flash column chromatography eluting with 7 % MeOH in DCM. The isolated was then dissolved into MeOH (10 mL), then treated with aqueous 6N HCl (10 mL). The resulting reaction mixture was stirred at rt O/N, concentrated under reduced pressure, ppt. filtered, and dried under reduced pressure to afford biotin amine hydrochloride **5.49** as a white solid (1.01g, 67 % 2-steps). ^{1}H and ^{13}C NMR consistent with literature.[7]

2,2-dichloro-*N*-(4-((3a*S*,4*S*,6aR)-2-oxohexahydro-1*H*-thieno[3,4-*d*]imidazol-4-yl)butyl)acetamide (**5.50**)

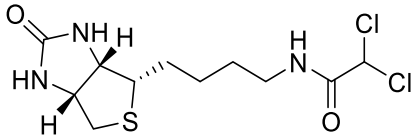

A solution of biotin amine hydrochloride **5.50** (0.100, 0.40 mmol), methyl dichloroacetate (0.045 mL, 0.44 mmol), and TEA (0.110 mL, 0.79 mmol) in anhydrous THF (5 mL) was heated under reflux for 16 h. The reaction mixture was concentrated under reduced pressure and purified by silica gel flash column chromatography eluting with 8 % MeOH in DCM to give the biotin dichloroacetamide **5.50** as a white solid (0.041 g, 32 %). **^{1}H NMR** (500 MHz, DMSO-

d_6) δ 8.55 (t, *J* = 5.6 Hz, 1H), 6.44 – 6.41 (m, 2H), 6.37 – 6.35 (m, 1H), 4.35 – 4.27 (m, 1H), 4.16 – 4.11 (m, 1H), 3.16 – 3.06 (m, 3H), 2.82 (dd, *J* = 12.4, 5.1 Hz, 1H), 2.58 (d, *J* = 12.4 Hz, 1H), 1.68 – 1.58 (m, 1H), 1.49 – 1.42 (m, 3H), 1.38 – 1.29 (m, 2H); **^{13}C NMR** (126 MHz, DMSO-d_6) δ 163.45, 162.69, 66.98, 66.96, 60.97, 59.17, 55.43, 39.11, 28.55, 27.92, 25.79; **HRMS** calcd. for (M + H^+) $C_{11}H_{18}Cl_2N_3O_2S^+$: requires 326.0491 found 326.0493.

2,2-dichloro-*N*-nitroso-*N*-(4-((3a*S*,4*S*,6a*R*)-2-oxohexahydro-1*H*-thieno[3,4-*d*]imidazol-4-yl)butyl)acetamide (**5.51**)

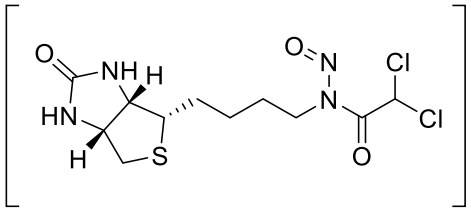

The biotin dichloroacetamide **5.50** (0.041 g, 0.13 mmol) was dissolved in 1/1 acetic anhydride / dichloroacetic acid (5 mL) and stirred in an ice bath at 0 ºC for 30 min. To the mixture was added solid sodium nitrite (0.26 mmol). The flask was capped with a rubber septum and vented with a syringe packed with anhydrous calcium sulfate and stirred for 4 h. The reaction mixture was diluted with EtOAc (10 mL) washed with H_2O, aqueous 10 % $NaCO_3$, washed with potassium phosphate monobasic (1 M aqueous, pH 5, 10 mL), dried with Na_2SO_4, filtered and used directly for the subsequent transformation without removing the solvent. Heating the organic phase at 40 ºC resulted in material decomposition as suggested by ^{1}H NMR analysis.

(3a*S*,4*S*,6a*R*)-4-(5-oxohexyl)tetrahydro-1*H*-thieno[3,4-*d*]imidazol-2(3*H*)-one (**5.53**)

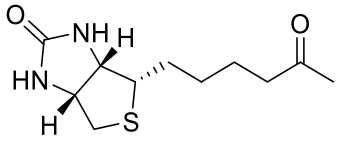

A solution of MeLi in diethyl ether (1.5M, 21.00 mL, 31.50 mmol) was added dropwise to a solution of biotin Weinreb Amide **4.06** (2.91 g, 10.13 mmol) in anhydrous THF (40 mL) over 1 min at -78 °C under a N_2 atmosphere, and the resulting solution was stirred for 3 h at -78 ºC. The reaction was quenched with aqueous sat. NH_4Cl (35 mL) and warmed to rt. The resulting mixture was extracted with EtOAc. The organic extracts were combined, concentrated under reduced pressure, and purified via silica gel flash column chromatography eluting with 12 % MeOH in DCM to give biotin methyl ketone **5.53** as a white solid (1.15 g, 47 %). **^{1}H NMR** (500 MHz, DMSO-d_6) δ 6.42 (s, 1H), 6.35 (s, 1H), 4.34 – 4.26 (m, 1H), 4.15 – 4.10 (m, 1H),

3.13 – 3.06 (m, 1H), 2.82 (dd, *J* = 12.4, 5.1 Hz, 1H), 2.57 (d, *J* = 12.4 Hz, 1H), 2.47 – 2.32 (m, 2H), 2.07 (s, 3H), 1.66 – 1.54 (m, 1H), 1.50 – 1.40 (m, 3H), 1.33 – 1.23 (m, 2H); **^{13}C NMR** (126 MHz, DMSO-d_6) δ 208.45, 162.68, 61.02, 59.17, 55.37, 42.56, 39.82, 29.65, 28.11, 28.08, 23.23; **HRMS** calcd. for (M + H^+) $C_{11}H_{19}N_2O_2S^+$: requires 243.1162 found 243.1164.

4-((3aS,4S,6aR)-5,5-dioxido-2-oxohexahydro-1H-thieno[3,4-d]imidazol-4-yl)butyl acetate (**5.54**)

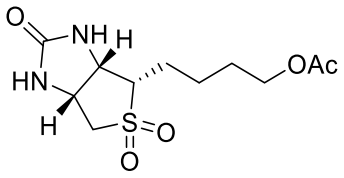

Attempt 1: To a mixture of biotin methyl ketone **5.53** (0.100 g, 0.41 mmol) in DCM (10 mL) was added *m*-CPBA (0.071, 0.41 mmol), and the reaction mixture was stirred at rt for 3 h, then concentrated under reduced pressure. The crude material was purified by silica gel flash column chromatography eluting with 10% MeOH in DCM to give a white solid, that LC-MS confirmed to be the corresponding sulfone **5.55**. An LC-MS of the crude material also only gave the mass peak for sulfone **5.55**.

Attempt 2: To a mixture of biotin methyl ketone **5.53** (0.100 g, 0.41 mmol) in DCM (20 mL) was added *m*-CPBA (0.376 g, 2.53 mmol), and the reaction mixture was heated under reflux for 3 h, then concentrated under reduced pressure. The crude material was purified by silica gel flash column chromatography eluting with 10% MeOH in DCM to give a white solid, that LC-MS confirmed to be the corresponding sulfone **5.55**. An LC-MS of the crude material also only gave the mass peak for sulfone **5.55**.

Attempt 3: As described in attempt 1. However, the *m*-CBPA was replaced with 10 % H_2O_2 (v = 5 mL) and DCM replaced with H_2O (v = 5 mL). The same results were obtained as reported for attempt 1 and 2.

Attempt 4: As described in attempt 1. However, the *m*-CBPA was replaced with 10 % H_2O_2 (v = 5 mL). and DCM replaced with H_2O (v = 5 mL). The reaction mixture was also heated at 80 ℃. The same results were obtained as reported for attempt 1 and 2.

5-((3a*S*,4*S*,6a*R*)-2-oxohexahydro-1*H*-thieno[3,4-*d*]imidazol-4-yl)pentyl phenyl carbonate (**5.56**)

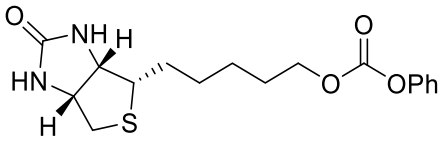

To a mixture of compound biotinol **5.57**[6] (0.540 g, 2.34 mmol) in DMF (10mL) was added diphenyl carbonate (0.50 g, 2.34 mmol) and DBU (0.385 mL, 2.58 mmol) and the reaction mixture was stirred at rt for 6 h. The mixture was poured into water (100 mL) and extracted with DCM. The organic extracts were combined, dried over Na_2SO_4, concentrated under reduced pressure, and purified by silica gel flash column chromatography eluting with 9 % MeOH in DCM to give biotin carbonate **5.56** as a white solid (0.353 g, 43 %).**^{1}H NMR** (500 MHz, DMSO-d_6) δ 7.43 (t, J = 7.9 Hz, 2H), 7.29 (t, J = 7.6 Hz, 1H), 7.23 (d, J = 7.9 Hz, 2H), 6.44 (s, 1H), 6.35 (s, 1H), 4.33 – 4.29 (m, 1H), 4.20 (t, J = 6.6 Hz, 2H), 4.17 – 4.11 (m, 1H), 3.13 – 3.09 (m, 1H), 2.83 (dd, J = 12.4, 5.1 Hz, 1H), 2.58 (d, J = 12.4 Hz, 1H), 1.72 – 1.61 (m, 3H), 1.53 – 1.33 (m, 5H); **^{13}C NMR** (126 MHz, DMSO-d_6) δ 162.68, 153.06, 150.75, 129.55, 126.04, 121.23, 68.45, 60.98, 59.18, 55.39, 39.94, 39.80, 28.15, 28.11, 27.81, 25.17; **HRMS** calcd. for (M + H^+) $C_{17}H_{23}N_2O_4S^+$: requires 351.1373 found 351.1371.

N-(9-(3-(sulfamoylamino)propyl)-9*H*-purin-6-yl)benzamide (**5.58**)

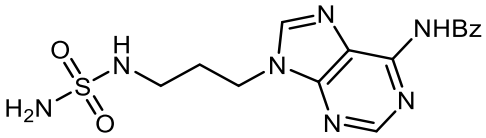

To a mixture of compound Boc-protected sulfonamide **5.65** (0.175 mg, 0.37 mmol) in DCM (5 mL) was added TFA (0.5 mL) and the mixture was stirred for 2 h. The mixture was concentrated under reduced pressure and the residue purified by silica gel flash column chromatography on silica eluting with 17 % MeOH in DCM to yield sulfonamide **5.58** as a white solid (0.121 g, 88 %) **^{1}H NMR** (600 MHz, DMSO-d_6) δ 11.12 (s, 1H), 8.74 (s, 1H), 8.48 (s, 1H), 8.05 (d, J = 6.9 Hz, 1H), 7.66 – 7.61 (m, 1H), 7.55 (t, J = 7.7 Hz, 2H), 6.65 (t, J = 6.1 Hz, 1H), 6.55 (s, 2H), 4.34 (t, J = 6.9 Hz, 2H), 2.90 (q, J = 6.5 Hz, 2H), 2.07 (p, J = 6.9 Hz, 2H); **^{13}C NMR** (150 MHz, DMSO-d_6) δ 165.55, 152.37, 151.35, 150.05, 144.76, 133.46, 132.36, 128.43, 128.41, 125.36, 48.57, 41.02, 29.02; **HRMS** calcd. for (M + H^+) $C_{15}H_{18}N_7O_3S^+$: requires 376.1186 found 376.1189.

N-(9-(4-sulfamoylbutyl)-9*H*-purin-6-yl)benzamide (**5.59**)

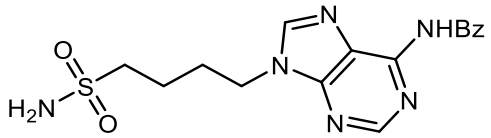

A solution of pyrimidinyl sulfone **5.68** (0.430 g, 0.98 mmol) in MeOH (8 mL) was cooled to 0 ℃, to which sodium methoxide, 25 wt. % solution in methanol (0.273 mL, 0.98 mmol) was added dropwise in one portion. The mixture was stirred at 0-5 ℃ for 20 min and then concentrated under reduced pressure, to give a crude residue of sulfinate **5.69** (0.98 mmol). This resulting residue was dissolved into a solution of NaOAc (0.101 g, 1.23 mmol) in H_2O (5 ml). To this solution was added a solution of HOSA (0.133 g, 1.18 mmol) in water (1 mL), and the resulting reaction mixture was stirred for 1 h at rt, concentrated under reduced pressure and purified by silica gel flash-column chromatography eluting with 10 % MeOH in DCM to give sulfonamide **5.11** as a white solid (0.165 g, 45 % over 2-steps). **^{1}H NMR** (500 MHz, DMSO-d_6) δ 11.14 (s, 1H), 8.74 (s, 1H), 8.50 (s, 1H), 8.04 (d, *J* = 7.7 Hz, 2H), 7.64 (t, *J* = 7.4 Hz, 1H), 7.55 (t, *J* = 7.6 Hz, 2H), 6.77 (s, 2H), 4.32 (t, *J* = 6.9 Hz, 2H), 3.09 – 3.01 (m, 2H), 2.00 (p, *J* = 7.2 Hz, 2H), 1.72 – 1.64 (m, 2H); **^{13}C NMR** (126 MHz, DMSO-d_6) δ 165.54, 152.48, 151.43, 151.42, 150.07, 144.72, 144.70, 133.43, 132.39, 128.46, 128.44, 125.39, 53.72, 42.73, 27.83, 20.84; **HRMS** calcd. for (M + H^+) $C_{16}H_{19}N_6O_3S^+$: requires 375.1234 found 375.1235.

3-(6-benzamido-9*H*-purin-9-yl)propyl sulfamate (**5.60**)

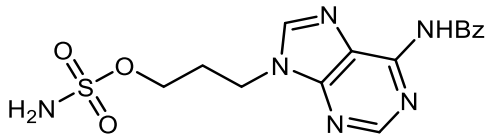

Formic acid (40 µL, 1.06 mmol) was added to neat CSI (0.090 mL, 1.06 mmol) at 0 ℃ under a N_2 atmosphere. The reaction mixture was stirred at 0 ℃ until a white solid appeared, then anhydrous MeCN (2 mL) was added, and the resulting mixture was stirred at rt O/N. The reaction mixture now containing sulfonating reagent **5.35** was cooled to 0 ℃, and a suspension of Bz-protected alcohol **5.72** (0.100 g, 0.46 mmol) in DMA (2 mL) was added dropwise. The resulting reaction mixture was stirred at 0 ℃ for 1.5 h, then warmed to rt and stirred for a further 2 h. The reaction mixture was quenched with water (1 mL), concentrated under reduced pressure, and purified by silica gel flash-column chromatography to give Bz-protected sulfamate **5.60** as white resin (0.056 g, 42 %). **^{1}H NMR** (500 MHz, DMSO-d_6) δ 11.43 (s, 1H), 8.54 (s, 1H), 8.43 (s, 1H), 8.00 (d, *J* = 7.6 Hz, 2H), 7.53 (t, *J* = 7.4 Hz, 1H), 7.49 (t, *J* = 7.6 Hz,

2H), 7.37 (s, 2H), 4.31 (t, *J* = 7.1 Hz, 2H), 4.10 (t, *J* = 6.3 Hz, 2H), 2.22 – 1.92 (m, 2H); **HRMS** calcd. for (M + H^+) $C_{15}H_{17}N_6O_4S^+$: requires 377.1027 found 377.1025.

tert-butyl (3-(6-amino-9*H*-purin-9-yl)propyl)carbamate (**5.61**)

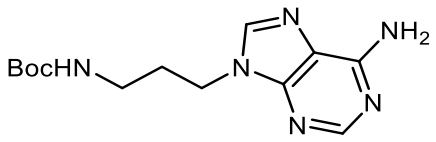

Adenine **5.15** (1.05 g, 7.7 mmol) was alkylated with 3-(Boc-amino)propylbromide (2.04 g, 8.55 mmol) in DMF (10 mL) in the presence of Cs_2CO_3 (3.80 g, 11.66 mmol), and the solution was stirred at rt O/N. The reaction mixture was diluted with water (80 mL), extracted with EtOAc, washed with water, brine, dried over Na_2SO_4, filtered, concentrated under reduced pressure and purified by silica gel flash column chromatography eluting with 6 % MeOH in DCM to give Boc-protected alkyl adenine **5.61** as a white solid (2.11 g, 93 %).**^{1}H NMR** (500 MHz, DMSO-d_6) δ 8.13 (d, *J* = 1.5 Hz, 2H), 7.19 (s, 2H), 6.93 (t, *J* = 5.7 Hz, 1H), 4.13 (t, *J* = 6.9 Hz, 2H), 2.91 (q, *J* = 6.5 Hz, 2H), 1.89 (p, *J* = 6.9 Hz, 2H), 1.37 (s, 9H); **^{13}C NMR** (126 MHz, DMSO-d_6) δ 155.95, 155.61, 152.35, 152.33, 149.48, 140.89, 140.87, 118.77, 77.65, 40.69, 37.12, 29.83, 28.23; **HRMS** calcd. for (M + H^+) $C_{13}H_{21}N_6O_2^+$: requires 293.1721 found 293.1720.

tert-butyl (3-(6-benzamido-9*H*-purin-9-yl)propyl)carbamate (**5.62**)

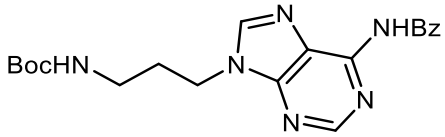

To a mixture of Boc-protected alkyl adenine **5.61** (1.62 g, 5.54 mmol) in pyridine (10 mL) was slowly added BzCl (0.708 mL, 6.09 mmol) and the mixture was stirred at 100 °C for 1 h. The mixture was concentrated under reduced pressure and the residue was purified by silica gel flash column chromatography eluting with 5 % MeOH in DCM to give **5.62** as a white foam (1.45 g, 66 %). **^{1}H NMR** (500 MHz, DMSO-d_6) δ 11.12 (s, 1H), 8.72 (s, 1H), 8.49 (s, 1H), 8.07 – 8.02 (m, 2H), 7.67 – 7.62 (m, 1H), 7.55 (t, *J* = 7.7 Hz, 2H), 6.95 (t, *J* = 5.8 Hz, 1H), 4.28 (t, *J* = 7.0 Hz, 2H), 2.96 (q, *J* = 6.5 Hz, 2H), 1.98 (p, *J* = 6.9 Hz, 2H), 1.38 (s, 9H); **^{13}C NMR** (126 MHz, DMSO-d_6) δ 155.63, 150.06, 149.61, 144.77, 133.46, 132.37, 129.25, 128.54, 128.45, 128.43, 125.41, 123.90, 77.69, 41.09, 37.11, 29.63, 28.24; **HRMS** calcd. for (M + H^+) $C_{20}H_{25}N_6O_3^+$: requires 397.1983 found 397.1985.

N-(9-(3-((2,2,2-trifluoroacetyl)-l4-azaneyl)propyl)-9*H*-purin-6-yl)benzamide (**5.63**)

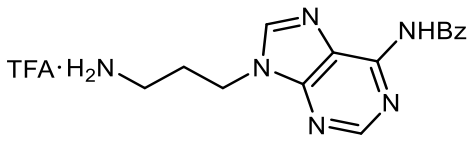

To a solution of **5.62** (1.10 g, 2.77 mmol) in DCM (10 mL) was added TFA (2 mL) and the resulting reaction mixture stirred at rt for 1 h. The mixture was then concentrated under reduced pressure to give **5.63** as a white solid which was used in subsequent steps without further purification (0.820, 99 %).**^{1}H NMR** (500 MHz, DMSO-d_6) δ 11.27 (s, 1H), 8.78 (s, 1H), 8.62 (s, 1H), 8.06 (d, *J* = 1.2 Hz, 1H), 7.86 (s, 2H), 7.68 – 7.64 (m, 1H), 7.56 (t, *J* = 7.7 Hz, 2H), 4.40 (t, *J* = 6.8 Hz, 2H), 3.53 – 3.44 (m, 2H), 2.83 (q, *J* = 7.2, 6.8 Hz, 2H), 2.18 (p, *J* = 7.0 Hz, 2H). **^{13}C NMR** (126 MHz, DMSO-d_6) δ 166.31, 152.09, 151.79, 149.01, 144.38, 132.82, 129.24, 128.64, 128.54, 41.52, 36.09, 27.01.

N-(9-(3-(sulfamoylamino)propyl)-9*H*-purin-6-yl)benzamide (**5.65**)

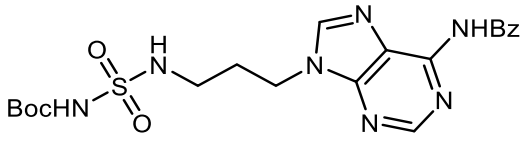

To a mixture of **5.63** (0.800 g, 2.69 mmol) in THF (20mL) were added TEA (1.50 mL, 10.76 mmol) and sulfamoylating agent **5.64** (1.62 g, 5.38 mmol) and the mixture was stirred at 60 °C O/N. The mixture was concentrated under reduced pressure and the residue was purified by silica gel flash column chromatography eluting with 1 % MeOH, and 25 % acetone in DCM to give **5.65** as a white solid (0.670 g, 46 %). **^{1}H NMR** (500 MHz, DMSO-d_6) δ 11.13 (s, 1H), 10.86 (s, 1H), 8.73 (s, 1H), 8.46 (s, 1H), 8.08 – 8.01 (m, 2H), 7.73 (s, 1H), 7.64 (t, *J* = 7.4 Hz, 1H), 7.55 (t, *J* = 7.7 Hz, 2H), 4.33 (t, *J* = 6.9 Hz, 2H), 2.91 (q, *J* = 6.6 Hz, 2H), 2.08 – 2.02 (m, 2H), 1.40 (s, 9H); **^{13}C NMR** (126 MHz, DMSO-d_6) δ 165.50, 152.39, 151.37, 151.35, 150.66, 150.06, 144.69, 144.66, 133.42, 132.36, 128.43, 128.40, 125.40, 81.18, 54.88, 40.85, 28.88, 27.71; **HRMS** calcd. for (M + H$^+$) $C_{20}H_{26}N_7O_5S^+$: requires 476.1711 found 476.1708.

9-(4-(pyrimidin-2-ylthio)butyl)-9*H*-purin-6-amine (**5.66**)

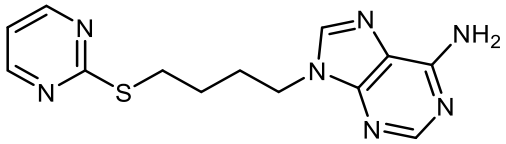

Adenine alkyl bromide **5.23** (1.00 g, 3.70 mmol) was alkylated with 2-mercaptopyrimidine (0.457 g, 4.07 mmol) in DMF (10 mL) in the presence of Cs_2CO_3 (1.80 g, 5.55 mmol), and the reaction suspension was stirred at rt O/N. The reaction mixture was diluted into H_2O (150 mL), extracted with DCM, washed with water, brine, dried over Na_2SO_4, filtered, concentrated under reduced pressure to give 2-pyrimidinyl thioether **5.66** as a yellow crystalline solid, which was used without further purification (1.10 g, 99 %.) **^{1}H NMR** (500 MHz, DMSO-d_6) δ 8.60 (d, J = 4.9 Hz, 2H), 8.15 (s, 1H), 8.12 (s, 1H), 7.21 – 7.15 (m, 3H), 4.17 (t, J = 7.0 Hz, 2H), 3.13 (t, J = 7.3 Hz, 2H), 1.94 (p, J = 7.2 Hz, 2H), 1.63 (tt, J = 9.7, 6.6 Hz, 2H); **^{13}C NMR** (126 MHz DMSO-d_6) δ 170.91, 157.70, 155.93, 152.34, 152.32, 149.52, 140.82, 118.72, 117.13, 42.39, 29.30, 28.57, 26.01; **HRMS** calcd. for (M + H^+) $C_{13}H_{16}N_7S^+$: requires 302.1182 found 302.1180.

N-(9-(4-(pyrimidin-2-ylthio)butyl)-9*H*-purin-6-yl)benzamide (**5.67**)

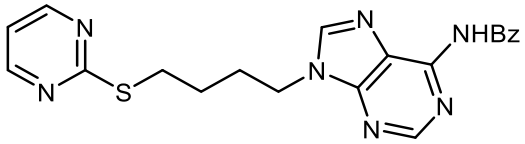

To a mixture of 2-pyrimidinyl thioether **5.66** (1.00 g, 3.48 mmol) in pyridine (5 mL) was slowly added BzCl (0.445 mL, 3.83 mmol) and the mixture was stirred at 100 °C for 1 h. The reaction mixture was concentrated under reduced pressure and the residue was purified by silica gel flash-column chromatography eluting with 5 % MeOH in DCM to yield Bz-protected 2-pyrimidinyl thioether **5.28** as a white solid (0.870 g, 62%). **^{1}H NMR** (500 MHz, DMSO-d_6) δ 11.13 (s, 1H), 8.72 (s, 1H), 8.60 (d, J = 4.9 Hz, 2H), 8.52 (s, 1H), 8.07 – 8.02 (m, 2H), 7.68 – 7.61 (m, 1H), 7.58 – 7.53 (m, 2H), 7.19 (t, J = 4.9 Hz, 1H), 4.33 (t, J = 7.0 Hz, 2H), 3.15 (t, J = 7.3 Hz, 2H), 2.02 (p, J = 7.2 Hz, 2H), 1.72 – 1.64 (m, 2H); **^{13}C NMR** (126 MHz, DMSO-d_6) δ 170.88, 157.72, 152.43, 151.32, 150.04, 149.60, 136.11, 132.35, 128.43, 128.42, 125.37, 123.88, 117.14, 42.79, 29.28, 28.36, 26.02; **HRMS** calcd. for (M + H^+) $C_{20}H_{20}N_7OS^+$: requires 406.1445 found 406.1444.

N-(9-(4-(pyrimidin-2-ylsulfonyl)butyl)-9*H*-purin-6-yl)benzamide (**5.68**)

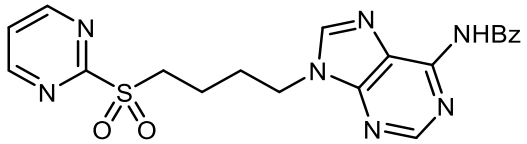

A solution of Bz-protected 2-pyrimidinyl thioether **5.66** (0.820 g, 2.02 mmol) in DCM (10 mL) at 0 °C was treated with *m*-CPBA (1.22 g, 7.08 mmol) and the resulting mixture was allowed to warm to rt and stirred for 3 h. The reaction mixture was concentrated under reduced pressure and purified by silica gel flash column chromatography eluting with 6 % MeOH in DCM to the pyrimidinyl sulfone **5.68** as a white solid (0.663 g, 75 %). **^{1}H NMR** (500 MHz, DMSO-d_6) δ 11.12 (s, 1H), 9.06 (d, *J* = 4.9 Hz, 1H), 8.72 (s, 1H), 8.49 (s, 1H), 8.05 (d, *J* = 7.6 Hz, 2H), 7.84 (t, *J* = 4.9 Hz, 1H), 7.65 (t, *J* = 7.4 Hz, 1H), 7.55 (t, *J* = 7.6 Hz, 2H), 4.32 (t, *J* = 6.9 Hz, 2H), 3.74 – 3.67 (m, 2H), 2.03 (p, *J* = 7.2 Hz, 2H), 1.73 – 1.65 (m, 2H); **^{13}C NMR** (126 MHz, DMSO-d_6) δ 165.54, 164.82, 159.18, 159.17, 152.43, 151.40, 150.06, 144.75, 144.73, 133.42, 132.38, 128.45, 125.37, 49.72, 42.48, 27.76, 19.15; **HRMS** calcd. for (M + H^+) $C_{20}H_{20}N_7O_3S^+$: requires 438.1343 found 438.1340.

3-(6-amino-9*H*-purin-9-yl)propyl acetate (**5.70**)

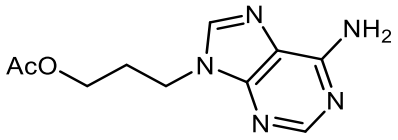

Adenine **5.15** (1.03 g, 7.6 mmol) was alkylated with 3-bromopropyl acetate (1.64 g, 8.70 mmol) in DMF (10 mL) in the presence of Cs_2CO_3 (3.73 g, 11.43 mmol), and the resulting suspension was stirred at rt O/N The reaction mixture was diluted with water (80 mL), extracted with DCM, washed with water, brine, dried over Na_2SO_4, filtered, concentrated and purified by silica gel flash column chromatography eluting with 10 % MeOH in DCM to give alkyl acetate **5.70** as a white solid (1.82 g, 90 %).**^{1}H NMR** (600 MHz, DMSO-d_6) δ 8.14 (s, 1H), 8.13 (s, 1H), 7.17 (s, 2H), 4.16 (t, *J* = 7.0 Hz, 2H), 4.00 (t, *J* = 6.6 Hz, 2H), 1.98 (s, 3H), 1.95 – 1.91 (m, 2H); **^{13}C NMR** (150 MHz, DMSO-d_6) δ 172.57, 154.95, 153.21, 148.14, 140.12, 116.72, 65.12, 40.46, 31.03, 28.11; **HRMS** calcd. for (M + H^+) $C_{10}H_{14}N_5O_2^+$: requires 236.1142 found 236.1142.

3-(6-amino-9*H*-purin-9-yl)propan-1-ol (**5.71**)

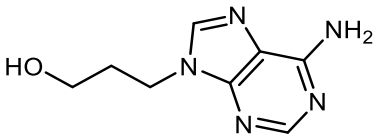

To a solution of alkyl acetate **5.70** (1.500 g, 6.21 mmol) in THF, MeOH and H_2O (3:1:1 = 15 mL) was added LiOH (0.456 g, 16.50 mmol), and the reaction mixture was stirred at 40 ℃ for 2 h, concentrated under reduced pressure and purified by silica gel flash column chromatography eluting with 17 % MeOH in DCM to give alcohol **5.71** as a white solid (1.38 g, 99 %). **^{1}H NMR** (600 MHz, DMSO-d_6) δ 8.13 (s, 1H), 8.10 (s, 1H), 7.15 (s, 2H), 4.50 (t, J = 5.2 Hz, 1H), 4.17 (t, J = 7.1 Hz, 2H), 3.38 – 3.34 (m, 2H), 2.94 – 2.90 (m, 2H); **^{13}C NMR** (150 MHz, DMSO-d_6) δ 157.23, 150.32, 147.14, 139.56, 116.47, 62.20, 42.83, 35.66.

N-(9-(3-hydroxypropyl)-9*H*-purin-6-yl)benzamide (**5.72**)

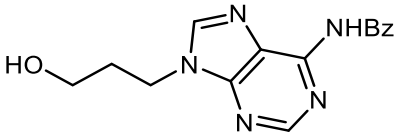

To a stirring solution of alcohol **5.71** (0.810 g, 4.10 mmol) in anhydrous pyridine (25 mL) was added TMSCl (4.94 mL, 39.09 mmol) under a N_2 atmosphere. After 30 min, BzCl (0.60 mL, 4.50 mmol) was added at 0 ℃. The resulting reaction mixture was warmed to rt and further stirred for 16 h. Then NH_4OH (10 mL) was added at 0 ℃, and the resulting reaction mixture was stirred at rt for 1 h; the solvent was removed under reduced pressure, and the resulting residue purified via silica gel flash column chromatography eluting with 10 % MeOH in DCM to give Bz-protected alcohol **5.34** (0.630 g, 50 %). **^{1}H NMR** (600 MHz, DMSO-d_6) δ 11.11 (s, 1H), 8.74 (s, 1H), 8.48 (s, 1H), 8.04 (d, J = 7.0 Hz, 1H), 7.69 – 7.65 (m, 1H), 7.56 (t, J = 7.8 Hz, 2H), 4.50 (t, J = 5.2 Hz, 1H), 4.29 (t, J = 7.1 Hz, 2H), 3.42 – 3.38 (m, 2H), 2.93 – 2.88 (m, 2H); **^{13}C NMR** (150 MHz DMSO-d_6) δ 164.41, 151.56, 150.34, 149.44, 144.71, 132.57, 131.47, 129.26, 126.33, 124.33, 60.09, 43.24, 33.52; **HRMS** calcd. for (M + H^+) $C_{15}H_{16}N_5O_2^+$: requires 298.1299 found 298.1302.

5-((3a*S*,4*S*,6a*R*)-2-oxohexahydro-1*H*-thieno[3,4-*d*]imidazol-4-yl)pentyl-(*N*-(3-(6-benzamido-9*H*-purin-9-yl)propyl)sulfamoyl)carbamate (**5.73**)

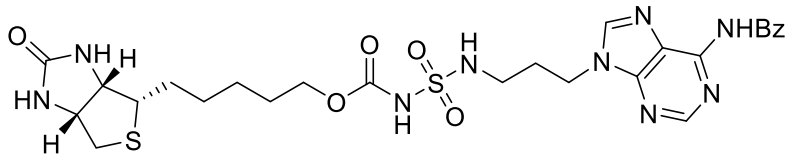

Biotin carbonate **5.56** (0.070 g, 0.20 mmol) and Bz-protected amino sulfonamide **5.58** (0.067g, 0.18 mmol) was reacted according to **general procedure 5C** and was purified by silica gel flash-column chromatography eluting with 9 % MeOH in DCM to give **5.73** as a white solid (0.059 g, 47 %). **^{1}H NMR** (500 MHz, DMSO-d_6) δ 11.13 (s, 1H), 9.83 (s, 1H), 8.73 (s, 1H), 8.45 (s, 1H), 8.15 – 7.93 (m, 2H), 7.64 (t, *J* = 7.4 Hz, 1H), 7.61 – 7.52 (m, 2H), 7.51 (s, 1H), 6.42 (d, *J* = 1.9 Hz, 1H), 6.35 (s, 1H), 6.25 (s, 1H), 4.33 (t, *J* = 6.9 Hz, 2H), 4.30 – 4.26 (m, 1H), 4.14 – 4.08 (m, 1H), 3.10 – 2.98 (m, 3H), 2.95 – 2.87 (m, 2H), 2.79 (dd, *J* = 12.4, 5.1 Hz, 1H), 2.56 (d, *J* = 12.4 Hz, 1H), 2.06 (p, *J* = 6.8 Hz, 2H), 1.67 – 1.56 (m, 2H), 1.54 – 1.22 (m, 4H); **^{13}C NMR** (150 MHz, DMSO-d_6) δ 165.56, 162.73, 152.42, 151.39, 150.08, 144.73, 133.45, 132.40, 128.47, 128.45, 125.38, 60.99, 59.20, 55.57, 55.45, 54.92, 40.89, 39.85, 38.81, 29.41, 28.88, 27.96, 25.81, 23.07; **HRMS** calcd. for (M + H^+) $C_{25}H_{33}N_{10}O_5S_2^+$: requires 617.2071 found 617.2068.

5-((3a*S*,4*S*,6a*R*)-2-oxohexahydro-1*H*-thieno[3,4-*d*]imidazol-4-yl)pentyl ((4-(6-benzamido-9*H*-purin-9-yl)butyl)sulfonyl)carbamate (**5.74**)

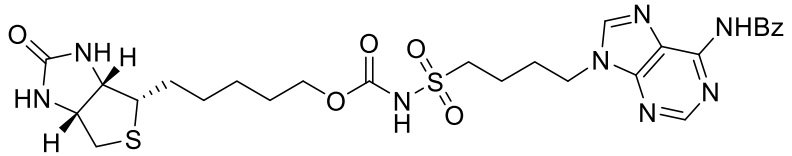

Biotin carbonate **5.56** (0.070 g, 0.20 mmol) and Bz-protected sulfonamide **5.59** (0.067 g, 0.18 mmol) was reacted according to **general procedure 5C** and was purified by silica gel flash-column chromatography eluting with 9 % MeOH in DCM to give **5.73** as a white solid (0.071 g, 56 %). **^{1}H NMR** (600 MHz, DMSO-d_6) δ 11.14 (s, 1H), 8.74 (s, 1H), 8.46 (s, 1H), 8.06 – 8.01 (m, 3H), 7.66 – 7.62 (m, 1H), 7.55 (t, *J* = 7.8 Hz, 3H), 6.43 (s, 0H), 6.35 (s, 1H), 4.38 – 4.27 (m, 3H), 4.16 – 4.10 (m, 1H), 4.04 (t, *J* = 6.7 Hz, 2H), 3.10 – 3.04 (m, 1H), 2.95 – 2.89 (m, 3H), 2.80 (dd, *J* = 12.4, 5.1 Hz, 1H), 2.57 (d, *J* = 12.4 Hz, 1H), 2.07 (pd, *J* = 6.7, 2.8 Hz, 2H), 1.66 – 1.52 (m, 3H), 1.45 (dtt, *J* = 13.2, 9.0, 4.8 Hz, 1H), 1.38 – 1.25 (m, 4H); **^{13}C NMR**

(150 MHz, DMSO-d_6) δ 165.53, 162.74, 162.72, 152.41, 151.39, 150.07, 144.81, 144.72, 133.43, 133.42, 132.39, 128.46, 128.43, 125.40, 65.17, 61.00, 60.65, 59.21, 59.20, 55.40, 54.91, 40.87, 40.00, 32.33, 29.04, 28.20, 28.10, 28.02, 25.16; **HRMS** calcd. for (M + H^+) $C_{27}H_{35}N_8O_6S_2^+$: requires 631.2115 found 631.2116.

3-(6-benzamido-9*H*-purin-9-yl)propyl-(((5-((3a*S*,4*S*,6a*R*)-2-oxohexahydro-1*H*-thieno[3,4-*d*]imidazol-4-yl)pentyl)oxy)carbonyl)sulfamate (**5.75**)

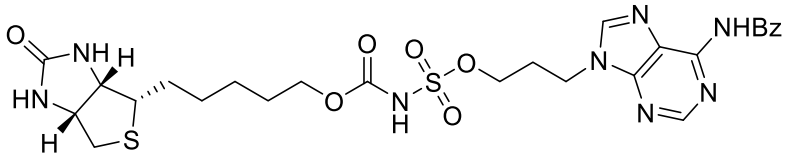

Biotin carbonate **5.56** (0.070 g, 0.20 mmol) and Bz-protected sulfamate **5.60** (0.055 g, 0.18 mmol) was reacted according to **general procedure 5C** and was purified by silica gel flash-column chromatography eluting with 20 % MeOH in DCM to give **5.75** as a white solid (0.021 g, 15 %). **^{1}H NMR** (600 MHz, DMSO-d_6, selected resonances due to signs of decomposition) δ 12.40 (s, 1H), 10.71 (s, 1H), 8.74(s, 1H), 8.58 (s, 1H), 8.10 (d, *J* = 7.7 Hz, 2H), 7.65(t, *J* = 7.4 Hz, 1H), 7.61 (t, *J* = 7.6 Hz, 2H), 6.40 (s, 1H), 6.39 – 6.32 (m, 2H), 4.31 (t, *J* = 7.1 Hz, 2H), 4.29 – 4.22 (m, 1H), 4.18 – 4.14 (m, 2H), 4.10 – 4.02 (m, 1H), 3.19 – 3.11 (m, 1H), 3.10 – 2.98 (m, 2H), 2.78 (dd, *J* = 12.4, 5.1 Hz, 1H), 2.55 (d, *J* = 12.3 Hz, 1H), 1.68 – 1.57 (m, 3H), 1.47 – 1.35 (m, 3H), 1.33 – 1.24 (m, 2H); **HRMS** calcd. for (M + H^+) $C_{27}H_{35}N_8O_6S_2^+$: requires 633.1908 found 633.1910.

5-((3a*S*,4*S*,6a*R*)-2-oxohexahydro-1*H*-thieno[3,4-*d*]imidazol-4-yl)pentyl-(*N*-(3-(6-amino-9*H*-purin-9-yl)propyl)sulfamoyl)carbamate (**5.76**)

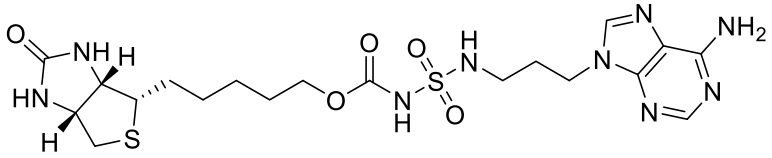

Bz-protected amino sulfonylcarbamate **5.73** (0.055 g, 0.09 mmol) was de-protected according to **general procedure 5A** and was purified by silica gel flash-column chromatography eluting with DCM:MeOH (v/v = 5:1) to give **5.76** as a white solid (0.032 g, 71 %). **^{1}H NMR** (600 MHz, DMSO-d_6) δ 11.12 (s, 1H), 8.13 (s, 1H), 8.10 (s, 1H), 7.20 (s, 2H), 6.53 (s, 1H), 6.50 (s, 1H), 6.36 (s, 1H), 4.32 – 4.29 (m, 1H), 4.22 – 4.16 (m, 2H), 4.16 – 4.11 (m, 1H), 4.05 – 4.00 (m, 2H), 3.12 – 3.07 (m, 1H), 2.90 – 2.85 (m, 2H), 2.82 (dd, *J* = 12.4, 5.1 Hz, 1H), 2.58 (d, *J* = 12.4 Hz, 1H), 1.99 (h, *J* = 6.8 Hz, 2H), 1.66 – 1.27 (m, 8H); **^{13}C NMR** (150 MHz, DMSO-d_6) δ

162.78, 155.94, 152.37, 152.34, 149.46, 140.89, 140.81, 118.73, 65.06, 61.04, 59.22, 55.41, 54.88, 48.58, 40.58, 40.46, 39.98, 29.23, 29.16, 28.23, 28.12, 28.03, 25.17; **HRMS** calcd. for (M + H^+) $C_{27}H_{35}N_8O_6S_2^+$: requires 528.1806 found 528.1810.

5-((3a*S*,4*S*,6a*R*)-2-oxohexahydro-1*H*-thieno[3,4-*d*]imidazol-4-yl)pentyl-((4-(6-amino-9*H*-purin-9-yl)butyl)sulfonyl)carbamate (**5.77**)

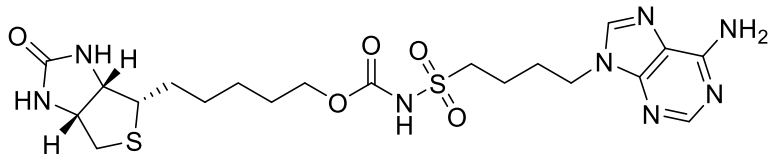

Bz-protected amino sulfonylcarbamate **5.74** (0.031 g, 0.05 mmol) was de-protected according to **general procedure 5A** and was purified by silica gel flash-column chromatography eluting with DCM:MeOH (v/v = 5:1) to give **5.77** as a white solid (0.015 g, 56 %). **^{1}H NMR** (500 MHz, DMSO-d_6) δ 11.49 (s, 1H), 8.19 – 8.09 (m, 2H), 7.20 (s, 2H), 6.53 – 6.47 (m, 1H), 6.36 (s, 1H), 4.34 – 4.27 (m, 1H), 4.18 – 4.11 (m, 3H), 3.98 (t, *J* = 6.6 Hz, 2H), 3.13 – 3.05 (m, 1H), 2.82 (dd, *J* = 12.4, 5.1 Hz, 1H), 2.57 (d, *J* = 12.4 Hz, 1H), 1.92 (p, *J* = 7.1 Hz, 2H), 1.65 – 1.51 (m, 6H), 1.47 – 1.29 (m, 6H); **^{13}C NMR** (126 MHz, DMSO-d_6) δ 162.75, 155.94, 152.39, 152.37, 149.52, 140.78, 118.70, 61.04, 60.65, 59.20, 55.44, 54.90, 53.75, 50.71, 42.27, 32.33, 28.20, 27.95, 25.30, 20.48; **HRMS** calcd. for (M + H^+) $C_{20}H_{35}N_8O_6S_2^+$: requires 526.1781 found 526.1784.

5-((3a*S*,4*S*,6a*R*)-2-oxohexahydro-1*H*-thieno[3,4-*d*]imidazol-4-yl)pentyl-((4-(6-amino-9*H*-purin-9-yl)butyl)sulfonyl)carbamate (**5.77**)

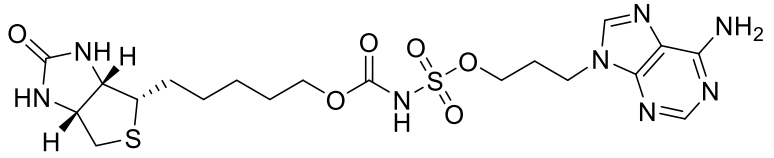

Bz-protected amino sulfonylcarbamate **5.74** (0.031 g, 0.05 mmol) was de-protected according to **general procedure 5A** and was purified by silica gel flash-column chromatography eluting with DCM:MeOH (v/v = 5:1) to give a white solid (0.002 g, 3 %). Due to instability issues, characterisation was limited to HRMS; **HRMS** calcd. for (M + H^+) $C_{20}H_{35}N_8O_6S_2^+$: requires 529.1646 found 529.1651.

6.4 References

(1) Stachura, D. L.; Nguyen, S.; Polyak, S. W.; Jovcevski, B.; Bruning, J. B.; Abell, A. D. A New 1,2,3-Triazole Scaffold with Improved Potency against Staphylococcus Aureus Biotin Protein Ligase. *ACS Infect. Dis.* **2022**, *8* (12), 2579-2585. https://doi.org/10.1021/acsinfecdis.2c00452.

(2) Sternicki, L. M.; Nguyen, S.; Pacholarz, K. J.; Barran, P.; Pendini, N. R.; Booker, G. W.; Huet, Y.; Baltz, R.; Wegener, K. L.; Pukala, T. L.; Polyak, S. W. Biochemical Characterisation of Class III Biotin Protein Ligases from Botrytis Cinerea and Zymoseptoria Tritici. *Arch. Biochem. Biophys.* **2020**, *691* (June), 108509. https://doi.org/10.1016/j.abb.2020.108509.

(3) Ng, B.; Polyak, S. W.; Bird, D.; Bailey, L.; Wallace, J. C.; Booker, G. W. Escherichia Coli Biotin Protein Ligase: Characterization and Development of a High-Throughput Assay. *Anal. Biochem.* **2008**, *376* (1), 131–136. https://doi.org/10.1016/j.ab.2008.01.026.

(4) Yung-Chi, C.; Prusoff, W. H. Relationship between the Inhibition Constant (KI) and the Concentration of Inhibitor Which Causes 50 per Cent Inhibition (I50) of an Enzymatic Reaction. *Biochem. Pharmacol.* **1973**, *22* (23), 3099–3108. https://doi.org/10.1016/0006-2952(73)90196-2.

(5) Feng, J.; Paparella, A. S.; Tieu, W.; Heim, D.; Clark, S.; Hayes, A.; Booker, G. W.; Polyak, S. W.; Abell, A. D. New Series of BPL Inhibitors To Probe the Ribose-Binding Pocket of Staphylococcus Aureus Biotin Protein Ligase. *ACS Med. Chem. Lett.* **2016**, *7* (12), 1068–1072. https://doi.org/10.1021/acsmedchemlett.6b00248.

(6) Paparella, A. S.; Lee, K. J.; Hayes, A. J.; Feng, J.; Feng, Z.; Cini, D.; Deshmukh, S.; Booker, G. W.; Wilce, M. C. J.; Polyak, S. W.; Abell, A. D. Halogenation of Biotin Protein Ligase Inhibitors Improves Whole Cell Activity against Staphylococcus Aureus. *ACS Infect. Dis.* **2018**, *4* (2), 175–184. https://doi.org/10.1021/acsinfecdis.7b00134.

(7) Lee, K. J.; Tieu, W.; Blanco-Rodriguez, B.; Paparella, A. S.; Yu, J.; Hayes, A.; Feng, J.; Marshall, A. C.; Noll, B.; Milne, R.; Cini, D.; Wilce, M. C. J.; Booker, G. W.; Bruning, J. B.; Polyak, S. W.; Abell, A. D. Sulfonamide-Based Inhibitors of Biotin Protein Ligase as New Antibiotic Leads. *ACS Chem. Biol.* **2019**, *14* (9), 1990–1997. https://doi.org/10.1021/acschembio.9b00463.

(8) Neves, M. A. C.; Totrov, M.; Abagyan, R. Docking and Scoring with ICM: The Benchmarking Results and Strategies for Improvement. *J. Comput. Aided. Mol. Des.* **2012**, *26* (6), 675–686. https://doi.org/10.1007/s10822-012-9547-0.